DOKUZ EYLÜL UNIVERSITY

GRADUATE SCHOOL OF NATURAL AND APPLIED SCIENCES

MINERALOGIC AND PETROGRAPHIC INVESTIGATION OF SKARN ALTERATION ZONES RELATED TO THE EVCİLER GRANITOID, KAZDAĞ NORTHWESTERN ANATOLIA

by

Yeşim YÜCEL ÖZTÜRK

September, 2006

İZMİR

MINERALOGIC AND PETROGRAPHIC INVESTIGATION OF SKARN ALTERATION ZONES RELATED TO THE EVCİLER GRANITOID, KAZDAĞ NORTHWESTERN ANATOLIA

A Thesis Submitted to the
Graduate School of Natural and Applied Sciences of Dokuz Eylül University
In Partial Fulfillment of the Requirements for the Degree of Doctor of Philosophy in Geological Engineering, Economic Geology Program

by
Yeşim YÜCEL ÖZTÜRK

September, 2006
İZMİR

Ph.D. THESIS EXAMINATION RESULT FORM

We have read the thesis entitled **"MINERALOGIC AND PETROGRAPHIC INVESTIGATION OF SKARN ALTERATION ZONES RELATED TO THE EVCİLER GRANITOID, KAZDAĞ NORTHWESTERN ANATOLIA"** completed by **Yeşim YÜCEL ÖZTÜRK** under supervision of **Prof. Dr. Cahit HELVACI** and we certify that in our opinion it is fully adequate, in scope and in quality, as a thesis for the degree of Doctor of Philosophy.

Prof. Dr. Cahit HELVACI

Supervisor

Prof. Dr. Hüseyin YILMAZ

Committee Member

Prof. Dr. Kadir YURDAKOÇ

Committee Member

Jury Member

Jury Member

Prof. Dr. Cahit HELVACI
Director
Graduate School of Natural and Applied Sciences

ACKNOWLEDGMENTS

I would like to express my sincere gratitude to my supervisor, Prof. Dr. Cahit Helvacı, for his patience, support, guidance and helpful suggestions during the preparation of this thesis.

I extend my thanks to Prof. Dr. Muharrem Satır for providing the use of his laboratories in the Institute of Geochemistry, Tübingen University, Germany and for his encouraging suggestions, which have improved significantly the content and clarity of the stable isotope study.

I thank to Dr. Heinrich Taubald, Gabriele Stoschek, Bernd Steinhilber and Gisela Bartholomä for the isotope analyses, and Dr. Thomas Weinzel for the microprobe analyses. My special thanks are extended to Prof. Dr. Yücel YILMAZ who made constructive comments during the field studies. I am indepted to Prof. Dr. Hüseyin YILMAZ who made great contributions for understanding of the skarn mineralization processes of the study area. I am also grateful to Prof. Dr. Sinan ÖNGEN for his contributions. I acknowladge Prof. Dr. Erdin BOZKURT for his helpful suggestions and Dr. Cüneyt AKAL for his helpful suggestions during the field studies.

This thesis was supported by two research project grants, (Project number 101Y018) from the Scientific & Technological Research Council of Turkey (TÜBİTAK) and (Project number 0922.01.01.17) from Dokuz Eylül University Scientific Research Projects (BAP) .

Lastly, I must thank to my parents Mestinaz and Cemil Yücel, my brother Oğuzkan Yücel and my husband Hasan Öztürk for their continuous support and encouragement throughout the preparation of this thesis.

Yeşim YÜCEL ÖZTÜRK

MINERALOGIC AND PETROGRAPHIC INVESTIGATION OF SKARN ALTERATION ZONES RELATED TO THE EVCİLER GRANITOID, KAZDAĞ NORTHWESTERN ANATOLIA

ABSTRACT

The purpose of this study is determination of the petrographic features, geology and alteration-mineralization style of the Evciler district with the aid of analytical data obtained by the electron probe microanalyses of the skarn mineral assemblage of Evciler, and establishment of the results of a stable isotope study of the skarn-forming minerals at the Evciler location. Stable isotope analyses of oxygen, hydrogen were made of appropriate mineral phases from the Evciler skarn with two broad objectives; (1) to derive estimates of fluid temperature from oxygen isotope geothermometry on appropriate mineral pairs, and (2) to model the isotopic composition and origin of skarn forming fluids (at each successive stage). This study also draws attention to the similarities of this occurrence with the other skarns of the world, some of which are well known for their ore potential.

Alteration and mineralization in the Evciler district (Kazdağ, Çanakkale) are related to I-type, magnetite-series, metaluminous and calc-alkaline body, which intrudes the Kazdağ Massif. Correlations between skarns and Evciler granitoid within the study area are evaluated using Harker-type diagrams with major and trace elements. The Evciler granitoid exhibits characteristic distribution patterns of the plutons associated with Au-Cu, and Fe skarns.

The skarn zones in the study area are both calcic exoskarn and endoskarn and have an oxidized mineralogy dominated by garnet, clinopyroxene, epidote, amphibole and chlorite. Skarn at Evciler contain up to 80 percent sulfides (pyrrothite, pyrite, and chalcopyrite) and massive pyrrothite-bearing mineralization body replaces prograde skarn and marble. The garnet-pyroxene skarn represent early skarn formation (prograde stage) and are composed of the anhydrous minerals, predominantly pyroxene with garnet. Epidote-amphibole skarn represent late skarn-forming phases (retrograde stage) and replace early mineral assemblages.

Microprobe analyses indicate that clinopyroxene has diopside-rich, whereas garnet composition has andradite-rich composition (typical for Au-Cu, Fe sulfide associations).

Stable isotope compositions of anhydrous and hydrous minerals from Evciler skarn indicates that garnet-pyroxene skarn was produced by predominantly magmatic fluids during initial skarn forming metasomatism in the study area and amphibole-epidote rich skarn was formed by magmatic water mixed with meteoric water. However, the delta-deuterium values of late amphibole and epidote indicate both magmatic and lighter values for Evciler skarn deposit that could be explained by mixing with meteoric water. We concluded that the isotopic evolution of the hydrothermal fluid can be accounted for by circulation of meteoric water through a convention system heated by the Evciler granitoid, causing exchange of oxygen isotopes with the granitoid and country rock, and possibly involving some admixture of magmatic water.

Keywords. Skarn, geochemistry, stable isotope, Evciler, Kazdağ, Northwestern Anatolia.

EVCİLER GRANİTOİDİNE (KAZDAĞ, KUZEYBATI ANADOLU) BAĞLI GELİŞEN SKARN ALTERASYON ZONLARININ MİNERALOJİK VE PETROGRAFİK İNCELEMESİ

ÖZ

Çalışmanın amacı, Evciler skarn mineral topluluğunun, elektron mikroprob analizleri ile saptanan analitik verileri ile birlikte, Evciler bölgesinin petrografik özellikleri, jeolojisi ve alterasyon-mineralizasyon tipini tespit etmek ve Evciler lokasyonunda gözlenen skarn oluşturan minerallere ait duraylı izotop çalışmalarının sonuçlarını ortaya koymaktır. Evciler skarnından alınan mineral fazlarından oksijen, hidrojen duraylı izotop analizleri, (1) mineral çiftleri ile oksijen izotop jeotermometrisinden akışkan sıcaklığının tahmin edilmesi ve (2) skarn oluşturan akışkanların (her bir evre için) izotopik bileşimi ve kökeninin modellenmesi için gerçekleştirilmiştir. Bu çalışma aynı zamanda, cevher potansiyeli açısından iyi bilinen Dünya'daki diğer skarn yatakları ile bu bölgedeki skarn oluşumunun benzerliklerini ortaya koymaktadır.

Evciler bölgesindeki (Kazdağ, Çanakkale) alterasyon ve mineralizasyon, Kazdağ Masifi'ne sokulmuş, I-tipi, magnetit-serili, metaluminyumlu, kalk alkalen kütle ile ilişkilidir. Çalışma alanında, Evciler granitoidi ve skarnlar arasında korelasyonlar, major ve iz elementlerle birlikte Harker-tip diyagramlar kullanılarak, değerlendirilmiştir. Buna göre Evciler granitoidi Au-Cu, ve Fe skarnları ile birlikte bulunan plutonların karakteristik dağılım özelliklerini göstermektedir..

Çalışma alanında skarn zonları, kalsik ekzoskarn ve endoskarn şeklindedir ve granat, klinopiroksen, epidot, amfibol ve kloritce baskın okside bir mineralojiye sahiptir. Evciler bölgesinde gözlenen skarn, %80'nin üzerinde sulfid (pirotin, pirit, ve kalkopirit) içermektedir ve masiv pirotin içeren mineralizasyon kütlesi, prograd evre skarnını ve mermeri ornatmaktadır. Granat-piroksen skarnı, erken skarn oluşumunu temsil etmektedir (prograd evre) ve granatla birlikte piroksence baskın susuz minerallerden oluşmaktadır. Epidot-amfibol skarnı ise geç skarn oluşum fazını temsil etmektedir (retrograd evre) ve erken mineral topluluklarını ornatmaktadır.

Mikroprob analizler, klinopiroksenin diyopsitce zengin, buna karşın granatın andraditce zengin bileşime sahip olduğuna işaret etmektedir (Au-Cu, Fe sülfid toplulukları için tipik).

Evciler skarnından alınan susuz ve sulu minerallerinin duraylı izotop bileşimleri, çalışma alanında ilk skarn-oluşturan metasomatizma boyunca, granat-piroksen skarnın baskın olarak magmatik akışkanlardan geliştiğine ve amfibol-epidotca zengin skarnın ise meteorik su ile karışmış magmatik su ile oluştuğuna işaret etmektedir. Bununla birlikte, geç evre amfibol ve epidota ait delta-döteryum değerleri Evciler skarnı için, hem magmatik ve hem de meteorik su ile karışım şeklinde açıklanabilen daha hafif değerlere işaret etmektedir. Bu şekilde, hidrotermal akışkanın izotopik evriminin, granitoid ve yan kayaç ile oksijen izotop değişimine neden olan, Evciler granitoidi tarafından ısıtılan bir sistem içinde, bir miktar magmatik suyun da karışımını içeren, meteorik su sirkülasyonu ile açıklanabileceği sonucu ortaya konmaktadır.

Anahtar Kelimeler. Skarn, jeokimya, duraylı izotop, Evciler, Kazdağ, Kuzeybatı Anadolu.

CONTENTS

Page

CHAPTER ONE
GENERAL OVERVIEW OF THE SKARNS

1.1 Definitions, Terminology and Classification of skarns

Skarn is relatively simple rock type defined by its mineralogy that reflects the physical and chemical stability of the constituent minerals rather than implying any particular geological setting or protolith composition (e.g. Meinert, 1992). Skarns occur on all continents and in rocks of almost all ages. Although the majority of skarns are found in lithologies containing at least some limestone, they can form in almost any rock type, including shale, sandstone, granite, iron formation, basalt, and komatiite.

Skarns are rocks consisting of Ca-Fe-Mg-Mn silicates formed by the replacement of carbonate-bearing rocks accompanied by regional or contact metamorphism and metasomatism (Einaudi, Meinert & Newbery, 1981) in response to the emplacement of intrusives of varying compositions. They are found adjacent to igneous intrusions, along faults and major shear zones, in shallow geothermal systems, on the bottom of the sea floor, and at lower crustal depths in deeply buried metamorphic terrains (Meinert, 1992). Complex mineralogy and polyphasal deposition are characteristic, typically with early high temperature anhydrous silicates ± iron oxides overprinted by later hydrous silicates and sulfides.

Skarns can be subdivided according to several criteria. Exoskarn and endoskarn are common terms used to indicate a sedimentary or igneous protolith, respectively (Figure 1.1). Magnesian and calcic skarns can be used to describe the dominant composition of the protolith and resulting skarn minerals. Calcic skarns are formed by replacement of limestone producing Ca-rich alteration products such are garnets (grossular-andradite) – clinopyroxene (diopside-hedenbergite), vesuvianite and wollastonite. Magnesian skarns are formed by replacement of dolomite, producing Mg-rich alteration phases such as diopside, forsterite and phlogopite.

Calc-silicate hornfels is a descriptive term often used for the relatively fine-grained calc-silicate rocks that result from metamorphism of impure carbonate units such as clayey and/or silty limestone or calcareous shale (Figure 1.2a). Reaction skarns can form from isochemical metamorphism of thinly interlayered shale and carbonate units where metasomatic transfer of components between adjacent lithologies may occur on a small scale (perhaps centimetres) (Figure 1.2b) (e.g. Vidale, 1969; Zarayskiy, Zharikov, Stoyanovskaya & Balashov, 1987).

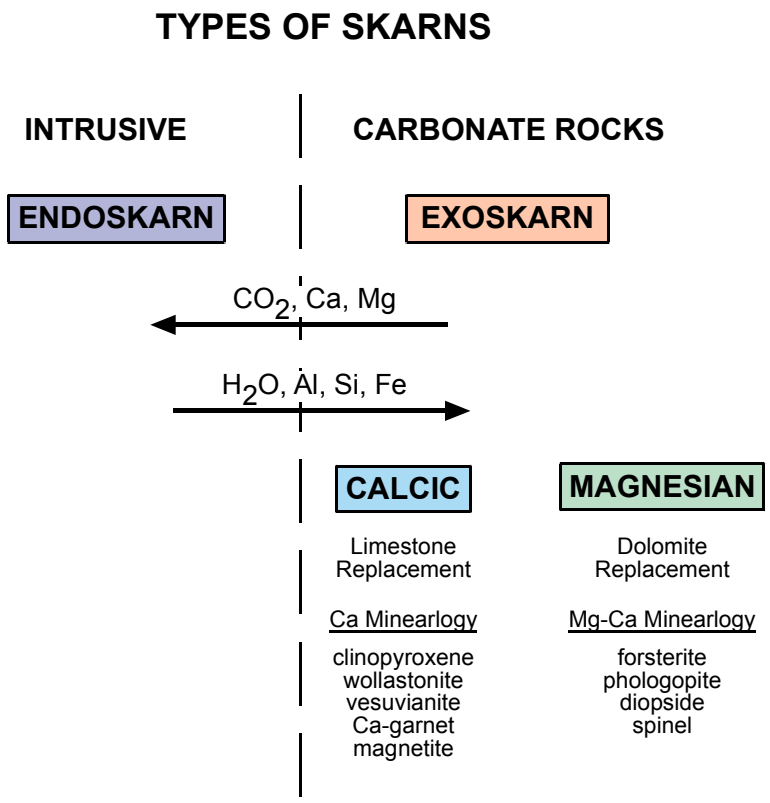

Figure 1.1. Host (protolith) compositions of the skarns.

Skarnoid is a descriptive term for calc-silicate rocks which are relatively fine-grained, iron-poor, and which reflect, at least in part, the compositional control of the protolith (Zharikov, 1970) (Figure 1.2c). Genetically, skarnoid is intermediate between a purely metamorphic hornfels and a purely metasomatic, coarse-grained skarn. For all of the preceding terms, the composition and texture of the protolith tend to control the composition and texture of the resulting skarn. In contrast, most economically important skarn deposits result from large scale metasomatic transfer,

where fluid composition controls the resulting skarn and ore mineralogy (Figure 1.2d).

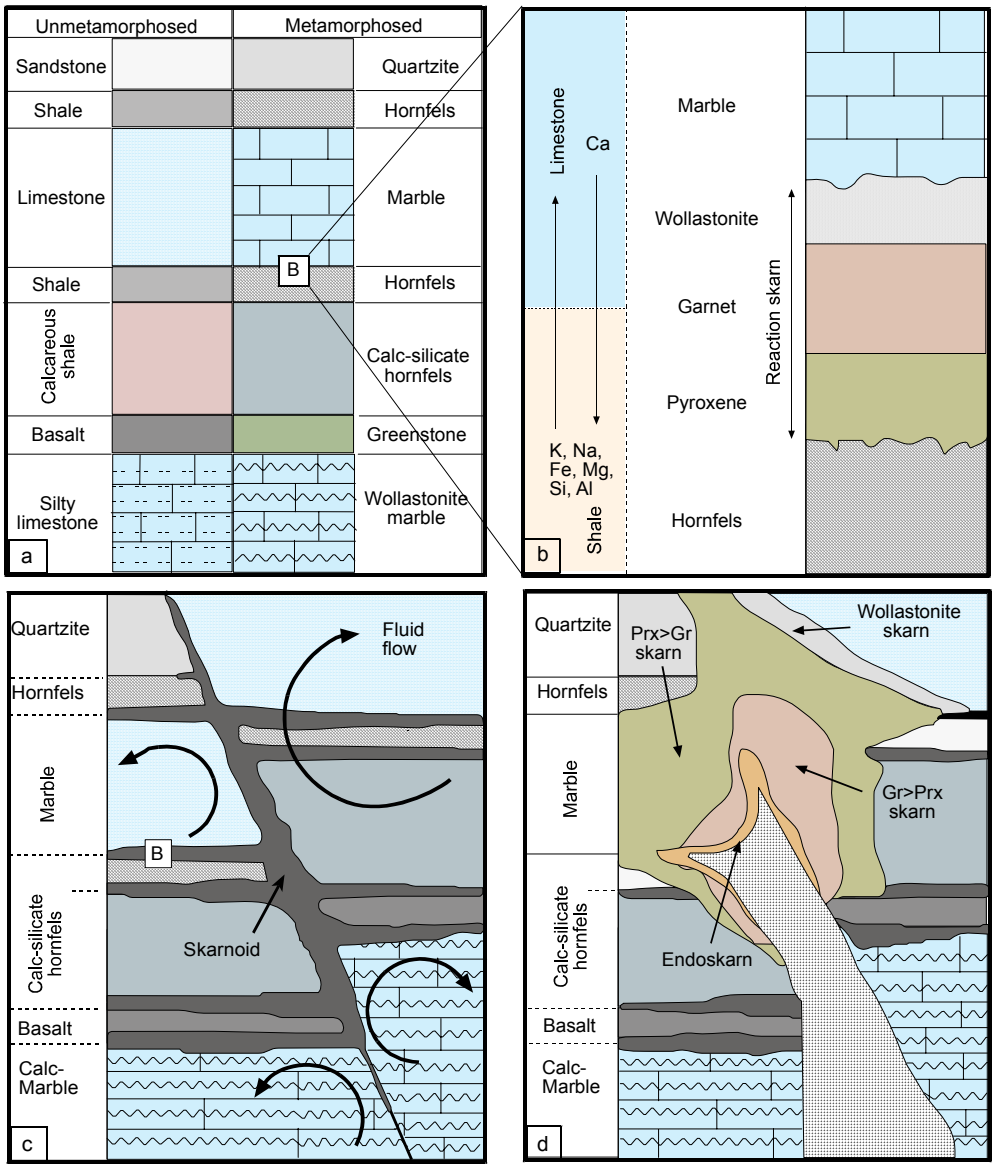

Figure 1.2. Types of skarn formation: (a) Isochemical metamorphism involves recrystallization and changes in mineral stability without significant mass transfer. (b) Reaction skarn results from metamorphism of interlayered lithologies, such as shale and limestone, with mass transfer between layers (bimetasomatism). (c) Skarnoid results from metamorphism of impure lithologies; some mass transfer by small scale fluid movement. (d) Metasomatic skarns; zonation of most skarns reflects the geometry of the pluton contact and fluid flow. Such skarns are zoned from proximal endoskarn to proximal exoskarn, domainated by garnet. (from http://www.wsu.edu:8080/~meinert/skarnHP.html).

1.2 Mineralogy of skarns

Mineralogy is the key to recognizing and defining skarns, it is also critical in understanding their origin and in distinguishing economically important deposits from interesting but uneconomic mineral localities. Skarn mineralogy is mappable in the field and serves as the broader "alteration envelope" around a potential ore body. Because most skarn deposits are zoned, recognition of distal alteration features can be critically important in the early exploration stages.

The mineralogy of the skarn depends on factors including the composition of both the intrusive and carbonate rocks; the structural or relative permeable nature of the host rocks; and the level of intrusion. The new minerals are typically coarse-grained crystals that grow over or replace the fine-grained or massive host rock of intrusion (endoskarn) and carbonate-rich rock (exoskarn). The calc-silicate minerals include garnet (calcium-rich grossularite and andradite to magnesium-rich pyrope), pyroxene (diopside to hedenbergite +/- johansennite), epidote, olivine (forsterite to fayalite), wollastonite, amphibole (actinolite-tremolite to hornblende) and scapolite. Table 1.1 lists many of the common skarn minerals and their end-member compositions.

Large amounts of compositional information can be summarized graphically. Triangular plots commonly are used to express variations in compositionally complex minerals such as garnet and pyroxene (Figure 1.3a and 1.3b).

Amphiboles are more difficult to portray graphically because they have structural as well as compositional variations. The main differences between amphiboles in different skarn types are variations in the amount of Fe, Mg, Mn, Ca, Al, Na, and K. Amphiboles from Au, W, and Sn skarns are progressively more aluminous (actinolite-hastingsite-hornblende), amphiboles from Cu, Mo, and Fe skarns are progressively more iron-rich in the tremolite-actinolite series, and amphiboles from zinc skarns are both Mn-rich and Ca-deficient, ranging from actinolite to dannemorite.

Table 1.1. Skarn mineralogy – common minerals, mineral groups, abbreviations and compositions.

Group End members	Abr.	Composition	Series
Garnet			
Grossularite	Gr	$Ca_3Al_2(SiO_4)_3$	Grandite
Andradite	Ad	$Ca_3Fe_2(SiO_4)_3$	
Spessartine	Sp	$Mn^3Al_2(SiO_4)_3$	
Almandine	Al	$Fe_3Al_2(SiO_4)_3$	Sub-calcic garnet
Pyrope	Py	$Mg_3Al_2(SiO_4)_3$	
Pyroxene			
Diopside	Di	$CaMgSi_2O_6$	Salite
Hedenbergite	Hd	$CaFeSi_2O_6$	
Johannsenite	Jo	$CaMnSi_2O_6$	
Fassaite	Fas	$Ca(Mg,Fe,Al)(Si,Al)_2O_6$	
Olivine			
Larnite	Ln	Ca_2SiO_4	Monticellite
Forsterite	Fo	Fe_2SiO_4	
Fayalite	Fa	Mg_2SiO_4	Knebelite
Tephrioite	Tp	Mn_2SiO_4	
Pyroxenoid			
Ferrosilite	Fs	$FeSiO_3$	Pyroxmangite
Rhodonite	Rd	$MnSiO_3$	
Wollastonite	Wo	$CaSiO_3$	Bustamite
Amphibole			
Tremolite	Tr	$Ca_2Mg_5Si_8O_{22}(OH)_2$	Actinolite
Ferroactinolite	Ft	$Ca_2Fe_5Si_8O_{22}(OH)_2$	
Manganese actinolite	Ma	$Ca_2Mn_5Si_8O_{22}(OH)_2$	
Hornblende	Hb	$Ca_2(Mg,Fe)_4Al_2Si_7O_{22}(OH)_2$	
Pargasite	Pg	$NaCa_2(Mg,Fe)_4Al_3Si_6O_{22}(OH)_2$	
Cummingtonite	Cm	$Mg_2(Mg,Fe)_5Si_8O_{22}(OH)_2$	
Dannemorite	Dm	$Mn_2(Fe,Mg)_5Si_8O_{22}(OH)_2$	Sub-calcic amphibole
Grunerite	Gru	$Fe_2(Fe,Mg)_5Si_8O_{22}(OH)_2$	

Table 1.1. Cont.

Group End members	Abr.	Composition	Series
Edipote			
Piemontite	Pm	$Ca_2(Mn,Fe,Al)_3(SiO_4)_3(OH)$	
Allanite	All	$(Ca,REE)_2(Fe,Al)_3(SiO_4)_3(OH)$	
Epidote	Ep	$Ca_2(Fe,Al)_3(SiO_4)_3(OH)$	
Clinozoisite	Cz	$Ca_2Al_3(SiO_4)_3(OH)$	
Plagioclase			
Anortite	An	$CaAl_2Si_2O8$	
Albite	Ab	$NaAlSi_3O8$	
Scapolite			
Marialite	Ml	$Na_4Al_3Si_9O_{24}(Cl,CO_3,OH,SO_4)$	
Meionite	Me	$Ca_4Al_3Si_6O_{24}(CO_3,Cl,OH,SO_4)$	
Other			
Axinite	Ax	$(Ca,Mn,Fe, Mg)_3Al_2BSi_4O_{15}(OH)$	
Vesuvianite (idocrase)	Vs	$Ca_{10}(Mg,Fe,Mn)_2Al_4Si_9O_{34}(OH,Cl,F)_4$	
Prehnite	Pr	$Ca_2Al_2Si_3O_{10}(OH)_2$	

1.3 Evolution of skarns in time and space

Formation of a skarn deposit is a dynamic process (e.g., Barrell, 1907; Goldschmidt, 1911; Knopf, 1918; Lindgren, 1902; Umpleby, 1913;). In most large skarn deposits there is a transition from early/distal metamorphism resulting in hornfels, reaction skarn, and skarnoid, to later/proximal metasomatism resulting in relatively coarse-grained ore-bearing skarn. One of the more fundamental controls on skarn size, geometry, and style of alteration is the depth of formation. The effect of depth on metamorphism is largely a function of the ambient wall rock temperature prior to, during, and post intrusion. The greater extent and intensity of metamorphism at depth can affect the permeability of host rocks and reduce the amount of carbonate available for reaction with metasomatic fluids. The depth of skarn formation also will affect the mechanical properties of the host rocks. In a deep skarn environment, rocks will tend to deform in a ductile manner rather than fracture. Intrusive contacts with sedimentary rocks at depth tend to be sub-parallel to bedding; either the pluton intrudes along bedding planes or the sedimentary rocks fold or flow until they are

aligned with the intrusive contact. Examples of skarns for which depth estimates exceed 5-10 km include Pine Creek, California (Brown, Bowman & Kelly, 1985) and Osgood Mountains, Nevada (Taylor, 1976). In deposits such as these, where intrusive contacts are sub-parallel to bedding planes, skarn is usually confined to a narrow, but vertically extensive, zone. At Pine Creek skarn is typically less than 10 m wide but locally exceeds one kilometre in length and vertical extent (Newberry, 1982).

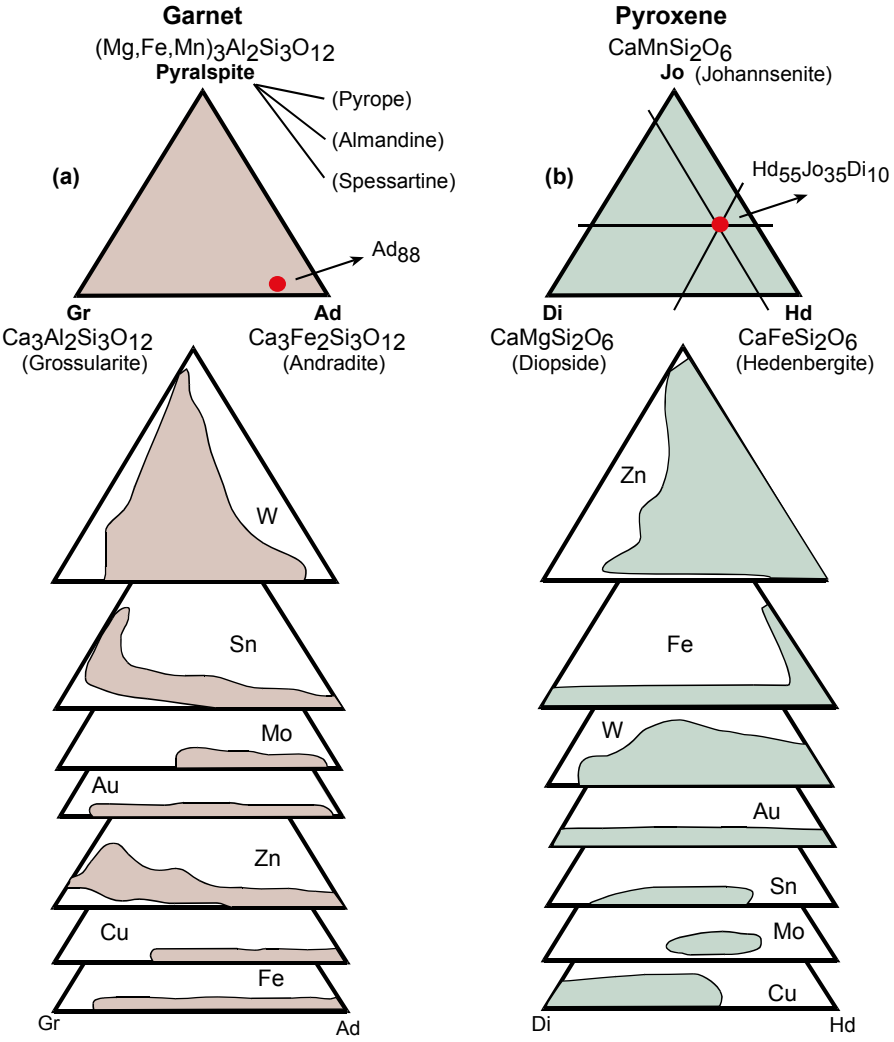

Figure 1.3. Ternary plots of (a) garnet and (b) pyroxene compositions from major skarn types. Data from Einaudi et al. (1981) and Meinert (1983, 1989).

Thus, skarn formed at greater depths can be seen as a narrow rind of small size relative to the associated pluton and its metamorphic aureole. In contrast, host rocks at

shallow depths will tend to deform by fracturing and faulting rather than folding. The strong hydrofracturing associated with shallow level intrusions greatly increases the permeability of the host rocks, not only for igneous-related metasomatic fluids, but also for later, possibly cooler, meteoric fluids (Shelton, 1983). The influx of meteoric water and the consequent destruction of skarn minerals during retrograde alteration is one of the distinctive features of skarn formation in a shallow environment.

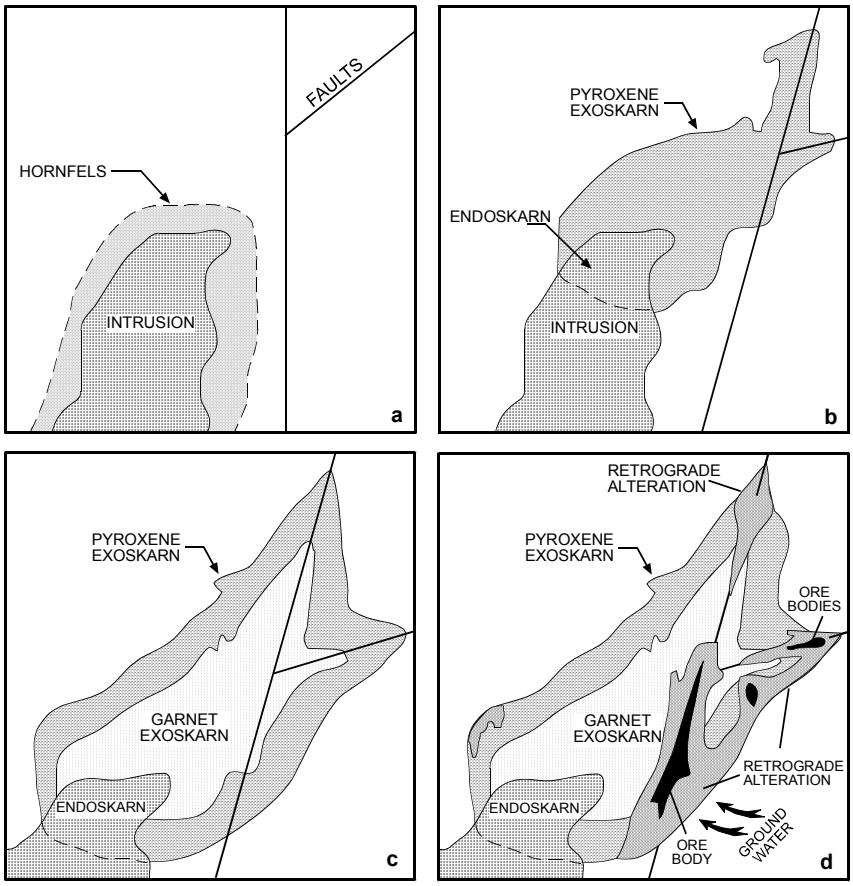

Figure 1.4. Schematic evolution of a calcic skarn deposit: (a) Intrusion of magma into carbonate-rich sequence and formation of contact hornfels, (b) Infiltration of hydrothermal fluids to produce endoskarn and pyroxene-rich exoskarn, (c) Continued infiltration with progressive expansion of exoskarn envelope and development of proximal garnet-rich exoskarn, (d) Hydrothermal system wanes and cools accompanied by retrograde overprinting. During this stage metals may be introduced or scavenged and redeposited to form economic orebodies. The structural/lithological controls and influence of meteoric water may result in irregularly distributed orebodies that are notoriously difficult to delineate in skarn (Ray & Webster, 1991a).

Skarn deposits are generally hosted within zones or halos of exoskarn alteration with morphologies that vary from stratiform, to vein-like, and sharply discordant. The amount of exoskarn developed ranges from narrow zones up to large envelopes that involved the generation of several cubic kilometers of skarn alteration. The associated mineralization is often volumetrically small compared to the total size of the skarn. Formation of the envelopes is an evolving, complex process, but the following paragenetic stages (Figure 1.4) are common to many infiltration calcic skarn: stage (1) Magmatic intrusion into relatively cool hostrocks leading to the production of an isochemical, contact metamorphic calcsilicate or biotite-rich hornfels (Figure 1.4a); stage (2) Infiltration of magmatic hydrothermal fluids into the surrounding country rocks, resulting in multiple stages of metasomatic garnet-pyroxene±amphibole prograde skarn assemblages (Figure 1.4b & c); stage (3) Retrograde alteration results in the formation of lower temperature hydrous phases such as chlorite, epidote, amphibole, ilvaite or, more rarely, scapolite (Figure 1.4d). Mineralization occurs either late in stage 2 or during the stage 3 retrograde alteration as temperatures decline (Figure 1.4d). Magnesian skarns often undergo similar evolutionary stages. Stages 1 and 2 in magnesian skarns typically result in the growth of olivine, spinel, phlogopite, pyroxene, pargasite and calcic plagioclase. In stage 3, retrograde alteration result in the formaiton of lower temperature hydrous phases such as serpentine, talc and amphibole.

1.4 Major skarn types

Groupings of skarn deposits can be based on descriptive features such as protolith composition, rock type, and dominant economic metal(s) as well as genetic features such as mechanism of fluid movement, temperature of formation, and extent of magmatic involvement. The general trend of modern authors is to adopt a descriptive skarn classification based upon the dominant economic metals and then to modify individual categories based upon compositional, tectonic, or genetic variations. This is similar to the classification of porphyry deposits into porphyry copper, porphyry molybdenum, and porphyry tin types; deposits which share many alteration and geochemical features but

are, nevertheless, easily distinguishable. Seven major skarn types (Au, Cu, Fe, Mo, Sn, W, and Zn-Pb) have received significant modern study and several others (including F, C, Ba, Pt, U, REE) are locally important. In addition, skarns can be mined for industrial minerals such as garnet and wollastonite.

1.4.1 Iron Skarns

Iron skarns are the largest skarn deposits and are mined for their magnetite content with minor uneconomic abundances of Cu, Co, Ni, and Au, although some are transitional to copper skarns. Major reviews of this deposit type include Einaudi et al. (1981), Sangster (1969) and Sokolov & Grigorev (1977). Calcic iron skarns in oceanic island arcs are associated with iron-rich diabase to diorite intrusives intruded into limestone. In some deposits, the amount of endoskarn may exceed exoskarn; whereas magnesian iron skarns are associated with a wide range of intrusives which have intruded into dolomitic wall rock and produce iron-free silicate skarn mineralogy.

1.4.2 Gold Skarns

Gold skarns are associated with diorite-granodiorite plutons and commonly contain sub-economic Cu, Pb and Zn. Proximal garnets are intermediate in composition, whereas distal pyroxenes are iron-rich. Potassium feldspar, scapolite, vesuvianite, apatite and Cl-rich amphiboles are common. Arsenopyrite and pyrrhotite are the dominant sulfide phases in many deposits, indicative of a reducing environment. Most gold occurs as electrum in close association with bismuth and telluride minerals. Gold skarns can form in distal portions of large skarns in which the proximal parts may form significant copper skarn deposits.

Although gold skarns had been mined since the late 1800s (Hedley district, British Columbia, Billingsley & Hume, 1941), there was so little published about them until recently that they were not included in the major world review of skarn deposits by Einaudi et al. (1981). In the past decade, multiple gold skarn discoveries have prompted new scientific studies and several overview papers, (Meinert, 1989;

Ray, Ettlinger & Meinert, 1990; Theodore, Orris, Hammarstrom & Bliss, 1991). The highest grade (5-15 g/t Au) gold skarn deposits (e.g. Hedley district, Ettlinger, 1990; Ettlinger, Meinert & Ray, 1992; Fortitude, Nevada, Myers & Meinert, 1991) are relatively reduced, are mined solely for their precious metal content, and lack economic concentrations of base metals. Other gold skarns (e.g. McCoy, Nevada, Brooks, Meinert, Kuyper, & Lane, 1991) are more oxidized, have lower gold grades (1-5 g/t Au), and contain subeconomic amounts of other metals such as Cu, Pb, and Zn. Several other skarn types, particularly Cu skarns, contain enough gold (0.01->1 g/t Au) for it to be a byproduct. A few skarn deposits, although having economic base metal grades, are being mined solely for their gold content (e.g. Veselyi mine, USSR, Ettlinger & Meinert, 1991).

The Fortitude deposit is part of a large zoned skarn system in which the proximal garnet-rich part was mined for copper (Theodore & Blake, 1978). Similarly, the Crown Jewel gold skarn in Washington is the pyroxene-rich distal portion of a large skarn system in which the proximal part is garnet-rich and was mined on a small scale for iron and copper (Hickey, 1990). Such zoned skarn systems suggest that other skarn types may have undiscovered precious metal potential if the entire skarn system has not been explored (e.g. Soler, Ayora, Cardellach & Delgado, 1990).

1.4.3 Tungsten Skarns

Major reviews of tungsten skarns include Kwak (1987), Newberry & Einaudi (1981), Newberry & Swanson (1986) and Newberry (1998). Tungsten skarns are associated with coarse grained calc-alkaline equigranular granodiorite to quartz-monzonite batholiths with related pegmatite and aplite dykes. The geology and mineralogy of tungsten skarns is indicative of a deep environment of formation associated with calc-alkaline intrusives, compared to the shallow environment proposed for copper and lead-zinc skarns. Plutons are typically fresh with only minor myrmekite and plagioclase-pyroxene endoskarn zones near contacts.

Newberry & Einaudi (1981) divides tungsten skarns into two types: reduced tungsten skarns formed in carbonaceous rocks or at greater depths, and are characterized by hedenbergitic pyroxene, magnetite, iron-rich biotite, trace native bismuth, and high pyrrhotite:pyrite ratios; locally they may also contain scapolite, vesuvianite and fluorite (Lowell, 1991). Oxidized tungsten skarns formed in either noncarbonaceous or hematitic rocks, or at shallower depths and have low pyrrhotite:pyrite ratios and their diagnostic minerals are salitic pyroxene, epidote and andraditic garnet.

1.4.4 Copper Skarns

Copper skarns are perhaps the worlds most abundant skarn type. They are particularly common in orogenic zones related to subduction, both in oceanic and continental settings. Most copper skarns are associated with I-type, magnetite series, calc-alkaline, porphyritic plutons, many of which have co-genetic volcanic rocks, stockwork veining, brittle fracturing and brecciation, and intense hydrothermal alteration. These are all features indicative of a relatively shallow environment of formation. Most copper skarns form in close proximity to stock contacts with a relatively oxidized skarn mineralogy dominated by andraditic garnet. Other phases include diopsidic pyroxene, idocrase, wollastonite, actinolite, and epidote. Hematite and magnetite are common in most deposits and the presence of dolomitic wall rocks is coincident with massive magnetite lodes which may be mined on a local scale for iron. As noted by Einaudi et al. (1981), copper skarns commonly are zoned with massive garnetite near the pluton and increasing pyroxene and finally idocrase and/or wollastonite near the marble contact. In general, pyrite and chalcopyrite are most abundant near the pluton with increasing chalcopyrite and finally bornite in wollastonite zones near the marble contact. The largest copper skarns are associated with mineralized porphyry copper plutons. The mineralized plutons exhibit characteristic potassium silicate and sericitic alteration which can be correlated with prograde garnet-pyroxene and retrograde epidote-actinolite, respectively, in the skarn. Intense retrograde alteration is common in copper skarns and in some porphyry-related deposits may destroy most of the prograde garnet and pyroxene (e.g. Ely, Nevada; James 1976).

Endoskarn alteration of mineralized plutons is rare. In contrast, barren stocks associated with copper skarns contain abundant epidote-actinolite- chlorite endoskarn and less intense retrograde alteration of skarn. Some copper deposits have coarse-grained actinolite-chalcopyrite-pyrite-magnetite ores but contain only sparse prograde garnet-pyroxene skarn (e.g. Monterrosas and Ral-Condestable deposits, Peru: Ripley & Ohmoto, 1977; Sidder 1984; Vidal, Injoque-Espinoza, Sidder, & Mukasa, 1990; Record mine, Oregon, Caffrey, 1982; Cerro de Mercado, Mexico, Lyons, 1988).

1.4.5 Zinc skarns

Most zinc skarns occur in continental settings associated with either subduction or rifting. They are mined for ores of zinc, lead, and silver although zinc is usually dominant. Related igneous rocks span a wide range of compositions from diorite through high-silica granite. They also span diverse geological environments from deep-seated batholiths to shallow dike-sill complexes to surface volcanic extrusions. Zinc skarns occur distal to associated intrusives, commonly grading outward from skarn-rich to skarn-poor zones, and in places skarn mineralogy may be almost totally absent. Almost all mineralogy in Zn-Pb skarns is enriched in manganese, with the pyroxene:garnet ratio and manganese content of pyroxenes increasing away from the intrusives. These skarns are therefore closely related to the carbonate-base metal gold vein systems (Corbett & Leach, 1998). Since Zn-Pb skarns occur in distal portions of major magmatic hydrothermal systems, vectors derived from mapping of alteration zones can lead to significant copper-gold skarns in the proximal parts of these systems.

1.4.6 Molybdenum skarns

Most molybdenum skarns are associated with leucocratic granites and range from high grade, relatively small deposits (Azegour, Morocco, Permingeat, 1957) to low grade, bulk tonnage deposits (Little Boulder Creek, Idaho, Cavanaugh, 1978). Most molybdenum skarns contain economic amounts of W, Cu with minor Zn, Pb, Bi, Sn and U, and commonly forming polymetallic deposits. Most molybdenum skarns occur in silty carbonate or calcareous clastic rocks. Fe-pyroxene dominates with

minor garnet, wollastonite, amphibole and fluorite. This skarn mineralogy indicates a reducing environment with high fluorine activities.

1.4.7 Tin skarns

Tin skarns are associated with high-silica granites generated by crustal melting within a continental rifting environments. Major reviews of tin skarn deposits include Einaudi et al. (1981) and Kwak (1987). Greisen alteration stage is commonly superimposed on early skarn, intrusive and carbonate sediments, and is characterised by high fluorine activities and by minerals such as fluorite, topaz, tourmaline, muscovite, ilmenite and abundant quartz (Corbett & Leach, 1998).

1.5 Zonation of skarn deposits

In most skarns there is a general zonation pattern of proximal garnet, distal pyroxene, and idocrase (or a pyroxenoid such as wollastonite, bustamite, or rhodonite) at the contact between skarn and marble. In addition, individual skarn minerals may display systematic color or compositional variations within the larger zonation pattern. For example, proximal garnet is commonly dark red-brown, becoming lighter brown and finally pale green near the marble front (e.g., Atkinson & Einaudi, 1978). The change in pyroxene color is less pronounced but typically reflects a progressive increase in iron and/or manganese towards the marble front (e.g., Harris & Einaudi, 1982). For some skarn systems, these zonation patterns can be "stretched out" over a distance of several kilometres and can provide a significant exploration guide (e.g., Meinert, 1987). Details of skarn mineralogy and zonation can be used to construct deposit-specific exploration models as well as more general models useful in developing grass roots exploration programs or regional syntheses. Reasonably detailed zonation models are available for copper (Figure 1.5a), gold (Figure 1.5b) , and zinc skarns (Figure 1.5c) (Meinert, 1997). Other models can be constructed from individual deposits which have been well studied such as the Hedley Au skarn (Figure 1.5d) (Ettlinger, 1992; Ray, Webster, Dawson, & Ettlinger, 1993) or the Groundhog Zn skarn (Meinert, 1982).

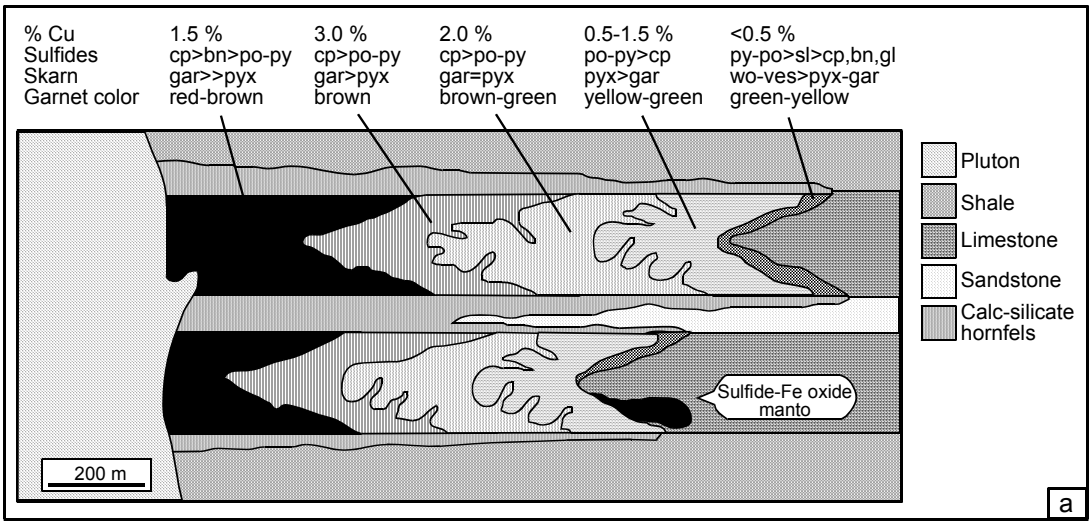

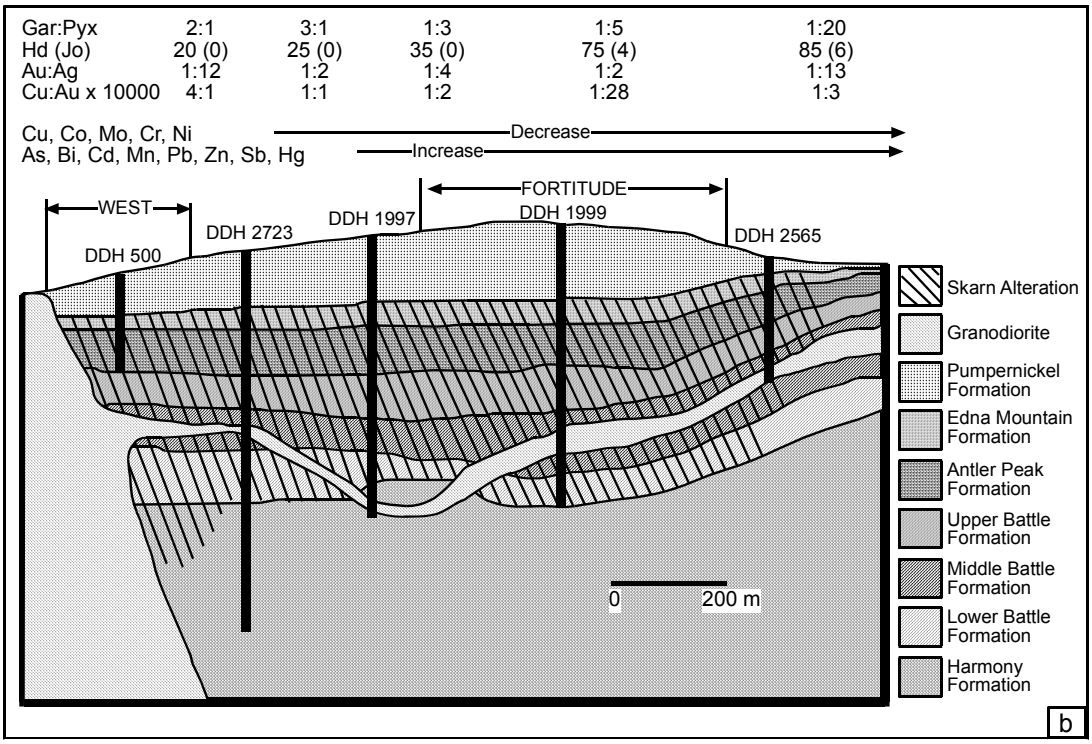

Figure 1.5. General models of skarn zonation: (a) copper skarns (after Atkinson and Einaudi, 1978); (b) gold skarns, cross section of the Fortitude deposit, Nevada (Myers & Meinert, 1991).

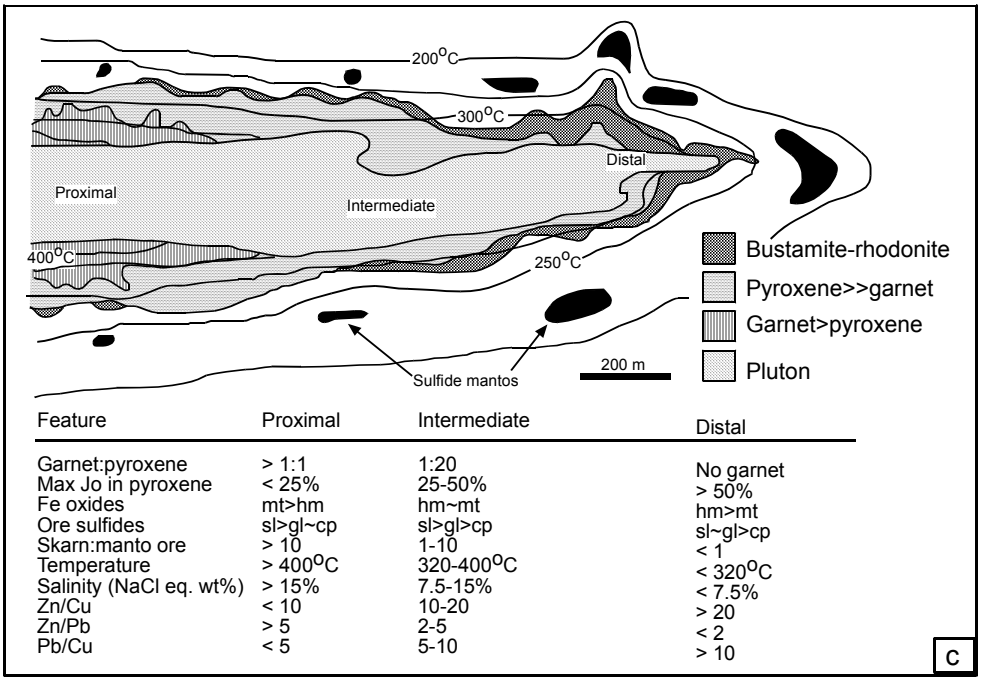

Feature	Proximal	Intermediate	Distal
Garnet:pyroxene	> 1:1	1:20	No garnet
Max Jo in pyroxene	< 25%	25-50%	> 50%
Fe oxides	mt>hm	hm~mt	hm>mt
Ore sulfides	sl>gl~cp	sl>gl>cp	sl~gl>cp
Skarn:manto ore	> 10	1-10	< 1
Temperature	> 400°C	320-400°C	< 320°C
Salinity (NaCl eq. wt%)	> 15%	7.5-15%	< 7.5%
Zn/Cu	< 10	10-20	> 20
Zn/Pb	> 5	2-5	< 2
Pb/Cu	< 5	5-10	> 10

c

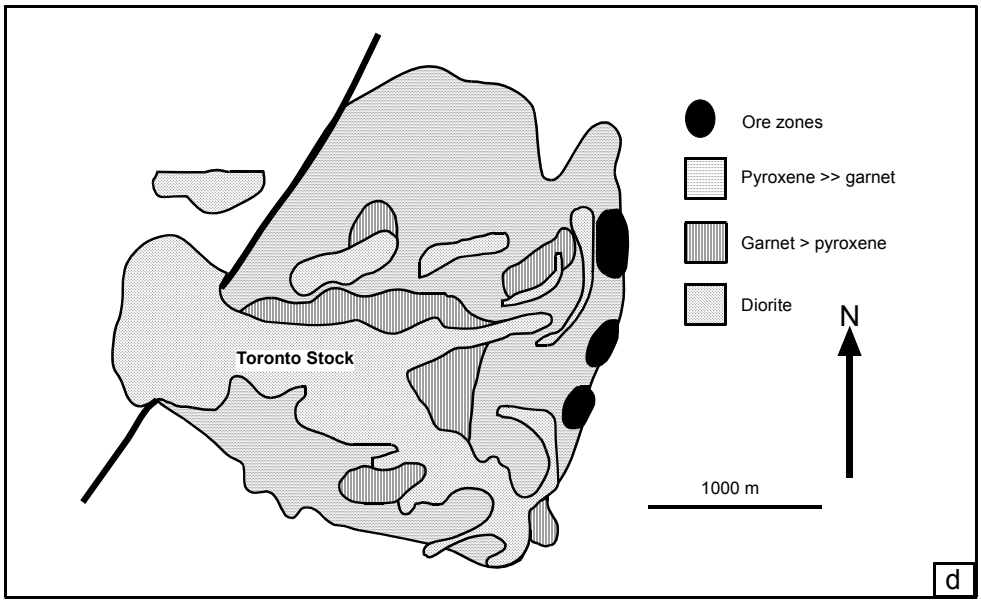

d

Figure 1.5. (Cont.) (c) zinc skarns (after Meinert, 1987); and (d) gold skarns, Hedley district, British Columbia (after Ray & Webster, 1991a).

1.6 Geochemistry of skarn deposits

Most geochemical studies of skarn deposits have focused on mineral phase equilibria, fluid inclusions, isotopic investigations of fluid sources and pathways, and determination of exploration anomaly and background levels. Experimental phase

equilibria studies are essential for understanding individual mineral reactions. Fractionation of elements between minerals (e.g. Ca:Mg in carbonate, Bowman & Essene, 1982; Bowman, Covert, Clark, & Mathieson, 1985) can be used to estimate conditions of skarn formation. A general review of phase equilibria applicable to skarn systems is presented by Bowman (1998). A more specialized treatment of the vector representation of skarn mineral stabilities is presented by Burt (1998). Recent work has incorporated standard phase equilbria treatment of skarn mineralogy along with fluid dynamics to model of the metasomatic evolution of skarn systems (Dipple and Gerdes, 1998).

Fluid inclusion studies of many ore deposit types focus on minerals such as quartz, carbonate, and fluorite which contain numerous fluid inclusions, are relatively transparent, and are stable over a broad T-P-X range. However, this broad T-P-X range can cause problems in interpretation of fluid inclusion data, because these minerals may grow and continue to trap fluids from early high temperature events through late low temperature events (Roedder, 1984). In contrast, high temperature skarn minerals such as forsterite, diopside, etc. are unlikely to trap later low temperature fluids (beyond the host mineral's stability range) without visible evidence of alteration. Thus, fluid inclusions in skarn minerals provide a relatively unambiguous opportunity to measure temperature, pressure, and composition of skarn-forming fluids. All the skarn types summarized in Meinert (1992) have fluid inclusion homogenization temperatures up to and exceeding 700^{o}C except for copper and zinc skarns, deposits in which most fluid inclusions are in the 300-550^{o}C range. This is consistent with the relatively shallow and distal geologic settings inferred respectively for these two skarn types.

Salinities in most skarn fluid inclusions are high; documented daughter minerals in skarn minerals include NaCl, KCl, $CaCl_2$, $FeCl_2$, $CaCO_3$, CaF_2, C, $NaAlCO_3(OH)_2$, Fe_2O_3, Fe_3O_4, AsFeS, $CuFeS_2$, and ZnS. Haynes & Kesler (1988) describe systematic variations in NaCl:KCl:$CaCl_2$ ratios in fluid inclusions from different skarns reflecting differences in the fluid source and the degree of mixing of magmatic, connate, and meteoric fluids. In general, magmatic fluids have

$KCl>CaCl_2$ whereas high-$CaCl_2$ fluids appear to have interacted more with sedimentary wall rocks.

Studies of fluid inclusions in specific skarn mineral phases are particularly useful in documenting the temporal and spatial evolution of skarn-forming fluids and how those changes correlate with compositional, experimental, and thermodynamic data (e.g. Kwak & Tan, 1981; Meinert, 1987). Fluid inclusions also provide direct evidence for the temperature and salinity shift in most skarn systems between prograde and retrograde skarn events. For example, most garnet and pyroxene fluid inclusions in iron skarns have homogenization temperatures of 370-700^{o}C and 300-690^{o}C, respectively, with salinities up to 50 wt. % NaCl equivalent, whereas retrograde epidote and crosscutting quartz veins have homogenization temperatures of 245-250^{o}C and 100-250^{o}C, respectively, with salinities of less than 25 wt. % NaCl equivalent.

Isotopic investigations, particularly the stable isotopes of C, O, H, and S, have been critically important in documenting the multiple fluids present in most large skarn systems (Bowman, 1998; Shimazaki, 1988). The pioneering study of Taylor & O'Neil (1977) demonstrated the importance of both magmatic and meteoric waters in the evolution of the Osgood Mountain W skarns. Bowman et al. (1985) demonstrated that in high temperature W skarns, even some of the hydrous minerals such as biotite and amphibole can form at relatively high temperatures from water with a significant magmatic component (see also Marcke de Lummen, 1988).

Specifically, garnet, pyroxene, and associated quartz from the skarn deposits summarized in Meinert (1992) all have $\delta^{18}O$ values in the +4 to +9 range consistent with derivation from magmatic waters. In contrast, $\delta^{18}O$ values for sedimentary calcite, quartz, and meteoric waters in these deposits are distinctly different. In most cases, there is a continuous mixing line between original sedimentary $\delta^{18}O$ values and calculated $\delta^{18}O$ values for magmatic hydrothermal fluids at the temperatures of prograde skarn formation. Similar mixing is indicated by $\delta^{13}C$ values in calcite, ranging from typical sedimentary $\delta^{13}C$ values in limestone away from skarn to

typical magmatic values in calcite interstitial to prograde garnet and pyroxene (Brown et al., 1985). Hydrous minerals such as biotite, amphibole, and epidote from different skarn deposits also display $\delta^{18}O$ and δD values ranging from magmatic to local sedimentary rocks and meteoric waters (Layne, Longstaffe & Spooner, 1991). Again, mixing of multiple fluid sources is indicated.

Overall, stable isotopic investigations are consistent with fluid inclusion and mineral equilibria studies which demonstrate that most large skarn deposits form from diverse fluids, including early, high temperature, highly saline brines directly related to crystallizing magma systems (e.g. Auwera & Andre, 1988). In many systems, the highest salinity fluids are coincident with sulfide deposition. In addition, at least partial mixing with exchanged connate or meteoric fluids is required for most deposits with the latest alteration events forming largely from dilute meteoric waters.

1.7 Petrogenesis and tectonic settings of skarn deposits

Most major skarn deposits are directly related to igneous activity and broad correlations between igneous composition and skarn type have been described by several workers (Einaudi et al., 1981; Kwak & White, 1982; Meinert, 1983; Newberry and Swanson, 1986; Newberry, 1987; Shimazaki, 1980; Zharikov, 1970). Averages of large amounts of data for each skarn type can be summarized on a variety of compositional diagrams to show distinctions among skarn classes. Tin and molydenum skarns typically are associated with high silica, strongly differentiated plutons. At the other end of the spectrum, iron skarns usually are associated with low silica, iron-rich, relatively primitive plutons.

Other important characteristics include the oxidation state, size, texture, depth of emplacement, and tectonic setting of individual plutons. For example, tin skarns are almost exclusively associated with reduced, ilmenite-series plutons which can be characterized as S-type or anorogenic. Many gold skarns are also associated with reduced, ilmenite-series plutons. However, gold skarn plutons typically are mafic, low-silica bodies which could not have formed by melting of sedimentary crustal material. In contrast, plutons associated with copper skarns, particularly porphyry

copper deposits, are strongly oxidized, magnetite-bearing, I-type and associated with subduction-related magmatic arcs. These plutons tend to be porphyritic and emplaced at shallow levels in the earth's crust. Tungsten skarns, on the other hand, are associated with relatively large, coarse-grained, equigranular plutons or batholithic complexes indicative of a deeper environment.

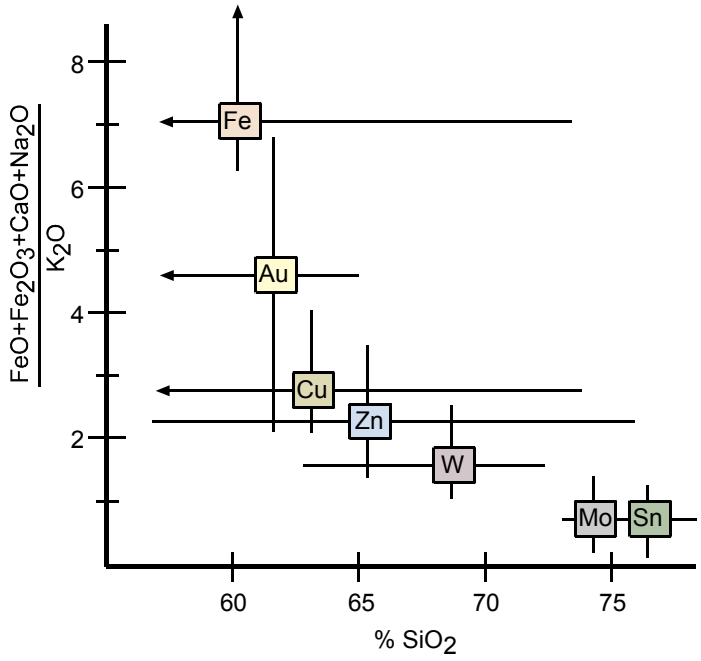

Figure 1.6. Average composition of plutons associated with different skarn types (Meinert, 1993).

Skarn deposits are encountered throughout a broad range of geological environments, however the different type of skarn deposits based on metal contents have been related to specific compositions of intrusives and tectonic settings (Figures 1.6 & 1.7) (Meinert, 1993). Fe skarns are associated with low-silica iron-rich primitive diabase to diorite plutons found in oceanic island-arc terranes. Au skarn plutons are typically mafic, low silica diorites, in places emplaced in back arc basins associated with island volcanic arcs (Ray, Dawson, & Simpson, 1988). Cu and Pb-Zn skarns are associated with calc-alkaline porphyries emplaced at shallow levels within magmatic arcs related to subduction beneath contenental crust; whereas W skarns form at deep levels in this same environment associated with large calc-alkaline granodiorite to monzonite batholiths. Mo skarns are typically associated with granitic intrusives

possibly associated with late stage subduction beneath stable continental crust. Sn skarns formed adjacent to high silica, strongly differentiated granite bodies associated with continental rifting and related crustal melting.

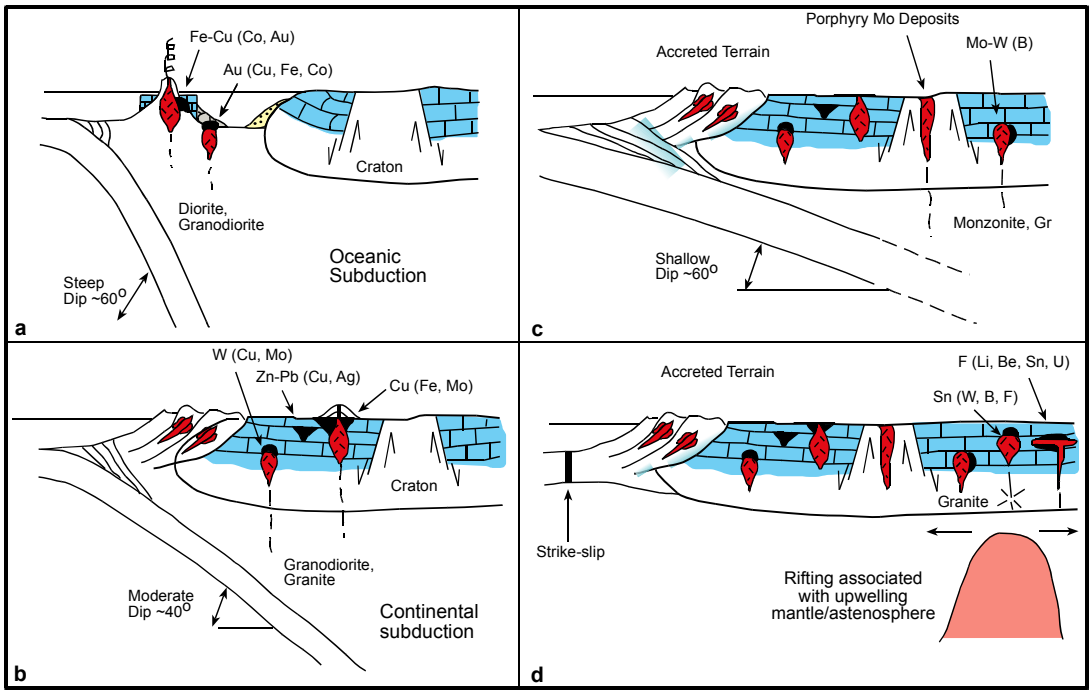

Figure 1.7. Tectonic models for skarn formation: (a) oceanic subduction and back-arc basin environment; (b) continental subduction environment with accreted oceanic terrane; (c) transitional low-angle subduction environment, and (d) post-subduction or continental rifting environment (modified from Meinert, 1983).

1.8. Skarn occurences in Western Turkey

Western Turkey includes several different types of mineral deposits such as epithermal, porphyry and skarn, related to the complicate tectonic and magmatic history of the region. This region has been well explored based mainly on geochemical prospecting, whereas detailed ore deposit studies, using modern analytical techniques, are relatively limited.

The field surveys and subsequent analytical works identify several different deposit types in western Turkey as follows.

- *Listwaenite Au:* Donbaycılar, Kaymaz
- *Skarn Fe:* Samulı, Atizi, Ayazmant, Kazmuttepe, Handeresi, Yaşyer, Kızılkesili, Demirlitepe
- *Hydrothermal replacement deposits;* Balya (Balıkesir) Pb-Zn, Efemçukuru (Menderes) Au, Çulfaçukuru (Havran) Au. This type of deposits grade into skarn-type mineralization (Jankoviç, 1997)
- *Porphyry Cu-Mo:* Tepeoba, Kışladağ, Muratdere, Domaniç, Tüfekçikonağı, Karacaali, Akkayaduzu, Sarıçayıryayla
- *Carbonate-hosted Au*: Söğüt, Beyköy, Bileylikyayla
- *Epithermal Au-Sb related to calc-alkaline volcanics:* Ovacık, İvrindi, Küçükdere, Kubaşlar, Madendağ, Kartaldağ, Terziali, Dereharman, Sebepli, Kırantepe, Sahinli
- *Xenothermal Pb-Zn:* Arapuçandere
- *Shear zone-hosted Pb-Zn-Ba:* Korudere, Yalakkayor, Papazlık
- *Stratiform Fe:* Eymir, Kuşçayırı

Skarn bodies occur in two major post-collisional magmatic activity of western Anatolia (Figure 1.8): (1) skarn type deposits associated with calc-alkaline plutons; Ayazmant (Ayvalık) Fe, Agonia district (Yenice), W-Mo, Cu, Zn and Fe, Atizi (Havran) Fe-Cu-W, Şamlı (Balıkesir) Fe-Cu, Demir Tepe, Tahtaköprü (Bursa) wollastonite-garnet skarn; (2) skarn-type deposits associated with alkaline intrusions; Kadıkalesi (Bodrum) Pb-Zn-Cu, Girelbelen skarn (Bodrum), Maden Adası (Ayvalık) Pb-Cu-Zn. During the last decades, many papers have been published on the skarns of western Anatolia.

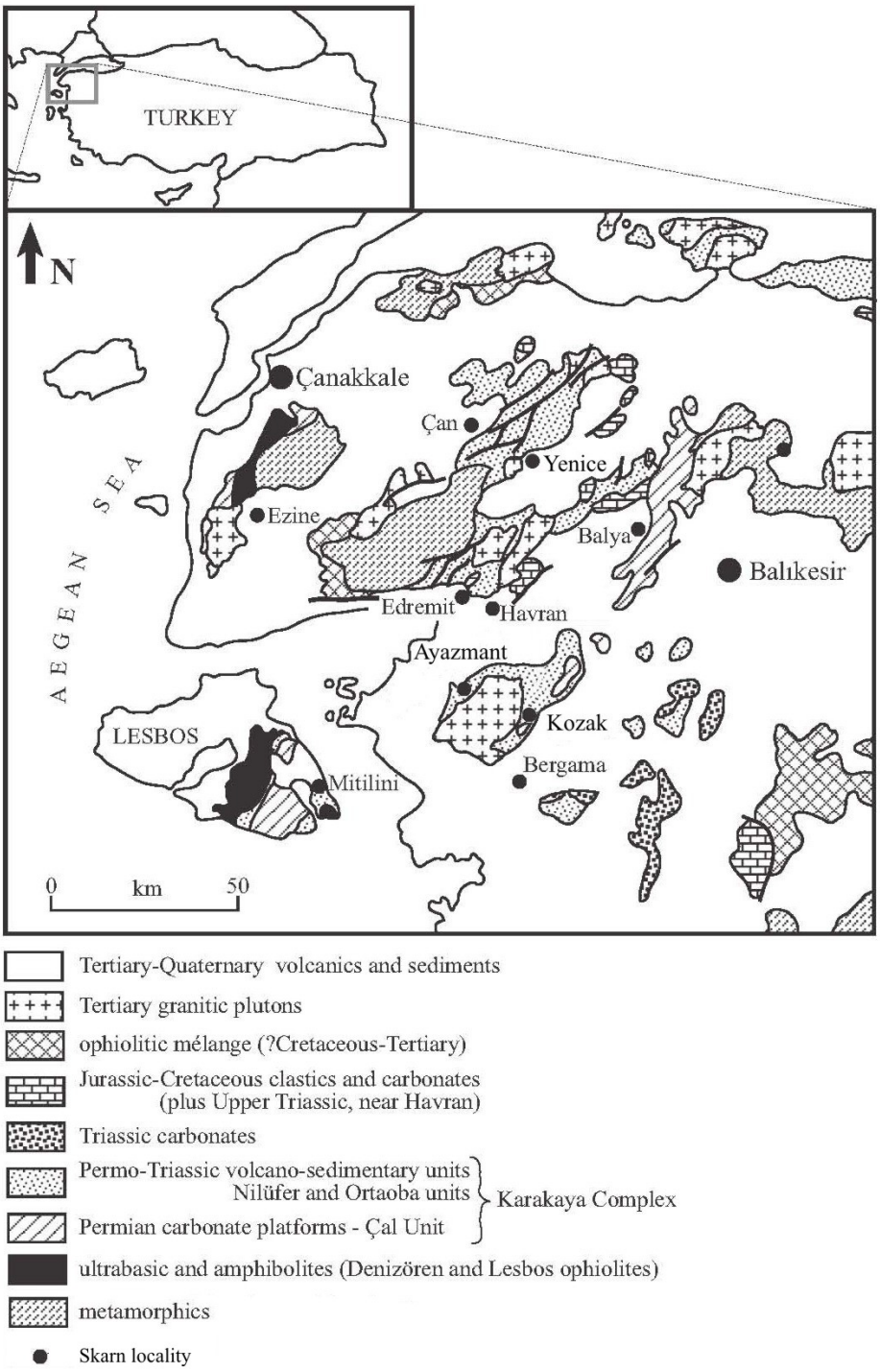

Figure 1.8. Simplified geological map of the Northwestern Anatolia, showing the skarn localities (modified from Pickett & Robertson, 2004).

Ayazmant (Ayvalık) Fe skarn is located on the SW contact of Kozak Magmatic Complex (KMC). It contains 5.8 million metric tons with a grade of 46 % Fe (Oyman, Pişkin, Özgenç, Akbulut & Minareci, 2005). KMC is a typical example of

the calc-alkaline volcanic products of a compressional tectonic regime which active between Paleogene-Middle Miocene in Western Anatolia. Granitic-granodioritic pluton and associated microdioritic and microgranodioritic dykes of KMC which crosscut the Triassic metamorphic basement gave rise to occur iron skarn formations. Contact metamorphism is identical with a well-developed calcium-silicate paragenesis and it is composed of widespread endoskarn and exoskarn formations. Exoskarn is represented mainly by pyroxene, garnet and amphibole group minerals. Retrograde stage is characteristic with K-feldspar, epidote, chlorite, tremolite-actinolite, calcite and quartz (Oyman et al., 2005). Magnetite, chalcopyrite-cubanite, valleriite, pyrrothite, molybdenite, pyrite, graphite and ilmenite are the products of early mineralization event. Galena, sphelarite, chalcopyrite, pyrite, bornite and idaite which were precipitated in veinlets (a few cm.) are products of hydrothermal stage (Oyman et al., 2005).

Agonia district (Çanakkale) contains more than 10 small occurrences of skarns. Most of them involve subeconomic contact metasomatic mineralization of W, Mo, Fe, Cu, Pb and Zn (Özgenç, Dayal & Oyman, 2000). Skarn related pollymetallic mineralization are coused by young magmatism which is a subset of the gological evolution of Biga Peninsula and consists of calc-alkalen plutonic and co-genetic volcanic rocks. The skarns occur within the thermal aureoles of the granodioritic to quartz monzonitic stocks which were emplaced into the epimetamorphic rocks (pelitic schists, feldspathic metasandstone, metabasic lavas). The skarns in the district display exoskarn properties. In general skarn evolution can be divided into the prograde development of anhydrous minerals (dominantly garnet and pyroxene) which occur in calc-silicate hornfels (Madenburnu, W skarn) and in marbles (Ayvacıkbaşı, Kireçlitepe, Cu skarns; Sameteli, Umurlar, Zn skarns; Engecetepe, Fe skarns) and retrograde development of hydrous minerals (epidote, amphibole, chlorite with quartz and carbonate assemblages).

Şamlı Fe-Cu deposits is located in the Balikesir Province in Western Turkey. The Şamlı granodiorite and related porphyry dikes irregularly intruded into the Triassic age Karakaya formation, which comprises various rock types such as siltstones and

graywackes, clastic calcareous sedimentary rocks, meta-basic rock (spilite) and subordinate limestone. The Karakaya formation was partly affected by contact metamorphism. The hornfelses are replaced by the skarn and ore minerals. While the main pluton is mostly granodiorite to quartz diorite in composition, Fe-Cu ore mineralisation is related to porphyr dikes in quartz diorite composition (Çolakoğlu, Murakami & Arıkal, 2004). Skarn occurrence is marked by the following zones in order of proximity to the intrusive contact: (1) massive garnet zone, with garnet and minor amounts of pyroxene. Massive garnet skarn occurs along both sides of the magnetite ore bodies; (2) pyroxene zone, which contains clinopyroxene and garnet.

Magnetite ore bodies are found within the contact metamorphic aureole including small pods of sulfide ore comprising in minor amount as; chalcopyrite, pyrite and pyrrhotite, bornite, galena, sphalerite, bismuth, bismuthinite, cobaltite, muschketowite, linnaeite, polybasite and gold. With supergene alteration, chalcopyrite and bornite were replaced by digenite, covellite-chalcocite, cuprite, malachite, azurite and native copper. Magnetite is martitized and altered to goethite(Çolakoğlu et al., 2004).

Located in NW Anatolia, near the village of Tahtaköprü (Bursa), the skarns of Demir Tepe, belong to the province of wollastonite skarns that streches to Çan and Çanakkale 200 km westwards (Öngen, 1992). Wollastonite-garnet skarns of Demir Tepe (Bursa) are developed in graphitic marbles, forming roof-pendants in the granodioritic Tertiary pluton of Göynükbelen, at the contact of stocks and veins of diorite-monzodiorites that intrude the main pluton (Demange et al., 1998). Skarn formation includes several superimposed stages as follows; (1) main stage: diopside-andesine and anorthite-diopside-grossular rich garnet (or anorthite-diopside-wollastonite) endoskarns and exoskarns made of massive wollastonite; (2) anorthite-diopside-andradite rich garnet veins; (3) scapolitisation; (4) development of massive garnet; (5) several late stages including copper mineralisation, alteration into zeolites.

1.9. References

Atkinson, W.W., & Einaudi, M.T., (1978). Skarn formation and mineralization in the contact aureole at Carr Fork, Bingham, Utah. *Economic Geology*, *73*, 1326-1365.

Auwera, J.V., & Andre, L., (1988). O, C and Sr isotopes as tracers of metasomatic fluids: application to the skarn deposit (Fe, Cu, W) of Traversella (Ivrea, Italy). *Chemical Geology*, *70*, 137.

Barrell, J. (1907). Geology of the Marysville mining district, Montana. *United States Geological Survey, Professional Paper*, *57*, 178p.

Billingsley, P., & Hume, C.B., (1941). The ore deposits of Nickel Plate Mountain, Hedley B.C. *Canadian Institute of Mining and Metallurgy Bulletin*, *44*, 524-590.

Bowman, J.R., & Essene, E.J., (1982). P-T-XCO_2 conditions of contact metamorphism in the Black Butte aureole, Elkhorn, Montana. *American Journal of Science*, *282*, 311-340.

Bowman, J.R., Covert, J.J., Clark, A.H., & Mathieson, G.A., (1985). The Can Tung E-zone scheelite skarn ore body, Tungsten, Northwest Territories: oxygen, hydrogen and carbon isotope studies. *Economic Geology*, *80*, 1872-1895.

Bowman, J.R. (1998). Stable-isotope systematics of skarns. *Mineralogical Association of Canada Short Course*, *26*, 99-145.

Brooks, J.W., Meinert, L.D., Kuyper, B.A., & Lane, M.L., (1991). Petrology and geochemisrty of the McCoy gold skarn, Lander County, N.V., *in* Raines, G.L., Lisle, R.E., Schafer, R.W., & Wilkinson, W.H., eds. Geology and Ore Deposits of the Great Basin; *Geological Society of Nevada, Reno*, *1*, 419-442.

Brown, P.E., Bowman, J.R., & Kelly, W.C., (1985). Petrologic and stable isotope constraints on the source and evolution of skarn-forming fluids at Pine Creek, California. *Economic Geology, 80*, 72-95.

Burt, D.M. (1998). Vector treatment of the compositions of some skarn minerals. *Mineralogical Association of Canada Short Course*, *26*, 51-70.

Caffrey, G.M. (1982). Petrology and alteration of ultramafic rocks of Bullrun Mountain, Baker County, Oregon. *Unpublished M.Sc. thesis, Washington State University*, 130p.

Cavanaugh, P.C. (1978). Geology of the Little Boulder Creek molybdenum deposit, Custer County, Idaho. *Unpublished M.Sc. thesis, University of Montana*, 82p.

Corbett, G.J., & Leach, T.M., (1998). Southwest Pacific Rim gold-copper systems: structure, alteration, and mineralization: *Society of Economic Geologists Special Publication*, *6*, 237 p.

Çolakoğlu, A.R., Murakami H., & Arikal T., (2004). Geology of the Şamlı Fe-Cu skarn deposit (Western Turkey). *5th International Symposium on Eastern Mediterranean Geology Thessaloniki, Greece*, *14-20 April 2004,* 1595-1596.

Demange, M., Berson, F., Fonteilles, M., Pascal, M.L., Öngen, S., & Forette, M.C., (1998). Wollastonite-garnet skarns of Demir Tepe, Tahtaköprü (province of Bursa, Turkey). *Academie des Sciences Paris, Sciences de la terre et des planètes/Earth & Planetary Sciences*, *326*, 771-778.

Dipple, G.M., & Gerdes, M.L., (1998). Reaction-infiltration feedback and hydrodynamics at the skarn front. *Mineralogical Association of Canada Short Course*, *26*, 71-98.

Einaudi, M.T., Meinert, L.D., & Newbery, R.J. (1981). Skarn deposits: *Economic Geology. 75th Anniversary Volume, Economic Geology Publication Co., Lencester Pres Inc.,* 317-391.

Ettlinger, A.D. (1990). A geological analysis of gold skarns and precious metals enriched iron and copper skarns in British Columbia, Canada. *Unpublished Ph.D. thesis, Washington State University*, 246p.

Ettlinger, A.D., & Meinert, L.D., (1991). Copper-gold skarn mineralization at the Veselyi Mine, Sinuikhinskoe district, Siberia, U.S.S.R. *Economic Geology*, *86*, 185-194.

Ettlinger, A.D., Meinert, L.D., & Ray, G.E., (1992). Gold skarn mineralization and evolution fluid in the Nickel Plate deposit, Hedley district, British Columbia. *Ecoomic Geology*, *87*, 1541-1565.

Goldschmidt, V.M. (1911). Die kontaktmetamorphose im Kristianiagebiet, Oslo Vidensk. Skr., I., *Mat.-Natur*, K1, 1, 483p.

Harris N.B., & Einaudi, M.T., (1982). Skarn deposits in the Yerington district, Nevada: Metasomatic skarn evolution near Ludwig. *Economic Geology*, *77*, 877-898.

Haynes, F.M., & Kesler, S.E., (1988). Compositions and sources of mineralizing fluid for chimney and manto limestone-replacement ores in Mexico. *Economic Geology*, *83*, 1985-1992.

Hickey, R.J., (1990). The geology of the Buckhorn mountain gold skarn, Okanagon County, Washington. *Unpublished M.Sc. thesis, Washington State University*, 171p.

James, L.P. (1976). Zoned alteration in limestone at porphyry copper deposits, Ely, Nevada. *Economic Geology*, *71*, 488-512.

Jankoviç, S. (1997). Lead-zinc deposits in the Serbo-Macedonian-Anatolian metallogenic province: types and distribution pattern. In: Pişkin, Ö., Ergün, M., Savaşcın, M.Y., Tarcen, G. (Eds.), *International Earth Sciences Colloquium On The Aegean Region, Proceedings, vol. II. Dokuz Eylül University, İzmir*, 535-548.

Japan-Turkey Project. Study on Hydrothermal Deposits and Metallogeny of Western Turkey. Between the Institute for Geo-Resources and Environment, AIST and Mineral Research and Exploration Department, General Directorate of Mineral Research and Exploration of Turkey from 2001 to 2004, 4p.

Knopf, A. (1918). Geology and ore deposits of the Yerington district, NV. *United States Geological Survey, Professional Paper*, *114*, 68p.

Kwak, T.A.P., & Tan, T.H., (1981). The geochemistry of zoning in skarn minerals at the King Island Dolphin mine. *Economic Geology*, *76*, 468-497.

Kwak, T.A.P., & White, A.J.R., (1982). Contrasting W-Mo-Cu and W-Sn-F skarn types and related granitoids. *Mining Geology*, *32*, 339-351.

Kwak, T.A.P. (1987). W-Sn skarn deposits and related metamorphic skarns and granitoids. *In Developments in Economic Geology, 24, Elsevier Publishing Company*, 445p.

Layne, G.D., Longstaffe, F.J., & Spooner, E.T.C., (1991). The JC tin skarn deposit, southern Yukon Territory: II. A carbon, oxygen, hydrogen and sulfur stable isotope study. *Economic Geology*, *86*, 48-65.

Lindgren, W. (1902). The character and genesis of certain contact deposits. *American Institute of Mining Engineers, Transactions*, *31*, 226-244.

Lowell, G.R. (1991). Tungsten-bearing scapolite-vesuvianite skarns from the upper Salcha River area, east-central Alaska. In Skarns-Their Genesis and Metallogeny. *Theophrastus Publications, Athens, Greece*, 384-418.

Lyons, J.I. (1988). Volcanogenic iron oxide deposits, Cerro de Mercado and Vicinity, Durango, Mexico. *Economic Geology*, *83*, 1886-1906.

Marcke de Lummen, G. van (1988). Oxygen and hydrogen isotope evidence for influx of magmatic water in the formation of W-Mo- and Sn-bearing skarns in pelitic rocks at Costaboone, France, and Land's End, England, *in* Zachrisson, E., ed., Proceedings *of the 7th Quadrennial IAGOD Symposium*: E. Schweizerbart'sche Verlagsbuchhandlung, Stuttgart, 355-362.

Meinert, L.D. (1983). Variability of skarn deposits – Guides to Exploration. *In:* Boardman, S.J. (eds.), *Revolution in the Earth Sciences*. Kendall-Hunt Publishing, Dubuque, Iowa, 301-316.

Meinert, L.D. (1987). Skarn zonation and fluid evolution in the Groundhog mine, Central Mining District, New Mexico. *Economic Geology*, *82*, 523-545.

Meinert, L.D. (1989). Gold skarn deposits – Geology and exploration criteria, in Groves, D., Keays, R., and Ramsay, R., ed., Proceedings of Gold'88: *Economic Geology Monograph* , *6*, 537-552.

Meinert, L.D. (1992). Skarns and skarn deposits. *Geoscience Canada*, 19, 145-162.

Myers G.L., & Meinert, L.D., (1991). Alteration, mineralization and gold distribution in the Fortitude gold skarn, *in* Raines, G.L., Lisle, R.E., Schafer, R.W. & Wilkinson, W.H., eds. Geology and Ore Deposits of the Great Basin; *Geological Society of Nevada, Reno*, *1*, 407-418.

Newberry, R.J., & Einaudi, M.T., (1981). Tectonic and geochemical setting of tungsten skarn mineralization in the Cordillera. *Arizona Geological Society Digest*, *14*, 99-112.

Newberry, R. J., & Swanson, S. E. (1986). Scheelite skarn granitoids: an evaluation of the roles of magmatic source and process. *Ore Geology Reviews, 1*, 57-58.

Newberry, R.J. (1982). Tungsten-bearing skarns of the Sierra Nevada. I. The Pine Creek Mine, California. *Economic Geology*, *77*, 823-844.

Newberry, R.J. (1987). Use of intrusive and calc-silicate compositional data to distinguish contrasting skarn types in the Darwin polymetallic skarn district, California, USA. *Mineralium Deposita*, *22*, 207-215.

Newberry, R.J. (1998). W- and Sn-skarn deposits: *Mineralogical Association of Canada Short Course Series*, *26*, 289-335.

Oyman, T., Pişkin, Ö., Özgenç, İ., Akbulut, M., & Minareci, F., (2005). Ayazmant (Ayvalık-Balıkesir) skarn tipi demir cevherleşmesinin jeolojisi, mineralojisi ve metasomatik gelişimi. *Türkiye Demir Yatakları Jeolojisi, Madenciliği ve Mevcut Sorunları Sempozyumu Bildiriler Kitabı*, 23-25 Haziran 2005, İstanbul, 417-418.

Öngen, S. (1992). Les échances métasomatiques entre granitoides et encaissant particuliers (calcaires, dolomies, ultrabasites, series manganiferes): I'example de la Turquie-NW. *Doctorat These. Université de Nancy, Faculté des Sciences de la Terre*, 554 p.

Özgenç, İ., Dayal, A., & Oyman, T., (2000). Characteristics of skarn types in Agonia district (Çanakkale) Biga Peninsula, Turkey. *International Earth Sciences Colloquium on the Aegean Region (IESCA-2000) Proceedings*, 113-117.

Permingeat, F. (1957). Le gisement de molybdène, tungstène et cuivre d'Azègour (Haut Atlas), étude pétrographique at metallogénique. *Maroc Service Geological Notes et Memoir*, *141*, 284p.

Pickett, E.A., & Robertson, A.H.F., (2004). Significance of the Volcanogenic Nil.fer Unit and Related Components of the Triassic Karakaya Complex for Tethyan Subduction/Accretion Processes in NW Turkey. *Turkish Journal of Earth Sciences*, *13*, 97-143.

Ray, G.E., & Webster, I.C.L., (1991a). Geology and mineral occurrences of the Merry Widow Skarn Camp, Northern Vancouver Island, 92L/6. B.C. *Ministry of Energy, Mines and Petroleum Resources*, *Open File 1991-8*.

Ray, G.E., Dawson, G.L., & Simpson, R., (1988). Geology, geochemistry and metallogenic zoning in the Hedley Gold-Skarn Camp: *British Columbia Ministry of Energy Mines and Petroleum Resources, Geological Fieldwork, 1987*, *Paper 1988-1*, 59-80.

Ray, G.E., Ettlinger, A. D., & Meinert, L.D., (1990). Gold skarns: Their distribution, characteristics, and problems in classification: *British Columbia Geological Survey Geological Fieldwork 1989*, *Paper 1990-1*, 237-246.

Ray, G.E., Webster, I.C.L., Dawson, G.L., & Ettlinger, A.D., (1993). A Geological Overview of the Hedley Gold Skarn District, Southern British Columbia; *B.C. Ministry of Energy, Mines and Petroleum Resources*, *Paper 1993-1*, 269-279.

Ripley, E.M., & Ohmoto, H., (1977). Mineralogic, sulfur isotope and fluid inclusion studies of the stratabound copper deposits at the Raul mine, Peru. *Economic Geology*, *72*, 1017-1041.

Roedder, E. (1984). Fluid inclusions. Mineralogical Society of America. *Reviews in Mineralogy*, *12*, 644p.

Sangster, D.F. (1969). The contact metasomatic magnetite deposits of southwestern British Columbia. *Geological Survey of Canada, Bulletin*, *172*, 79p.

Shelton, K.L. (1983). Composition and origin of ore-forming fluids in a carbonate-hosted porphyry copper and skarn deposit: A fluid inclusion and stable isotope study of Mines Gaspé, Quebec. *Economic Geology*, *78*, 387-421.

Shimazaki, H. (1980). Characteristics of skarn deposits and related acid magmatism in Japan. *Economic Geology*, *75*, 173-183.

Shimazaki, H. (1988). Oxygen, carbon and sulfur isotope study of skarn deposits in Japan, *in* Zachrisson, E., eds., *Proceedings of the 7th Quadrennial IAGOD Symposium: E. Schweizerbart'sche Verlagsbuchhandlung, Stuttgart*, 375-381.

Sidder, G.B. (1984). Ore genesis at the Monterrosas deposit in the Coastal Batholith, Ica, Peru. *Unpublished Ph.D. thesis, Oregon State University*, 247p.

Sokolov, G.A., & Grigorev, V.M., (1977). Deposits of iron, *in* Smirnov, V.I., eds., *Ore Deposits of the USSR: Pittman, London*, *1*, 7-113.

Soler, A., Ayora, C., Cardellach, E., & Delgado, J., (1990). Gold-bearing hedenbergite skarnsfrom the SW contact of the Andora granite (Central Pyrenees, Spain). *Mineralium Deposita*, *25*, S59-S68.

Taylor, B.E. (1976). Origin and significance of C-O-H fluids in the formation og Ca-Fe-Si skarn, Osgood Mountains, Humboldt County, Nevada. *Unpublished Ph.D. thesis, Stanford University*, 149p.

Taylor, B.E., & O'Neil, (1977). Stable isotope studies of metasomatic Ca-Fe-Al-Si skarns and associated metamorphic and igneous rocks, Osgood Mountains, Nevada. *Contributions on Mineralogy and Petrology*, *63*, 1-49.

Theodore, T.G., & Blake, D.W., (1978). Geology and geochemistry of the West orebody and associated skarns, Copper Canyon porphyry copper deposits, Lander County, Nevada (with a section on electron micropbobe analyses of andradite and diopside by N.G. Banks). *United State Geological Survey, Professional Paper, 798-C*, 85p.

Theodore, T.G., Orris, G.J., Hammarstrom, J.M., & Bliss, J.D., (1991). Gold-bearing skarns. *United State Geological Survey, Bulletin, 1930*, 61p.

Umpleby, J.B. (1913). Geology and ore deposits of Lemhi County, Idaho. *United State Geological Survey, Bulletin, 528*, 182p.

Vidal, C., Injoque-Espinoza, J., Sidder, G.B., & Mukasa, S.B., (1990). Amphibolitic Cu-Fe skarn deposits in the central coast of Peru. *Economic Geology*, *85*, 1447-1461.

Vidale, R. (1969). Metasomatism in the chemical gradient and the formation of calc-silicate bands. *American Journal of Science*, *267*, 857-874.

Zarayskiy, G.P., Zharikov, V.A., Stoyanovskaya, F.M., & Balashov, V.N., (1987). The experimental study of bimetasomatic skarn formation. *International Geology Review*, *29*, 761-858.

Zharikov, V.A. (1970). Skarns. *International Geology Review 12*, 541-559, 619-647 and 760-775.

CHAPTER TWO
GENETIC RELATIONS BETWEEN SKARN MINERALIZATION AND PETROGENESIS OF THE EVCILER GRANITOID (KAZDAĞ, ÇANAKKALE, NW TURKEY) AND COMPARISON WITH WORLD SKARN GRANITOIDS

This chapter was published in the Turkish Journal of Earth Sciences, edited by E. Bozkurt, as; Yücel Öztürk, Y., Helvacı, C. & Satır, M. (2005). Genetic Relations between Skarn Mineralization and Petrogenesis of the Evciler Granitoid, Kazdağ, Çanakkale, Turkey and Comparison with World Skarn Granitoids.Turkish Jourrnal of Earth Sciences, 14, 255-280.

2.1. Abstract

Most skarn deposits are directly related to magmatic activity and there is a systematic correlation between the composition of causative plutons and the metal content of the related skarns. This paper documents the composition of facies within the Evciler pluton and correlations between intrusion composition and the metal content of associated skarns. There are previous works on mine (e.g., Cu mine) in the Evciler district, however, there has been no detail geological study of such ore deposits or associated skarn mineralization. In the Evciler district both calcic exoskarn (garnet-pyroxene) and endoskarn (pyroxene-epidote) occur along the contact between granitoid and marble. Calc-silicate mineral compositions in Evciler skarns are similar to those in Au-Cu and Fe-Cu skarns.

Based on mineralogy and geochemistry, three main facies are observed in the Evciler pluton; (1) the Çavuşlu monzodiorite, (2) the Karaköy granodiorite and (3) Evciler quartz diorite-granodiorite named as the mezocratic type of the Evciler pluton. At the Evciler district, monzogranitic rocks has also limited distribution compared to mezocratic-type Evciler and named as leucocratic-type Evciler. The field evidence for relative timing of intrusions and trace element geochemistry of individual facies suggest that the Evciler pluton formed in a magmatic arc or post-

collisional setting from a hybrid source, having crustal and mantle components contaminated by interaction with the upper crust.

Whole rock $\delta^{18}O$ values of the Evciler granitoid decrease from 8.5 to 2.5‰ towards the intrusive contact, which is closest to the calcic skarn mineralization (Au-Cu), and quartz $\delta^{18}O$ composition of the Evciler granitoid varies from 7.2 to 10.9‰. These values are normal for I-type, primary unaltered value for this intrusive rock, but it is too large to be accounted for by simple magmatic differentiation. Therefore, the Evciler granitoid was subjected to post-emplacement open-system hydrothermal alteration and exchanged with external fluid (probably meteoric water) which changed the original magmatic $\delta^{18}O$ values.

The present study shows that the geochemical characteristics of the Çavuşlu monzodiorite, Karaköy granodiorite and mezocratic-type Evciler are similar to the averages for Au-Cu and Fe-skarn granitoids, whereas the geochemical characteristics of the leucocratic-type Evciler are similar to the averages for Sn- and Mo-skarn granitoids. The Evciler granitoid is also characterized by relatively unevolved to moderately evolved and oxidized suite like the most worldwide Au-Cu core metal associations.

Keywords. Gold, copper, skarn, mineralization, Evciler granitoid, Kazdağ, NW Turkey

2.2. Introduction

The Evciler granitic pluton is located in Kazdağ, northwestern Anatolia. It is an elliptical metaluminous calc-alkaline body of Late Oligocene-Early Miocene age (25±3 Ma; Birkle 1992), which intrudes the Kazdağ Massif, with the long axis trending WSW-ENE, and covers an area of approximately 170 km^2 (Figure 2.1).

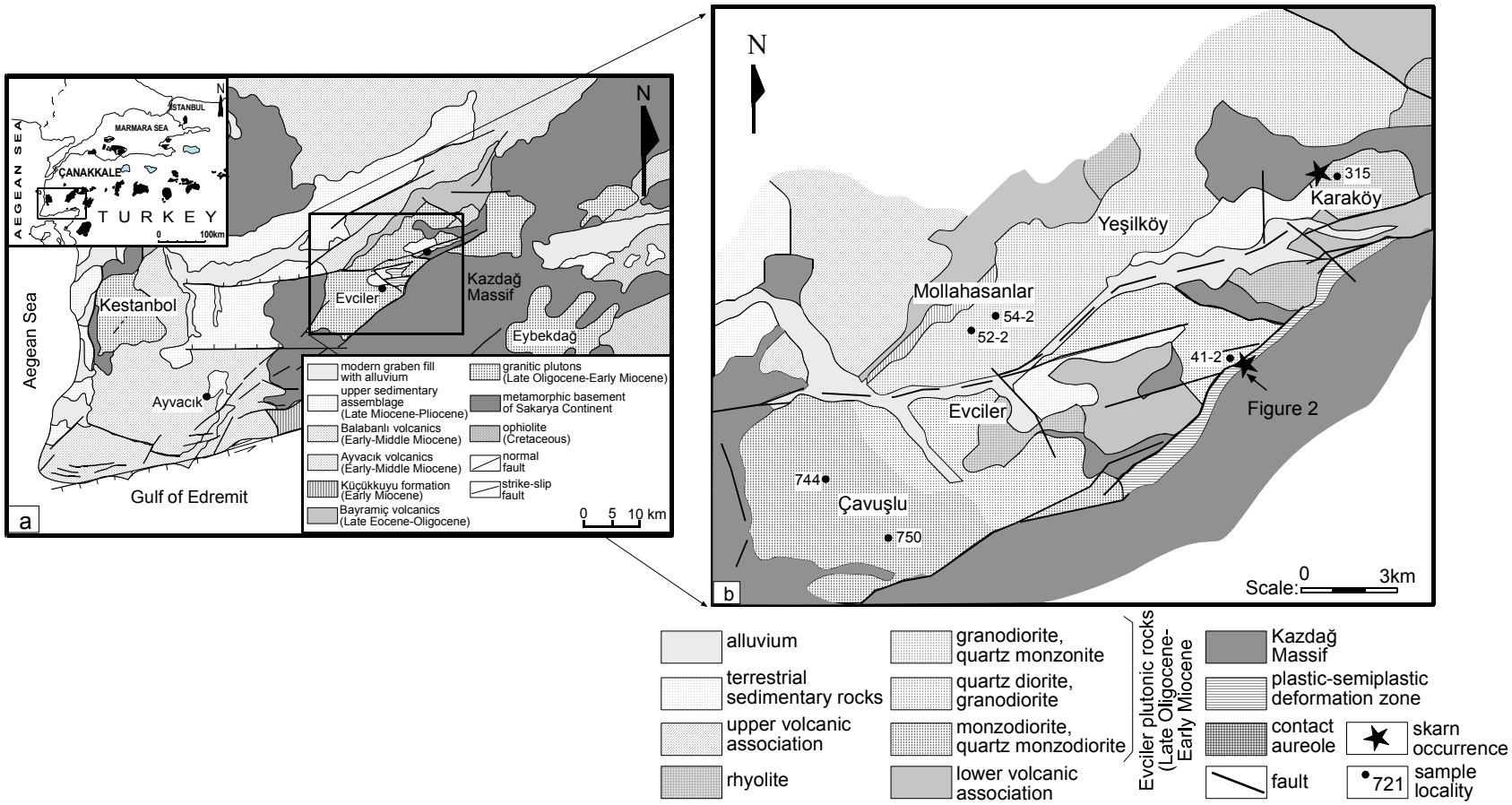

Figure 2.1. **(a)** Regional geologic map showing location of the Evciler district (simplified fromYılmaz & Karacık 2001); **(b)** geologic map of the Evciler district (simplified from Genç 1998).

Although there are historical workings (mainly Cu mine) in the Evciler district, no modern exploration occurred until 1996 when a company conducted detailed stream sediment geochemical surveys to identify anomalies caused by hydrothermal alteration. Numerous copper and gold anomalies were found associated with exoskarn. The exploration studies by this company focused on geology and ore-reserve estimation of mineralization within individual bodies such as the pyrrhotite-rich Au skarn zone at the south end of the Evciler pluton (H. Yılmaz, personel communication, May, 2000). However, the relationship between skarns and associated plutons, and the potential for different types of mineralization associated with the Evciler granitoid has not been studied yet.

Broad correlation between igneous composition and the metal content of associated skarns has been described by several workers (Blevin & Chappell 1992; Ishihara & Sasaki 1991; Keith *et al.* 1989; Kwak & White 1982; Martin-Izard *et al.* 2000; Meinert, 1983, 1995; Meinert *et al.* 1990; Meza-Figueroa *et al.* 2003; Naldrett 1992; Newbery & Swanson 1986; Newbery 1987; Newbery *et al.* 1990; Nicolescu *et al.* 1999; Paktunc 1990; Ray *et al.* 1995; Shimazaki 1975, 1980; Srivastava & Sinha 1997; Zharikov 1970;). These studies have documented the relationship between metal contents in mineral deposits and major and trace element composition, degree of crystallization, and tectonic setting of the related plutons.

The present study is the first report of correlations between skarns and the related Evciler granitoid in the Kazdağ region, northwestern Anatolia, Turkey.

2.3. Geological Setting

Studies on the geology, tectonics, petrology and geochronology of the Kazdağ Massif have been studied by several workers some of which are Duru *et al.* (2004), Genç (1998), Öngen (1992), Okay *et al.* (1990, 1996), Okay & Satır (2000), Şengör & Yılmaz (1981), Şengör *et al.* (1993) and Yılmaz (1989 1990 1995 1997). The high-grade metamorphic rocks of the Kazdağ mountain range, named as the Kazdağ group, crop out as a tectonic window under the Karakaya complex (Göncüoğlu *et al.*

2004; Okay & Göncüoğlu 2004; Okay & Altıner 2004; Pickett & Robertson 2004) in the northwestern Turkey. The Kazdağ group forms a doubly plunging, NE-SW-trending anticliniorium.

Duru *et al.* (2004) subdivided the metamorphic rocks into four formations. The lowermost unit is the Fındıklı formation, which comprises amphibole-gneiss, marble and minor amphibolite. It crops out mainly in the southern part of the Kazdağ Massif. The overlying unit, comprising metadunite and orthoamphibolite, is the Tozlu formation, which in turn is overlain by the Sarıkız marble. The uppermost unit, which crops out in the northern parts of Kazdağ Massif, is the Sutuven formation that comprises sillimanite-gneiss, migmatite, marble, amphibolite and granitic gneiss.

The Sutuven formation rests with a sharp contact on the Sarıkız marble and Fındıklı formation (Duru *et al.* 2004), and is intruded by the Oligo-Miocene Evciler granodiorite. The Sutuven formation comprises mainly grey, dark grey and brown, well-banded quartzo-feldspathic gneisses. These gneisses, which constitute the dominant lithology, comprise marble, amphibolite and granitic gneiss horizons and lenses (Duru *et al.* 2004).

Metamorphism in the Kazdağ Group has been dated by using zircon Pb-Pb and mica Rb-Sr and K-Ar methods on gneisses from the Fındıklı and Sutuven formations. Pb-Pb data from the gneisses yield Mid-Carboniferous ages (308±16 Ma, Okay *et al.* 1996), whereas the biotite and muscovite Rb-Sr and K-Ar ages from the gneisses are Oligo-Miocene (19-22 Ma: Bingöl 1968 1969; Okay & Satır 2000). These isotopic data have been interpreted as indicating two periods of high-grade metamorphism; the initial one during the Mid-Carboniferous and a later one in the Oligo-Miocene. The P-T conditions of the high-grade metamorphism have been estimated as 640±50^{o}C and 5±1 kbar (Okay & Satır 2000).

2.4. Magmatism in Western Anatolia

Several studies have been published on granitoids to understand the geodynamic evolution of western and northwesten Anatolia (Altherr *et al.* 1988; Bingöl 1977, 1978; Bingöl *et al.* 1982; Bozkurt *et al.* 1993, 1995; Bozkurt & Park 1994; Bozkurt 2004; Delaloye & Bingöl 2000; Erdoğan & Güngör 2004; Genç 1998; Gessner *et al.* 2001, 2004; Gülen 1990; Harris *et al.* 1994; Işık & Tekeli 2001; Işık *et al.* 2004; Karacık & Yılmaz 1998; Koralay *et al.* 2001, 2004; McKenzie & Yılmaz 1991; Okay *et al.* 1996; Şengör & Yılmaz 1981). Delaloye & Bingöl (2000) subdivided the granitoids, in western and northwestern Anatolia, according to their ages; (1) the young granitoids (Late Cretaceous to Late Miocene) caused high-temperature metamorphic aureoles. They are defined by six isochronous belts which become progressively younger from north to south, and (2) the old granitoids (Cambrian to Middle Jurassic) are present in the northwestern and northern part of Anatolia (Delaloye & Bingöl 2000).

During the Oligocene-Middle Miocene period widespread magmatic activity had developed in western Anatolia, following the collision between the Sakarya Continent and the Tauride-Anatolide platform (Şengör & Yılmaz 1981; Şengör *et al.* 1993; Yılmaz 1989, 1990, 1995, 1997). Bingöl *et al.* (1982, 1992) suggested that the young granites formed in a post-collisional environment as a result of crustal thickening. However, complementary data presented by Delaloye & Bingöl (2000) are more consistent with a subduction-related origin. The Aegean subduction zone is an especially good candidate to play this role for Eocene-Miocene granitoid belts (Delaloye & Bingöl 2000). The chemical signature of the granites is volcanic-arc granites (VAG) and can be related to N-dipping subduction. The still-active subduction zone must have begun by Oligocene time, but Delaloye and Bingöl (2000)'s data suggest that it may have started earlier. This widespread magmatic activity produced both intrusive and extrusive rocks (Genç 1998), which appear to be associated in space and time in this region. In the Bayramiç area, magmatic activity started with intrusion of the Evciler granite, coeval with the lower volcanic

association. This was followed by an upper volcanic association. These rock groups form collectively the Bayramiç Magmatic Complex (Genç 1998).

2.5. Local Geology

Two main rock units are exposed in the Evciler district: Kazdağ metamorphic rocks and the Evciler granitoid. The metamorphic rocks consist mainly of grey, dark grey, and brown well-banded quartzofeldisphatic gneisses which include marble, amphibolite and granitic gneiss horizons and lenses. Gneisses are characterized petrographically by the presence of biotite, sillimanite, garnet and hornblende along with ubiquitous quartz and feldspar. The marble has a granoblastic texture and is fine-grained. The grain size increases towards igneous contacts. Diopside-bearing amphibolites occur as bands, up to several meters thick, in gneiss and marble (Okay & Satır 2000).

The Evciler pluton occurs as a WSW-ENE trending elliptical body that intruded gneiss and marbles of the Kazdağ Massif in the south, and its volcanic equivalents in the north. The Evciler pluton consists mainly of granodiorite to quartz-diorite, medium grained and granular in the center, and porphyritic and fine-grained toward the margin (Genç 1998). The pluton contains numerous aplite dykes, veins and rounded to lensoidal mafic microgranular enclaves.

2.6. Mineralogy and Petrology of the Evciler Granitoid

The Evciler pluton consists mainly of granodiorite, quartz monzonite, monzodiorite and quartz diorite. Öngen (1992) and Genç (1998) subdivided the pluton into main three facies (Figure 2.1b): (1) Çavuşlu monzodiorite is the earliest facies of the pluton and has a equigranular and coarse-grained texture. It mainly consists of intermediate microcline (%15, Or_{89-90}), automorph plagioclase (%48, An_{45-35}), quartz (%14), biotite (%10), poikilitic magnesium hornblende (%9) and augite (%4). (2) Karaköy granodiorite is the main facies of the pluton and occurs at the northeasthern part of the pluton. It is fine to medium grained and porphyritic in

texture. It consists essentially of plagioclase (%39, An_{40-27}), interstitial orthoclase (%24, Or_{80-85}), quartz (%24), actinolitic hornblende (%8) and coarse-grained biotite (%5). (3) The contact between these two plutonic members is graditional and represented by melanocrate granodiorite including coarse-grained magnesium hornblende, named as mesocratic-type Evciler. It is medium to dark gray in colour due to its higher abundance of mafic components. Phenocryst mineralogy includes major K-feldspar, plagioclase and quartz; minor amphibole, and pyroxene; and accessory titanite, apatite and magnetite. The presence of primary titanite and magnetite, combined with the absence of ilmenite, indicates that these are relatively oxidized magmas. Secondary minerals, formed due to alteration, are epidote, sericite and chlorite with pyroxene altered to amphibole. At the south of the pluton monzogranitic rocks has limited distribution compared to mesocratic-type Evciler and named as leucocratic-type Evciler. It is light gray in colour, fine- to medium-grained and equigranular to porphyritic in texture. It consists mainly of K-feldspar, plagioclase, quartz, and secondary epidote and amphibole crystals; and accessory titanite, apatite, and pyroxene. The K-feldspar is medium to coarse grained and shows perthitic and myrmecitic textures. The leucocratic- and mesocratic-type boundaries are poorly mapped at the Evciler district since their contacts are not clearly observed. Although they are geochemically classified as two different granitoids, the field relations fail to discriminate clearly the contacts between them.

2.7. Skarn Occurences

Skarns in the Evciler district; (1) are mostly calcic, (2) have an oxidized mineralogy dominated by garnet, clinopyroxene, epidote and amphibole, (3) have epidote endoskarn close to the contact between marble and granitoid, (4) contain pyrrhotite, chalcopyrite, magnetite, garnet, pyroxene, epidote, actinolite and chlorite in Ayazma, SE of Evciler village (Figure 2.2).

2.7.1 Endoskarn

Endoskarn formation begins with epidotization, and is coincident with sericitization during metasomatic reactions. Endoskarn consists mainly of epidote and pyroxene. Along the contact with exoskarn, replacement of granodiorite by massive epidote and minor garnet-pyroxene endoskarns over widths of centimeters to 0.5 m may result in complete destruction of the original igneous texture. This zone consists of fine- to medium-grained epidote accompanied by interstitial quartz (Figure 2.3a & b). Endoskarn located at Evciler also contains garnet and pyroxene accompanying the above mineral association. Further within the granite, endoskarns

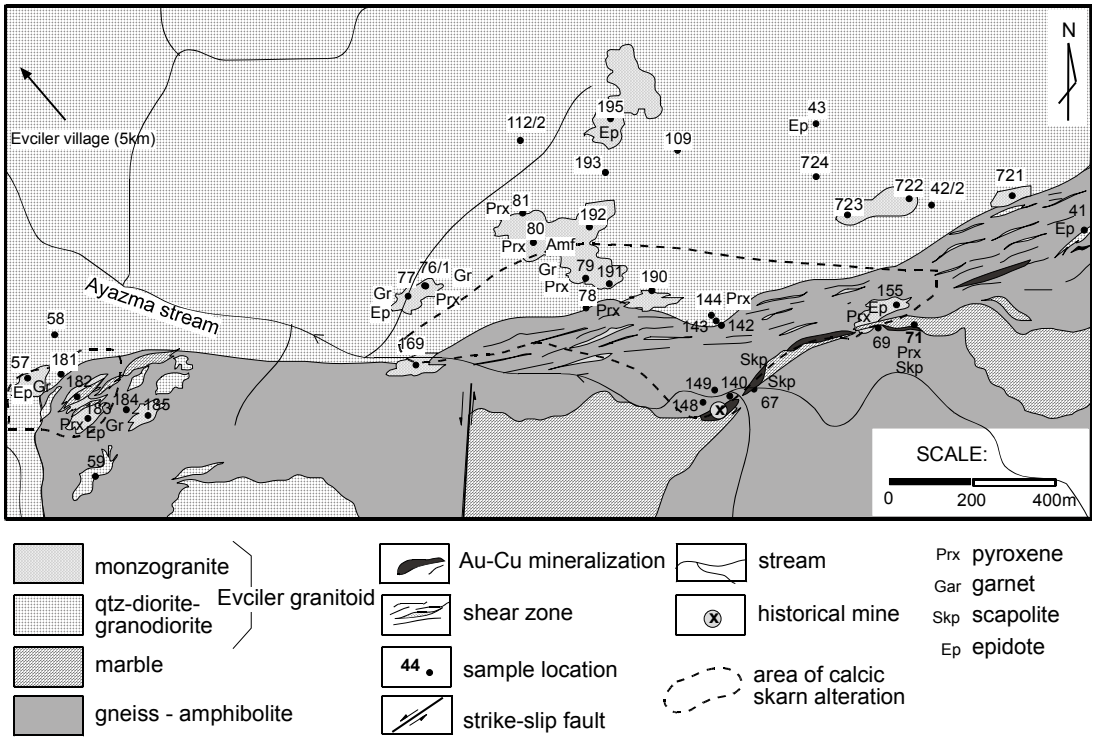

Figure 2.2. Geological map showing location of the skarn alteration and mineralization.

occur only as disseminated epidote skarns, and are enriched in garnet towards the marble. The garnet-rich skarn predominantly comprises exoskarn. However, garnet was locally developed by the dissolution and replacement of primary igneous minerals, particularly feldspar, in the granodiorite (Figure 2.3c & d). Most garnets in

the granodiorite are isotropic, whereas some garnets display anizotrophy and sector and oscillatory zoning (Figure 2.3e & f).

2.7.2 Exoskarn

The alteration of the host rock (marble and gneiss) at the Evciler district is marked by the formation of coarsely crystalline skarn lenses due to the ingress of Si-, Al-, Fe-, and Mg-rich fluids in the host rock. At the contact between Evciler granitoid and Kazdağ Massif, the earliest changes observed in the protolith involve recrystallization to fine-grained, dark grey-green hornfels containing an assemblage of clinopyroxene-feldspar-quartz. Metasomatism of carbonate litology in Evciler produced grossular-andradite/pyroxene exoskarn. The dominant minerals of the exoskarn are pyroxene and garnet as prograde assemblages, and epidote, tremolite/actinolite, chlorite and/or calcite and quartz as retrograde mineral assemblages.

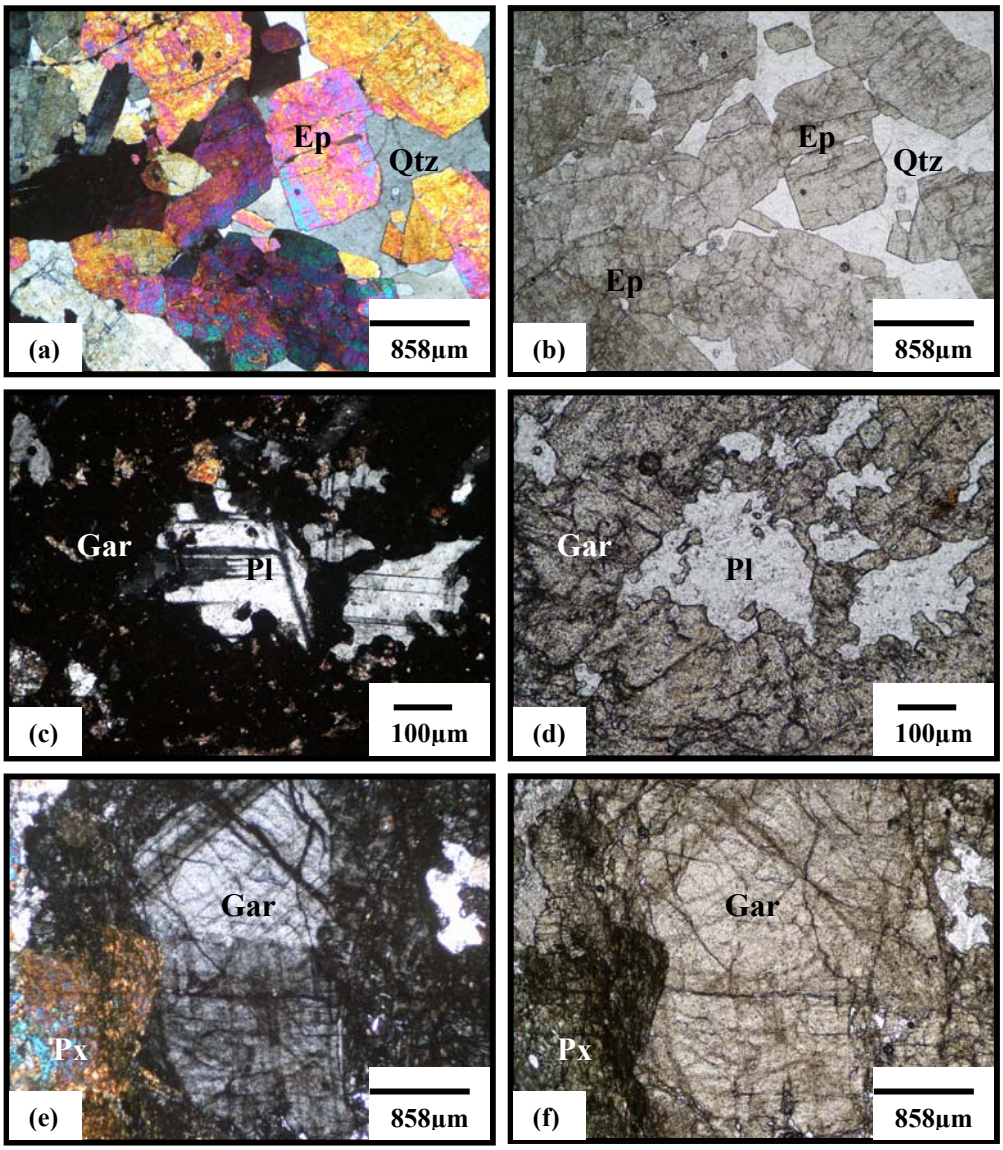

Figure 2.3. Typical endoskarn textures in the Evciler district; (a, b) massive epidote with interstitial quartz, (CPL-cross polarized transmitted light & PPL-plane polarized transmitted light); (c, d) replacement of primary igneous minerals (plagioclase) by garnet (CPL & PPL); (e, f) garnet showing oscillatory and sector zoning within the granodiorite (CPL & PPL). Ep= Epidote, Qtz= Quartz, Gar= Garnet, Pl= Plagioclase, Px= Pyroxene.

In the Evciler skarn, the exoskarn shows slightly zoning to pyroxene-epidote assemblages, with plagioclase, scapolite and sphene, close to marble front (distal skarn) and as garnet-pyroxene with chlorite, epidote, close to endoskarn zone (pyroximal skarn). The width of individual zones ranges from centimeters scale to 2-3 m (even locally 15-25 m). Epidote, tremolite/actinolite, chlorite and/or quartz and

calcite typically represent the retrograde assemblages formed by the alteration of pyroxene and garnet at the advanced stages of skarn formation.

The prograde skarn mineral assemblage comprises garnet, clinopyroxene and scapolite (Figure 2.4a & b). Garnet and pyroxene are intimately intergrown, suggesting synchronous growth of these minerals. The garnet consists of anisotropic and isotropic zoned andradite to grossular ($Ad_{70-50}Gr_{30-50}$). Two types of garnets are observed in exoskarns, smaller and isotropic garnets and largely anisotropic garnets (with oscillatory-zoning) (Figure 2.4c & d). Their compositions are close to those of garnets from Au-Cu and Fe-Cu skarns (Einaudi *et al.* 1981; Meinert 1992). Pyroxenes are generally anhedral to subhedral and hedenbergitic to diopsidic in composition ($Hd_{50-75}Di_{50-25}$) and are close to those of pyroxenes from Au-Cu and Fe-Cu skarns (Einaudi *et al.* 1981; Meinert 1992). These were converted into tremolite/actinolite during the retrograde stages. Calcic-scapolite (meionite) is commonly formed during prograde alteration. Its presence in the Evciler exoskarn indicates a low-temperature scapolite variety or a former skarn assemblage. As the Ca-scapolite grains are intergrown with clinopyroxene and garnets, the latter hypothesis is favored (Figure 2.4c & d).

The main pyrrhotite-rich mineralization is observed within exoskarn and is resulted from the retrograde alteration of prograde calc-silicate assemblages to chlorite and/or calcite. Magnetite-pyrrhotite-chalcopyrite assemblage is common and magnetite is replaced by both pyrrhotite and chalcopyrite. Pyrrhotite occur as the main sulfide phase that was replaced by chalcopyrite. The sulfide mineralization typically developed within the pyroxene exoskarns and occurs intermittently along ca. 600 m of the contact between gneiss and marble belong to the Sutuven formation (Kazdağ Massif).

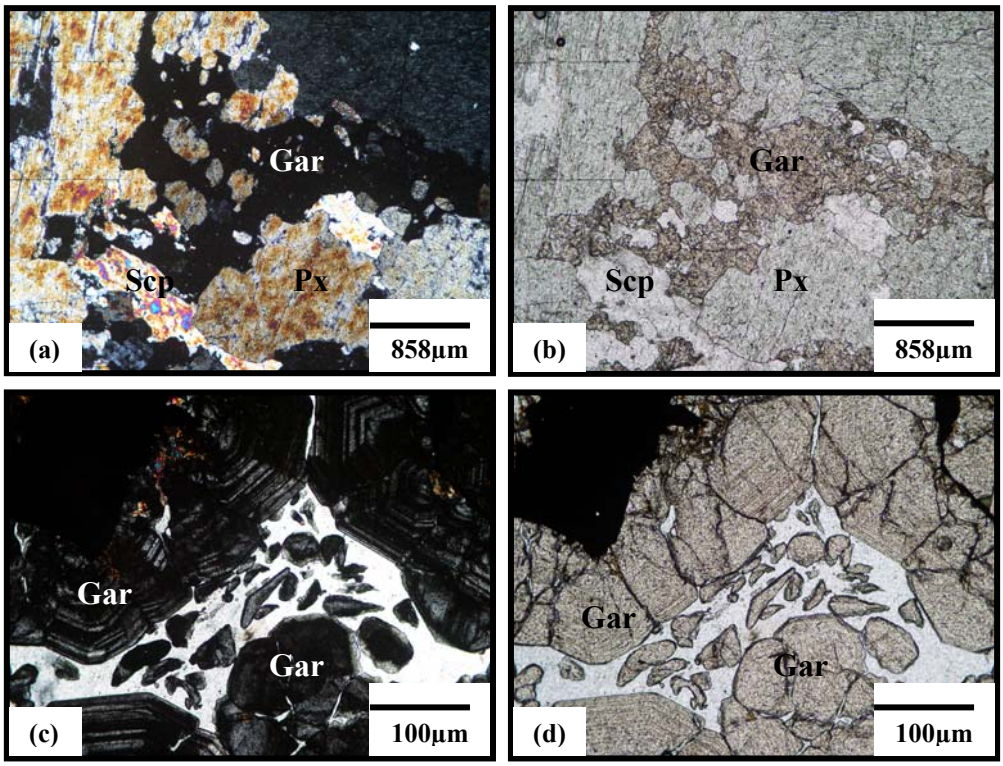

Figure 2.4. Typical exoskarn textures in the Evciler district; (a, b) the prograde skarn mineral assemblage comprising garnet, clinopyroxene and scapolite (CPL & PPL) ; (c, d) the garnet exoskarn consisting of anisotropic and isotropic zoned andradite to grossular (CPL & PPL).

2.8. Geochemistry and Petrogenesis

30 samples were collected for geochemical analysis from the several localities of the Evciler pluton and were analysed for both major and trace element contents. The results are presented in Table 2.1.

Table 2.1. Major- and trace-element compositions of the Evciler pluton.

Örnek no	720-2	721	722-1	723-3	42-1	223/3	41-2	744	750	52-2	54-2	315
	Evciler leucogranite					Evciler granodiorite		Çavuşlu monzodiorite		Karaköy granodiorite		
SiO_2 (%)	73.71	72.64	73.81	74.41	73.34	68.66	56.46	62.14	58.22	61.7	64.79	66.55
TiO_2	0.08	0.12	0.10	0.05	0.09	0.23	0.72	0.57	0.65	0.55	0.47	0.37
Al_2O_3	13.91	14.14	13.32	13.25	14.04	15.15	16.81	15.81	16.25	16.41	15.73	15.18
Fe_2O_3	1.23	1.58	1.17	0.78	0.89	0.96	5.97	5.82	6.91	5.10	4.55	3.59
MnO	0.02	0.03	0.02	0.01	0.01	0.02	0.10	0.10	0.13	0.11	0.10	0.06
MgO	0.16	0.24	0.25	0.11	0.33	0.86	3.28	2.10	2.91	2.10	1.97	1.51
CaO	1.27	1.51	1.56	0.95	1.39	3.14	8.11	4.52	6.19	5.11	4.65	3.77
Na_2O	3.06	3.22	2.82	2.41	2.92	2.83	3.58	3.08	3.22	3.45	3.14	3.28
K_2O	5.40	4.83	5.41	6.40	5.87	6.51	2.36	4.17	3.20	2.97	3.43	3.73
P_2O_5	0.01	0.01	0.01	0.03	0.07	0.15	0.22	0.18	0.19	0.14	0.11	0.10
Ba (ppm)	699	817	1046	634	925	2611	1097	944	722	697	840	826
Sc	2	2	2	1	2	3	14	10	12	10	9	6
Co	1	2	3	1	2		15	15	20	12	11	7
Cs	2	1	1	3	1	1	1	3	6	2	10	6
Ga	20	20	17	16	17	20	19	18	20	18	17	17
Hf	3	4	3	2	2	6	5	6	6	5	4	4
Nb	10	5	6	6	3	14	9	10	12	9	8	9
Rb	196	152	142	231	151	188	61	139	129	93	112	133
Sn	1	2	1	< 1	< 1	< 1	3	1	2	1	< 1	< 1
Sr	196	381	260	205	188	1005	677	525	616	462	448	427
Ta	1	0	1	2	1	1	1	1	1	1	1	1
Th	25	17	26	19	7	32	6	21	21	35	14	21
U	7	5	6	12	8	7	2	6	6	7	4	7

Table 2.1. Cont.

Örnek no	720-2	721	722-1	723-3	42-1	223/3	41-2	744	750	52-2	54-2	315
	Evciler leucogranite					Evciler granodiorite		Çavuşlu monzodiorite		Karaköy granodiorite		
V	13	23	15	13	10	25	178	132	155	103	98	73
W	2	3	1	1	2	2	2	2	2	2	5	2
Zr	66	111	63	47	43	197	160	198	176	144	116	124
Y	19	9	11	12	11	18	27	23	28	23	21	17
Mo	9	8	7	0	0	3	1	7	1	1	1	2
Cu	7	7	40	1	1	2	2	49	45	7	5	12
Pb	5	7	4	6	4	4	23	6	22	3	148	5
Zn	10	17	11	7	11	5	34	39	39	45	115	15
Ni	8	8	7	2	4	5	3	9	4	5	5	4
As	1	< .5	< .5	< .5	< .5	< .5	< .5	1	1	< .5	1	1
Au	< .5	< .5	< .5	1	9	< .5	1	1	1	1	< .5	< .5
La	18	28	21	12	16	63	32	32	38	26	32	41
Ce	30	44	33	22	45	95	54	56	62	41	46	56
Pr	3	6	4	3	3	11	7	7	8	5	5	6
Nd	13	21	14	10	12	41	30	26	32	22	20	21
Sm	3	4	3	3	2	6	6	6	6	4	4	3
Eu	1	1	1	1	1	1	1	1	1	1	1	1
Gd	2	2	2	2	2	4	5	4	5	4	3	3
Tb	0	0	0	0	0	1	1	1	1	1	1	1
Dy	2	2	2	2	2	3	5	4	4	3	3	2
Ho	1	0	0	0	0	1	1	1	1	1	1	1
Er	2	1	1	1	2	1	3	2	3	2	2	2
Yb	2	1	1	2	1	2	3	2	3	3	2	2

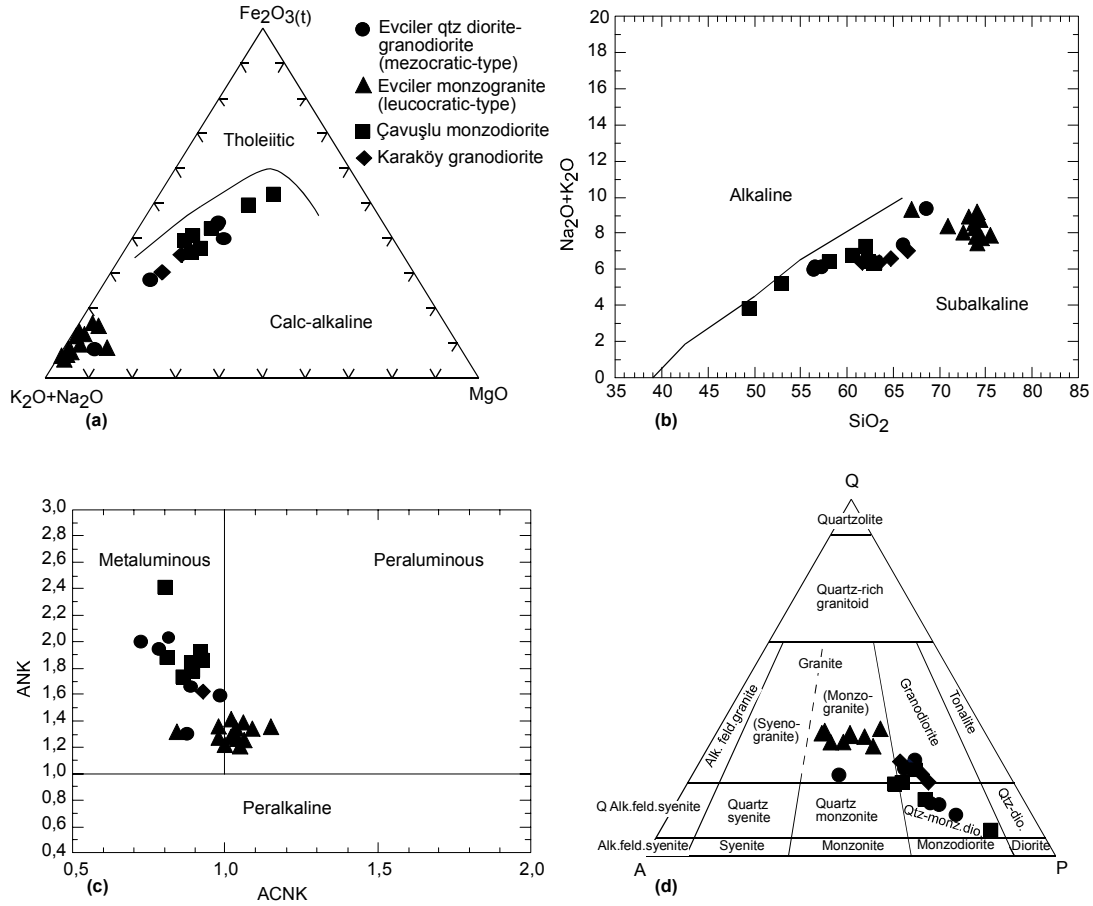

Figure 2.5. Classification of (a) calcalkaline, (b) subalkaline, (c) Al-saturation (according to Peacock, 1931) and (d) nomenclature (according to Streckeisen 1976) index diagrams of the Evciler granitoid associated with skarn occurrence.

In terms of major elements, most pluton associated with skarn deposits is fairly normal calc-alkaline rocks. For the Evciler granitoid, all values plot in calcalkaline (Figure 2.5a) and subalkaline (Figure 2.5b) type on the basis of the Irvine & Baragar (1971) classification scheme. The mesocratic- (quartz diorite-granodiorite) and leucocratic- (monzogranite) types, distinguished by field observations and petrographically also appear as two distinct groups on these diagrams, suggesting that these are the products of two different magmas or the leucocratic-type is the late stage products of the same magma. The mesocratic-type Evciler plots in high MgO (Figure 2.5a) and low SiO_2 fields (Figure 2.5b). However, all values of the Evciler pluton plot in the metaluminous to mildly peraluminous fields. The mesocratic-type Evciler is characterized by a higher alkaline content (Figure 2.5c). In the classification diagram of Debon & Le Fort (1983) (Figure 2.5d), the Evciler granitoid

form a continuous spectrum from quartz diorite to the granite. The mesocratic-type Evciler is granodiorite to quartz monzodiorite in composition, whereas the leucocratic-type Evciler is monzogranite in composition.

In the K_2O versus SiO_2 diagram (Figure 2.6a), the Evciler granitoid shows high-K characteristics. The K_2O contents correlate positively with the silica. In contrast, the MgO, Fe_2O_3, TiO_2, Al_2O_3, P_2O_3 and CaO display a clear negative trend against the silica increase (Figures 2.6b-g), suggesting that the Evciler pluton was derived from highly evolved melts (Genç 1998). In these diagrams, MgO, Fe_2O_3, TiO_2 and P_2O_3 values appear more depleted for the Evciler leucogranite, with exception of K_2O which appears more enriched, than the Evciler granodiorite (Figure 2.6).

The SiO_2 and Na_2O contents, molecular A/CNK ratio , K_2O/Na_2O ratio, key CIPW minerals and key modal minerals (such as amphibole, sphene) all suggest that the Evciler granitoid shows I-type characteristics on the basis of the Chappel & White (1974) and Raymond (1995) schemes.

The use of trace-element data is the discrimination of tectonic or geologic provinces associated with particular magma types (e.g., Pearce *et al.* 1984). By using the Rb versus Y+Nb (Figure 2.7a) and Nb versus Y (Figure 2.7b), values of the Evciler pluton plot VAG and VAG + Syn-COLG fields, respectively. However, The Rb/Zr versus SiO_2 diagram indicates crustal contamination (Figure 2.7c).

REE data are also presented in Table 2.1. The mesocratic-type Evciler, Çavuşlu monzodiorite and Karaköy granodiorite are enriched in REE. They have smaller negative Eu anomalies and a horizontal normalized pattern for the HREE (Figure 2.8). However, normalized patterns for leucocratic-type Evciler are characterized by LREE enrichment, strong negative Eu anomalies and well-defined a positive sloping HREE. A characteristic feature of the leucocratic-type Evciler is that it is extremely depleted in HREE compared to other associations (Figure 2.8). These rocks indicate

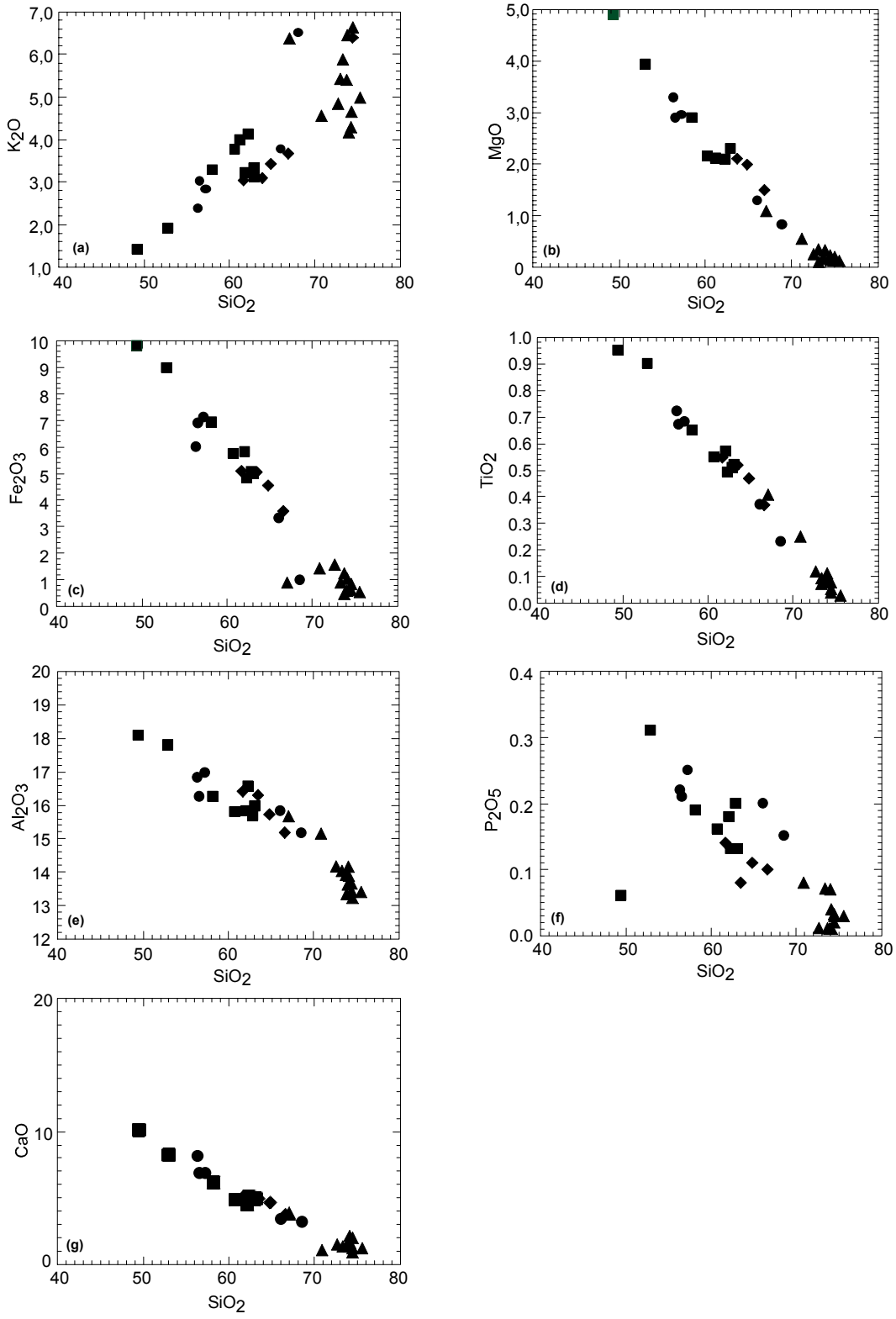

Figure 2.6. Harker variation diagrams of major elements of Evciler granitoid (see Figure 2.5 for symbols).

little or no residual plagioclase in the source magma. These data are consistent with numerous examples from continental or continental margin settings (Delaloye & Bingöl 2000).

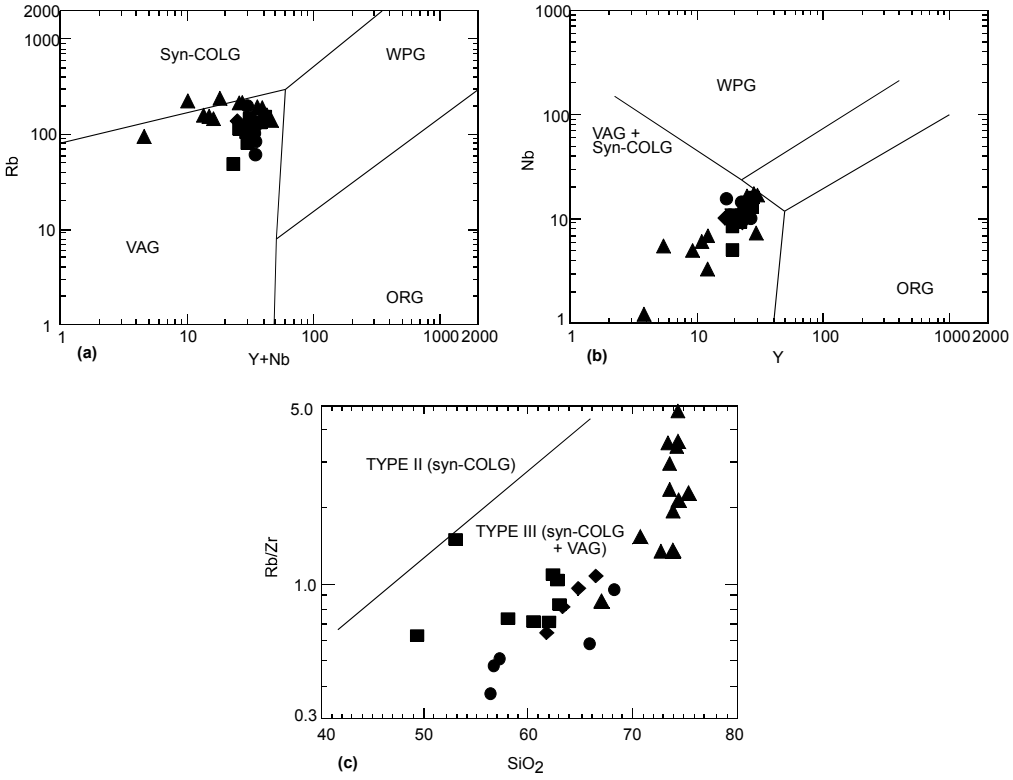

Figure 2.7. (a) Rb vs (Y+Nb), (b) Nb vs Y and (c) (Rb/Zr) vs SiO_2 granitoid discrimination diagram to discriminate the magma characteristics of the Evciler granitoid (field boundries and nomenclature after Pearce *et al*. 1984).

The mesocratic-type Evciler, Çavuşlu monzodiorite and Karaköy granodiorite are exceptionally rich in Ce, Pr, Nd, and Sm in comparison with leucocratic-type Evciler. Occurrences of accessory minerals such as apatite are responsible for this enrichment (Delaloye & Bingöl 2000).

ORG (Ocean Ridge Granite) – normalized patterns for the Evciler granitoid are characterized by K_2O, Rb, Ba and Th enrichment. However, the Evciler granitoid is depleted in Zr and Y (Figure 2.9a), indicating that it had interacted with the crust.

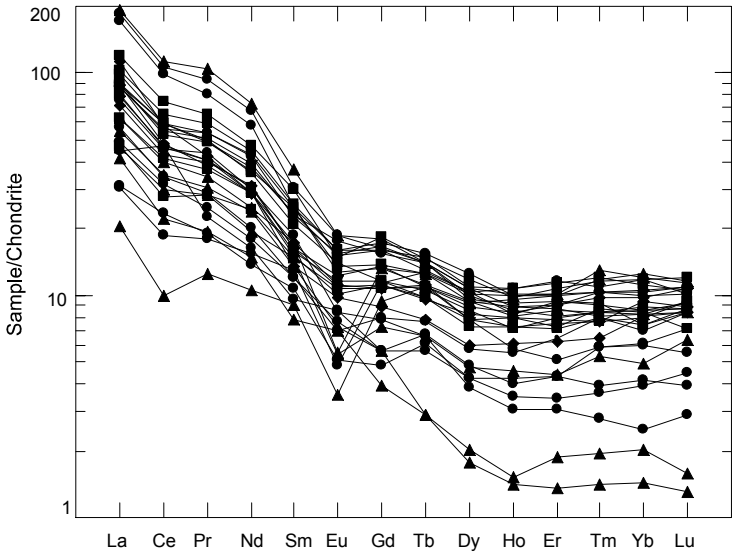

Figure 2.8. Chondrite-normalized REE patterns for Evciler granitoid.

The comparison of the trace element contents of the Evciler granitoid with those of lower and upper crust (Wilson 1989) shows that the Evciler granitoid is fairly similar to that of upper crust (Figures 2.9a & b), in that LIL elements are enriched with respect to HFS elements. The enrichment in Th and Nb indicates that the source rocks are also enriched in these elements. According to Genç (1998), the Evciler pluton yields a cafemic trend on the A-B diagram of Debon & Le Fort (1983). The cafemic associations are known to have been derived mostly from a hybrid source, having crustal and mantle components (Debon & Le Fort 1983). This conclusion is supported by the ORG-normalized trace element systematics of the Evciler granitoid as discussed above. These features indicate a source region in the mantle, enriched by subduction processes (e.g., Harris *et al.* 1986; Pearce *et al.* 1984; Rogers *et al.* 1985). Therefore, the trace element and REE patterns of the Evciler granitoid compares with the magmas formed in a magmatic arc or in the post-collisional setting (Genç 1998).

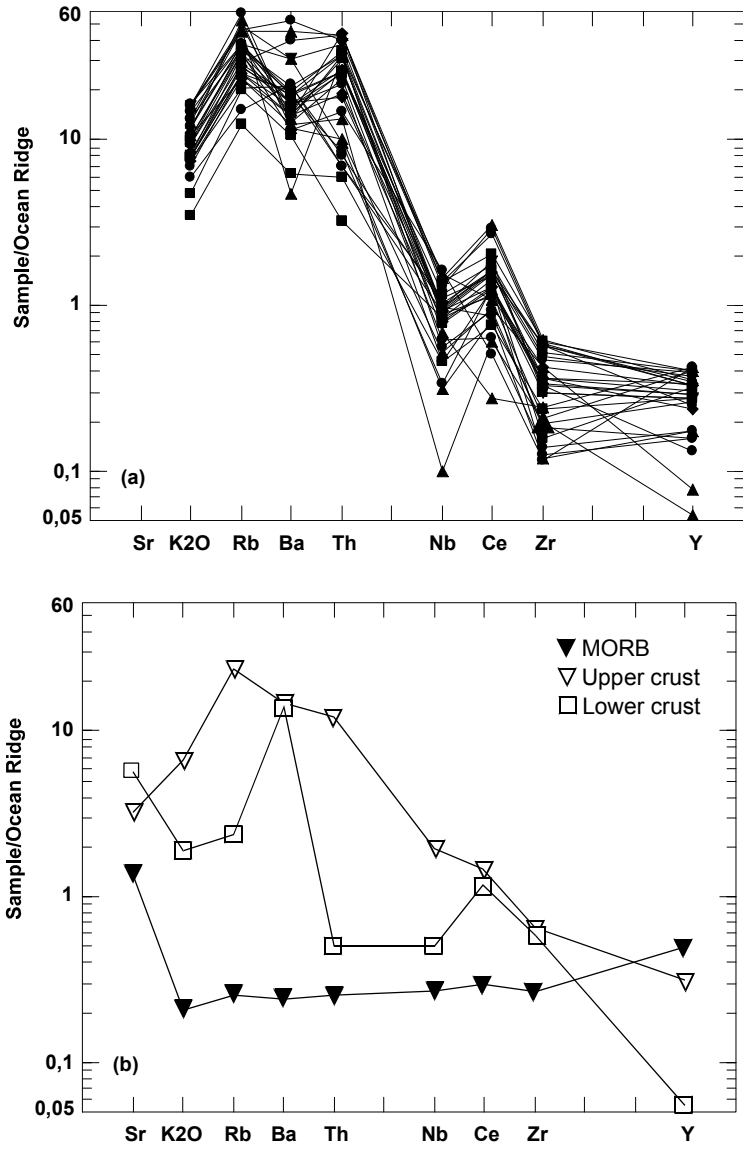

Figure 2.9. Ocean ridge granite (ORG)-normalized spider diagrams for (a) the Evciler granitoid and (b) MORB, upper crust and lower crust, for comparison. Normalizing values are from Pearce *et al.* (1984).

2.9. Oxygen Isotope Chemistry

Because of its proximity to the skarn mineralization and its possible role in genesis of the ore-forming fluids, we analyzed oxygen isotopes for samples of whole rocks and seperated minerals from the Evciler granitoid collected close to the pyrrhotite-bearing mineralization at the Evciler district. Oxygen isotope analyses of

the granite reported here (Table 2.2) were performed on mineral seperates (quartz and amphibole) in preference to whole-rock powders because oxygen isotope ratios of the whole-rock are vulnerable to effects of post-crystallization, sub-solidus alteration.

Table 2.2. $\delta^{18}O$ values and locations of samples from Evciler granitoid.

Sample no.	$\delta^{18}O$ (‰)			$\delta^{18}O_{magma}$ (‰)
	Quartz	Amphibole	Whole rock	
195	10.2			
193	10.4			
112/2	10.4	6.6	7.2	8.0
191	8.9		8.1	
79	10.9		8.3	
192/2	1.3		6.1	
109	7.2		6.0	
58	10.2		8.7	
76/1	7.2		5.7	
42/2	10.2	5.9	2.5	7.2
148/2	9.0	5.2	6.5	6.5
184	3.7	-0.6		7.2
140/S_5	4.5		7.1	
222/1	8.5	5.2	4.8	6.6

Quartz and amphibole were seperated and purified by magnetic seperation and hand picking. The purity of all mineral seperates was checked by X-Ray diffraction, and is better than 95%. The oxygen isotope composition (^{18}O, ^{16}O) of the samples were measured, using a method similar to that described by Sharp (1990) and Rumble & Hoering (1994). Between 0.5 to 2 mg of sample was loaded onto a small Pt-sample holder and pumped out to a vacuum of about 10^{-6} mbar. After preflourination of the sample chamber overnight, the samples were heated with a CO_2-laser in 50 mbars of pure F_2. Excess F_2 is seperated from the O_2 produced by conversion to Cl_2 using KCl held at 150^{o}C. The extracted O_2 is collected on a molecular sieve (13X) and subsequently expanded and analyzed using a Finnigan MAT 252 isotope ratio mass spectrometer at the Tübingen University, Germany. The results are reported as conventional permil $\delta^{18}O$ values relative to SMOW. The

reproducibility is better than ±0.1‰. The mean value for the NBS-28 standard obtained during the present study was +9.64 ‰.

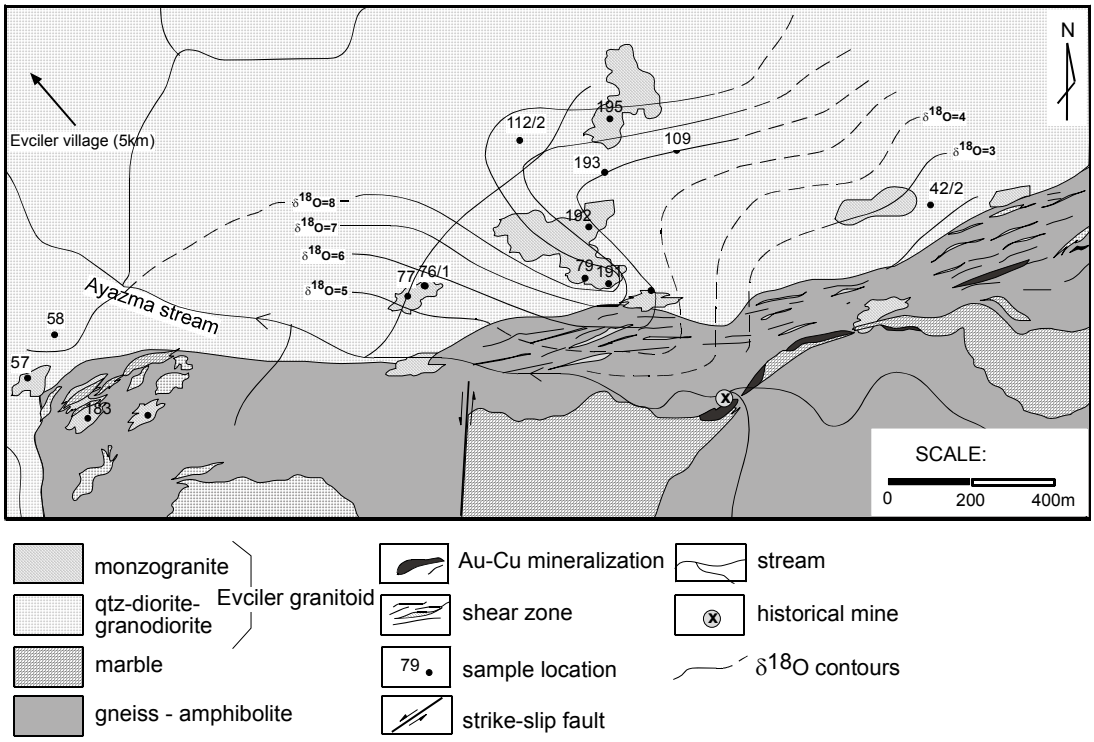

Figure 2.10. Geological map showing $\delta^{18}O$ values of the Evciler qtz diorite-granodiorite.

The whole rock $\delta^{18}O$ values of the Evciler granitoid decrease toward the intrusive contact, which happens to be the region closest to the pyrrhotite-bearing mineralization at the Evciler district (Figure 2.10). The whole-rock $\delta^{18}O$ values of samples, collected only a few meters from the skarn mineralization is 2.5, 5.7 and 6.0 ‰, lower than the normal range for fresh granites (Taylor 1968), and suggest that granite at this locality has been altered.

Note that the range of $\delta^{18}O$ values for quartz from the granite samples collected furthest from the skarn mineralization is restricted, ranging from +7.2 to +10.9 ‰, which may be close to the primary unaltered value for this intrusive rock. This range is normal for I-type granitic rocks (e.g., Taylor & Sheppard 1986; +8 ‰ - +10 ‰).

In this chapter, the $\delta^{18}O$ value for the original magma (δ_{magma}) has been estimated from the $\delta^{18}O$ values of quartz. In theory, the $\delta^{18}O$ value of the fresh rock (and hence δ_{magma}) can be calculated from the mineral $\delta^{18}O$ values and modal proportions, provided that oxygen isotope data are available for all of the constituent minerals (Harris *et al.* 1997). The $\delta^{18}O$ values calculated for the granite magmas from quartz $\delta^{18}O$ values at the Evciler granitoid range from 6.0 to 8.0 ‰.

In slowly cooled coarse-grained rocks (e.g., the Cape granites, Harris *et al.* 1997), the difference between the $\delta^{18}O$ value of quartz and δ_{magma} is not only dependent on $\Delta_{qtz\text{-}melt}$, but is also dependent on grain-size, the rate of cooling, and the temperature of closure of the mineral to oxygen diffusion (e.g., Giletti 1986; Jenkin *et al.* 1991). Larger grain size generally results from slower cooling, which in turn means that oxygen diffusion and re-equilibrium continues for a greater period of time.

The difference between the $\delta^{18}O$ value of quartz and the other constituent minerals in a slowly cooled rock will be larger than for a more rapidly cooled rock. To correct for these 'closure' effects $\Delta_{quartz\text{-}magma}$ was assumed to be +1‰ in the quartz porphyries (e.g., Taylor & Sheppard 1986) and +2 ‰ in the remaining granites which relatively coarse-grained (see Giletti 1986). Calculated $\Delta_{quartz\text{-}magma}$ for the Evciler granitoid range from +1.8 to +3.0 ‰. Under equilibrium conditions, the O-isotope fractionation between quartz and constituent minerals (e.g., $\Delta_{qtz\text{-}feld}$) should fall in the range of 0.5-2.0 ‰ at magmatic temperatures (Chiba *et al.* 1989). For the granitoid at the Evciler district, the only readily applicable fractionation for equilibrium conditions was quartz-amphibole. Quartz-feldspar, the fractionation most often chosen for felsic igneous rocks is not applicable at Evciler due to the lack of measured $\delta^{18}O$ values for feldspar. The average $\Delta_{qtz\text{-}amph}$ observed in the Evciler granitoid ranges from 3.0 to 4.2 ‰, indicating that the O-isotopes did not reach equilibrium in these samples. Therefore, the present isotopic characteristics demonstrate that the Evciler granitoid has experienced post emplacement open-system hydrothermal alteration. Meteoric water was the most probable fluid involved in the water-rock interactions for the granitic intrusion.

2.10. Discussion

2.10.1 Comparison of the Compositional Variation of the Evciler Granitoid with World Skarn Granitoids

Broad correlation between igneous composition and skarn type with respect to their metal contents have been described by several workers (Blevin & Chappell 1992; Ishihara & Sasaki 1991; Keith *et al.* 1989; Kwak & White 1982; Meinert 1983, 1990, 1993, 1995, 1997; Meinert *et al.* 1990; Naldrett 1992; Newbery & Swanson 1986; Newbery 1987; Newbery *et al.* 1990; Nicolescu *et al.* 1999; Paktunc 1990; Ray *et al.* 1995; Shimazaki 1975, 1980; Srivastava & Sinha 1997; Zharikov 1970). Parameters that are most important in determining the overall metallogenic "flavour" of intrusive igneous suites comprise; granite type, compositional evolution, degree of fractionation and oxidation state (Blevin 2004).

In terms of major elements, the Evciler granitoid was compared with the worldwide average of granitoids associated with Au-Cu and Fe skarns (Meinert 1995) and with skarn granitoids of Ertsberg, Indonesia (Meinert *et al.* 1997); Bocşa and Ocna de Fier, Romania (Nicolescu *et al.* 1999); McKenzie, Canada (Moore & Lentz 1996); Millstream, Canada (Lentz *et al.* 1995); British Columbia, Canada (Meinert 1984) and Rio Narcea gold belt (RNGB), Spain (Martin-Izard *et al.* 2000) by using Harker diagrams similar to those used by Meinert (1993, 1995).

As it is illustrated in the Harker-type diagrams, Au- and Fe-skarn averages are characterized by higher MgO and lower K_2O and SiO_2 contents compared to Cu-skarn and other types (W-, Mo-, Sn-, Zn-, and Pb-skarns). The MgO contents of the Evciler monzogranite (leucocratic-type) and Evciler quartzdiorite-granodiorite (mesocratic-type) are 0.28% and 2.30%, respectively. However this value is 3% for Fe-skarn granitoids, 3.2% for Au-skarn granitoids, and 1.8% for Cu-skarn granitoids (Meinert 1995). The MgO contents of the mesocratic-type Evciler is close to Fe- and Au-skarn granitoids, Çavuşlu monzodiorite and Karaköy granodiorite are close to Cu-skarn granitoid (Figure 2.11a). In contrast, the MgO contents of the leucoratic-

type Evciler is fairly similar values of Mo- and Sn-skarn granitoids and plots close to Mo-Sn granitoid averages (Figure 2.11a). Therefore it is suggested that the

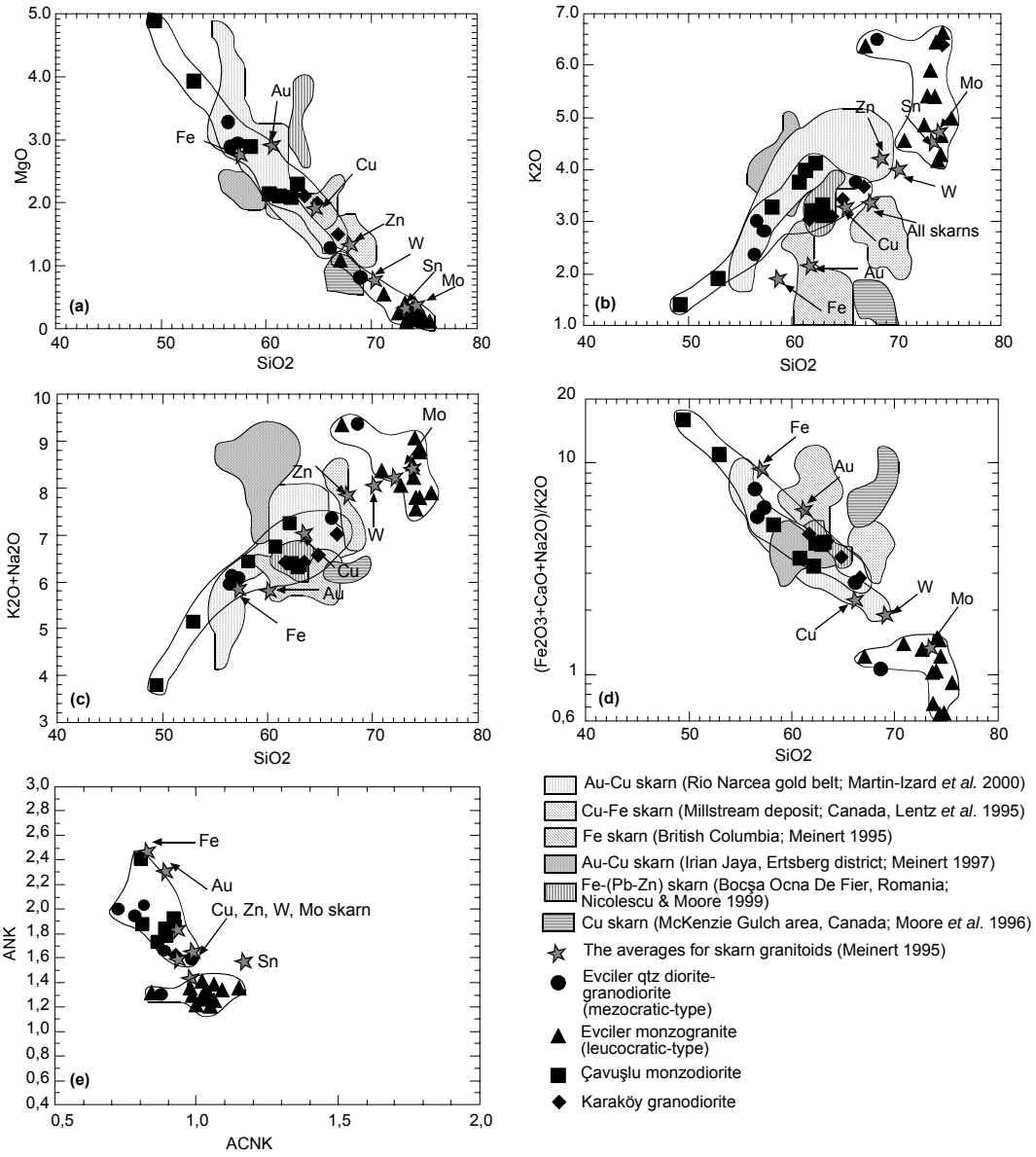

Figure 2.11. Harker-type (a) MgO vs SiO_2, (b) K_2O vs SiO_2, (c) total alkalies vs SiO_2 (d) Fe_2O_3+CaO+Na_2O/K_2O ratio vs SiO_2 and (e) ANK (molar $Al_2O_3/(Na_2O+K_2O)$ratio) vs ACNK (molar $Al_2O_3/(CaO+Na_2O+K_2O)$ratio) diagrams for the Evciler granitoid and comparison with world skarn granitoids (the averages for skarn granitoids are taken from Meinert 1995).

Evciler quartzdiorite-granodiorite could be associated with Cu-Au and Fe skarns and Evciler monzogranite could be associated with the Mo and Sn skarns. Similarly,

in terms of the K_2O contents of these rocks, Evciler values appear to trending towards Au-, Cu- and Fe-bearing granitoids (Figure 2.11b).

The total alkali content of the Evciler quartzdiorite-granodiorite (mesocratic-type), Çavuşlu monzodiorite and Karaköy granodiorite are fairly similar values of Au-Cu and Fe-skarn granitoids and value of these rocks plot close to Au-Cu and Fe-granitoid averages (Figure 2.11c). The Evciler granitoid, in general, has a single trend in terms of iron content and other major oxides (Figure 2.11d).

Consequently, In terms of major element contents, the overall geochemistry of the Evciler granitoid, except the leucocratic-type Evciler, is comparable to Au-Cu and Fe-skarn granitoids. Although it is not clear in the field, geochemistry of the leucocratic-type is comparable to Mo- and Sn-skarn granitoids (Figures 2.11a-d). Pyrrhotite-bearing Au-Cu mineralization in Ayazma (Evciler) district should be related to the Evciler quartz diorite-granodiorite (mesocratic-type).

According to Meinert (1995), in terms of Al-saturation, most composition of skarn- related plutons cluster close to the division between metaluminous and peraliminous, and almost none would be classified as peralkaline. The Evciler quartz diorite-granodiorite (mesocratic-type), Çavuşlu monzodiorite and Karaköy granodiorite are characterized by higher ANK and lower ACNK values than the leucocratic-type Evciler (Figure 2.11e). In this diagram, the Evciler granitoid shows lower ANK and higher ACNK values than typical Fe-skarn granitoids. In terms of Al-saturation index, Fe-skarn granitoids are interpreted as skarns derived from mantle granitoids with little or no crustal interaction (Meinert 1984). Because Al-saturation index of the Evciler granitoid is lower than that of Fe-skarn granitoids, unlike the average Fe-skarn granitoids, this suggests more crustal interaction. The Evciler granitoid, except the leucocratic-type appear to trending towards Cu- and Zn-skarn granitoids. However the leucocratic-type is fairly similar to those of the values for Mo- and Sn-skarn granitoids.

The degree and type of fractionation is important in determining both the potential for mineralisation and the type of mineralization with which a granite suite

is associated. Fractional crystallization can be measured in many ways: use of compatible/incompatible element ratios (e.g., Rb/Sr ratio) and the behaviour of selected trace elements that indicate the incoming and outgoing of crystallizing phases (Blevin 2004). For example, Rb should increase and Sc should decrease as crystallization and differentiation proceed for magmatic rocks. Figure 2.12a illustrates this relationship for the Evciler granitoid. The Evciler monzogranite (leucocratic-type) is characterized by higher Rb and lower Sc content than the Evciler quartz diorite-granodiorite, Karaköy granodiorite and the Çavuşlu monzodiorite. However, the Evciler (mesocratic-type), Çavuşlu and Karaköy plots are very close to those of Cu-, and Au-skarn granitoids, but higher than Fe-skarn granitoids. The Evciler monzogranite plots are also higher than those of Fe-skarn granitoids but lower than those of Mo- and Sn-skarn granitoids (Figure 2.12a). The variation of "mobile" large-ion lithophile trace elements such as Rb and Sr relative to "immobile" high-field-strength elements such as Zr, Nb, and P is also important to understand the petrogenesis of plutons associated with skarn deposits. For example, Newberry & Swanson (1986) has been noted that W, Sn, and Mo deposits have high Rb/Sr ratios, and this suggests that the process of differentiation, rather than a particular magma composition, is critical in the formation of these deposits. In contrast, Zn-, Cu-, Au-, and Fe-skarn systems have low Rb/Sr ratios, and show little evidence for differentiation. In Figure 12b, the Evciler granitoid is characterized by lower Rb/Sr ratios than Mo-, W-, and Sn-skarn granitoids but the leucocratic-type Evciler has slightly higher Rb/Sr ratios than the other associations. However, the Evciler quartz diorite-granodiorite (mesocratic-type) is fairly close to Au-, Cu-, and Fe-skarn granitoids, suggesting an Au-, and Cu- potential in the area.

As metallogenic associations depend on the compositional character of granites, K/Rb ratio is particularly useful in highly fractionated melts. According to Blevin (2004), suites that show classic petrographic and compositional behaviour consistent with the processes of fractional crystallization are most commonly associated with significant mineralization. In K/Rb versus SiO_2 diagram, there is a progressive decrease in K/Rb values with granite evolution (Figure 2.13a & b). This diagram

shows that the Evciler pluton is similar to I-type granites from continental margins (Figures 2.13c) and was also derived from moderately evolved melts (Figure 2.13d).

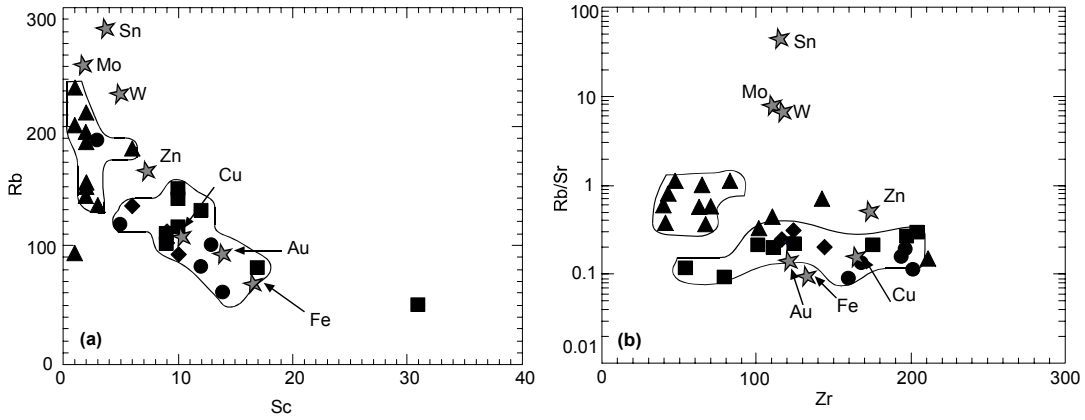

Figure 2.12. Trace element contents of Evciler granitoid and skarn granitoid averages taken from Meinert (1995). (a) Rb vs Sc and (b) Rb/Sr vs Zr.

Relative metal abundances in magmas and different types of intrusion-related deposits are a function of compositional evolution, fractionation and oxidation state. It is the core element association that most closely relates to magma composition. For example, Cu-Au deposits are associated with oxidized, relatively unevolved suites (Blevin 2004). In Fe_2O_3/FeO versus Rb/Sr plot (Figure 2.14a), The Evciler granitoid are characterized by relatively unevolved to moderately evolved and oxidized suites and are fairly close to Au-Cu deposits.

Combination of the parameters above can be used on a district to regional scale to interpret relationships between igneous rocks and ore deposits. Deposit zoning and mineral occurrence data can also be used as a key input in recognising magmatic-hydrothermal "districts". The most intrusion-proximal, high temperature metal association within these districts is defined as the "core metal association" (Figure 2.14b). In this diagram, there are five core metal associations recognized, and the Evciler granitoid are fairly close to Au-Cu association and similar to those of Cadia district, Australia (Blevin 2004). Such an approach has a predictive capacity in being able to recognize potential for particular metallic element associations in poorly explored Evciler pluton and other young granitoids from northwestern Anatolia.

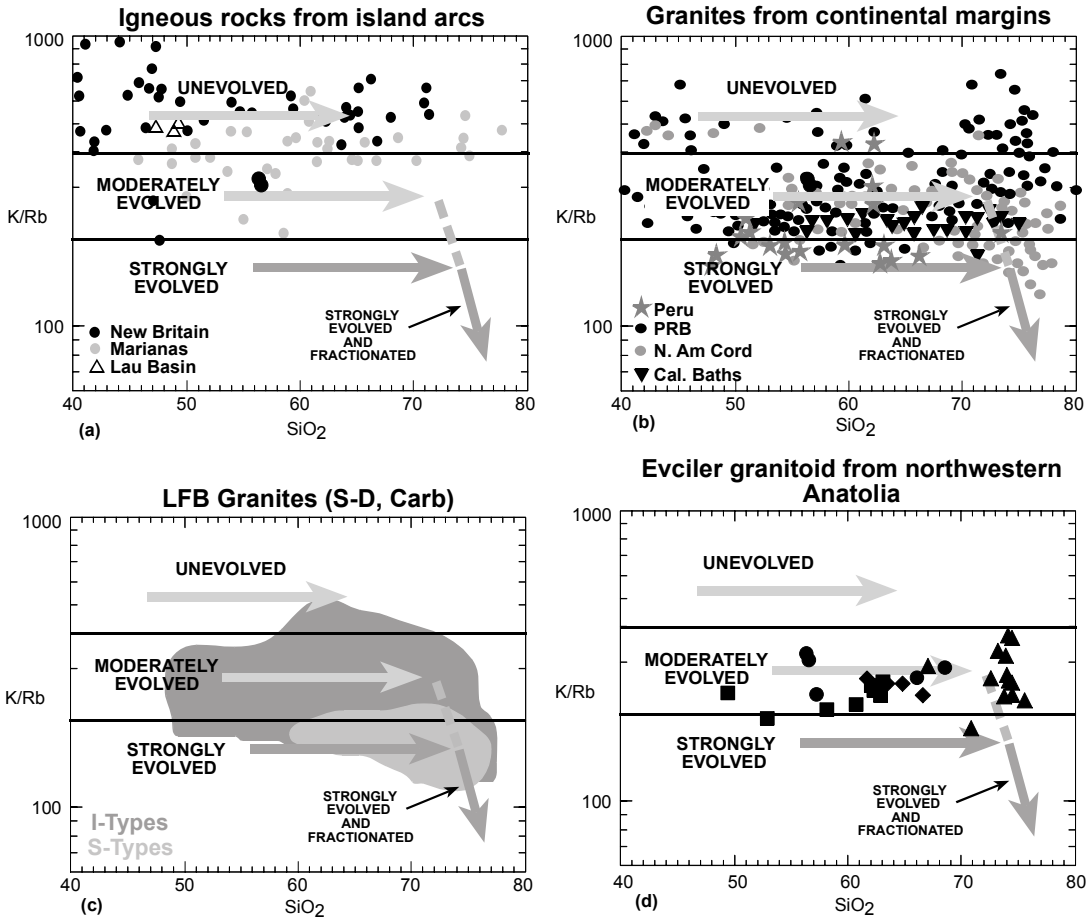

Figure 2.13. K/Rb classification scheme showing classification fields typical trends for (a) igneous rocks from island arcs, (b) granites from continental margins, (c) I- and S-type granites (all data from Blevin 2004) and (d) Evciler granitoid.

2.10.2 Oxygen Isotopic Constraint on Petrogenesis of Evciler Granitoid

For some granites, little or no interaction with external fluids seems to have taken place (e.g., the Berridale batholith in eastern Australia, O'Neil & Chappell 1977; Manaslu granite, Himalaya, France-Lanord *et al.* 1988) and the whole-rock oxygen isotope ratios probably reflect quite closely the original magma values. Other granites have been subjected to extensive exchange with external fluids which has changed the original magmatic $\delta^{18}O$ values. Some Hercynian granites of the Pyrenees (Wickham & Taylor 1987), the Idaho batholith and many other Tertiary

batholiths of the western USA (Criss *et al.* 1991) and some Caledonian granites of Britain (Harmon 1984) can be classified in this category.

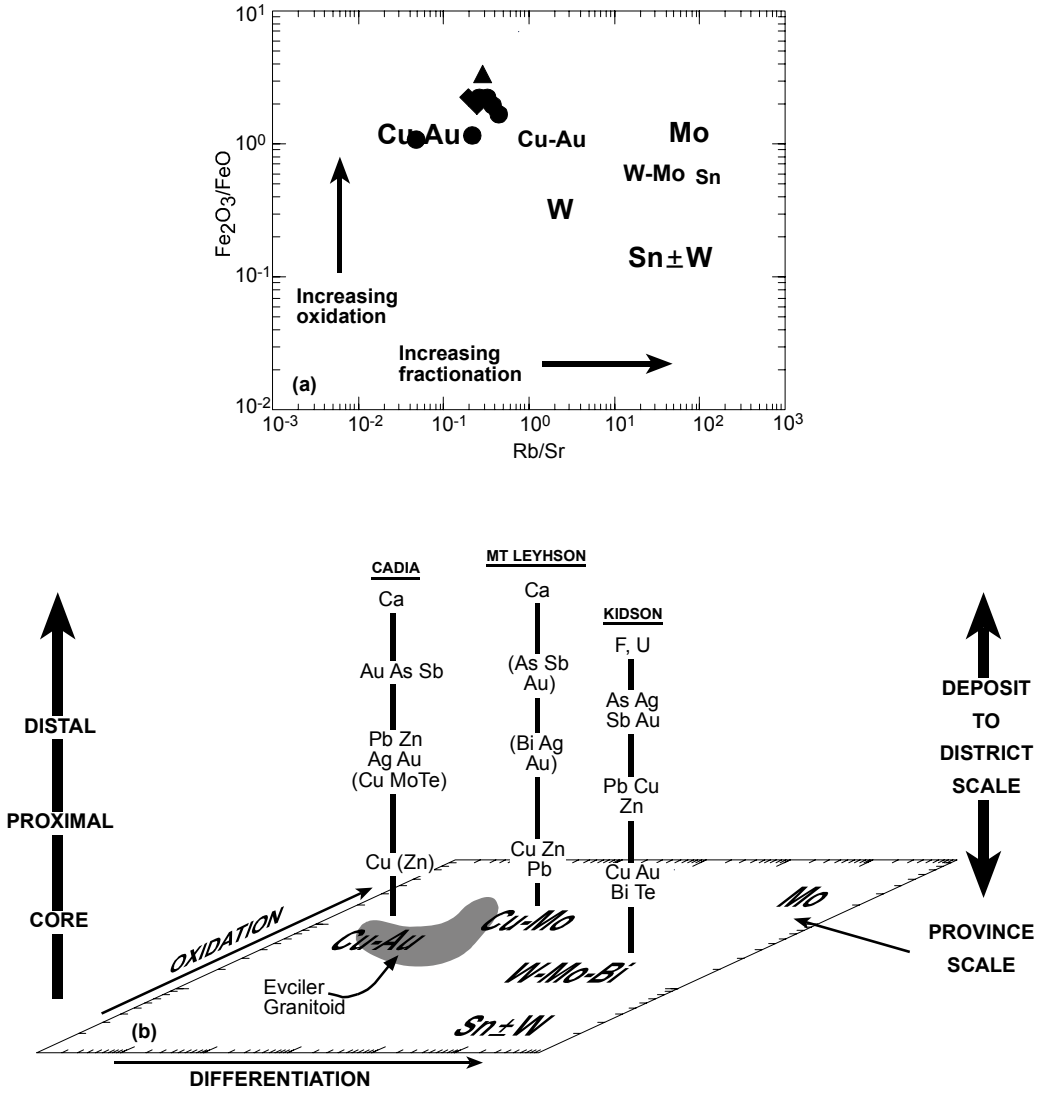

Figure 2.14. (a) Fe_2O_3/FeO vs Rb/Sr diagram for the Evciler granitoid and (b) conceptual diagram illustrating relationships between metal zonation at the deposit or district scale, and how it relates back to higher-temperature proximal igneous-centred systems (Cu-Au, Cu-Mo, W-Mo, Sn-W, Mo) (Blevin 2004).

Whole rock samples from Evciler granitoid, collected only a few meters from the skarn mineralization have $\delta^{18}O$ between 4.8 and 6.0 ‰, with the most altered samples having lowest $\delta^{18}O$ value like other world skarn granitoids (e.g., Edough granitoid, Annaba, Northeast Algeria; Laouar *et al.* 2002). In order to create granites

with low $\delta^{18}O$ values observed in the Evciler samples, it is necessary to call upon hydrothermal alteration. Compared to normal granites, meteoric waters have relatively low $\delta^{18}O$ values (Figure 2.15). During water-rock interaction at the Evciler district, each isotopic value of the granitoid and meteoric water normalize the value of other as $\delta^{18}O$ is exchanged. Thus, the Evciler granitoid $\delta^{18}O$ values would decrease to lower values during hydrothermal alteration and skarnization at the district.

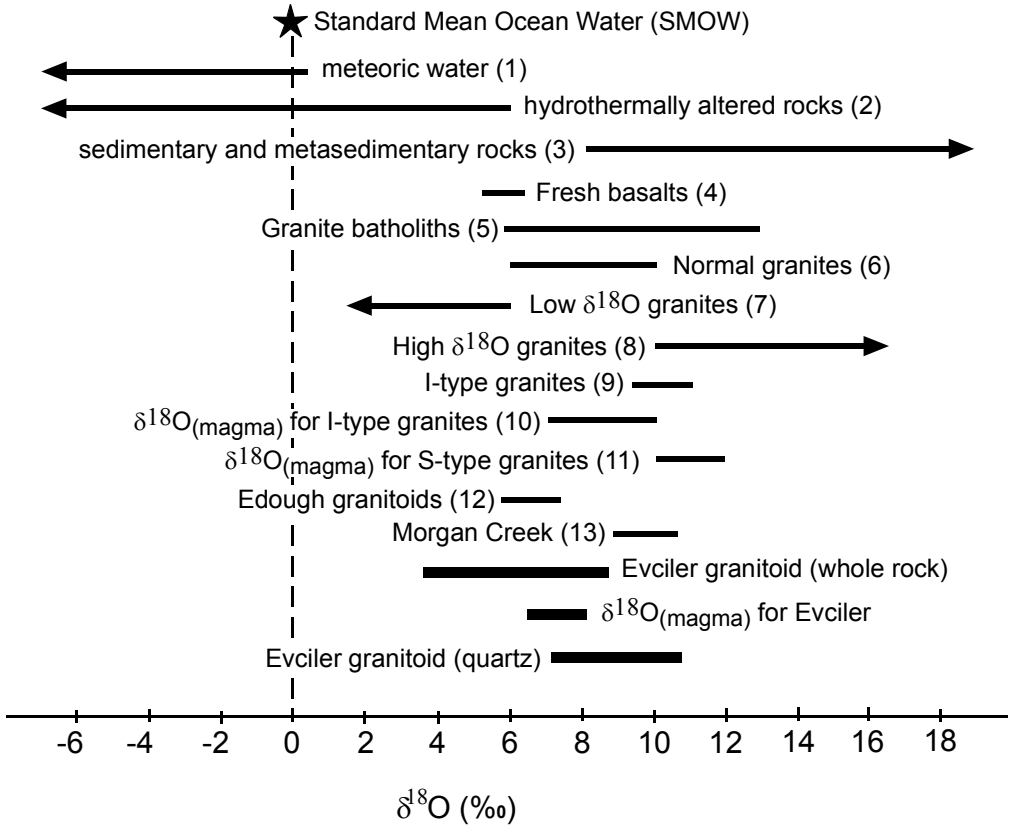

Figure 2.15. Oxygen isotopic composition of the Evciler granitoid compared to those of typical terrestrial materials and other world skarn granitoids. (1) Craig (1961); (2) Ohmoto (1986); (3), (4) and (5) Taylor & Sheppard (1986); (6), (7) and (8) Taylor (1978); (9), (10) and (11) Harris *et al.* (1997); (12) Laouar *et al.* (2002); and (13) Brown *et al.* (1985).

$\delta^{18}O$ values of the original magma of the Evciler granitoid (δ_{magma}), calculated from quartz $\delta^{18}O$ values, range from 6.0 to 8.0 ‰, suggesting similar to those of slowly cooled coarse-grained I-type granites (e.g., Cape granites, Harris *et al.* 1997)

(Figure 2.15). Although, range of $\delta^{18}O$ value for quartz (7.2-10.9 ‰) of fresh granitoid samples is normal for I-type granitic rocks, this range is too large for by simple magmatic differentiation (Sheppard 1986).

2.11. Conclusions

Major element chemistry indicates that the Evciler granitoid has a metaluminous, mildly peraluminous and calc-alkaline character. In terms of trace-element data, the Evciler granitoid is classified as VAG (volcanic arc granites) and syn-collision granites. In the study area two different rock types are observed: the mezocratic-type Evciler is quartz diorite to granodiorite in composition, whereas the leucocratic-type Evciler is monzogranite in composition and they both show I-type characteristics. Pyrrhotite-bearing calcic skarn mineralization occur at the contact between Evciler quartz diorite-granodiorite and marble lenses belong to the Kazdağ Massif at the south of the Evciler granitoid.

Oxygen isotope analyses of quartz and calculated δ_{magma} from the Evciler granitoid support I-type affinity as suggested by previous geochemical studies. The whole rock $\delta^{18}O$ values of the Evciler granitoid decrease toward the intrusive contact, which happens also to be the region closest to the pyrrhotite-bearing mineralization at the Evciler district. There is a significant evidence for the possibility of meteoric water hydrothermal alteration which generated low $\delta^{18}O$ values as down to 5.7 ‰.

Relative metal abundances in magmas and different types of intrusion-related deposits are a function of compositional evolution, fractionation and oxidation state. It is the core element association that most closely relates to magma composition. Cu-Au deposits are associated with oxidized, relatively unevolved to moderately evolved suites. The Evciler quartz diorite-granodiorite are characterized by relatively unevolved to moderately evolved and oxidized suite and are fairly close to Au-Cu deposits. The geochemical characteristics of the Evciler quartz diorite-granodiorite, Çavuşlu monzodiorite and Karaköy granodiorite are also similar to some of the Cu-,

Fe-, Cu-Au-, and Fe-Cu skarn granitoids in Canada, Indonesia, Spain and British Columbia. However, the geochemical characteristics of the Evciler monzogranite are similar to the averages for Sn- and Mo- skarn granitoids.

The results of this study suggest that the composition and petrologic evolution of the Evciler pluton are the primary controls on skarn alteration, mineralization, and metal content (e.g. copper, gold, iron). The combination of all these parameters can be used on a district to regional scale to interpret relationships between Evciler pluton and related ore deposits. However, the Evciler pluton and other young granitoids in western Anatolia are analoguous with Au-Cu association of the core metal associations, like Cadia district, Australia. Thus, the field relations and igneous petrology has a predictive capacity in being able to recognize potential for particular metallic element associations in poorly explored the Evciler pluton and other young granitoids from northwestern Anatolia.

2.12. References

Altherr, R., Henjes-Kunst, F., Matthews, A., Fiedrichsen, H., & Hansen, B.T. (1988). O-Sr isotopic variations in Miocene granitoids from the Aegean: Evidence for an origin by combined assimilation and fractional crystallization. *Contribution to Mineralogy and Petrology*, *100*, 528-541.

Bingöl, E. (1968). Constribution a l'etude geologique de la partie centrale et Sud-Est du masif de Kazdağ (Turqie). *PhD Thesis, Universite de Nancy, France*.

Bingöl, E. (1969). Kazdağ Masifi'nin merkezi ve güneydoğu kesiminin jeolojisi [Geology of central and southwestern parts of the Kazdağ Massif]. *MTA Dergisi*, *72*, 110-123 [in Turkish with English abstract].

Bingöl, E. (1977). Muratdağı jeolojisi ve anakayac birimlerinin petrolojisi [Geology of Muratdağı and petrology of rock units]. *Geological Society of Turkey Bulletin*, *20*, 13-67 [in Turkish with English abstract].

Bingöl, E. (1978). Explanatory notes to the metamorphic map of Turkey, *In.* Zwart, H.J. (eds), Me*tamorphic Map of Europe, Explanatory Text. Leiden, UNESCO*, Subcommission for the cartography of the metamorphic belts of the World, 148-154.

Bingöl, E., Akyürek, B., & Korkmazer, B. (1973). Biga yarımadasının jeolojisi ve Karakaya formasyonunun bazı özellikleri [Geology of the Biga Peninsula and some features of the Karakaya Formation]. *Cumhriyetin 50. Yılı Yerbilimleri Kongresi Tebliğleri*, MTA Ankara [in Turkish with English abstract].

Bingöl, E., Delaloye, M., & Ataman, G. (1982). Granitic intrusion in Western Anatolia: a contribution to the geodynamic study of this area. *Eclogae Geologicae Helvetiae*, *75*, 437-446.

Bingöl, E., Delaloye, M., Pişkin, Ö., & Genç, S. (1992). Significance of the granitoids Eastern and southern Marmara Sea within the framework of the regional geotectonic evolution. *International Symposium on the Geology of the Black Sea Region, Abstracts* 3.

Birkle, P. (1992). Petrologie-Geochem'e and Geochronogic des Miozanen Magmatismus auf der Biga-halbinhsel (Ezine, NW-Turkei). *Diplomarbiet an der Geowissenschaft Lichen* Fakultat der Eberhard-Karls-Universtat, Tübingen.

Blevin, P.L. (2004). Metallogeny of granitic rocks. *The Ishihara Symposium: Granites and Associated Metallogenesis, ©Geoscience Australia*, 1-4.

Blevin, P.L., & Chappell, B.W. (1992). The role of magma sources, oxidation states and fractionation in determining the granite metallogeny of eastern Australia. *Transactions of the Royal Society of Edinburgh: Earth Sciences, 83*, 305-316.

Bozkurt, E. (2004). Granitoid rocks of the southern Menderes Massif (southwestern Turkey): field evidence for Tertiary magmatism in an extensional shear zone. *International Journal of Earth Sciences, 93*, 52-71.

Bozkurt, E., & Park, R.G. (1994). Southern Menderes Massif: An incipient metamorphic core complex in Western Anatolia, Turkey. *Journal of Geological Society, London*, *151*, 213-216.

Bozkurt, E., Park, R.G., & Winchester, J.A. (1993). Evidence against the core/cover interpretation of the southern sector of the Menderes Massif, west Turkey. *Terra Nova*, *5*, 445-451.

Bozkurt, E., Winchester, J.A., & Park, R.G. (1995). Geochemistry and tectonic significance of augen gneisses from the southern Menderes Massif (West Turkey). *Geological Magazine*, *132*, 287-301.

Brown, P.E., Bowman, J.R., & Kelly, W.C. (1985). Petrologic and stable isotope constraints on the source and evolution of skarn-forming fluids at Pine Creek, California. *Economic Geology, 80*, 72-95.

Chappell, B.W., & White, A.J.R. (1974). Two contrasting granite types: expanded abstract. *Pacific Geology*, *8*, 173-174.

Chiba, H., Chacko, T., Clayton, R.N., & Goldsmith, J.R. (1989). Oxygen isotope fractionations involving diopside, forsterite, magnetite and calcite: application to geothermometry. *Geochimica Cosmochimica Acta*, *53*, 2985-2995.

Craig, H. (1961). Standard for reporting concentrations of deuterium and oxygen-18 in natural waters. *Science*, *133*, 1833-1834.

Criss, R.E., Fleck, R.J., & Taylor, H.P. (1991). Tertiary meteoric hydrothermal systems and their relation to ore deposition, northwestern United States and southern British Columbia. *Journal of Geophysical Research, 96*, 13335-13356.

Debon, F., & Le Fort, P. (1983). A chemical-mineralogical classification of common plutonic rocks and associations. *Transactions of the Royal Society of Edinburgh: Earth Sciences*, *73*, 135-149.

Delaloye, M., & Bingöl, E. (2000). Granitoids from Western and Northwestern Anatolia: Geochemistry and modeling of geodynamic evolution. *International Geology Review*, *42*, 241-268.

Duru, M., Pehlivan, Ş., Şentürk, Y., Yavaş, F., & Kar, H. (2004). New results on the lithostratigraphy of the Kazdağ Massif in Northwest Turkey. *Turkish Journal of Earth Sciences*, *13*, 177-186.

Einaudi, M.T., Meinert, L.D., & Newbery, R.J. (1981). Skarn deposits: *Economic Geology. 75th Anniversary Volume, Economic Geology Publication Co.*, Lencester Pres Inc., 317-391.

Erdoğan, B., & Güngör, T. (2004). The problem of the core-cover boundary of the Menderes Massif and an emplacement mechanism for regionally extensive gneissic granites, Western Anatolia (Turkey). *Turkish Journal of Earth Sciences*, *13*, 15-36.

France-Lanord, C., Sheppard, S.M.F., & Le Fort, P. (1988). Hydrogen and oxygen isotope variations in the High Himalaya peraluminous Manaslu leucogranite: evidence for heterogeneous sedimentary source. *Geochimica Cosmochimica Acta*, *52*, 513-526.

Genç, Ş.C. (1998). Evolution of the Bayramiç magmatic complex, northwestern Anatolia. *Journal of Volcanology and Geothermal Research*, *85*, 233-249.

Gessner K., Piazolo, S., Güngör, T., Ring, U., Kröner, A., & Passchier, C.W. (2001). Tectonic significance of deformation patterns in granitoid rocks of the Menderes nappes, Anatolide belt, southwest Turkey. *International Journal of Earth Sciences* , *89*, 766-780.

Gessner K., Collins, A.S., Ring, U., & Güngör, T. (2004). Structural and thermal history of poly-orogenic basement: U-Pb geochronology of granitoid rocks in the southern Menderes Massif, Western Turkey. *Journal of Geological Society, London*, *161*, 93-101.

Giletti, B.J. (1986). Diffusion effects on oxygen isotope temperatures of slowly cooled igneous and metamorphic rocks. *Earth and Planetary Science Letters*, *77*, 218-228.

Göncüoğlu, M.C., Kuwahara, K., Tekin, U.K., & Turhan, N. (2004). Upper Permian (Changxingian) Radiolarian cherts within the Clastic Successions of the "Karakaya Complex" in NW Anatolia. *Turkish Journal of Earth Sciences*, *13*, 201-213.

Gözler, M.Z. (1986). Kazdağ batısı Mıhlı dere vadisinin jeolojik ve petrografik incelemesi [Geological and petrographic investigation of Mıhlı Dere valley, western Kazdağ]. *Geological Society of Turkey Bulletin*, *29*, 133-142 [in Turkish with English abstract].

Gülen, L. (1990). Isotopic characterization of Aegean magmatism and geodynamic evolution of the Aegean subduction. *In:* Savaşcın, M.Y. & Eronat, A.H. (eds), *IESCA Proceedings*, İzmir, Turkey, *2*, 143-166.

Harmon, R.S. (1984). Stable isotope geochemistry of Caledonian granitoids from the British Isles and east Greenland. *Physics of the Earth and Planetary Interiors*, *35*, 105-120.

Harris, N.B.W., Pearce, J.A., & Tindle, A.G. (1986). Geochemical characteristics of collision-zone magmatism. *In:* Coward, M.P. & Ries, A.C. (eds), *Collision Tectonics, Geological Society, London, Special Publications*, *19*, 67-81.

Harris, N.B.W., Kelley, S., & Okay, A.I. (1994). Post-collisional magmatism and tectonics in northwest Anatolia. *Contributions to Mineralogy and Petrology*, *117*, 241-252.

Harris, C., Faure, K., Diamond, R.E., & Scheepers, R. (1997). Oxygen and hydrogen isotope geochemistry of S- and I-type granitoids: the Cape granite suite, south Africa. *Chemical Geology*, *143*, 95-114.

Irvine, I.C., & Baragar, W.R.A. (1971). A guide to chemical classification of the common volcanic rocks. *Canadian Journal of Earth Sciences*, *8*, 523-548.

Ishihara, S., & Sasaki, A. (1991). Ore deposits related to granitic magmatism in Japan: a magmatic point of view. *Episodes* 14, 286-292.

Işık, V., & Tekeli, O. (2001). Late orogenic crustal extension in the northern Menderes Massif (western Turkey): evidence for metamorphic core complex formation. *International Journal of Earth Sciences*, *89*, 757-765.

Işık, V., Tekeli, O., & Seyitoğlu, G. (2004). The $^{40}Ar/^{39}Ar$ age of extensional ductile deformation and granitoid intrusion in the northern Menderes core complex: implications for the initiation of extensional tectonics in western Turkey. *Journal of Asian Earth Sciences*, *23*, 555-566.

Jenkin, G.R.T., Fallick, A.E., Farrow, C.M., & Bowes, G.M. (1991). COOL: A FORTRAN 77 computer program for modelling stable isotopes in cooling closed systems. *Computer Geosciences*, *17*, 391-412.

Karacık, Z., & Yılmaz, Y. (1998). Geology of the ignimbrites and the associated volcano-plutonic complex of the Ezine area, northwestern Anatolia. *Journal of Volcanology and Geothermal Research*, *85*, 251-264.

Keith, J.D., Van Middelaar, W.T., Clark, A.H., & Hodgson, C.J. (1989). Granitoid textures, compositions and volatile fugacities associated with the formation of tungsten-dominated skarn deposits. *In*: Robertson, J.M. (eds), *Ore Deposition Associated with Magmas, Reviews in Economic Geology*, *4*, 235-250.

Koralay, O.E., Satır, M., & Dora, O.Ö. (2001). Geochemical and geochronological evidence for Early Triassic calc-alkaline magmatism in the Menderes Massif, western Turkey. *International Journal of Earth Sciences*, *89*, 822-835.

Koralay, O.E., Dora, O.Ö., Chen, F., Satır, M., & Candan, O. (2004). Geochemistry and Geochronology of Orthogneisses in the Derbent Alaşehir) Area, Eastern Part of the Ödemiş-Kiraz Submassif, Menderes Massif: Pan-African Magmatic Activity. *Turkish Journal of Earth Sciences* , *13*, 37-61.

Kwak, T.A.P., & White, A.J.R. (1982). Contrasting W-Mo-Cu and W-Sn-F skarn types and related granitoids. *Mining Geology*, *32*, 339-351.

Laouar, R., Boyce, A.J., Ahmed-Said, Y., Ouabadi, A., Fallick, A.E., & Toubal, A. (2002). Stable isotope study of the igneous, metamorphic and mineralized rocks of the Edough complex, Annaba, Northeast Algeria. *Journal of African Earth Sciences*, *35*, 271-283.

Lentz, D.R., Walker, J.A., & Stirling, J.A.R. (1995). Millstream Cu-Fe skarn deposits: an example of a Cu-bearing magnetite-rich skarn system in northern New Brunswick. *Exploration and Mining Geology, 4*, 15-31.

Martin-Izard, A., Fuertes Fuente, M., Cepedal, A., Moreiras, D., Nieto, J.G., Maldonado, C., & Pevida, L.R. (2000). The Rio Narcea gold belt intrusions: geology, petrology, geochemistry and timing. *Journal of Geochemical Exploration*, *71*, 103-117.

McKenzie, D., & Yılmaz, Y. (1991). Deformation and volcanism in Western Turkey and the Aegean. *Bulletin of Technical University of İstanbul*, *44*, 345-373.

Meinert, L.D. (1983). Variability of skarn deposits – Guides to Exploration. *In:* Boardman, S.J. (eds), *Revolution in the Earth Sciences*. Kendall-Hunt Publishing, Dubuque, Iowa, 301-316.

Meinert, L.D. (1984). Mineralogy and petrology of iron skarns in western British Columbia, Canada. *Economic Geology*, *79*, 869-882.

Meinert, L.D. (1990). Skarn deposits in Nevada – Geology, mineralogy and petrology of Au, Cu, W, and Zn skarns. *In*: Meinert, L.D., Myers, G.L. & Brooks, J.W. (eds), *Geological Society of Nevada Fieldtrip 2 Guidebook*. Geological Society of Nevada, Reno. NV, 41-72.

Meinert, L.D. (1992). Skarns and skarn deposits. *Geoscience Canada*, *19*, 145-162.

Meinert, L.D. (1993). Igneous petrogenesis and skarn deposits. *In:* Kirkham, R.V., Sinclair, V.D., Thorpe, R.I., Duke, J.M. (eds), Mineral Deposit Modelling. *Geological Association of Canada, Special Puplications*, *40*, 569-583.

Meinert, L. D. (1995). Compositional variation of igneous rocks associated with skarn deposits - Chemical evidence for a genetic connection between petrogenesis and mineralization. *In.* Thompson, J. F. H. (eds), Magmas, fluids, and ore deposits. *Mineralogical Association of Canada, Short Course Series, 23*, 401-418.

Meinert, L.D. (1997). Application of skarn deposit zonation models to mineral exploration. *Exploration and Mining Geology*, *6*, 185-208.

Meinert, L.D., Brooks, J.W., & Myers, G.L. (1990). Whole rock geochemistry and contrast among skarn types. *In:* Meinert, L.D., Myers, G.L. & Brooks, J.W. (eds), Skarn Deposits in Nevada. *Great Basin Symposium – Geology and Ore Deposits of the Great Basin. Geological Society of Nevada Field 2 Guidebook.* Geological Society of Nevada, Reno, NV, 179-192.

Meinert, L.D., Hefton, K.K., Mayes, D., & Tasıran, I. (1997). Geology, zonation and fluid evolution of the Big Gossan Cu-Au skarn deposit, Ertsberg district, Irian Jaya. *Economic Geology*, *92*, 509-526.

Meza-Figueroa, D., Valencia-Moreno, M., Valencia, V.A., Ochoa-Landin, L., Perez-Segura, E., & Diaz-Salgado, C. (2003). Major and trace element geochemistry and $^{40}Ar/^{39}Ar$ geochronology of Laramide plutonic rocks associated with gold-bearing Fe skarn deposits in Guerrero state, southern Mexico. *Journal of South American Earth Sciences*, *16*, 205-217.

Moore, C.E., & Lentz, D.R. (1996). Copper skarn-associated felsic intrusive rocks in the McKenzie Gulsh area (NTS 21o/10) Restigouche County, New Brunswick. *In.* Carroll, B.M W. (eds), *Current Research* 1995. New Brunswick Department of Natural Resources and Energy, Mineral and Energy Division, Fredericton, New Brunswick , *96*, 121-153.

Naldrett, A.J. (1992). A model for the Ni-Cu-PGE ores of the Noril'sk region and its application to other areas of flood basalt. *Economic Geology*, *87*, 1945-1962.

Newberry, R.J. (1987). Use of intrusive and calc-silicate compositional data to distinguish contrasting skarn types in the Darwin polymetallic skarn district, CA, U.S.A. *Mineralium Deposita*, *22*, 207-215.

Newberry, R. J., & Swanson, S. E. (1986). Scheelite skarn granitoids: an evaluation of the roles of magmatic source and process. *Ore Geology Reviews*, *1*, 57-58.

Newberry, R.J., Burns, L.E., Swanson, S.E., & Smith, T.E. (1990). Comparative petrologic evolution of the Sn and W granites of the Fairbanks-Circle area, Interior Alaska. *In:* Stein, H.J. & Hannah, J.L. (eds). *Ore-bearing Granite Systems; Petrogenesis and Mineralizing Processes, Geological Society of America Special Publications*, *246*, 121-142.

Nicolescu, D., Cornell, D.H., & Bojar, A.N. (1999). Age and tectonic settings of Bocşa and Ocna de Fier-Dogneca granodiorites (southwest Romania) and of associated skarn mineralization. *Mineralium Deposita, 34*, 743-753.

Ohmoto, H. (1986). Systematics of metal ratios and sulfur isotopic ratios in low-temperature basemetal deposits. *Terra Cognita*, *6*, 134-135.

Okay, A.İ., Siyako, M., & Bürkan, K.A. (1990). Biga Yarımadası'nın jeolojisi ve tektonik evrimi [Geology and tectonic evolution of the Biga Peninsula]. *Türkiye Petrol Jeologları Derneği Bülteni, I 3*, 83-121 [in Turkish with English abstract].

Okay, A.İ., Satır, M., Maluski, H., Siyako, M., Metzger, R., & Akyüz, S. (1996). Paleo- and Neo-Tethyan events in Northwestern Turkey: geological and geochronological constraints. *In:* An, Y. & Harrison, M. (eds), *Tectonics of Asia*. Cambridge University Press, 420-441.

Okay, A.İ., & Satır, M. (2000). Coeval plutonism and metamorphism in a latest Oligocene metamorphic core complex in northwest Turkey. *Geological Magazine*, *137*, 495-516.

Okay, A.İ., & Altıner, D. (2004). Uppermost Triassic Limestone in the Karakaya Complex- Stratigraphic and Tectonic Significance. *Turkish Journal of Earth Sciences*, *13*, 187-199.

Okay, A.İ., & Göncüoğlu, M.C. (2004). The Karakaya Complex: review of data and concepts. *Turkish Journal of Earth Sciences*, *13*, 77-95.

O'Neil, J.R., & Chappell, B.W. (1977). Oxygen and hydrogen isotope relations in the Berridale batholith. *Journal of Geological Society of London*, *133*, 559-571.

Öngen, S. (1992). Les échances métasomatiques entre granitoides et encaissant particuliers (calcaires, dolomies, ultrabasites, series manganiferes): I'example de la Turquie-NW. *Doctorat These. Université de Nancy, Faculté des Sciences de la Terre,* 554 p.

Paktunc, A. D. (1990). Origin of podiform chromite deposits by multistage melting, melt segregation and magma mixing in upper mantle. *Ore Geology Reviews*, *5*, 211-222.

Peacock, M.A. (1931). Classification of igneous rock series. *Journal of Geology*, *39*, 54-67.

Pearce, J. A., Harris, N. B., W., & Tindle, A. G., (1984). Trace-element discrimination diagrams for the tectonic interpretation of granitic rocks. *Journal of Petrology*, *25*, 956-983.

Pickett, E.A., & Robertson, A.H.F. (2004). Significance of the Volcanogenic Nilüfer Unit and Related Components of the Triassic Karakaya Complex for Tethyan Subduction/Accretion Processes in NW Turkey. *Turkish Journal of Earth Sciences*, *13*, 97-143.

Ray, G.E., Webster, I.C.L., & Ettlinger, A.D. (1995). The distribution of skarns in British Columbia and the chemistry and ages of their related plutonic rocks. *Economic Geology*, *90*, 920-937.

Raymond, L.A. (1995). *Petrology: The Study of Igneous, Sedimentary and Metamorphic Rocks.* WC Brown, 742 p.

Rogers, N.W., Hawkesworth, C.J., Parker, R.J., & Marsh, J.S. (1985). The geochemistry of potassium lavas from Vulsini, central Italy and implications for mantle enrichment processes beneath the Roman region. *Contributions to Mineralogy and Petrology*, *90*, 244-257.

Rumble, D.III., & Hoering, T.C. (1994). Analysis of oxygen and sulfur isotope ratios in oxide and sulfide minerals by spot heating with a carbon dioxide laser in a fluorine atmosphere. *Accounts of Chemical Research*, *27*, 237-241.

Sharp, Z. D. (1990). A laser-based microanalytical method for in situ determination of oxygen isotope ratios in silicates and oxides. *Geochimica Cosmochimica Acta*, *54*, 1353-1357.

Sheppard, S.M.F. (1986). Characterization and isotopic variations in natural waters. *Mineralogy*, *16*, 165-183.

Shimazaki, H. (1975). The ratios of Cu/Zn-Pb of pyrometasomatic deposits in Japan and their genetic implications. *Economic Geology*, *70*, 717-724.

Shimazaki, H. (1980). Characteristics of skarn deposits and related acid magmatism in Japan. *Economic Geology*, *75*, 173-183.

Srivastava, K.P., & Sinha, A.K. (1997). Geochemical characterization of tungsten bearing granites from Rajasthan, India. *Journal of Geochemical Exploration*, *60*, 173-184.

Streckeisen, A. (1976). To each plutonic rock its proper name. *Earth Science Reviews, 12*, 1-33.

Şengör, A. M. C., & Yılmaz, Y. (1981). Tethyan evolution of Turkey: a plate tectonic approach. *Tectonophysics*, *75*, 181-241.

Şengör, A.M.C., Cin, A., Rowley, D. B., & Nie, S.Y. (1993). Space-time patterns of magmatism along the tethysides: a preliminary study. *Journal of Geology, 101*, 51-84.

Taylor, H.P. (1968). The oxygen isotope geochemistry of igneous rocks. *Contributions to Mineralogy and Petroogy, 19*, 1-71.

Taylor, H.P. (1978). Oxygen and hydrogen isotope studies of plutonic granitic rocks. *Earth and Planetary Science Letters*, *38*, 177.

Taylor, H.P., & Sheppard, S.M.F. (1986). Igneous rocks: I Processes of isotopic ractionation and isotope systematics. *In:* Valley, J.W., Taylor, H.P. & O'Neil, J.R. (eds). *Stable Isotopes in High-Temperature Geological Processes. Reviews in Mineralogy, 16*, 227-271.

Wichkam, S.M., & Taylor, H.P. (1987). Stable isotope evidence for large-scale seawater infiltration in a regional metamorphic terrane: the Trois Seigneurs Massif, Pyrenees, France. *Contribution to Mineralogy and Petrology, 91*, 122-137.

Wilson, M. (1989). *Igneous Petrogenesis.* A Global Tectonic Approach. Chapman and Hall, London.

Yılmaz, Y. (1989). An approach to the origin of young volcanic rocks of western Turkey. *In:* Şengör, A.M.C. (eds), *Tectonic Evolution of the Tethyan Region.* Kluwer Academic Publications. The Hague, 159-189.

Yılmaz, Y. (1990). Comparison of the young volcanic associations of the west and east Anatolia under the compressional regime: a review. *Journal of Volcanology and Geothermal Research, 44*, 69-87.

Yılmaz, Y. (1995). Ege bölgesinde genç magmatizmanın oluşumu ile litosferin evrimi arasındaki ilişki üzerine düşünceler [Remarks on the relation between formation of young magmatism and evolution of the lithosphere in Aegean region]. *Jeofizik, 9*, 107-110 [in Turkish with English abstract].

Yılmaz, Y. (1997). Geology of western Anatolia. Active tectonics of Northwestern Anatolia. *In: The Marmara Poly-Project.* VDF, Hochschulverlag Ag an der ETH, Zürich, 1-20.

Yılmaz, Y., & Karacık, Z. (2001). Geology of the northern side of the gulf of Edremit and its tectonic significance for the development of the Aegean grabens. *Geodynamica Acta, 14*, 31-43.

Zharikov, V.A. (1970). Skarns. *International Geology Review, 12*, 541-559, 619-647 and 760-775.

CHAPTER THREE
SKARN ALTERATION AND Au-Cu MINERALIZATION ASSOCIATED WITH TERTIARY GRANITOIDS IN NORTHWESTERN TURKEY: EVIDENCE FROM EVCILER GRANITOID, KAZDAĞ MASSIF

This chapter was submitted to the Economic Geology, edited by Mark Hannington, as; Yücel Öztürk, Y., & Helvacı, C. Skarn Alteration and Au-Cu Mineralization Associated with Tertiary Granitoids in Northwestern Turkey: Evidence from Eevcıler Granitoid, Kazdağ Massif.

3.1 Abstract

The Evciler district, located in Kazdağ of northwest Anatolia (Turkey), has the following features; (1) alteration and mineralization are related to an elliptical I-type, magnetite-series, metaluminous, calc-alkaline body, which intrudes the Kazdağ Massif, with the long axis trending WSW-ENE; (2) skarns have an oxidized mineralogy dominated by garnet ($Ad_{70-50}Gr_{30-50}$), clinopyroxene ($Hd_{50-75}Di_{50-25}$), epidote, amphibole and chlorite; (3) skarn at Evciler contains up to 80 percent sulfides (pyrrhotite>>pyrite+chalcopyrite); (4) massive pyrrhotite-bearing mineralization replaces prograde skarn and marble.

At least two paragenetic stages of skarn formation and ore deposition have been recognized; stage-I, clinopyroxene ± garnet ± scapolite ± quartz; stage-II, amphibole ± epidote ± chlorite ± quartz ± calcite; and magnetite + pyrrhotite + chalcopyrite ± pyrite.

Stage-I mineral assemblages represent early skarn formation and are dominated by the anhydrous minerals, clinopyroxene and garnet. Stage-II minerals represent late skarn-forming phases and replace early mineral assemblages. Microprobe analyses indicate that the majority of the skarn minerals are calcic and have high Fe^{3+}/Fe^{2+}. Clinopyroxene is diopside rich, whereas garnet is andradite rich. Chemistry of clinopyroxene and garnet suggest that the Evciler skarn occurrence was formed under relatively oxidized conditions. Overall, Evciler skarn is similar to worldwide Cu-Au-, Fe-bearing skarn systems emplaced at shallow levels.

Keywords. Alteration, calcic skarn, Au-Cu mineralization, Evciler pluton, Kazdağ

3.2 Introduction

Skarns are known to carry economically significant deposits of W, Sn, Cu, Mo, Fe, Zn, Pb and are also considered potential sources for Co, Au, Ag, Bi, Sn, Be, F, B, U and rare earth elements (Einaudi et al., 1981; Meinert, 1992, 1993; Misra, 2000). Skarns are characterized by variegated and distinct mineral assemblages (Meinert, 1993; Misra, 2000) whose mineralogical aspects have attracted many scientific studies (Deer et al., 1993), and have provided constraints for the characteristics and genesis of skarns and skarn deposits (e.g., Gaspar and Inverno, 2000; Zaw and Singoyi, 2000).

Several studies have been published on granitic rocks to emphasize the geodynamic evolution of western and northwesten Anatolia (Altherr *et al.* 1988; Bingöl 1977 1978; Bingöl *et al.* 1982; Delaloye & Bingöl 2000; Genç 1998; Gülen 1990; Harris *et al.* 1994; Karacık & Yılmaz 1998; McKenzie & Yılmaz 1991; Okay *et al.* 1996; Şengör & Yılmaz 1981). Although similar skarn-style mineralization is known around the Evciler granitic pluton, there has been relatively little scientific study of the deposits or associated skarn and mineralization. Skarn zones are developed in the northern part of the Evciler pluton, and include the wollastonite-dominated skarn of Karaköy, studied in detail by Öngen (1992). The Karaköy skarn consists of calcic garnet, wollastonite, epidote, clinopyroxene, calcite, tremolite-actinolite, and quartz.

The recently identified skarn is in the southern part of the Evciler granitic pluton (Öngen, 1992) (Figure 3.1). Although there was a Cu and Au mine in the Evciler district only in 1996. Eurogold Co. were detailed geochemical surveys made to identify anomalies caused by hydrothermal alteration. Copper and gold anomalies were located within the exoskarn. A geochemical study of stream sediments and rocks delineated Au, Cu anomalies in the area. The alteration zones at the Evciler have not been studied yet, but extensive alteration and mineralization in contact between igneous rock and Kazdağ metamorphic suite and related skarns enabled detailed study of the hydrothermal system.

In this paper, we focus on the Evciler deposit, a Cu-Au skarn-type deposit. The skarn consists dominantly of garnet- calcic pyroxene assemblages; typical magnesian minerals such as forsterite, monticellite, spinel and serpentine are absent. We supplements geological and petrographic features with analytical data obtained by electron-probe microanalysis (EPMA) of the skarn mineral. We summarize the geology and style of mineralization in the Evciler district. We also draw upon the similarities of this occurrence with the other skarns of the world, some of which are well known for their ore potential, as described by Einaudi et al. (1981), Kwak (1994), Meinert (1992) and Newberry (1998).

3.3 Geological Setting

The high-grade metamorphic rocks of the Kazdağ Group, exposed in the Kazdağ Range, crop out as a tectonic window in the overlying Karakaya Ophiolitic Complex in northwestern Turkey. The Kazdağ group forms a doubly plunging, NE-SW-trending anticlinorium. Duru et al. (2004) have subdivided the metamorphic suite into four formations. The lowermost unit is the Fındıklı Formation, which comprises amphibole gneiss, marble and minor amphibolite. This unit crops out mainly in the southern part of the Kazdağ Massif. The overlying unit, comprising metadunite and orthoamphibolite, is the Tozlu Formation, which in turn is overlain by the Sarıkız marble. The uppermost unit, which crops out in the northern parts of Kazdağ Massif, is the Sutuven Formation which comprises sillimanite gneiss, migmatite and minor marble, amphibolite and granitic gneiss.

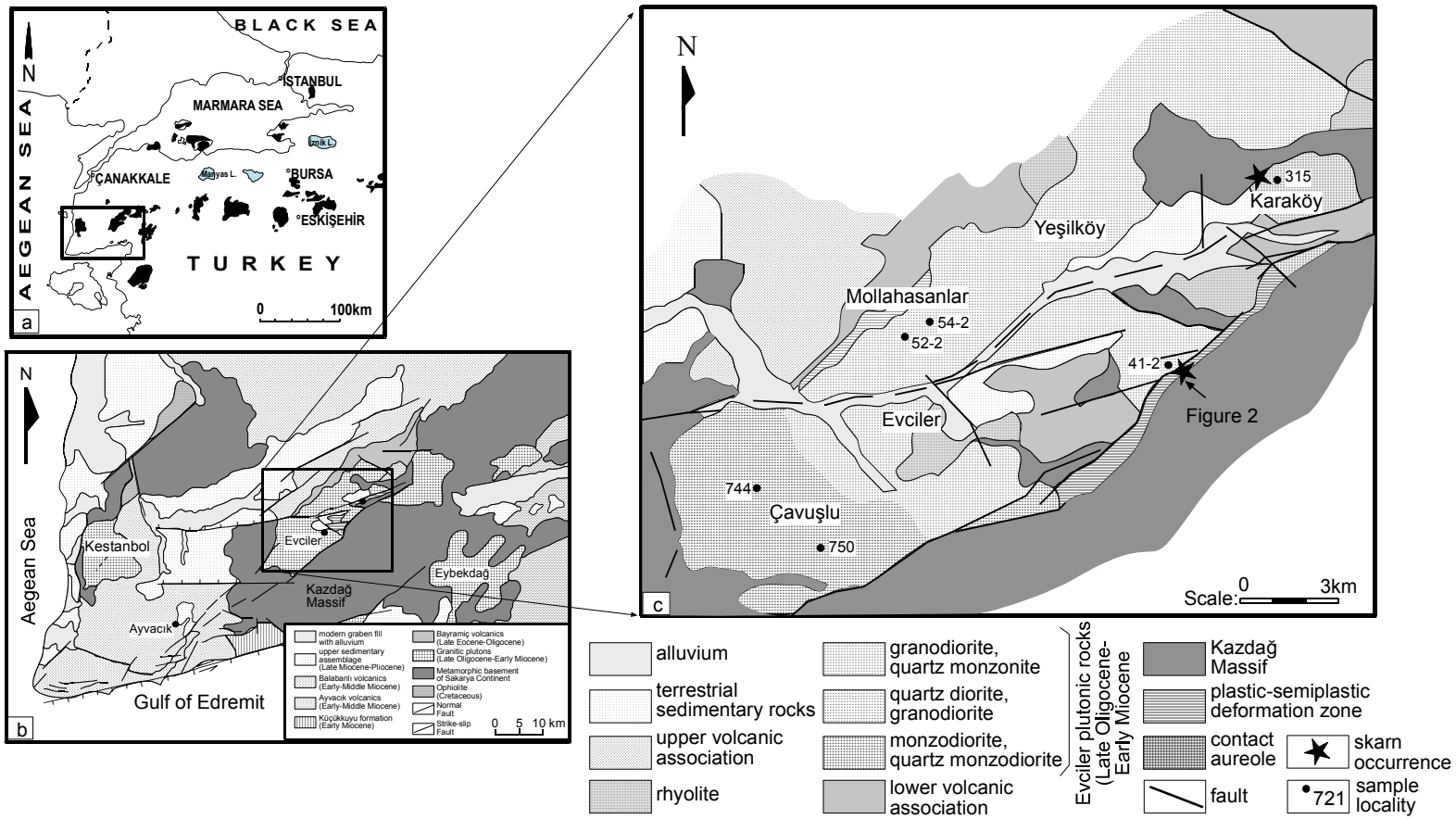

Figure 3.1. (a) Geographic location of the study area; (b) regional geologic map showing location of the Evciler district (simplified fromYılmaz & Karacık (2001)); (c) geologic map of the Evciler district (simplified from Genç (1998)).

The Sutuven Formation rests with a sharp contact on the Sarıkız marble and Fındıklı Formation, and is intruded by Oligo-Miocene Evciler granodiorite. The Sutuven Formation comprises mainly grey, dark grey and brown, well-banded quartzofeldspathic gneisses. In these gneisses, which constitute the dominant lithology, there are thin horizons and lenses marble, amphibolite and granitic gneiss.

The metamorphism in the Kazdağ Group has been dated using zircon Pb-Pb and mica Rb-Sr and K-Ar methods on gneisses from the Fındıklı and Sutuven formations (Duru et al., 2004). Pb-Pb data from the gneisses yield Mid-Carboniferous ages (308±16 Ma, Okay et al., 1996), whereas the biotite and muscovite Rb-Sr and K-Ar ages are Oligo-Miocene (19-22 Ma, Bingöl, 1968, 1969; Okay and Satır, 2000). These isotopic data have been interpreted as indicating two periods of high-grade metamorphism; the initial one during the Mid-Carboniferous and a later accompanying the emplacement of the granitoid. The P-T conditions of the high-grade metamorphism have been estimated as 640±50 ^{o}C and 5±1 kbar (Okay and Satır, 2000).

A zone of skarn mineralization containing pyrrhotite, chlorite, actinolite, garnet, pyroxene and epidote is located in Ayazma Dere 5 km SE of Evciler (Figure 3.2). The pyrrhotite-rich skarn occurs intermittently for some 600 m along the contact between gneiss and marble of the Sutuven Formation; it is 2 to 3 m thick. Distal metasomatic skarn mineralization is developed up to 150 m away from the main zone along the contact of the marble and the gneiss, now altered to calc-silicate and marbles intercalated with amphibolite, indicating the mineralization to be an exoskarn.

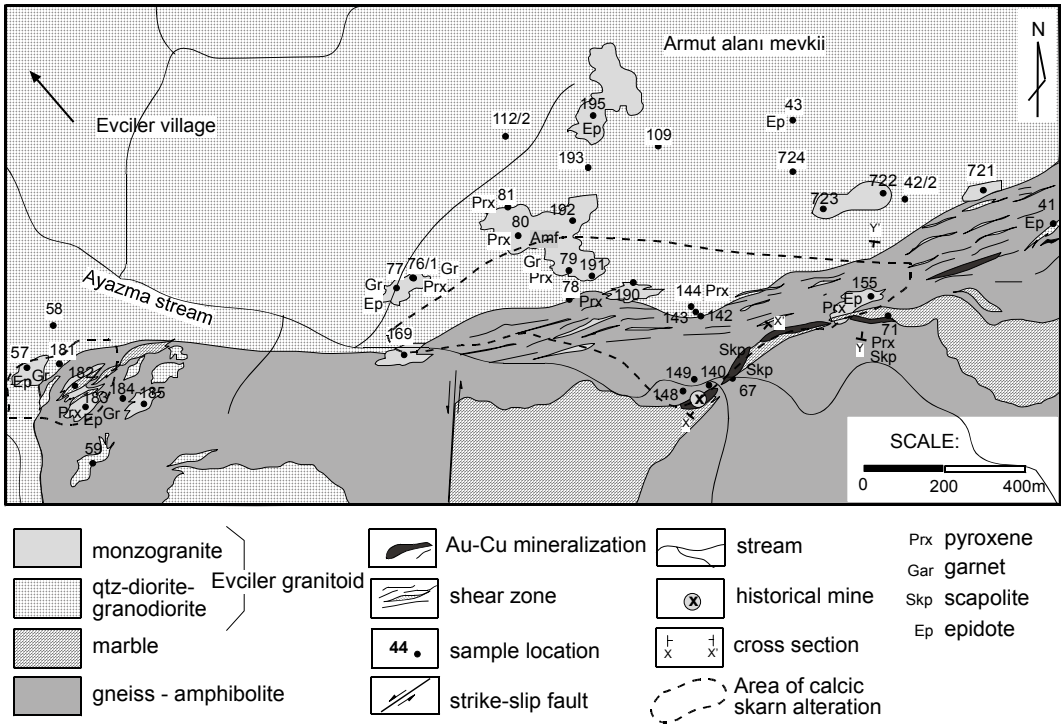

Figure 3.2. Geological map showing location of the skarn alteration and mineralization at the Evciler district.

3.3.1 Igneous Rock

During the Oligocene to Middle Miocene period, widespread magmatic activity developed in Western Anatolia, following the continental collision between the Sakarya continent and the Tauride-Anatolide platform (Şengör and Yılmaz, 1981; Şengör et al., 1993; Yılmaz, 1989, 1990, 1995, 1997;). This produced both intrusive and extrusive rocks. In the Bayramiç area, magmatic activity started with the intrusion of the Evciler granitoid, and is covered by the lower volcanic association. This was followed by the development of the upper volcanic association (Genç, 1998). According to Genç (1998), these units collectively form the Bayramiç Magmatic Complex. The Evciler granitic pluton, an elliptical metaluminous, calc-alkaline body of Late Oligocene-Early Miocene age (25±3 Ma, Birkle, 1992), intrudes the Kazdağ Massif. Its long axis trends WSW-ENE, and it covers an area of approximetaly 170 km^2 (Figure 3.1).

Petrographically, the Evciler pluton can be classified as quartz monzonite to granodiorite. Phenocryst mineralogy includes plagioclase K-feldspar and quartz; minor amphibole, biotite and pyroxene, with accessory titanite, apatite and magnetite. The presence of primary titanite and magnetite, combined with the absence of ilmenite, indicates that these are relatively oxidized magmas. Like plutons associated with Cu-Au and Fe skarns (Meinert, 1995), the Evciler intrusion are very similar, being more silicic and less differentiated (as measured by Rb/Sr; Yücel Öztürk et al. 2005).

3.4 Geology of the Study Area

Two main rock units are exposed in the Evciler district: Kazdağ metamorphic rocks and Evciler granitoid. The metamorphic rocks consist mainly of grey, dark grey, and brown well-banded quartzofeldsphatic gneisses, which include marble, amphibolite and granitic gneiss horizons and lenses. Gneisses are petrographically characterized by the presence of biotite, sillimanite, garnet and hornblende along with ubiquitous quartz and feldspar. The marble has granoblastic texture and is fine-grained. The grain size increases toward igneous contact. Diopside-bearing amphibolites occur as bands up to several meters thick (1-2 m), in gneiss and marble (Okay & Satır 2000).

The pluton has a petrological composition of granodiorite, quartz monzonite and quartz diorite, and are medium grained and granular at the center, which pass gradually into the porphyritic and fine-grained textured rocks toward the margin (Genç 1998). Numerous aplite dykes and veins were injected into the pluton along the fractures and the pluton contains rounded to lensoidal mafic microgranular enclaves. On the basis of mineralogical and textural features, the Evciler pluton is subdivided into three main facies (Genç 1998; Öngen 1992), (Figure 3.1c): (1) Çavuşlu monzodiorite is the earliest facies of the pluton and has a equigranular, coarse-grained texture. (2) The Karaköy granodiorite is the main facies of the pluton and occurs in the northeastern part of the pluton. It is fine to medium grained and porphyritic in texture. (3) The contact between these two plutonic members is

graditional and represented by granodiorite including coarse-grained magnesian hornblende, named as mesocratic-type Evciler. At the south of the pluton monzogranitic rocks have limited distribution compared to mesocratic-type Evciler and named as leucocratic-type Evciler. It is light gray in colour, fine- to medium-grained and equigranular to porphyritic in texture. The leucocratic- and mesocratic-type boundaries are poorly mapped at the Evciler district, as their contacts are not clearly observed.

3.5 Alteration and Mineralization

3.5.1 Alteration in Igneous Rock (Endoskarn)

The endoskarn is characterized by epidote and white mica of metasomatic origin. Endoskarn zones are represented mainly by epidote-pyroxene skarns. Along the contact with exoskarn, replacement of granodiorite by massive epidote and minor garnet-pyroxene endoskarns over widths of centimeters to 0.5 m may result in complete destruction of the original igneous texture. This zone consists of fine- to medium-grained epidote accompanied by interstitial quartz (Figure 3.3a & b). Further within the granite, endoskarns occur only as disseminated epidote skarns, and are enriched in garnet toward the marble. The garnet-rich skarn predominantly comprises exoskarn. However, garnet was locally developed by the dissolution and replacement of primary igneous minerals, particularly feldspar, in the granodiorite (Figure 3.3c & d). Similar development of endoskarn in the associated pluton and replacement of plagioclase by garnet have been reported by Lentz et al. (1995) and Somarin (2004). Following possible reaction for this process has been reported by Somarin (2004);

$3NaAlSi_3O_8 + 8FeCl_2 + 12CaCO_3 + 8H_2O + 2O_2 + 3Si(OH)_4 =$
(Feldspar)
$4Ca_3Fe_2Si_3O_{12} + 3NaOH + 3Al(OH)_3 + 16HCl + 12CO_2$
(Andradite)

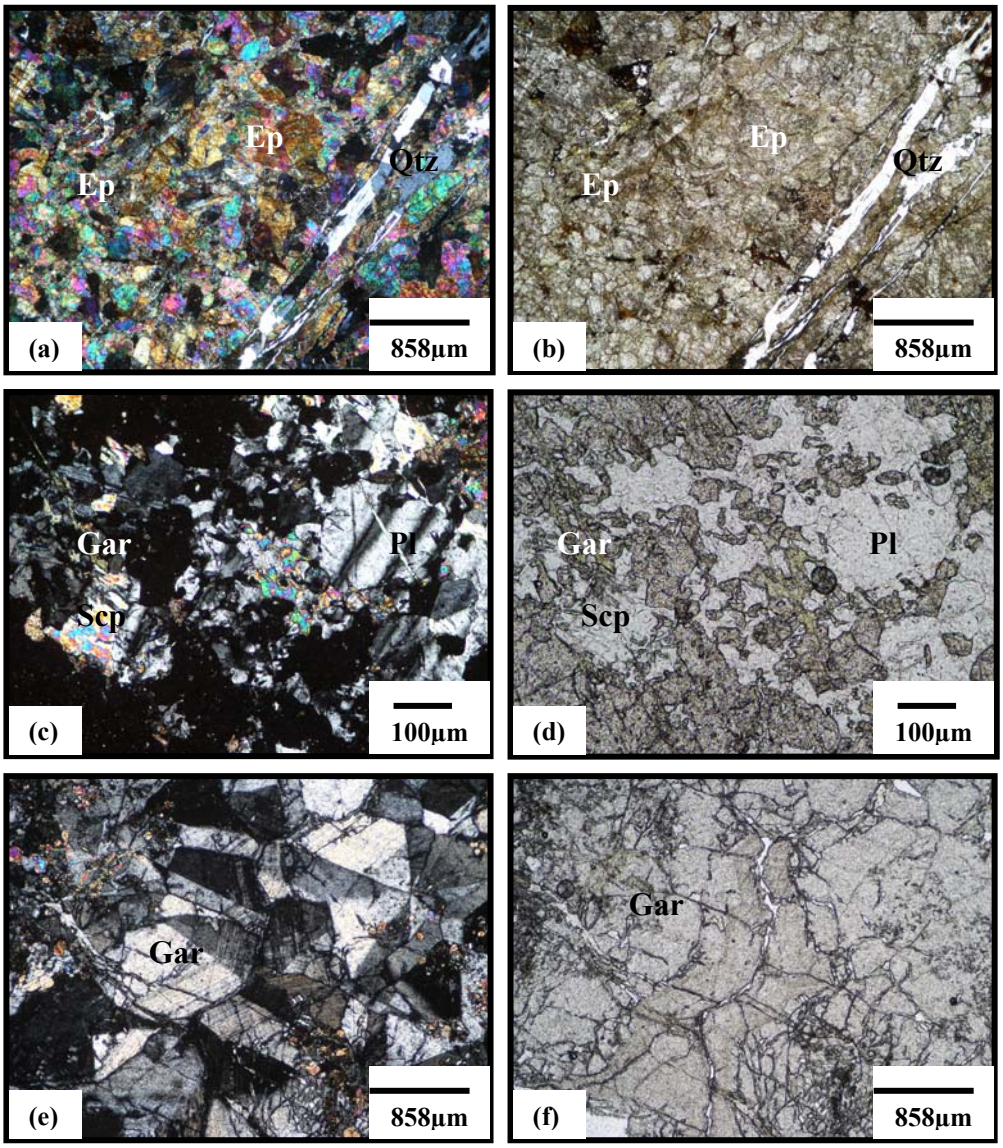

Figure 3.3. Typical endoskarn textures in the Evciler district; (a,b) massive epidote with interstitial quartz, (CPL-cross polarized transmitted light & PPL-plane polarized transmitted light); (c,d) replacement of primary igneous minerals (plagioclase) by garnet (CPL & PPL); (e,f) garnet showing oscillatory and sector zoning within the granodiorite (CPL & PPL). Ep= Epidote, Qtz= Quartz, Gar= Garnet, Pl= Plagioclase, Px= Pyroxene.

In this reaction, $CaCO_3$ and $8FeCl_2$ originate from the marble wallrock and magma, respectively.

However some grains of garnets in the endoskarn display anizotrophy, and sector and oscillatory zoning (Figure 3.3e & f).

3.5.2 Alteration in Wallrock (Exoskarn)

The alteration of the host rock (marble and gneiss) is marked by the formation of coarsely crystalline lenses of skarn owing to the ingress of Si-, Al-, Fe-, and Mg-rich fluids in the host rock. At the contact between the Evciler granodiorite and the Kazdağ metamorphic rocks, the earliest changes observed in the protolith involve recrystallization to fine-grained, dark grey-green hornfels containing an assemblage of clinopyroxene-feldspar-quartz. There is a recrystallization of the protolith into a pyroxene skarn via diffusion-controlled bimetasomatic interaction between the litologies. Metasomatism of the carbonate lithology at Evciler produced grossular-andradite/pyroxene exoskarn. Massive pyrrhotite bodies with magnetite and chalcopyrite occur in the exoskarn (Figure 3.4).

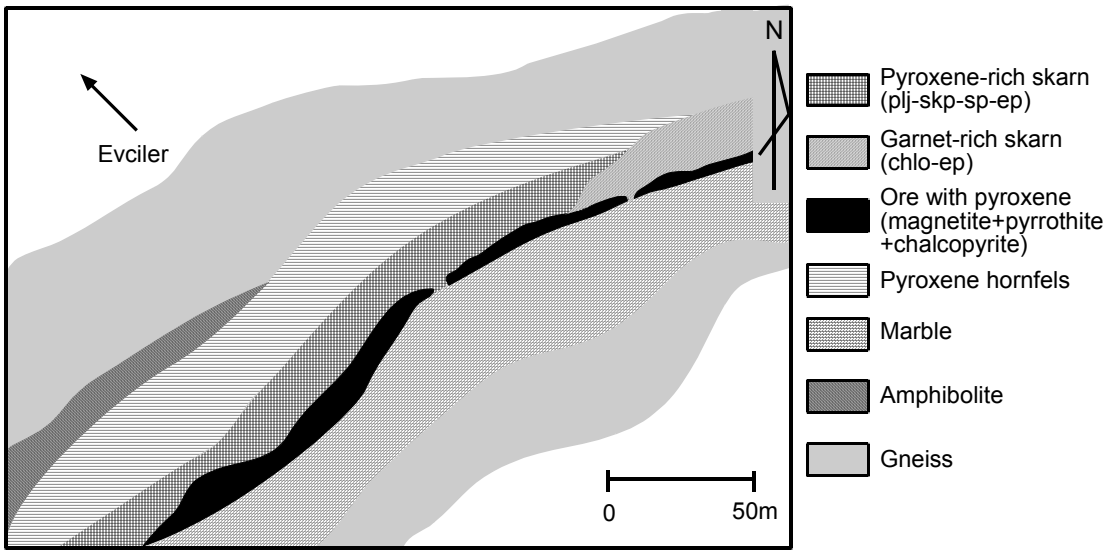

Figure 3.4. Mineral zonation of calcic skarn in the Ayazma occurrence.

The prograde skarn assemblage comprises garnet, clinopyroxene and scapolite (Figure 3.5a & b). The garnet consists of anisotropic and isotropic zoned andradite to grossular (Figure 3.5c & d). Metasomatism of the marble in the northwestern part of the skarn body produced a pyroxene-rich skarn (Figure 3.6a&b). The pyroxene exoskarn contains clinopyroxene+plagioclase+scapolite + epidote (Figure 3.6c & d). The clinopyroxene consists principally of diopside to hedenbergite.

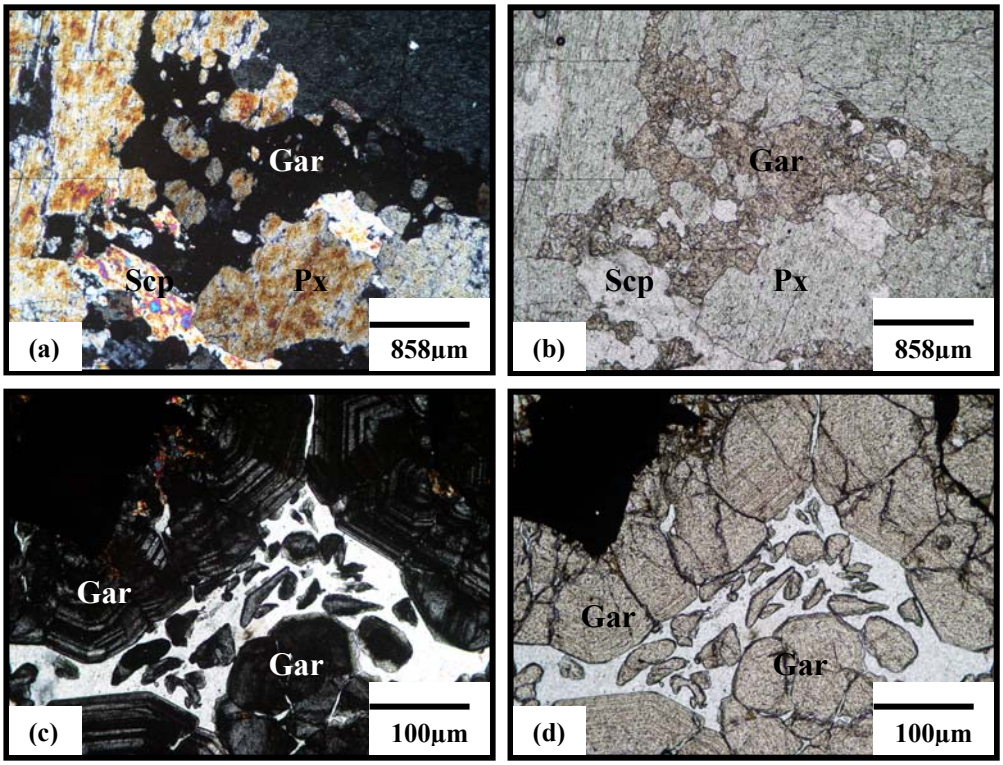

Figure 3.5. Typical exoskarn textures in the Evciler district; (a,b) the prograde skarn mineral assemblage comprising garnet, clinopyroxene and scapolite (CPL & PPL); (c,d) the garnet exoskarn consisting of anisotropic and isotropic zoned andradite to grossular (CPL & PPL).

3.6 Paragenesis of Skarn and Ore Minerals

The principal skarn minerals at Evciler are garnet, clinopyroxene, scapolite, epidote, and amphibole together with quartz, chlorite, titanite, calcite and apatite as subordinate or accessory minerals. At least two stages of skarn formation and ore deposition have been recognized at Evciler as follows: stage-I, clinopyroxene ± garnet ± scapolite ± quartz; stage-II, amphibole ± epidote ± chlorite ± quartz ± calcite; and magnetite + pyrrhotite + chalcopyrite ± pyrite.

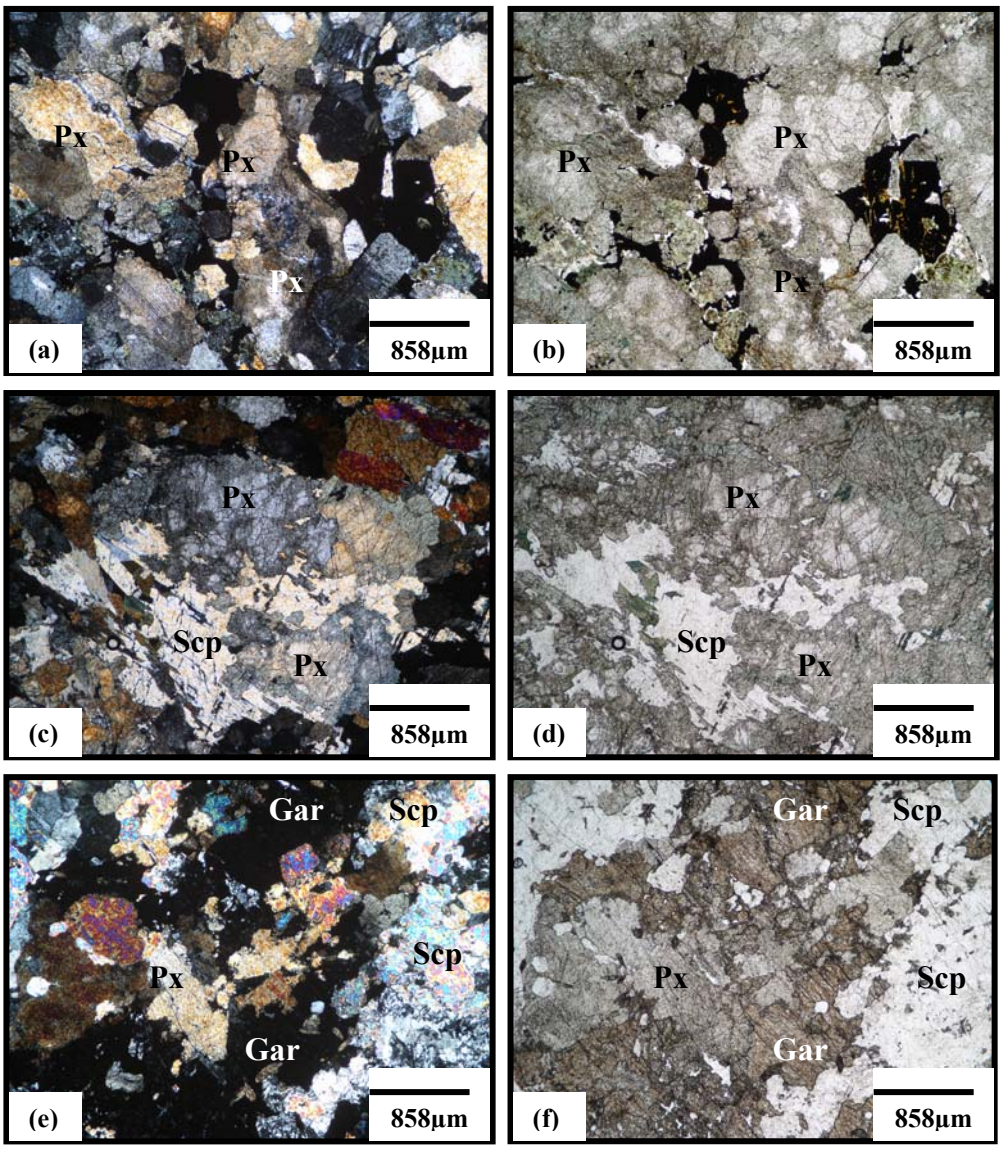

Figure 3.6. Photomicrographs of the pyroxene-rich exoskarn in the Ayazma occurrance. (a,b) pyroxenes show color zonation (CPL & PPL); (c-f) Calcic-scapolite (meionite) intergrown with clinopyroxene and garnet (CPL & PPL).

Textures can play an important role in understanding the evolution of a skarn system (Ciobanu and Cook, 2004). The range of textures formed during several events, such as infiltration-driven metasomatism, and devolatilization, can be used to discriminate between prograde and retrograde stages. Skarns are composed largely of minerals that form solid-solution series, such as garnet and pyroxene; which helps to establish trends of zonation and evolution.

Paragenetic studies based on macro- and micro-textures show that skarn formation at Evciler occurred in a number of stages, as in other skarns worldwide (Einaudi et al., 1981; Kwak, 1994; Meinert, 1992; Newberry, 1998). The early skarn mineral facies such as garnet and pyroxene are partially replaced by later mineral phases (e.g. amphibole, epidote and chlorite). The textural features further indicate that later minerals have developed largely by pervasive and diffusive replacement of earlier minerals such as garnet and pyroxene. Early mineral facies are largely anhydrous, whereas later ones are predominantly hydrous.

The Stage-I assemblage is dominated by clinopyroxene, garnet and scapolite. Calcic scapolite (meionite) is commonly formed during prograde alteration or regional metamorphism at high temperatures (Beran et al., 1985; Labotka, 1991; Rebbert and Rice, 1997; Pan, 1998). Its presence in the Evciler skarn shows that scapolite can appear at a low-temperature, as the meionite grains postdate the clinopyroxene and garnet the former hypothesis is favored (Figure 3.6e & f).

All skarn silicates (i.e., garnet, pyroxene) at Evciler represent intermediate members in solid solution series, and each of them displays a broad field of compositional variation. However, it is only garnet that shows oscillatory zonation with a variable compositional range (Figure 3.7a-d). Even though pyroxene shows significant compositional variation (and colour zonation), a tendency toward zonation is only rarely developed, e.g., rims of pyroxene slightly richer in Fe (Figure 3.7e & f).

Stage-II minerals represent late skarn-forming phases and replace early mineral (stage-I) assembleges. All textures that indicate superposition of a new mineral assemblage upon a former one, or modification of the pre-existing assemblage, are considered retrograde (Ciobanu & Cook, 2004). Retrograde textures are particularly marked within irregular envelopes, varying from cm to m in width.

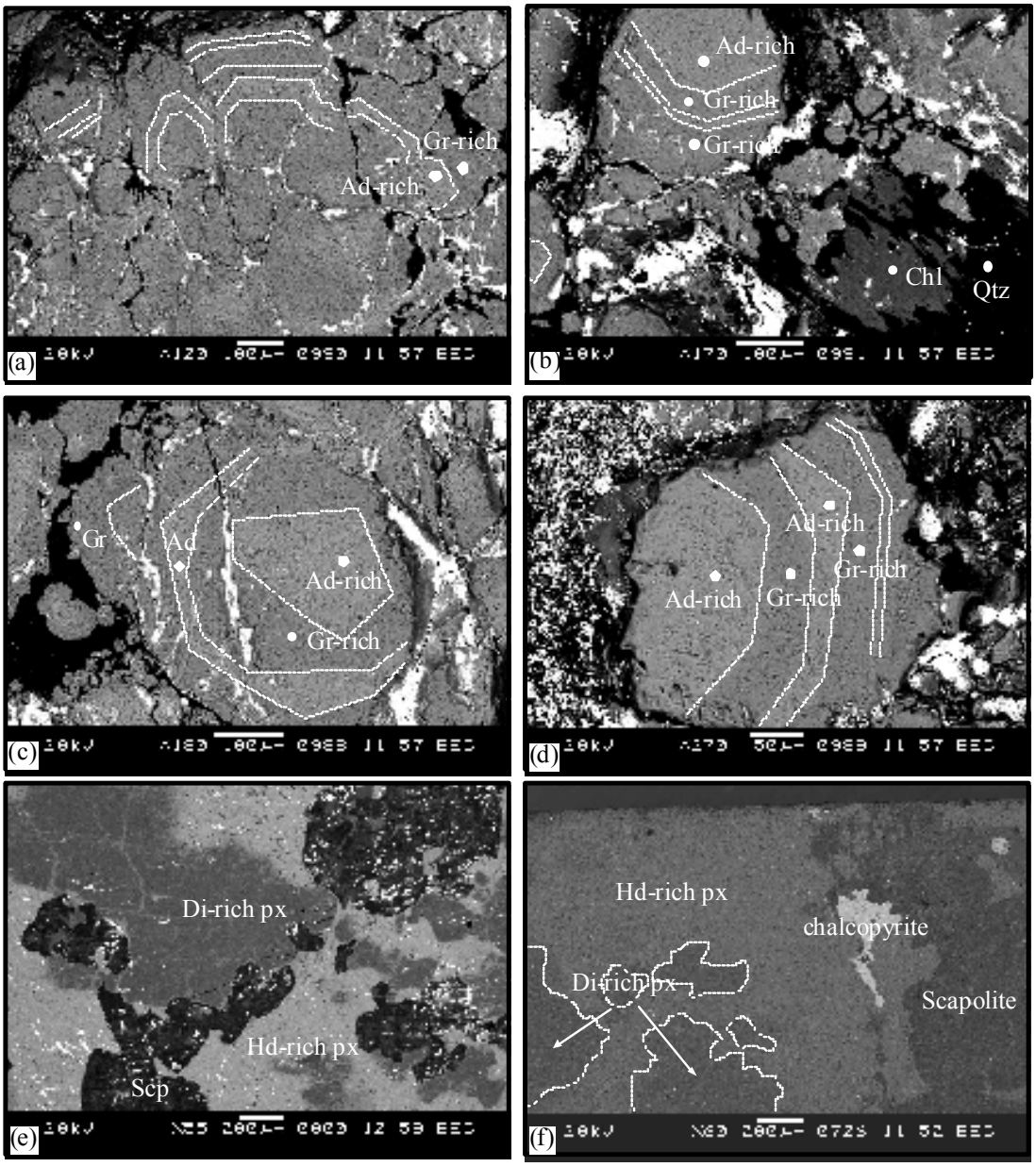

Figure 3.7. Back-scattered electron images showing (a-d) oscillatory zoning patterns in garnet from the Evciler district; (e,f) pyroxenes showing significant compositional variation, a tendency towards zonation is only rarely developed, e.g., rims of pyroxene slightly richer in Fe.

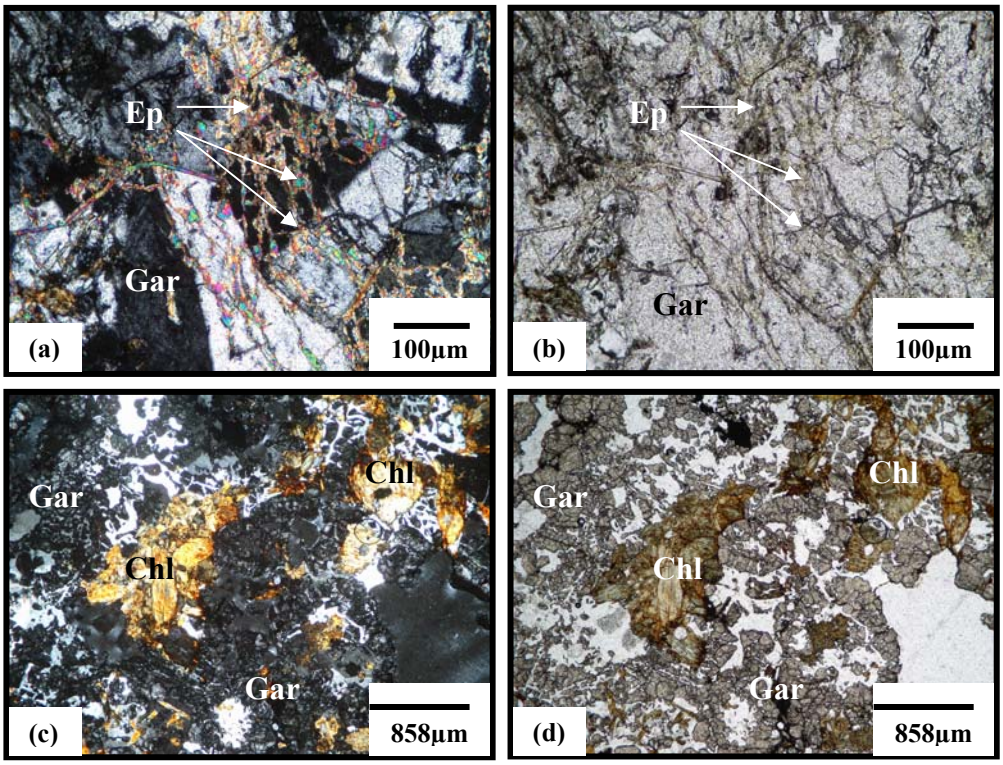

Figure 3.8. (a,b) Emplacements of filaments/patches of epidote that overprint an earlier, pre-existing sector zoning garnet (CPL & PPL); (c,d) retrograde brecciation in garnets. The garnet fragments are seperated by quartz-carbonate infill, as well as a series of hydrated minerals, e.g., chlorite(CPL & PPL).

In garnet displaying anomalous birefringence with prograde sector zoning, the appearence of scales and chaotic birefringence is followed by emplacements of filaments and patches of epidote (piercing texture) (Figure 3.8a & b). In the Evciler district, disruptive brecciation occurs in the "blown-apart" fabrics that characterize the garnet assemblages (Figure 3.8c & d). Here, the garnet fragments are separated by quartz-carbonate infill, as well as a series of hydrated minerals, e.g., chlorite. However, oscillatory zoned garnet shows brittle brecciation (Figure 7a). Zones of Di-rich pyroxene corrode into pre-existing Hd-rich pyroxene (Figure 3.9). Such textures are reported in metasomatic fronts from metamorphic terranes, where they are considered indicative of changes in permeability-porosity at skarn front in response to infiltration-driven decarbonation (Yardley & Lloyd, 1995)

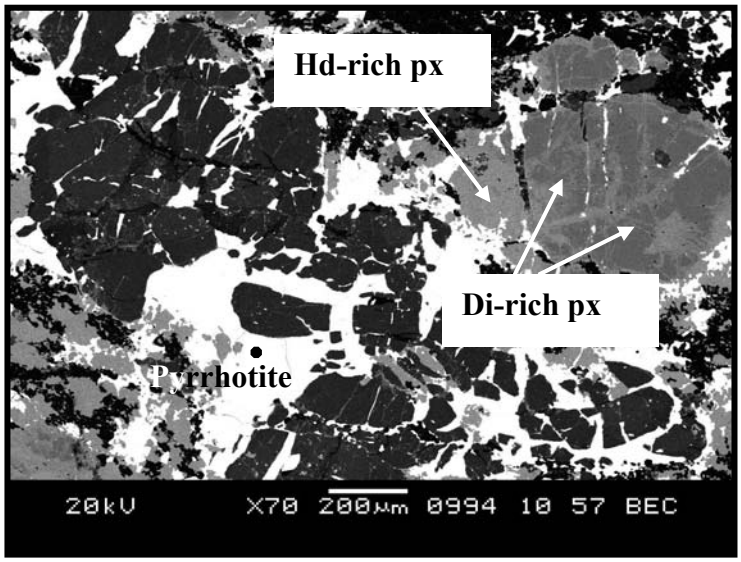

Figure 3.9. Back-scattered electron image showing zones of Di-rich pyroxene that corrode into former Hd-rich pyroxene.

3.6.1 Ore Minerals

The sulfides and oxide minerals overprint the pyroxene-rich calcic skarn, therefore, the Evciler deposit can be termed a skarn deposit. The term skarn deposit not only includes deposits emplaced at the pluton - carbonate rock contact, but also those occurring in distal zones. The Evciler skarn mineralization consists of shallowly-dipping (Au-Cu-bearing) massive pyrrhotite – pyrite – sulfide – quartz mineralization within quartz – biotite – amphibole gneiss and marble intruded by Tertiary porphyritic Evciler granodiorite. The mineralization appears to be controlled strongly by the amphibole gneiss-marble intercalation, which is cut by granodiorite (Figure 3.10).

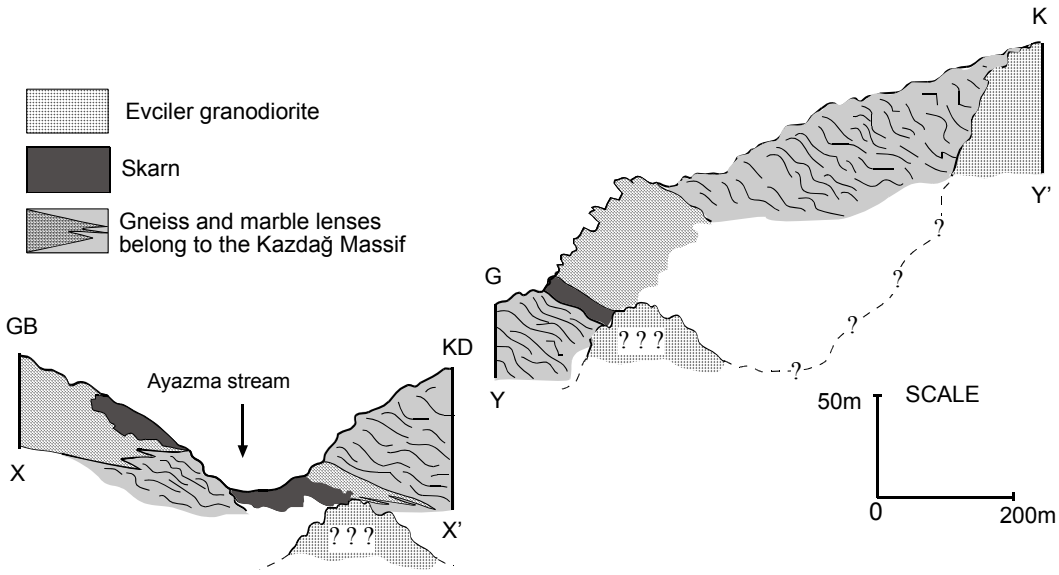

Figure 3.10. The cross-section showing the position of the skarn mineralization at the Evciler district (Ayazma occurrence).

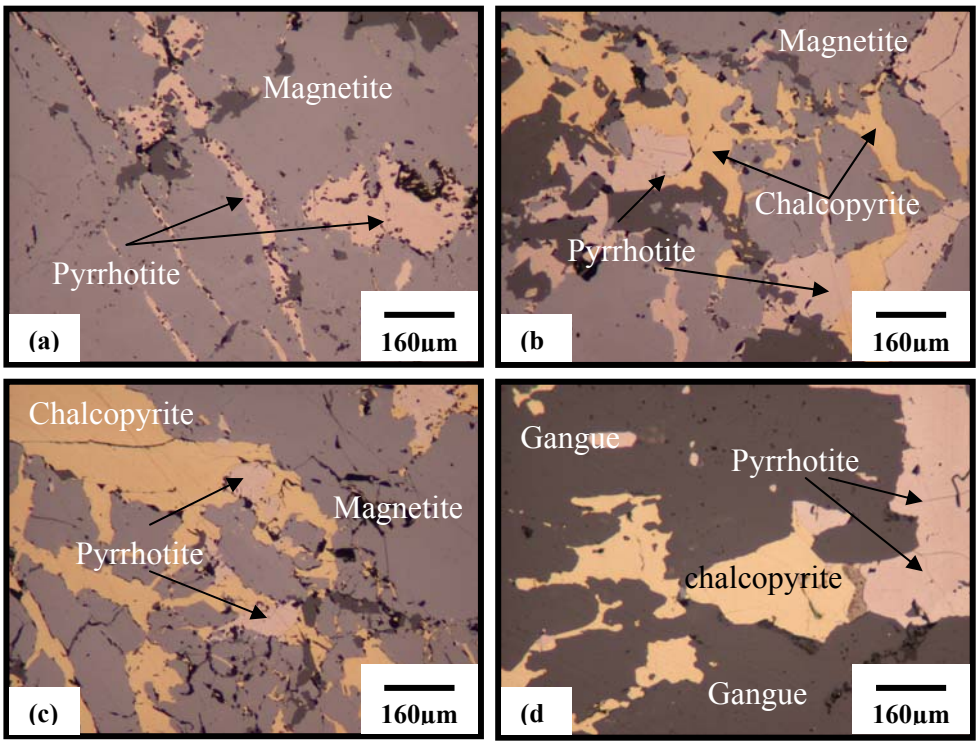

Figure 3.11. Polished sections showing (a-d) magnetite - phyrrothite - chalcopyrite assemblage. Magnetite is replaced by both phyrrothite and chalcopyrite.

The most abundant opaque minerals present are magnetite, pyrrhotite, chalcopyrite, melnicovite pyrite and goethite. Magnetite was the first opaque mineral

formed. Locally it is cross-cut by sulfide veins (pyrrhotite) (Figure 3.11a-d) and Deposition of pyrrhotite followed the magnetite formation. Pyrrhotite, the most abundant sulfide, formed in stage-II and generally shows a close spatial assocation with anhydrous minerals (e.g., pyroxene) and quartz. Pyrrhotite occurs as anhedral crystals disseminated in the fine-grained skarn and as massive aggregates replacing pyroxene. Microscale investigation of the transition zone between the banding and wigglite textures in Figure 3.12 shows regular oscillations between intervals of pyrrhotite and diopside-rich pyroxene (Figure 3.12a & b). As seen in Figure 3.12c and 3.12d, the boundary between these two minerals is generally sharp, and interfingering of the phases commonly occur.

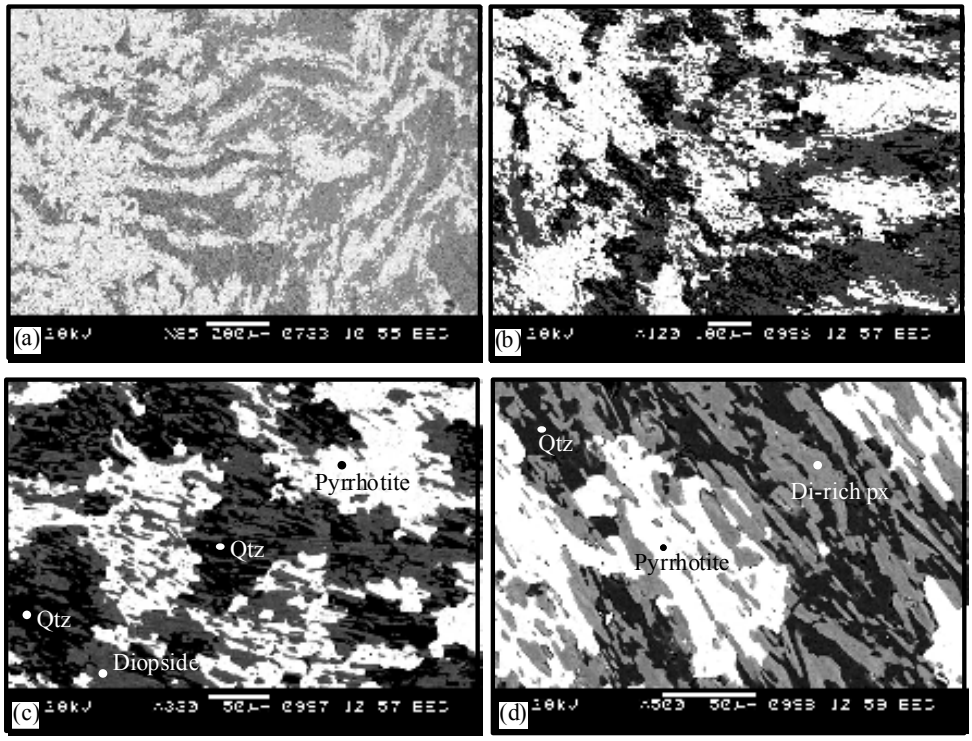

Figure 3.12. Back-scattered electron images showing prograde textures. (a) transition between banding and wiggle textures, showing regular swinging texture between phyyrrothite (light) and diopside (dark). (b), (c) and (d) illustrates details from (a).

Among the replacement textures, the characteristic alteration of pyrrhotite to a fine mixture of pyrite and marcasite results in the birds-eye texture. In the Evciler

skarn, this special texture can be seen in pyrrhotite (Figure 3.13a-c). However, goethite developed in pyrrhotite as veins (Figure 3.13d).

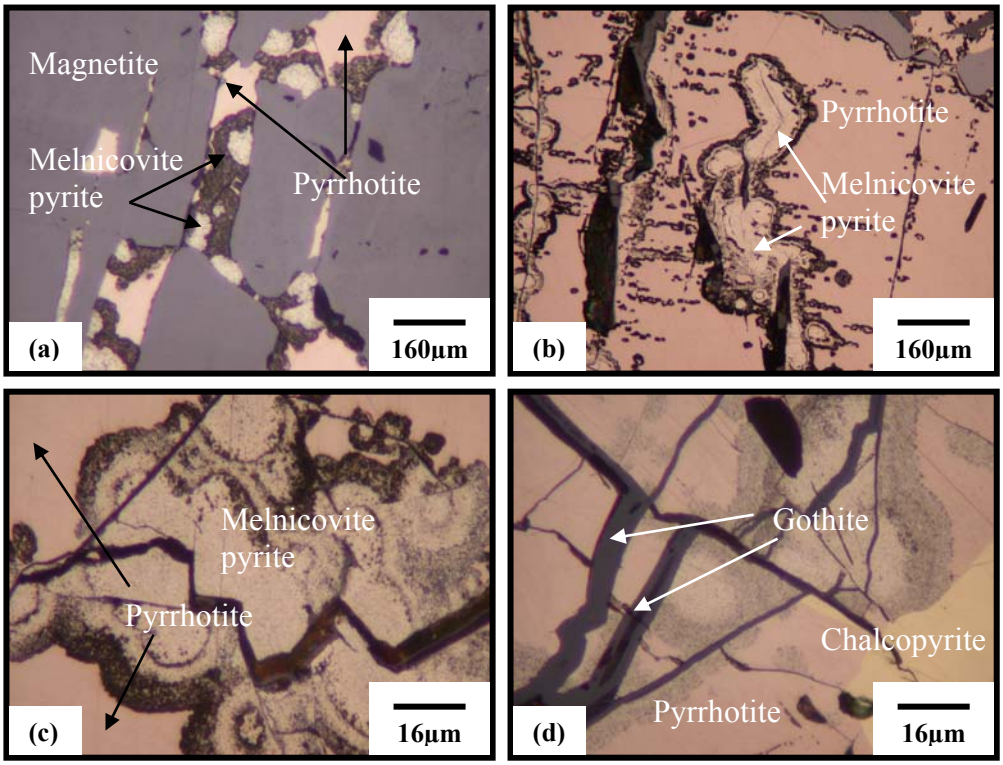

Figure 3.13. Polished sections showing (a-c) well-developed "bird's-eye" texture composed of pyrite, formed along a fracture during weathering of pyrrhotite; (d) gothite that is developed in pyrrhotite as veins.

The next deposited minerals were chalcopyrite accompanied by gold mineralization. This is the most important economical association. Chalcopyrite replaced both magnetite and pyrrhotite (Figure 3.11b-d).

3.7 Composition of Skarn Minerals

Most skarn minerals have compositional variations that can yield significant information about the skarn and ore-forming environment and can subsequently be used to differentiate between skarn types (e.g., Einaudi et al., 1981; Kwak, 1994; Meinert, 1992; Sato, 1980). Garnet and pyroxene composition in skarns are particularly important, as they can indicate redox conditions of a skarn system

(Brown and Essene, 1985). Knowledge of the redox condition of a skarn may have important exploration implications (Zaw and Singoyi, 2000). For example, Meinert (1992) pointed out that there is a tendency for oxidized tungsten skarns to form small deposits, whereas reduced ones generally form large deposits.

Previous mineral compositional determinations in the Karaköy skarn minerals were undertaken by Öngen (1992) on clinopyroxene and garnet. In this present study, chemical analyses of major elements were undertaken on garnet and pyroxene from stage I and epidote from stage II to (1) determine their compositional variations, (2) constrain nature of fluids during skarn evolution, and (3) classify the skarn types. Electron microprobe analyses were carried out for clinopyroxene, garnet and epidote.

3.7.1 Analytical Techniques

Compositional variations of skarn minerals were determined using a JEOL JXA 8900RL electron microprobe at the EMS Laboratory of the Geochemistry Institute of the University of Tübingen, Germany. We analyzed the silicates for Si, Al, Ti, Fe, Cr, Mn, Mg, Ca and Na. For these minerals, the operating conditions were as follows; accelerating voltage 15 kV, beam current 15 nA, and a beam diameter of 10 μm. TiO_2, Cr_2O_3 and K_2O were mostly below 0.07 wt percent and didn't show any meaningful relation to geochemical factors including mineral assemblages, host rock compositions and metal types. Analytical results for the skarn minerals are briefly described below.

3.7.2 Clinopyroxene

The geochemistry of skarn pyroxene is a potential indicator of the complex interaction between metal composition and other geochemical characteristics, since pyroxene occurs throughout the skarn system, is commonly associated with ores, and displays a significant solid-solution variability (Nakano et al., 1994).

The compositional variation of the pyroxenes is given in Table 3.1. The pyroxenes were analyzed for SiO_2, TiO_2, Al_2O_3, $FeO_{(T)}$, MnO, MgO, CaO and Na_2O. The SiO_2 contents of the pyroxenes from the Evciler district range from 50.0 to 52.3%. TiO_2 contents of the pyroxenes are very low and similar to those observed in several skarns in the world (Einaudi et al., 1981; Nakano et al., 1994) and range from 0.0 to 0.93%. Al_2O_3 compositions range from 0.09 to 1.55%, $FeO_{(T)}$ contents range from 10.38 to 23.01%. MnO and MgO contents range from 0.10 to 0.68% and from 3.82 to 11.84%, respectively. CaO contents range from 22.37 to 24.67%. Na_2O contents range from 0.10 to 0.83%.

Binary plots between $FeO_{(T)}$ and other oxides are shown on Figure 3.14. The correlation matrix (Table 3.2) for major oxides indicate that the correlation coefficient for $Fe_2O_{3(T)}$- SiO_2, $FeO_{(T)}$-MnO, $FeO_{(T)}$-CaO and $FeO_{(T)}$-MgO are -0.90, 0.43, -0.69 and -0.99, respectively.

The compositional variation of the pyroxene also plotted in Figure 3.15. This figure also shows pyroxene compositions from the Karaköy skarn. Skarn pyroxene is commonly expressed by a ternary proportion of its diopside-johannsenite-hedenbergite component, as expressed by $Ca(Mg,Mn,Fe)Si_2O_6$. The Evciler and the Karaköy clinopyroxenes distinctly fall in the diopside-hedenbergite end-member field, but close to hedenbergite.

However, previous studies have revealed that the Mg/Mn/Fe proportion varies widely in a single deposit, dependent on the mineral assemblage and the protolith composition (e.g., Einaudi, 1977; Morgan, 1975). It is notable that the Mg and Fe content (or Mg/Fe ratio) of pyroxenes are highly variable, whereas their Mn/Fe ratio is relatively restricted for these two skarn locations. The Evciler clinopyroxene shows Mn/Fe ratios of 0.02 to 0.05, with an average of 0.03. A similar positive relationship between the Mn and Fe content is observed in pyroxenes from the Karaköy wollastonite skarn (Öngen, 1992). The Mn/Fe ratio of Karaköy wollastonite skarn pyroxenes ranges from 0.01 to 0.4, the mean Mn/Fe value is 0.21 (Öngen, 1992).

Table 3.1. Representative Microprobe Analyses of Pyroxene from Evciler Skarn.

SAMPLE	57/4 (1)	57/4 (6)	57/4 (8)	76 (3)	76 (4)	76 (6)	76 (7)	76 (8)	76 (10)	140/S3 (1)	140/S3 (5)	144 (2)	144 (6)	144 (7)
wt %														
SiO_2	50.43	50.43	50.53	50.46	50.61	49.95	50.46	52.07	52.29	49.42	50.27	50.38	50.89	51.2
TiO_2	0.06	0.07	0.09	0.01	0.07	0.11	0.93	0.04	0.00	0.01	0.05	0.027	0.095	0.086
Al_2O_3	0.68	0.94	1.15	1.22	1.18	1.55	0.09	0.76	0.45	0.17	0.91	0.554	1.252	1.154
Cr_2O_3	0.00	0.00	0.00	0.12	0.15	0.15	0.13	0.00	0.04	0.00	0.03	0.00	0.00	0.03
FeO(Tot)	17.11	16.67	16.75	15.64	15.34	16.26	16.00	10.38	10.36	23.01	17.13	18.81	16.09	16.53
MnO	0.44	0.57	0.55	0.42	0.45	0.48	0.44	0.24	0.32	0.56	0.45	0.413	0.105	0.094
MgO	7.23	7.68	7.75	8.21	8.37	7.79	7.96	11.84	11.57	3.82	7.40	6.22	8.23	8.43
CaO	23.26	22.37	22.35	23.57	23.42	23.37	23.41	24.64	24.67	22.93	23.52	23.51	23.04	22.73
Na_2O	0.43	0.83	0.83	0.46	0.45	0.48	0.47	0.16	0.14	0.18	0.29	0.118	0.208	0.213
Total	99.64	99.56	100.00	100.12	100.03	100.14	99.89	100.13	99.84	100.10	100.05	100.03	99.91	100.47
						Number of ions on the base of 6 atoms of oxygen								
Si	1.968	1.958	1.952	1.944	1.950	1.929	1.960	1.961	1.978	1.978	1.954	1.979	1.970	1.971
Al	0.031	0.043	0.052	0.056	0.054	0.071	0.004	0.034	0.020	0.008	0.042	0.026	0.057	0.052
Ti	0.002	0.002	0.003	0.000	0.002	0.003	0.027	0.001	0.000	0.000	0.001	0.001	0.003	0.002
Cr	0.000	0.000	0.000	0.004	0.005	0.005	0.004	0.000	0.001	0.000	0.001	0.000	0.000	0.001
Fe^{3+}	0.061	0.101	0.099	0.086	0.072	0.095	0.053	0.055	0.033	0.050	0.068	0.024	0.013	0.015
Mg	0.421	0.444	0.446	0.472	0.481	0.449	0.461	0.665	0.653	0.228	0.429	0.364	0.475	0.484
Fe^{2+}	0.497	0.440	0.442	0.418	0.423	0.430	0.467	0.272	0.295	0.720	0.488	0.594	0.508	0.517
Mn	0.014	0.019	0.018	0.014	0.015	0.016	0.014	0.008	0.010	0.019	0.015	0.014	0.003	0.003
Ca	0.973	0.930	0.925	0.973	0.967	0.967	0.974	0.994	1.000	0.983	0.980	0.990	0.956	0.938
Na	0.033	0.063	0.062	0.034	0.034	0.036	0.035	0.012	0.010	0.014	0.022	0.009	0.016	0.016
Sum	4.000	4.000	4.000	4.000	4.000	4.000	4.000	4.000	4.000	4.000	4.000	4.000	4.000	4.000
Xfe	0.542	0.498	0.497	0.470	0.468	0.489	0.503	0.291	0.311	0.760	0.532	0.620	0.517	0.517
wt% Fe_2O_3	2.09	3.45	3.42	2.96	2.47	3.29	1.81	1.93	1.14	1.65	2.34	0.80	0.46	0.51
wt% FeO	15.23	13.57	13.68	12.97	13.12	13.30	14.37	8.64	9.33	21.52	15.02	18.09	15.68	16.07
Ferrous Tot.	99.64	99.56	100.00	100.12	100.03	100.14	99.89	100.13	99.84	100.10	100.05	100.03	99.91	100.47
Ferric Tot.	99.85	99.91	100.34	100.41	100.28	100.47	100.07	100.32	99.95	100.27	100.28	100.11	99.96	100.52

Table 3.2. Correlation matrix for the major oxides in pyroxenes from the Evciler district.

	SiO_2	TiO_2	Al_2O_3	Cr_2O_3	$FeO_{(T)}$	MnO	MgO	CaO	Na_2O
SiO_2	1	-0.11	-0.02	-0.17	-0.89	-0.63	0.92	0.63	-0.33
TiO_2		1	-0.42	0.40	-0.01	0.06	-0.02	-0.05	0.18
Al_2O_3			1	0.25	-0.15	-0.20	0.17	-0.26	0.32
Cr_2O_3				1	-0.15	0.16	0.10	0.17	0.17
$FeO_{(T)}$					1	0.43	-0.99	-0.69	0.10
MnO						1	-0.49	-0.29	0.60
MgO							1	0.65	-0.12
CaO								1	-0.61
Na_2O									1

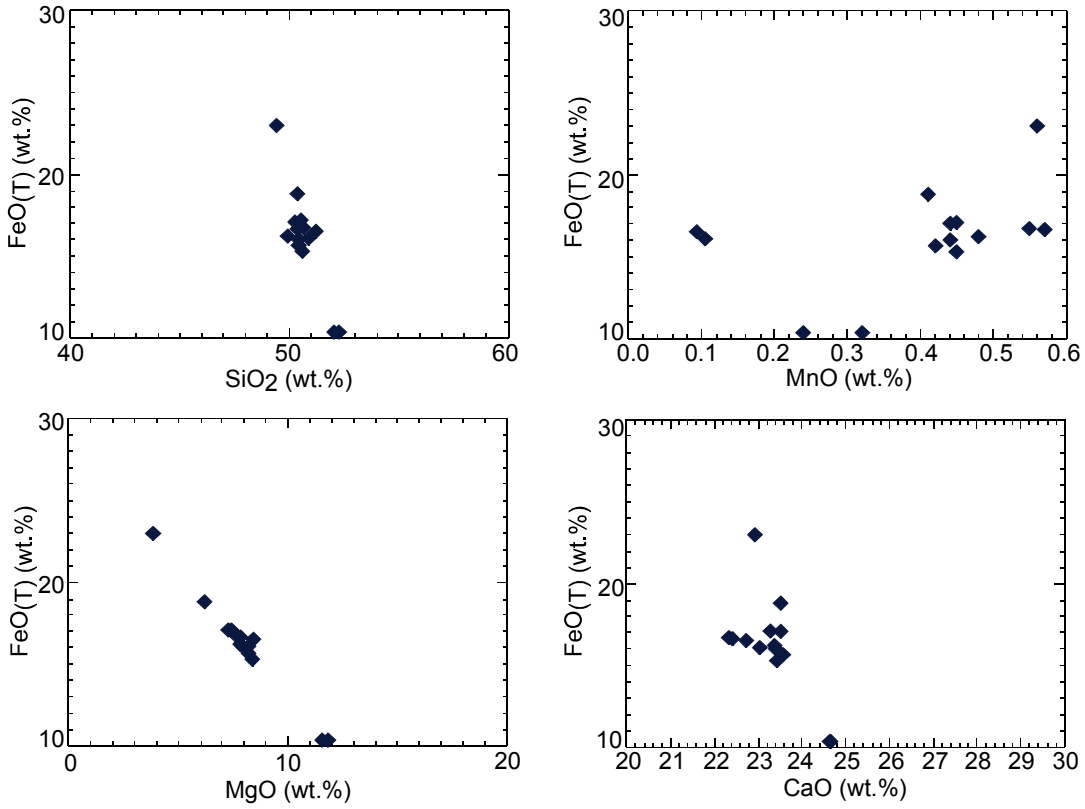

Figure 3.14. The relationships between $FeO_{(T)}$ and SiO_2, MnO, CaO and MgO in the pyroxenes.

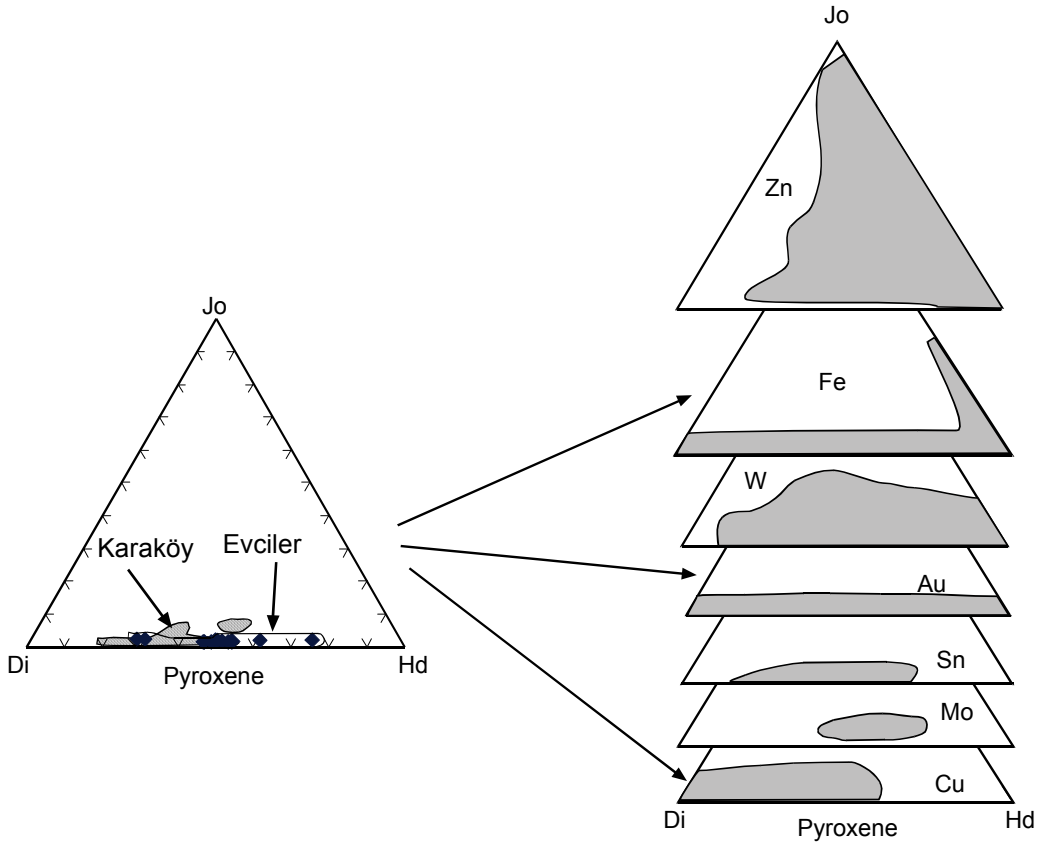

Figure 3.15. Jo-Di-Hd (Mn-Mg-Fe) ternary diagram showing compositional variations of clinopyroxene from the Evciler district compared with major skarn types. End members are Jo=Johannsenite, Di=Diopside, Hd=Hedenbergite. Data from Einaudi et al. (1981) and Meinert (1983, 1989).

The mean Mn/Fe ratio of pyroxenes for the Evciler skarn is similar to those of Cu-Fe and Au type skarn deposits (Figure 3.15). This data is strongly supported by the proposition of Einaudi and Burt (1982) that pyroxenes with a high hedenbergite-diopside component, or pyroxenes with a low Mn/Fe ratio according to Nakano et al. (1994), occur mostly in Cu-Fe and Au skarn deposits. Iiyama (1979, 1982) noted that Mg has a tendency to be highly concentrated and Mn less concentrated in the clinopyroxene. Therefore, if skarn pyroxene crystallizes from a relatively homogeneous fluid with respect to the Mg/Mn/Fe proportion, then the Mg fraction in the fluid would be readily modified. This leads to the formation of a suite of fluids with a relatively homogeneous Mn/Fe ratio, but with variable Mg/Fe ratios in accordance with the modification of the Mg fraction in the original fluid.

3.7.3 Garnet

Microprobe analyses were undertaken for the garnets from the Evciler skarn (stage-I). The compositional variations of the Evciler skarn garnets are summarized in Table 3.3. The garnets were analysed for SiO_2, TiO_2, Al_2O_3, $FeO_{(T)}$, MnO, MgO, CaO and Na_2O. The results of electron microprobe analyses from the garnets indicate that SiO_2 contents of the garnets from the Evciler district range from 34.79 to 37.61%. TiO_2 contents of the garnets range from 0.0 to 0.98%. Al_2O_3 compositions range from 0.35 to 11.54%, $FeO_{(T)}$ contents range from 14.32 to 28.66%. MnO and MgO contents range from 0.38 to 6.85% and 0.0 to 0.17%, respectively. CaO contents range from 27.02 to 34.29%.

Al_2O_3 displays significant relationships with $FeO_{(T)}$, SiO_2, CaO and MnO (Figure 3.16). Al_2O_3 contents are negatively correlated to $FeO_{(T)}$ contents (-1, Table 3.4) (Figure 3.16a). However, Al_2O_3 increases with the increase of SiO_2 and CaO contents. This results in the oscillations in grossular and andradite. There is no good correlation between Al_2O_3 and MnO (Figure 3.16d).

Table 3.3. Representative Microprobe Analyses of Garnet from Evciler Skarn.

SAMPLE	57/4 (4)	57/4 (11)	57/4 (12)	57/4 (13)	57/4 (17)	76 (1)	76 (2)	76 (3)	76 (4)	76 (5)	76 (7)	76 (9)	76 (13)
wt %													
SiO_2	35.18	35.68	36.08	36.24	36.63	37.61	36.96	37.34	37.17	37.18	36.74	37.38	37.13
TiO_2	0.00	0.01	0.00	0.00	0.35	0.73	0.99	0.97	0.57	0.57	0.70	0.47	0.51
Al_2O_3	0.61	3.15	6.41	7.61	7.99	11.17	9.35	11.03	8.30	8.81	7.66	9.25	8.62
Cr_2O_3	0.00	0.05	0.00	0.00	0.00	0.01	0.08	0.12	0.02	0.00	0.00	0.1	0.01
FeO(Tot)	28.66	25.16	20.69	19.11	18.57	14.87	17.37	15.92	18.70	18.23	19.30	18.01	18.00
MnO	5.72	5.79	5.83	6.83	2.97	0.38	0.46	0.49	0.56	0.50	0.43	0.66	0.46
MgO	0.01	0.03	0.00	0.01	0.01	0.13	0.17	0.16	0.08	0.09	0.12	0.05	0.09
CaO	27.36	28.71	29.12	28.40	32.17	34.09	33.19	33.25	33.46	33.35	33.56	32.67	33.79
Na_2O	0.00	0.00	0.00	0.00	0.00	0.00	0.01	0.02	0.00	0.00	0.03	0.02	0.00
Total	97.54	98.58	98.13	98.20	98.69	98.99	98.57	99.31	98.86	98.73	98.54	98.61	98.61
					Number of ions on the base of 24 atoms of oxygen								
Si	5.985	5.935	5.947	5.952	5.930	5.969	5.942	5.927	5.978	5.977	5.938	6.014	5.973
Al	0.123	0.618	1.245	1.473	1.524	2.089	1.772	2.063	1.573	1.669	1.459	1.754	1.634
Ti	0.000	0.001	0.000	0.000	0.043	0.087	0.119	0.116	0.069	0.069	0.085	0.057	0.062
Cr	0.000	0.006	0.000	0.000	0.000	0.002	0.010	0.015	0.002	0.000	0.000	0.013	0.001
Fe^{3+}	3.907	3.503	2.861	2.623	2.531	1.796	2.100	1.841	2.329	2.240	2.505	2.098	2.295
Mg	0.003	0.007	0.000	0.003	0.002	0.030	0.040	0.037	0.020	0.022	0.028	0.012	0.022
Fe^{2+}	0.171	0.000	0.000	0.002	0.000	0.178	0.236	0.272	0.186	0.211	0.104	0.325	0.126
Mn	0.824	0.816	0.814	0.950	0.407	0.051	0.062	0.066	0.076	0.068	0.059	0.090	0.062
Ca	4.987	5.117	5.142	4.997	5.580	5.797	5.717	5.655	5.766	5.744	5.812	5.631	5.824
Na	0.000	0.000	0.000	0.000	0.000	0.000	0.003	0.006	0.000	0.000	0.011	0.006	0.000
Sum	16.000	16.003	16.010	16.000	16.017	16.000	16.000	16.000	16.000	16.000	16.000	16.000	16.000
Xfe	0.985	0.000	None	0.382	0.000	0.855	0.854	0.881	0.902	0.906	0.790	0.964	0.851
wt% Fe_2O_3	30.51	27.96	22.99	21.22	20.64	15.04	17.36	15.41	19.25	18.51	20.59	17.33	18.96
wt% FeO	1.20	0.00	0.00	0.01	0.00	1.34	1.75	2.05	1.38	1.57	0.77	2.41	0.94
FerrousTot	97.54	98.58	98.13	98.20	98.69	98.99	98.57	99.31	98.86	98.73	98.54	98.61	98.61
Ferric Tot.	100.60	101.38	100.43	100.33	100.76	100.50	100.31	100.85	100.79	100.58	100.60	100.35	100.51

Table 3.4. Correlation matrix for the major oxides in garnets from the Evciler district.

	SiO_2	TiO_2	Al_2O_3	Cr_2O_3	$FeO_{(T)}$	MnO	MgO	CaO	Na_2O
SiO_2	1	0.80	0.95	0.35	-0.93	-0.88	0.68	0.92	0.32
TiO_2		1	0.76	0.49	-0.73	-0.91	0.95	0.88	0.52
Al_2O_3			1	0.34	-0.99	-0.73	0.65	0.82	0.31
Cr_2O_3				1	-0.27	-0.34	0.47	0.24	0.52
$FeO_{(T)}$					1	0.70	-0.62	-0.81	-0.27
MnO						1	-0.81	-0.97	-0.46
MgO							1	0.76	0.49
CaO								1	0.38
Na_2O									1

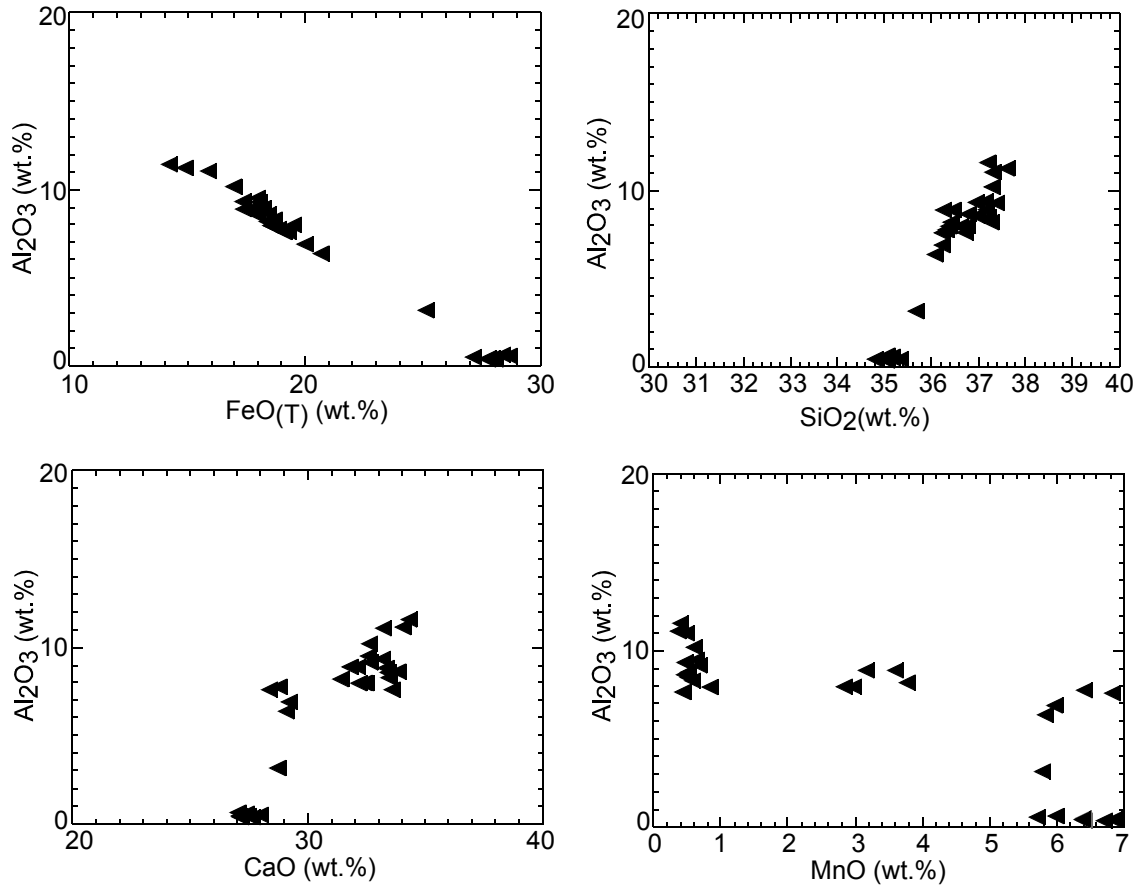

Figure 3.16. The relationships of Al_2O_3 contents with $FeO_{(T)}$, SiO_2, CaO and MnO contents in the garnets.

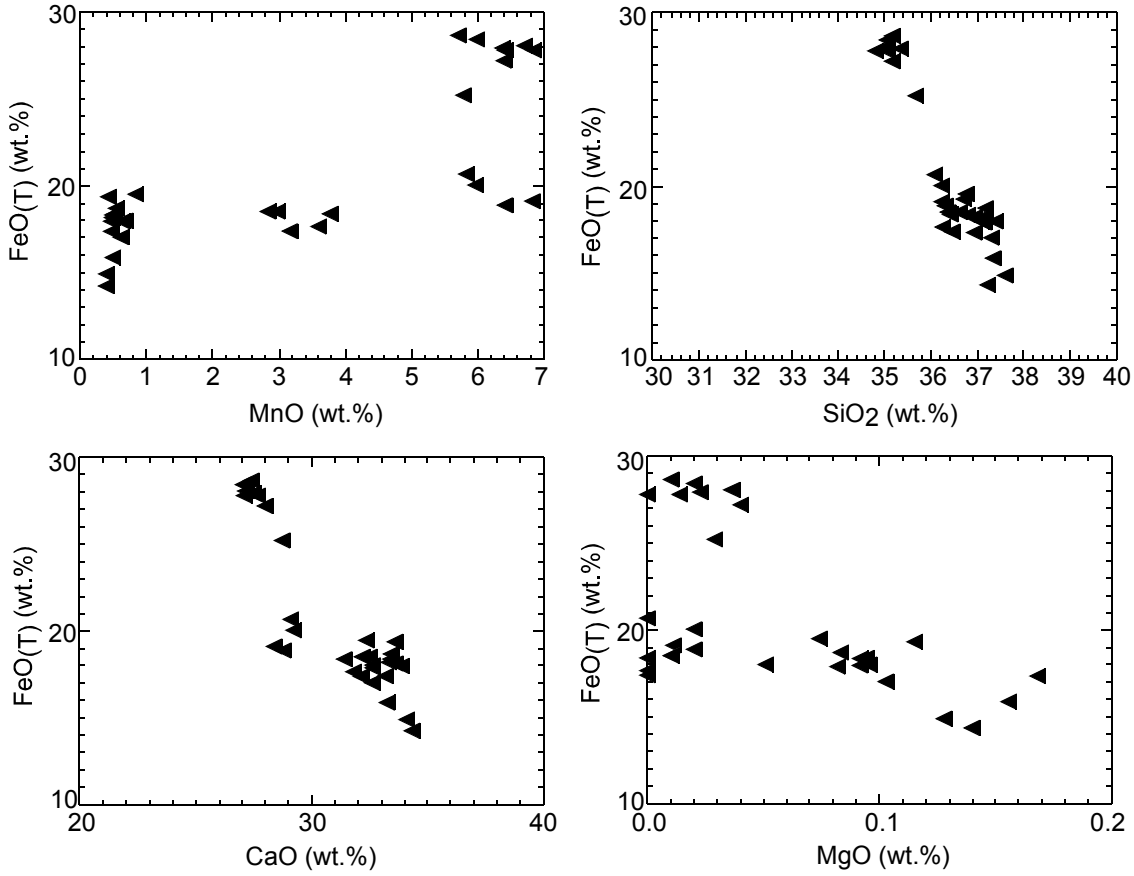

Figure 3.17. The relationships of $FeO_{(T)}$ contents with MgO, MnO, SiO_2 and CaO contents in the garnets.

$FeO_{(T)}$ displays additional significant relationships with MnO, SiO_2, CaO and MgO in the garnets. $FeO_{(T)}$ content decreases with the increases in SiO_2, CaO and MgO, but it increases with the increases of MnO contents (Figure 3.17). The similar correlations are also observed in many skarn districts in the world such as Darwin Pb-Zn-Ag skarn, California-USA (Newberry et al., 1991), Ban Ban zinc skarn, Queensland-Australia (Ashley, 1980) skarn deposits in Oslo Rift, Norway (Jamtveit et al., 1993; 1995) and in Turkey such as Akdağmadeni, Akçakışla skarn district, central Anatolia (Kuşçu, 1997, 2001). This relationship is explained by these authors as due to the exchange between Al^{3+} and Fe^{3+} in the garnet composition during metasomatic processes leading to skarn formation.

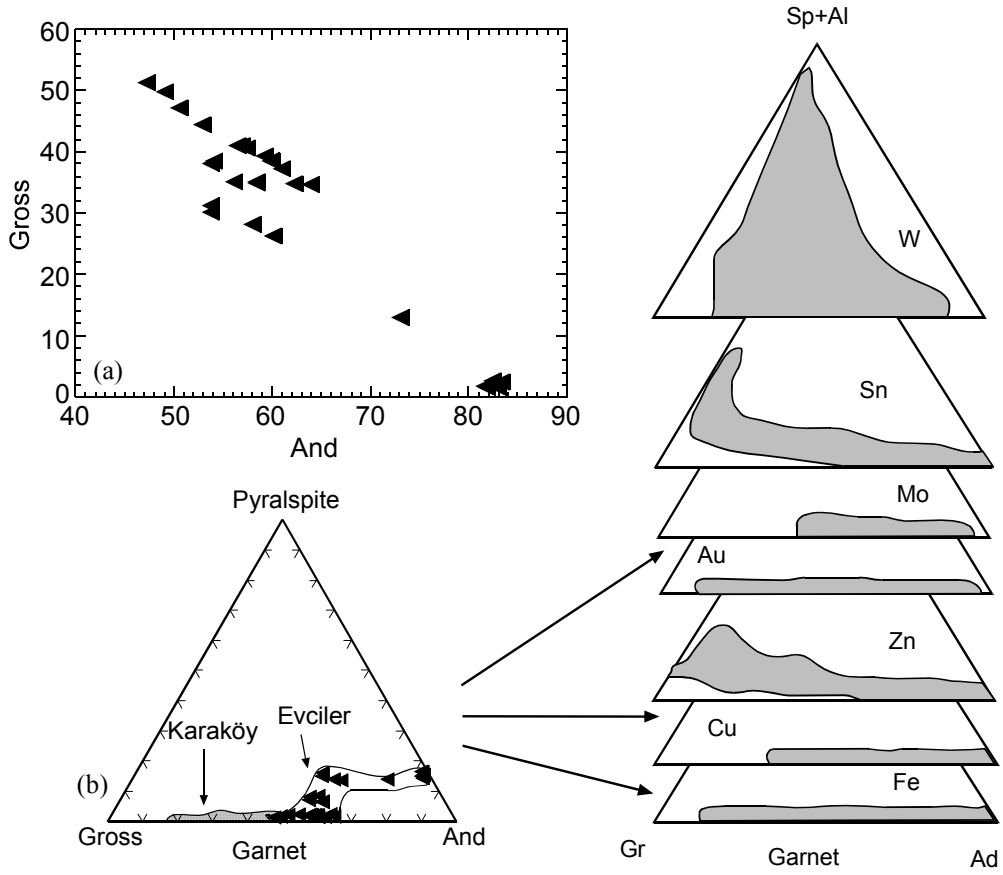

Figure 3.18. (a) The relationship between grossular (Gross) and andradite (And) in the Evciler district; (b) The compositional ternary variation diagram for the garnets from the Evciler district compared with major skarn types. Data from Einaudi et al. (1981) and Meinert (1983, 1989).

Skarn garnet is also commonly expressed by a ternary proportion of its grossular-pyralspite-andradite component, as expressed by $(Ca, Mn, Mg, Fe)_3(Al, Fe)_2(SiO_4)_3$. The garnets in the Evciler district contain grossular ($Ca_3Al_2(SiO_4)_3$), andradite ($Ca_3Fe_2(SiO_4)_3$), spessartine ($Mn_3Al_2(SiO_4)_3$) and pyrope ($Mg_3Al_2(SiO_4)_3$) end members. The grossular mole percent of the garnets range from 1.5 to 51.3%. The andradite mole percent of the garnets range from 47.3 to 83.3%. The spessartine and pyrope mole percent of the garnets are very low compared to those of andradite and grossular, and they range from 0.9 to 16.7% and 0.0 to 0.7%, respectively. Therefore, the garnets in the Evciler district are regarded as grossular-andradite (grandite) garnets, because of their high grossular-andradite contents, and low pyrope-spessartine-almandine (pyralspite) contents. The compositional distribution

of garnets are graphically presented in Figure 3.18a, together with garnets from the Karaköy (data from Öngen, 1992) and other skarn deposits (data from Einaudi et al., 1981; Meinert, 1983; 1989). Al_2O_3 and $FeO_{(T)}$ contents substitute for each other in the garnets during skarnification. The Evciler garnets distinctly fall in the grossular-andradite end-member field, but close to andradite. The composition of the Evciler garnets are similar to those from the Karaköy, though the Karaköy garnets extend more to the grossular field (Figure 3.18a). The examination of Figure 18b shows that the grossular and andradite end-members of the garnets in the Evciler district is inversely related to each other. Grossular decreases as andradite increases (Figure 3.18b). The Evciler skarn garnets contain high iron and low aluminum. Stoichiometric calculation (Table 3) shows that nearly all the iron is in the oxidized state (Fe^{3+}), resulting in the formation of andradite-rich garnets.

3.7.4 Epidote

The compositional variation of epidotes in the Evciler district are shown in Table 3.5. SiO_2 contents of epidotes range from 36.49 to 38.09%. Al_2O_3 contents range from 20.42 to 25.80%. $FeO_{(T)}$ contents range from 9.88 to 15.52%. MnO contents range from 0.027 to 0.623%. TiO_2, MgO and CaO contents range from 0.014 to 0.423, 0.00 to 0.066 and 22.76 to 23.76%, respectively. Significant relationships are observed between Al_2O_3, $FeO_{(T)}$ and MnO contents of epidotes. Al_2O_3 contents decrease as $FeO_{(T)}$ contents increase, whereas it increase with MnO content. $FeO_{(T)}$ contents slightly decrease as MnO content increases (Figure 3.19). The correlation matrix shows the coefficients between SiO_2, TiO_2, Al_2O_3, $FeO_{(T)}$, MnO, MgO, CaO and Na_2O. The most significant relationship is observed between Al_2O_3 and MgO. The correlation coefficient for these represent maximum observed negative correlation (-0.83) (Tablo 3.6). The maximum observed positive correlation occurs between TiO_2 and MnO (0.83). The Mn-Al, Mn-Fe, Fe and Mn classification diagram indicates that the samples plot in the epidote field of the diagram (Figure 3.20).

Table 3.5. Representative microprobe analyses of epidote from Evciler skarn.

SAMPLE	155 (1)	155 (2)	155 (3)	155 (4)	155 (5)	155 (6)	155 (7)	155 (8)	57/4 (1)	57/4 (2)	57/4 (3)	57/4 (4)	57/4 (5)	57/4 (6)	57/4 (7)	57/4 (8)	76/1 (1)	76/1 (2)	76/1 (3)	76/1 (4)	76/1 (5)
wt %																					
SiO_2	37.89	37.84	37.69	37.60	37.64	38.09	37.52	37.14	36.63	36.80	36.49	36.83	36.87	37.03	36.93	36.91	37.23	37.62	37.60	37.69	35.51
TiO_2	0.28	0.08	0.06	0.09	0.08	0.20	0.08	0.07	0.16	0.01	0.18	0.15	0.42	0.211	0.038	0.048	0.162	0.159	0.169	0.189	0.156
Al_2O_3	23.69	25.08	24.68	24.22	24.75	24.77	24.15	24.57	21.70	22.67	20.42	21.24	20.46	23.12	21.82	22.17	24.45	24.18	24.04	23.77	24.12
$FeO_{(T)}$	11.52	9.88	10.55	10.82	10.55	10.27	10.96	10.42	14.02	12.76	15.52	14.56	14.93	12.31	13.67	13.27	10.21	0.42	10.45	10.47	10.34
MnO	0.15	0.08	0.12	0.09	0.14	0.07	0.09	0.10	0.19	0.25	0.54	0.19	0.18	0.282	0.214	0.623	0.028	0.027	0.031	0.036	0.043
MgO	0.02	0.02	0.02	0.00	0.01	0.01	0.01	0.02	0.01	0.01	0.01	0.03	0.03	0.014	0.010	0.021	0.065	0.060	0.054	0.054	0.066
CaO	23.30	23.55	23.34	23.58	23.67	23.56	23.60	23.70	23.34	23.29	22.84	23.33	23.17	23.23	23.20	22.76	23.62	23.47	23.71	23.33	23.42
Na_2O	0.00	0.00	0.00	0.00	0.00	0.00	0.00	0.00	0.00	0.01	0.02	0.01	0.01	0.031	0.010	0.000	0.000	0.009	0.000	0.000	0.020
Total	96.85	96.53	96.46	96.40	96.84	96.96	96.41	96.02	96.05	95.80	96.01	96.34	96.07	96.22	95.89	95.80	95.76	85.94	96.05	95.54	93.68
									Number of ions on the base of 13 atoms of oxygen												
Si	3.099	3.077	3.078	3.081	3.066	3.088	3.077	3.054	3.078	3.076	3.097	3.093	3.113	3.071	3.098	3.094	3.064	3.269	3.088	3.109	3.003
Al	2.284	2.403	2.375	2.339	2.376	2.367	2.334	2.381	2.149	2.233	2.043	2.103	2.036	2.260	2.158	2.190	2.371	2.476	2.327	2.311	2.404
Ti	0.017	0.005	0.004	0.006	0.005	0.012	0.005	0.004	0.010	0.001	0.011	0.010	0.027	0.013	0.002	0.003	0.010	0.010	0.010	0.012	0.010
Mg	0.002	0.003	0.003	0.000	0.001	0.001	0.001	0.002	0.001	0.001	0.001	0.003	0.004	0.002	0.001	0.003	0.008	0.008	0.007	0.007	0.008
Fe^{2+}	0.788	0.672	0.721	0.742	0.719	0.696	0.752	0.716	0.985	0.892	1.102	1.023	1.054	0.854	0.959	0.930	0.703	0.031	0.718	0.722	0.731
Mn	0.010	0.005	0.008	0.006	0.010	0.005	0.006	0.007	0.014	0.018	0.039	0.013	0.013	0.020	0.015	0.044	0.002	0.002	0.002	0.003	0.003
Ca	2.042	2.052	2.042	2.070	2.066	2.047	2.074	2.088	2.101	2.086	2.077	2.099	2.096	2.064	2.086	2.044	2.083	2.185	2.086	2.062	2.122
Na	0.000	0.000	0.000	0.000	0.000	0.000	0.000	0.000	0.000	0.002	0.003	0.002	0.002	0.005	0.002	0.000	0.000	0.002	0.000	0.000	0.003
Sum	8.242	8.217	8.231	8.244	8.242	8.216	8.250	8.252	8.338	8.308	8.372	8.347	8.344	8.288	8.321	8.308	8.240	7.983	8.238	8.224	8.286
Xfe	0.997	0.996	0.996	1.000	0.998	0.998	0.999	0.997	0.999	0.999	0.999	0.997	0.996	0.999	0.999	0.997	0.989	0.797	0.991	0.991	0.989

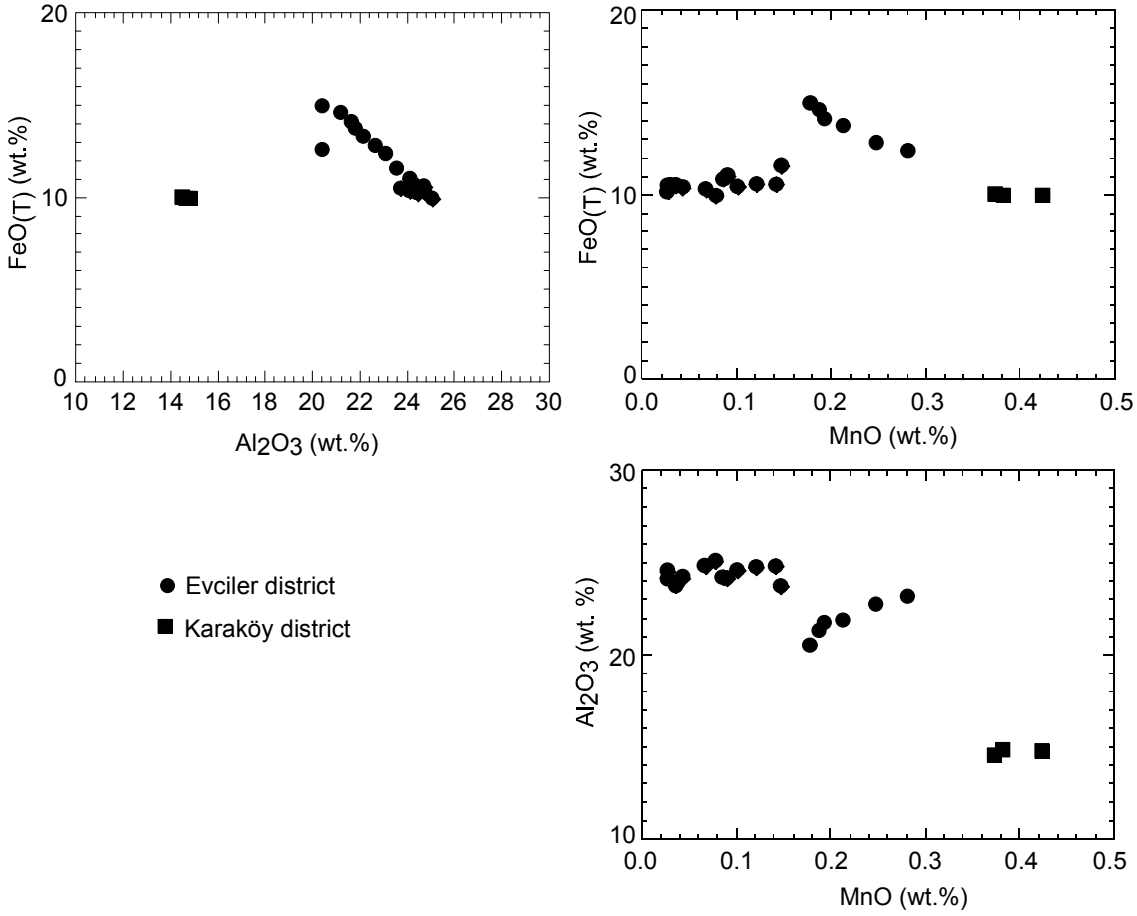

Figure 3.19. The relationships between Al_2O_3, $Fe_2O_{3(T)}$ and MnO in epidotes.

Table 3.6. Correlation matrix for the major oxides in epidotes from the Evciler district.

	SiO_2	TiO_2	Al_2O_3	$FeO_{(T)}$	MnO	MgO	CaO	Na_2O
SiO_2	1	0.27	-0.09	-0.53	-0.15	0.28	0.11	-0.44
TiO_2		1	-0.83	-0.18	0.34	0.84	-0.13	0.38
Al_2O_3			1	-0.03	-0.67	-0.83	0.13	-0.41
$FeO_{(T)}$				1	0.30	-0.45	-0.08	0.21
MnO					1	0.32	-0.14	0.37
MgO						1	-0.16	0.28
CaO							1	-0.16
Na_2O								1

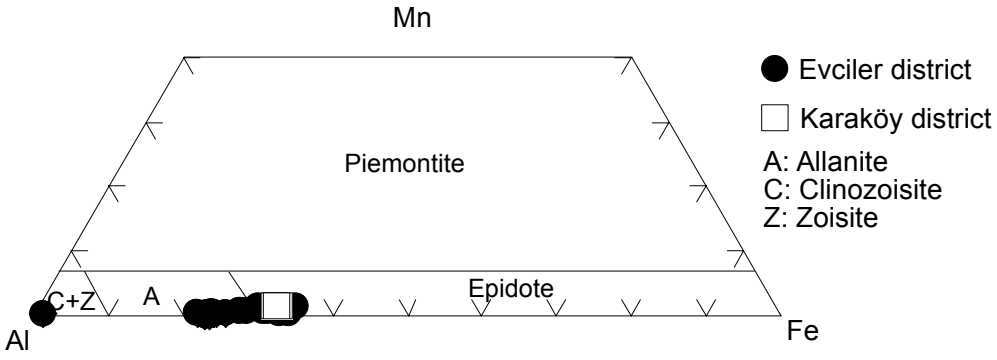

Figure 3.20. Mn-Al, Mn-Fe, Fe and Al classification diagram for the epidotes.

3.7.5 Redox Conditions

Redox conditions prevailing during skarn evolution influence the skarn type formed and can be inferred from the determination of relative ratios of Fe^{2+}/Fe^{3+} in skarn minerals (Zaw and Singoyi, 2000). Sato (1980) and other authors have shown that reduced skarns typically have relatively high Fe^{2+}/Fe^{3+} ratios, whereas oxidized skarns have relatively low Fe^{2+}/Fe^{3+} ratios. Brown and Essene (1985) suggested that redox can only be calculated from garnet and pyroxene phases, because either mineral phases are end-member in composition (e.g., quartz, wollastonite, and amphibole) or have end-member equilibria with insufficient thermodynamic data for redox determination (e.g., vesuvianite and epidote).

Most of the Evciler skarn minerals have compositions that are indicative of an oxidizing environment of deposition. The pyroxene at Evciler is diopsidic clinopyroxene (Mg-rich, Fe^{2+}-poor) and coexists or is overprinted by andradite-rich (Fe^{3+}-rich) garnet. Kwak (1994) has pointed out that there is a tendency to produce Mg-rich pyroxene and andradite in oxidized environments and hedenbergite (plus grossular) in reduced skarns.

The occurrence of diopside and andradite with little hedenbergite at Evciler suggests that conditions during skarn formation of the Evciler skarn were oxidizing. The widespread occurrence of epidote is also consistent with oxidizing conditions

(e.g., Kwak, 1994). In contrast, the occurrence of pyrrhotite-bearing mineralization with minor chalcopyrite and pyrite is of reduced condition.

These variations may be related to availability of pyrrothite-forming elements in the fluids; if they are related to changes in the oxidation-reduction state of the skarn, then they represent minor fluctuations within a dominantly oxidized skarn. Therefore, late-stage skarn formation at Evciler was reducing based on the presence of the pyrrhotite. It is known that pyrrhotite forms a very significant proportion of the early-stage skarn mineralogy. Zaw and Singoyi (2000) indicated that redox conditions can be estimated from more predominant minerals (garnet, clinopyroxene, epidote etc.). The reducing conditions may have existed at Evciler, but only locally as the predominant skarn minerals from stages I and II indicate oxidized conditions as discussed above.

3.8 Discussion and Conclusions

The paragenetic studies at Evciler show that skarn evolution occurred in two stages. Stage-I mineral assemblage is dominated by clinopyroxene and garnet. This stage is considered to represent prograde anhydrous skarn development, whereas stage-II, which is dominated by hydrous minerals (amphibole, epidote), is considered to represent retrograde alteration of the skarn and main sulfide deposition, which comprises pyrrhotite, pyrite, chalcopyrite, chlorite and/or quartz, calcite.

Chemical determinations of minerals from the Evciler and the Karaköy skarns showed that large proportions of minerals at these locations are calcium-rich (grossular-andradite, amphibole, epidote, titanite). This observation suggests high calcium activity during skarn formation, most likely emanating from the dissolution of the calcic carbonate protolith (Kazdağ marble lenses). Mineral chemistry also provide information, which can be used to classify the skarn type. In their attempts to classify skarns on the basis of pyroxene and garnet compositions, Nakano et al. (1994) reported that Mn/Fe ratios of pyroxene in each deposit are relatively constant and that they tend to vary regionally in accordance with metal type. They found that

tungsten skarns have pyroxene composition with an intermediate Mn/Fe (avg. around 0.15), Cu-Fe deposits have low Mn/Fe (<0.1), whereas Zn-Pb deposits have high Mn/Fe ratios (>0.2). The average clinopyroxene Mn/Fe ratio of 0.03 at the Evciler skarn is consistent with the classification of Nakano et al. (1994).

However, Einaudi and Burt (1982) noted that the chemical composition of pyroxenes in skarn deposits is variable dependent on the dominant metal. They classified skarn deposits into six groups based on metal association, Cu, Fe, Au Zn-Pb, W and Sn, and noted that johannsenitic pyroxene accompanies Pb-Zn deposits, whereas diopside-ferrosalite pyroxene is present in Cu-Fe deposits (Nakano et al., 1994). Previous data on skarn mineral compositions appear to be consistent with this classification (e.g. Meinert, 1987; Newberry et al., 1991).

3.8.1 Comparison to Other Cu-Fe and Au Skarns and Genetic Model

The Evciler and the Karaköy skarn occurrences show many similarities and a few differences with other calcic Fe-Cu and Au skarns (e.g., Einaudi et al., 1981; Meinert, 1983, 1989). The deposits occur in carbonate host litologies of various ages that are associated with felsic intrusions of varying ages. Other important features associated with these deposits include oxidation state of the skarns, plumbing system or channel ways for fluids, metal source, and level of emplacement of the associated intrusion (Zaw & Singoyi, 2000). These deposits are generally characterized by early anhydrous mineral assemblages that are overprinted by later hydrous retrograde mineral assemblages.

The Evciler deposit is extremely rich in pyrrothite, magnetite and chalcopyrite, and appear to be oxidized, but pyrrothite characterizes a reduced environment. The difference in oxidation levels of the skarn is revealed by varying Fe^{2+}/Fe^{3+} ratios, which are generally manifested in the type of garnet and clinopyroxene formed.

The genesis of the Evciler deposit is demonstrated schematically in Figure 3.21, which shows the development of the skarn following the Late Oligocene/Early

Miocene granitoid intrusion into Kazdağ metamorphic rocks. Skarns develop in the marble lenses, which have direct contact with the intrusion. During the early stage (stage-I), skarn-forming fluids are largely anhydrous and derived from granite, with no convection cell to focus fluids from meteoric sources from the country rocks. Major pyrrhotite-bearing mineralization occurs within the pyroxene skarn. The late stage (stage-II), magmatic fluids mix with meteoric fluids, and are focussed into permeable early-formed skarns and marble to form late-stage skarns and mineralization, which are dominantly hydrous. This late-stage is also accompanied by the formation of endoskarn due to metasomatic alteration of the igneous protolith in areas where fluids have permeated intensely.

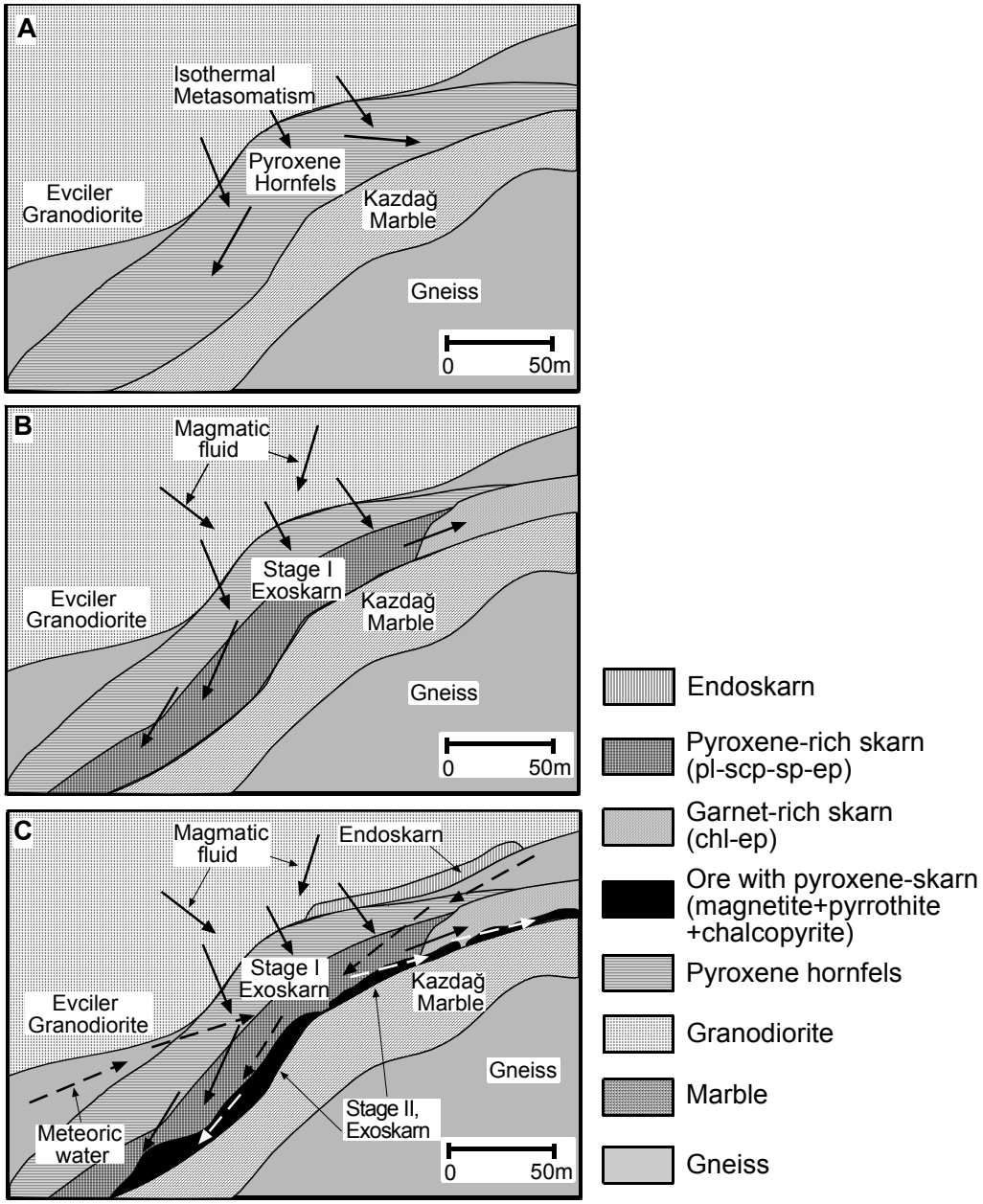

Figure 3.21. Idealized cross sections showing the genesis of the Evciler skarn deposit, southeastern Evciler village, Kazdağ. (a) isothermal metasomatism, (b) prograde alteration (stage-I) and (c) retrograde alteration and mineralization (stage-II).

3.9. References

Ashley, P.M. (1980). Geology of the Ban Ban zinc deposit: a sulfide-bearing skarn, Southeast Queensland, Australia. *Economic Geology*, *75*, 15-29.

Altherr, R., Henjes-Kunst, F., Matthews, A., Friedrichsen, H., & Hansen, B.T. (1988). O-Sr isotopic variations in Miocene granitoids from the Aegean: Evidence for an origin by combined assimilation and fractional crystallization. *Contribution to Mineralogy and Petrology*, *100*, 528-541.

Baren, A., Göd, R., Götzinger, M., & Zemman, J. (1985). A scheelite mineralization in calc-silicate rocks of Moldanubicum (Bohemian massif) in Austria. *Mineralium Deposita*, *20*, 16-22.

Bingöl, E. (1977). Muratdağı jeolojisi ve anakayac birimlerinin petrolojisi. *Turkiye Jeoloji Kurumu Bülteni*, *20*, 13-67.

Bingöl, E. (1978). Explanatory notes to the metamorphic map of Turkey, *In.* Zwart, H.J. (ed.). *Metamorphic map of Europe, explanatory text. Leiden, UNESCO*, Subcommission for the cartography of the metamorphic belts of the World, 148-154.

Bingöl, E., Delaloye, M., & Ataman, G. (1982). Granitic intrusion in Western Anatolia: a contribution to the geodynamic study of this area. *Eclogae Geologicae Helvetiae*, *75*, 437-446.

Birkle, P. (1992). Petrologie-Geochem'e and Geochronogic des Miozanen Magmatismus auf der Biga-halbinhsel (Ezine, NW-Turkei). *Diplomarbiet an der Geowissenschaft Lichen Fakultat der Eberhard-Karls-Universtat, Tübingen*.

Brown, P.E., & Essene, J.E. (1985). Activity variations attending tungsten skarn formation, Pine Creek, California. *Contribution to Mineralogy and Petrology*, *89*, 358-369.

Ciobanu, C.L., & Cook, N.J. (2004). Skarn textures and a case study: the Ocna de Fier-Dognecea orefield, Banat, Romania. *Ore Geology Reviews*, *24*, 315-370.

Deer, W.A., Howie, R.A., & Zussman, J. (1993). Rock-forming Minerals, Framework Silicates: Feldspars. Geological Society. London, *4A*, 972 p.

Delaloye, M., & Bingöl, E. (2000). Granitoids from Western and Northwestern Anatolia: Geochemistry and modeling of geodynamic evolution. *International Geology Reviews*, *42*, 241-268.

Duru, M., Pehlivan, Ş., Şentürk, Y., Yavaş, F., & Kar, H. (2004). New results on the lithostratigraphy of the Kazdağ Massif in Northwest Turkey. *Turkish Journal of Earth Sciences*, *13*, 177-186.

Einaudi, M.T. (1977). Petrogenesis of copper-bearing skarn at the Mason Valley Mine. Yerington district, Nevada. *Economic Geology*, *72*, 769-795.

Einaudi, M.T., Meinert, L.D., & Newberry, R.J. (1981). Skarn deposits. *Economic Geology (75th anniversary volume)* 317-391.

Einaudi, M.T., & Burt, D.M. (1982). Terminology, classification and composition of skarn deposits. *Economic Geology*, *77*, 745-754.

Gaspar, L.M., & Inverno, C.M.C. (2000). Mineralogy and metasomatic evolution of distal strata-bound scheelite skarns in the Riba de Alva Mine, Northeastern Portugal. *Economic Geology, 95*, 1259-1275.

Genç, Ş., C. (1998). Evolution of the Bayramiç magmatic complex, northwestern Anatolia. *Journal of Volcanology and Geothermal Research*, *85*, 233-249.

Gülen, L. (1990). Isotopic characterization of Aegean magmatism and geodynamic evolution of the Aegean subduction. *In.* Savaşcın, M.Y. & Eronat, A.H. (ed.), *IESCA Proceedings*, İzmir, Turkey, *2*, 143-166.

Harris, N.B.W., Kelley, S., & Okay, A.I. (1994). Post-collisional magmatism and tectonics in northwest Anatolia. *Contributions to Mineralogy and Petrology*, *117*, 241-252.

Iiyama, J.T. (1979). Experimental study of the material transport in the earth's crust, in Sunagawa, I., et al., eds., the materials science of the earth's interior: Tokyo, Ministry *of Education, Science, and Culture in Japan*, 50-53.

Iiyama, J.T. (1982). Material transport in the earth's crust and properties of mineral: *Japanese Association of Mineralogists, Petrologists and Economic Geologists Journal Special Issue*, *3*, 291-304.

Jamtveit, B., Wogelius, R.A., & Fraser, D.G. (1993). Zonation patterns of skarn garnets, records of hydrothermal system evolution. *Geology, 21* (2), 113-116.

Jamtveit, B., Ragnarsdattir, K.V., & Wood, B.J. (1995). On the origin of zoned grossular-andradite garnets in hydrothermal systems. *European Journal of Mineralogy*, *7*, 1399-1410.

Karacık, Z., & Yılmaz, Y. (1998). Geology of the ignimbrites and the associated volcano-plutonic complex of the Ezine area, northwestern Anatolia. *Journal of Volcanology and Geothermal Research*, *85*, 251-264.

Kuşçu, İ. (1997). Mineralogical and geochemical comparison of skarns in the Akmağdeni, Akçakışla and Keskin districts, central Anatolia, Turkey. *PhD Thesis, the Middle East Technical University, Turkey*.

Kuşçu, İ. (2001). Geochemistry and mineralogy of the skarns in the Çelebi District, Kırıkkale, Turkey. *Turkish Journal of Earth Sciences*, *10*, 121-132.

Kwak, T.A.P. (1994). Hydrothermal alteration in carbonate-replacement deposits: *Geological Association of Canada Short Course Notes*, *11*, 381-402.

Labotka, T.C. (1991). Chemical and physical properties of fluids. *Reviews in Mineralogy*, *26*, 43-104.

Lentz, D.A., Walker, J., & Stirling, J. (1995). Millstream Cu-Fe skarn deposit: an example of a Cu mineralised magnetite-rich skarn system in Northern New Brunswick. *Exploration and Mining Geology*, *4*, 15-31.

McKenzie, D., & Yılmaz, Y. (1991). Deformation and volcanism in Western Turkey and the Aegean. *Bulletin of Technical University of İstanbul*, *44*, 345-373.

Meinert, L.D. (1983). Variability of skarn deposits – Guides to exploration, in Boardman, S.J., ed., *Revolution in the Earth Sciences: Kendall-Hunt Publishing Co*., 301-316.

Meinert, L.D. (1987). Skarn zonation and fluid evolution in the Groundhog mine, Central Mining District, New Mexico. *Economic Geology*, *82*, 523-545.

Meinert, L.D. (1989). Gold skarn deposits – Geology and exploration criteria, in Groves, D., Keays, R., and Ramsay, R., ed., Proceedings of Gold'88: *Economic Geology Monograph*, *6*, 537-552.

Meinert, L.D. (1992). Skarns and skarn deposits: *Geoscience Canada*, *19*, 145-162.

Meinert, L.D. (1993). Igneous petrogenesis and skarn deposits. *In.* Kirkham, R.V., Sinclair, V.D., Thorpe, R.I., Duke, J.M. (ed), *Geological Association of Canada Special Paper, Toronto*, *40*, 569-583.

Meinert, L.D. (1995). Compositional variation of igneous rocks associated with skarn deposits - Chemical evidence for a genetic connection between petrogenesis and mineralization: in Thompson, J. F. H., ed., Magmas, fluids, and ore deposits, *Mineralogical Association of Canada Short Course Series*, *23*, 401-418.

Misra, K.C. (2000). Understanding Mineral Deposits. *Kluwer Academic Publishers, Dordrecht, the Netherlands*.

Morgan, B.A. (1975). Mineralogy and origin of skarns in the Mount Morrison pendent, Sierra Nevada, California. *American Jorunal of Science*, *275*, 119-142.

Nakano, T., Yoshino, T., Shimazaki, H., & Shimizu, M. (1994). Pyroxene composition as an indicator in the classification of skarn deposits. *Economic Geology*, *89*, 567-1580.

Newberry, R.J., Einaudi, M.T., & Eastman, A.H. (1991). Zoning and genesis of the Darwin Pb-Zn-Ag skarn deposit, California: a reinterpretation based on new data. *Economic Geology*, *86*, 960-982.

Newberry, R.J. (1998). W- and Sn-skarn deposits: *Mineralogical Association of Canada Short Course Series*, *26*, 289-335.

Okay, A., I., Satır, M., Maluski, H., Siyako, M., Metzger, R., & Akyüz, S. (1996). Paleo- and Neo-Tethyan events in Northwestern Turkey: geological and geochronological constraints. In: An, Y., Harrison, M. (Eds), *Tectonics of Asia. Cambridge Univ. Press*, 420-441.

Okay, A., I., & Satır, M. (2000). Coeval plutonism and metamorphism in a latest Oligocene metamorphic core complex in northwest Turkey. *Geological Magazine*, *137* (5), 495-516.

Öngen, S. (1992). Les échances métasomatiques entre granitoides et encaissant particuliers (calcaires, dolomies, ultrabasites, series manganiferes): I'example de la Turquie-NW. *Doctorat These. Université de Nancy, Faculté des Sciences de la Terre*, 554 p.

Pan, Y. (1998). Scapolite in skarn deposits: Petrogenetic and geochemical significance. *Mineralogical Association of Canada Short Course Series*, *26*, 169-209.

Rebbert, C.R., & Rice, J.M. (1997). Scapolite-plagioclase exchange: Cl-CO_3 scapolite solution chemistry and implications for peristerite plagioclase. *Geochimica et Cosmochimica Acta*, *61*, 555-567.

Sato, K. (1980). Tungsten skarn deposit of the Fujigatani mine, southwest Japan. *Economic Geology*, *75*, 1066-1082.

Somarin, A.K. (2004). Geochemical effects of endoskarn formation in the Mazreah Cu-Fe skarn deposit in northwestern Iran. *Geochemistry: Exploration, Environment, Analysis*, *4*, 307-315.

Şengör, A.M.C., & Yılmaz, Y. (1981). Tethyan evolution of Turkey: a plate tectonic approach. *Tectonophysics*, *75*, 181-241.

Şengör, A.M.C., Cin, A., Rowley, D.B., & Nie, S.-Y. (1993). Space-time patterns of magmatism along the Tethysides: a preliminary study. *Journal of Geology*, *101*, 51-84.

Yardley, B.W.D., & Lloyd, G.E. (1995). Why metasomatic fronts are really metasomatic sides. *Geology*, *23*, 53-56.

Yılmaz, Y. (1989). An approach to the origin of young volcanic rocks of western Turkey. In: Şengör, A.M.C., (eds.), *Tectonic evolution of the Tethyan Region. Kluwer Academic Publ.*, p. 159.

Yılmaz, Y. (1990). Comparison of the young volcanic associations of the west and east Anatolia under the compressional regime: a review. *Journal of Volcanology and Geothermal Research*, *44*, 69-87.

Yılmaz, Y. (1995). Ege bölgesinde genç magmatizmanın oluşumu ile litosferin evrimi arasındaki ilişki üzerine düşünceler. *Jeofizik*, *9*, 107-110.

Yılmaz, Y. (1997). Geology of western Anatolia. *Active tectonics of Northwestern Anatolia-The Marmara Poly-Project. VDF, Hochschulverlag Ag an Der ETH, Zürich*, 1-20.

Yücel-Öztürk, Y., Helvacı, C., & Satır, M. (2005) Genetic relations between skarn mineralization and petrogenesis of the Evciler granitoid (Kazdağ, Çanakkale-Turkey) and comparison with world skarn granitoids. *Turkish Journal of Earth Sciences*, *14*, 255-280.

Zaw, K., & Singoyi, B. (2000). Formation of magnetite-scheelite skarn mineralization at Kara, Northwestern Tasmania: evidence from mineral chemistry and stable isotopes. *Economic Geology*, *95*, 1215-1230.

CHAPTER FOUR
OXYGEN AND HYDROGEN ISOTOPE STUDY OF EVCİLER SKARN OCCURRENCE, KAZDAĞ, ÇANAKKALE/TURKEY

4.1. Abstract

Stable isotope compositions of calc-silicate minerals from skarn deposits have been used to interpret the evolution of fluid sources during sequential stages of skarn formation. Aim of the analyses was the determination of temperatures of formation, the extent of equilibration amongst the mineral phases and/or of possible alteration through fluid-mineral isotopic exchange.

Generally, skarn ore deposits are characterized by two distinctly different alteration styles. An early prograde stage with anhydrous minerals, such as garnet and pyroxene, which forms in the presence of relatively high-temperature fluid. A later retrograde stage with hydrous minerals, such as epidote, amphibole, and chlorite plus sulfide ore minerals, which forms in the presence of in the lower temperature fluid. These two alteration stages commonly have been thought to reflect a dominance of magmatic and meteoric water, respectively, with relevance to the source of ore metals. We report data from the Evciler Au-Cu skarn deposit (Kazdağ, NW Anatolia). Stable isotope compositions of anhydrous and hydrous alteration minerals from this deposit indicate that garnet-pyroxene skarn (prograde stage) was produced by predominantly magmatic fluids during initial skarn forming metasomatism in the study area and amphibole-epidote rich skarn (retrograde stage) was formed by magmatic water mixed with meteoric water. The $\delta^{18}O$ values of garnet from the Evciler district range from 4.6 to 8.2‰ (average 6.7‰), the $\delta^{18}O$ values of pyroxene range from 6.2 to 10.3‰ (average 8.2‰), and the $\delta^{18}O$ values of amphibole range from 6.3 to 8.2‰ (average 7.4‰) and the $\delta^{18}O$ values of epidote range from -3.3 to 5,1‰ (average 0.9‰). However, the δD values of retrograde alteration minerals such as amphibole and epidote indicate both magmatic and lighter values for Evciler skarn deposit that could be explained by mixing with meteoric water.

We concluded that the isotopic evolution of the hydrothermal fluid can be accounted for by circulation of meteoric water through a convection system heated by the Evciler granitoid, causing exchange of oxygen isotopes with the granitoid and country rock, and possibly involving some admixture of magmatic water.

Keywords. Evciler granitoid, ore deposit, stable isotopes, hydrothermal alteration.

4.2. Introduction

Studies of skarn deposits generally begin with comprehensive analyses of field relationships, mineral compositions, and paragenetic relations; however, these alone usually have been insufficient to constrain pressure-temperature-fluid composition (P-T-X) conditions of skarn formation adequetaly, in large part due to the high variance assemblages that typically result from metasomatic processes (Hall *et al.,* 1988). Bowman & Essene (1984), Bowman *et al.* (1985), and Rose *et al.* (1985) have succesfully combined petrologic and stable isotope studies to delineate conditions of skarn formation.

Many studies have demonstrated multiple sources of fluids responsible for forming ore deposits (e.g., Meinert *et al.*, 2003). A variety of theories of ore genesis invoke interactions among such fluids, particularly those of magmatic and meteoric origin (Giggenbach, 1997; and Taylor, 1997, respectively). Since most skarn ores have an intimate spatial relationship with magmatic intrusions, their minerals should provide a clear record of the fluid(s) that were present in the intrusive environment during ore formation.

Previous studies of multistage proximal skarns (e.g., Taylor & O'Neil, 1977, Osgood Mountains, Nevada; Bowman et al., 1985a, Elkhorn, Montana; Brown *et al.*, 1985, Pine Creek, California) have established the utility of stable isotope analyses in recognizing variation in fluid sources and in estimating the degree of interaction between skarn-forming minerals and carbonate wall rock. These studies all concluded that magmatic fluid or fluid that had equilibrated with the adjacent intrusion was predominant during the initial stages of skarn-forming metasomatism

(Layne *et al.*, 1991). Subsequent lower temperature stages, however, may display an increasing involvement of meteroric water, which becomes the predominant fluid component in the latest stages of skarn formation (Bowman *et al.*, 1985a; Taylor & O'Neil, 1977).

The Evciler skarn evolved through early stages typified by garnet-pyroxene (stage I) and amphibole-epidote-calcite (stage II) and chlorite-pyrothite-pyrite (stage III) assemblages. Stage III mineralization has a particular economic interest. In this deposit, there was a transition from high temperature fluid associated with prograde garnet-pyroxene skarn to lower temperature fluid associated with retrograde epidote-amphibole skarn alteration.

This paper presents the results of a stable isotope study of the skarn-forming minerals at Evciler. Stable oxygen and hydrogen isotope analyses were made of appropriate mineral phases from the Evciler skarn with two broad objectives; to derive estimates of fluid temperature from oxygen isotope geothermometry on appropriate mineral pairs, and to model the isotopic composition and origin of skarn forming fluids (at each successive stage).

4.2.1. Terminology, Notation and Isotopic Fractionation

Stable isotopic compositions are expressed in the δ or "delta" notation:

$$\delta = \left(\frac{R_{sa} - R_{std}}{R_{std}} \right) x1000 \qquad (1)$$

where R_{sa} and R_{std} are the atomic ratios of the heavy to light isotope in the sample or standard, respectively (in this case $^{18}O/^{16}O$). Hence a sample depleted in the heavy isotope with respect to the standard will have a negative δ value, whereas a sample enriched in the heavy isotope with respect to the standard will have a positive δ value. Values of δ are in parts per thousand or per mil. The internationally recognized standards are: VSMOW (Vienna Standard Mean Ocean Water) for

hydrogen and oxygen, PDB (Peedee Bellemnite) for carbon and oxygen, and CDT (troilite from Canyon Diablo meteorite) for sulfur.

An important term expressing the extent of isotopic fractionation between two coexisting compounds or phases 1 and 2 is the fractionation factor, α:

$$\alpha_{1-2} = \frac{R_1}{R_2} \tag{2}$$

In terms of δ-values, the fractionation factor α is expressed as:

$$\alpha_{(1-2)} = \left(\frac{\delta_1 + 1000}{\delta_2 + 1000} \right) \tag{3}$$

For fractionations of less than 10 per mil (absolute value), a good approximation is:

$$\Delta_{(1-2)} = \delta_1 - \delta_2 \cong 10^3 \ln \alpha_{(1-2)} \tag{4}$$

The value of the fractionation factor α is a function of temperature. For many pairs of compounds and phases, the fractionation factor decreases with increasing temperature; as a function of $1/T^2$ at low temperature and as a function of $1/T^2$ at elevated temperature. This inverse temperature dependence is the basis of stable isotope geothermometry. The theoretical justifications for these temperature dependencies and the behaviour of specific compound and mineral pairs have been reviewed extensively and summarized in O'Neil (1986) and Kyser (1987).

4.2.2. Rock and Fluid Reservoir

Many of Earth's major reservoirs of rock and water are isotopically distinct in δD and $\delta^{18}O$ value, or both. The field for magmatic water, water in hydrogen- and oxygen-isotope equilibrium with unaltered igneous rock at high temperature, is

subdivided into I-type and S-type ranges along which $^{18}O/^{16}O$ ratio increases from I-type to S-type.. The δD values of meteoric and magmatic water overlap in the range -40 to -80 per mil, but even these relatively D-rich meteoric waters have $\delta^{18}O$ values (-7 or lower) that are well lower than those of magmatic waters. Magmatic fluids have much lower $\delta^{18}O$ values than marine carbonate rocks. The result is that any interaction between magmatic waters and marine carbonate rocks should be reflected by modification of the $\delta^{18}O$ values of one or both of these isotopically distinct reservoirs. As a result, hydrogen and oxygen isotopes are inherently powerful tracers of the origins of hydrothermal fluids and for monitoring magmatic fluid-carbonate-rock interactions common in skarn systems.

In applications of hydrogen and oxygen isotopes as tracers of the origins of skarn or other hydrothermal fluids, two basic approaches are used to determine the δD and $\delta^{18}O$ values of the skarn-forming fluids. The first is direct analysis of the hydrothermal fluids, but that is not possible in other than modern geothermal systems, except through liberation of fluid trapped in inclusions in minerals from paleohydrothermal systems. This approach has the adventage of direct isotopic analysis of the hydrothermal fluid, but fluid inclusion water is known to exchange oxygen isotopes with the enclosing minerals (Ohmoto, 1986), and extraction of fluids from a single generation of fluid inclusions is fraught with practical difficulties. The second and more common approach is to analyze the isotopic composition of a mineral or minerals formed in the hydrothermal system and then calculate the isotopic composition of the hydrothermal fluid using available fractionation factors and temperature limits. For this approach to yield valid information, two basic assumptions must hold: (1) the minerals must have formed in isotope exchange equilibrium with hydrothermal fluid; and (2) the original δ value of the mineral at the time of its formation must be preserved. These assumptions should always be evaluated in applications of stable-isotope geochemistry to hydrothermal systems, including skarn systems. The usual test for exchange equilibrium is to analyze two or more coexisting minerals and determine whether or not they have compatible isotopic compositions by applying the appropriate mineral-mineral fractionation factors.

An additional requirement for determining the δD and $\delta^{18}O$ value of the skarn fluid from the measured δ values of the mineral(s) is that the temperature of formation of the mineral(s) be known. In principle, the temperature of formation can be deduced from the measured differences in δ values of coexisting minerals in skarn systems. If well-calibrated mineral pairs do not coexist in a particular skarn system or are not in isotope exchange equilibrium, than it is critical to conduct stable-isotope studies of skarns in conjuction with phase equilibria and fluid-inclusion studies to provide the necessary information on formation temperatures.

4.2.3. Stable-isotope geothermometry in skarn systems

Stable-isotope geothermometry is potentially very useful in skarn systems because isotopic fractionation is independent of pressure, unlike fluid-inclusion, cation exchange, and phase-equilibria geothermometry. Further, often phase-equilibria geothermometry depends on the presence of a few or even a single limiting mineral assemblage. Because of the typically high variance of skarns, such assemblages are rare, and applications of phase equilibria usually provide only upper of lower limits to temperature.

4.2.3.1 Assumptions and Criteria

As a consequence of its $1/T^2$ dependence at elevated temperature, the temperature dependence of fractionation factors for specific mineral (or compound)-water pairs are generally expressed in the form:

$$10^3 \ln \alpha_{(1-2)} = A_{(1-2)}\left(10^6 T^{-2}\right) + B_{(1-2)} \tag{5}$$

for coexisting compounds 1 and 2, and where the constants A and B are determined experimentally, empirically, from theoretical considerations, or from some combination of these approaches (Bottinga & Javoy, 1973, 1975; Friedman & O'Neil, 1977; Kyser, 1987; O'Neil, 1986).

Constant A and B for mineral-water systems, including those relevant to skarn systems, are compiled in O'Neil (1986) and Kyser (1987). Fractionation factors for mineral pairs are derived in a straightforward manner by algebraic combination of the appropriate mineral-water factors. For example, the quartz-pyroxene factor is generated by substracting the pyroxene-water factor from the quartz-water factor (Bottinga & Javoy, 1973, 1975):

$$10^3 \ln \alpha_{(Qz-H_2O)} = 4.1\left(10^6 T^{-2}\right) - 3.7 \tag{6}$$

$$-\left[10^3 \ln \alpha_{(Px-H_2O)} = 1.42\left(10^6 T^{-2}\right) - 3.7\right] \tag{7}$$

$$10^3 \ln \alpha_{(Qz-Px)} = 2.68\left(10^6 T^{-2}\right) \tag{8}$$

To obtain geologically meaningful temperatures with isotope geothermometry, the following assumptions and conditions must hold: (1) the mineral pair(s) must attain isotopic exchange equilibrium at the time of their formation; (2) the minerals must preserve their original δ values; (3) the isotopic fractionation between the mineral pairs should be a regular and sensitive function of temperature; and (4) these fractionation factors must be calibrated reasonably well.

In a number of skarns, the results of isotope geothermometry are generally consistent with the results of phase-equilibria and fluid inclusion geothermometry. In the Osgood Mountains skarn (Nevada), ^{18}O fractionation between quartz and amphibole from the early retrograde skarn development (Stage II) yields temperatures from 480 to 540ºC (average 523ºC) that are comparable with upper limits of 475ºC defined by phase equilibria (Taylor & O'Neil, 1977). In the Cantung W-skarn deposit (N.W.T.), isotope temperatures for both anhydrous (stage I) and hydrous (stage II) skarn development (Bowman, Covert, Clark & Mathieson, 1985a) are compatible with phase-equilibria limits of maximum temperature, and are somewhat higher than the results of fluid-inclusion microthermometry (Mathieson & Clark, 1984).

There are also several instances of disaggrement between isotopic temperatures and those based on other methods. Where textural criteria indicate that minerals did not co-precipitate, applications of isotope geothermometry using these minerals yield, not surprisingly, incompatible results. Taylor & O'Neil (1977) determined from textural criteria that quartz and garnet did not co-precipitate in the Osgood Mountains skarns; as a result, their calculated temperatures using this mineral pair, ranging from 330 to 640ºC (average 381ºC), are well below the phase-equilibria limits for early (stage I) skarn development and are also below the isotopic temperatures from co-precipitated quartz-amphibole pairs for the later stage (II) of retrograde (hydrous) skarn development. Similar incompatibilities occur in the Hanover skarn. Textural criteria distinguish igneous quartz and later epidote+calcite+chlorite alteration (stage I) in pre-ore dykes. Whereas ^{18}O fractionation among epidote, calcite, and chlorite yields reasonable temperatures, thermometry pairs involving the pre-existing igneous quartz (Qtz-Cal or Qtz-Ep) yield a very wide range of temperature generally incompatible with the other isotopic, phase-equilibria, and fluid inclusion results. These results emphasize the importance of evaluating textural criteria for mineral coexistence in interpreting isotopic data, including applications of isotopic geothermometry. The ideal procedure in applications of stable-isotope geothermometry is to analyze and then test for attainment of isotopic equilibrium among a minimum of three coexisting minerals. This test is often illustrated with isotherm or concordancy diagrams (O'Neil, 1986).

4.3. Geological Setting of the Evciler District

The main geologic units of the area are Kazdağ metamorphic rocks and the Evciler granitoid (Figure 4.1). The metamorphic rocks consist mainly of grey, dark grey, and brown well-banded quartzofeldisphatic gneisses which include marble, amphibolite lenses and granitic gneiss horizons. Gneisses are characterized petrographically by the presence of biotite, sillimanite, garnet and hornblende along with ubiquitous quartz and feldspar. The marble has a granoblastic texture and is fine-grained. The grain size increases towards igneous contacts. Diopside-bearing

amphibolites occur as bands, up to several meters thick (3-4m.), in gneiss and marble (Okay & Satır 2000).

The Evciler pluton is a metaluminous, calc-alkaline granitoid of Late Oligocene-Early Miocene age (21±3 Ma, Okay & Satır, 2000) which intrudes the Kazdağ Metamorphic Complex in the south, and its volcanic equivalents in the north (Figure 4.1). The bulk of the pluton is comprised of granodiorite to quartz-diorite, medium grained and granular in the center, and porphyritic and fine-grained toward the margin (Genç 1998). The pluton contains numerous aplite dykes, veins and rounded to lensoidal mafic microgranular enclaves.

Skarn mineralization containing pyrrhotite-bearing chlorite, actinolite, garnet, pyroxene and epidote is located in Ayazma Dere 5 km SE of Evciler (Figure 4.2). The pyrrhotite-rich skarn is focused along the narrow alongate contact between gneiss and marble of the Kazdağ Massif, close to the granitoid contact. The skarn extends for more than 500 m in a direction roughly parallel to the strike of the granitoid contact, reaching a width of at least 2m. Distal metasomatic skarn mineralization is developed up to 150m away from the main zone along the contact of a gneiss, now altered to calc-silicate and marbles intercalated with amphibolite indicating the mineralization to be an exoskarn. The skarn itself has been divided into several paragenetic stages, based on stable mineral assemblages. These stages are sequential in time, with each stage partially replacing its predecessors.

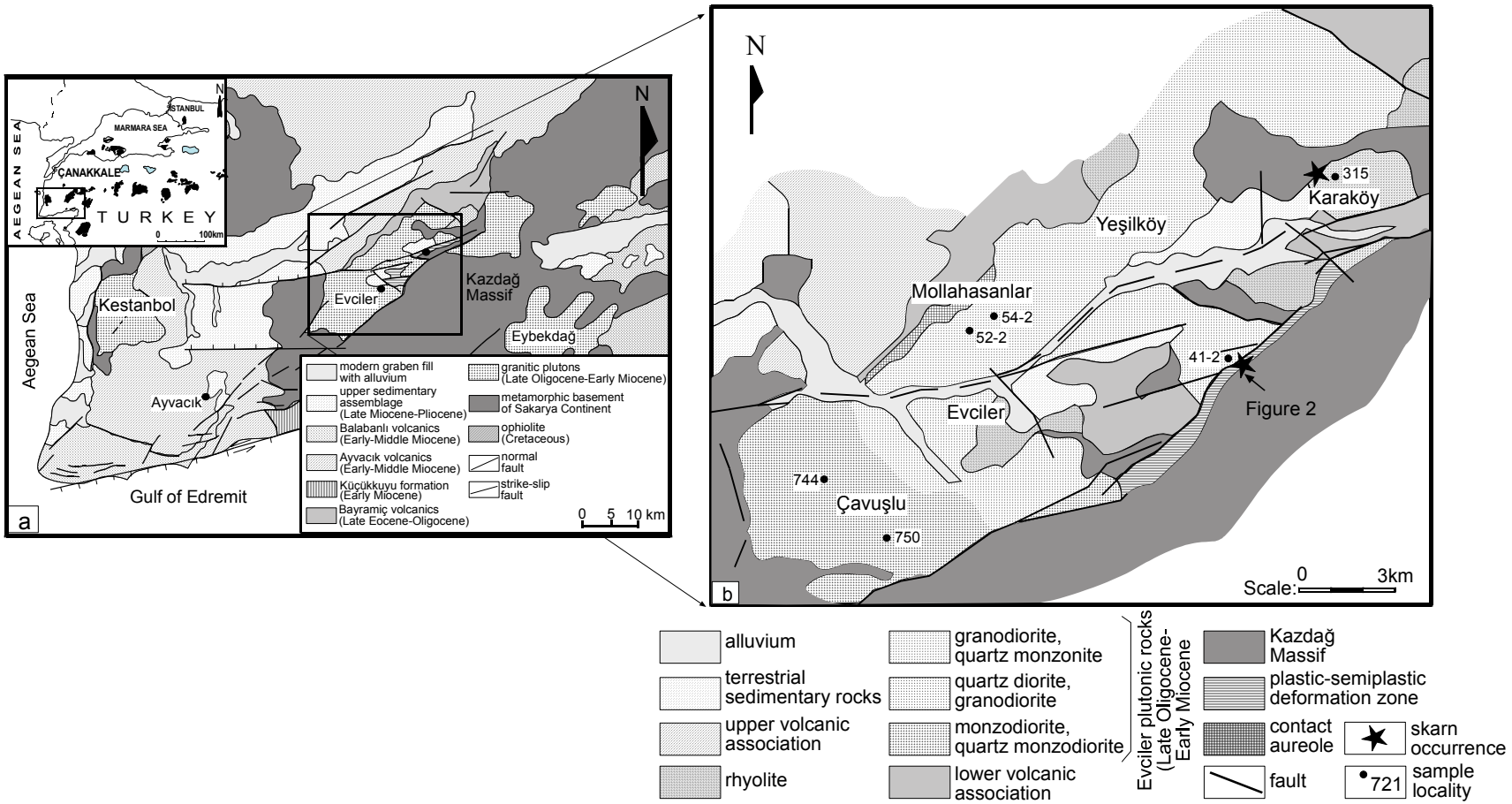

Figure 4.1. (a) Regional geologic map showing location of the Evciler district (simplified fromYılmaz & Karacık 2001); (b) geologic map of the Evciler district (simplified from Genç 1998).

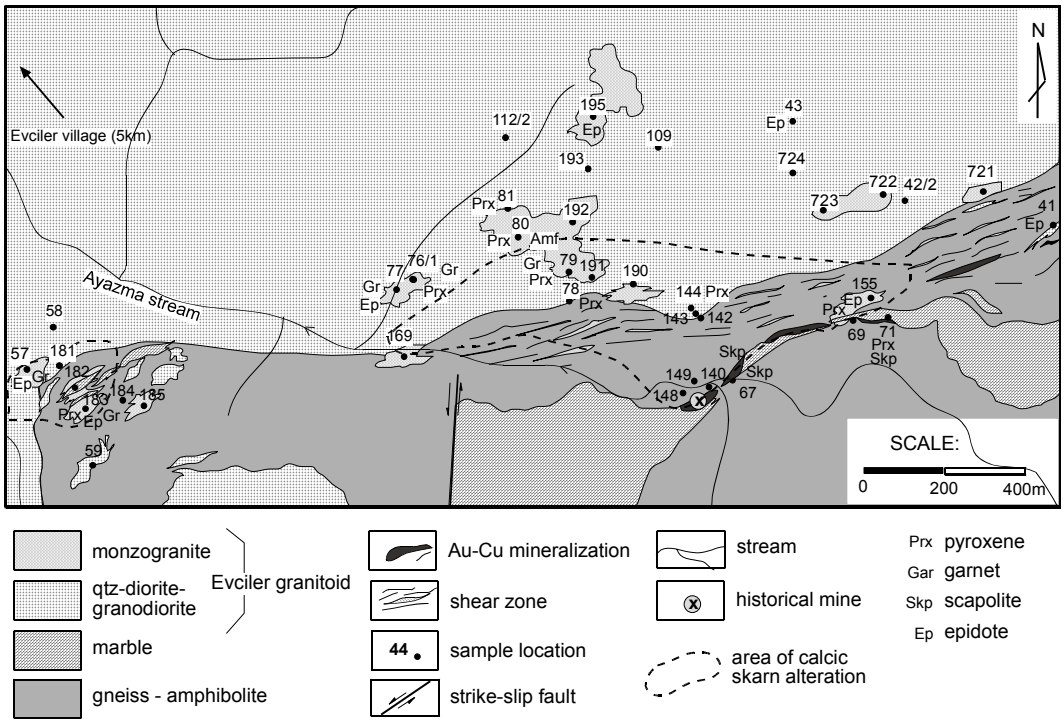

Figure 4.2. Geological map showing location of the skarn alteration and mineralization (after Yücel-Öztürk et al., 2005).

4.4. Characteristics of the Evciler Granitoid

The Evciler pluton consists mainly of granodiorite, quartz monzonite, monzodiorite and quartz diorite. Öngen (1992) and Genç (1998) subdivided the pluton into three main facies (Figure 4.1c): (1) Çavuşlu monzodiorite is the earliest facies of the pluton and has a equigranular and coarse-grained texture. It mainly consists of intermediate microcline 15%, Or_{89-90}), automorph plagioclase 48%, An_{45-35}), quartz 14%), biotite 10%), poikilitic magnesium hornblende 9%) and augite (4%). (2) Karaköy granodiorite is the main facies of the pluton and occurs at the northeasthern part of the pluton. It is fine to medium grained and porphyritic in texture. It consists essentially of plagioclase 39%, An_{40-27}), interstitial orthoclase 24%, Or_{80-85}), quartz 24%), actinolitic hornblende 8%) and coarse-grained biotite 5%). (3) The contact between these two plutonic members is gradational and represented by granodiorite including coarse-grained magnesium hornblende, named as mesocratic-type Evciler (Yücel-Öztürk *et al.*, 2005). It is medium to dark gray in colour due to its higher abundance of mafic components. Phenocryst mineralogy

includes major K-feldspar, plagioclase and quartz; minor amphibole, and pyroxene; and accessory titanite, apatite and magnetite. The presence of primary titanite and magnetite, combined with the absence of ilmenite, indicates that these are relatively oxidized magmas. Secondary minerals, formed due to alteration, are epidote, sericite and chlorite with pyroxene altered to amphibole. Compared to mesocratic-type Evciler rocks, the monzogranitic rocks are of minor occurce only at the south of the pluton. These monzogranitic rocks are named leucocratic-type Evciler. It is light gray in colour, fine- to medium-grained and equigranular to porphyritic in texture. It consists mainly of K-feldspar, plagioclase, quartz, and secondary epidote and amphibole crystals; and accessory titanite, apatite, and pyroxene. The K-feldspar is medium to coarse grained and shows perthitic and myrmecitic textures. The leucocratic- and mesocratic-type boundaries are poorly mapped at the Evciler district since their contacts are not clearly observed. Although they are geochemically classified as two different granitoids, the field relations fail to discriminate clearly the contacts between them (Yücel-Öztürk et al., 2005).

4.5. Skarn Occurences

Both endo- and exo-skarn can be observed in the Evciler district. Skarns in the district; (1) are mostly calcic, (2) have an oxidized mineralogy dominated by garnet, clinopyroxene, epidote and amphibole, (3) have epidote endoskarn close to the contact between marble and granitoid, (4) contain pyrrhotite, chalcopyrite, magnetite, garnet, pyroxene, epidote, actinolite and chlorite in Ayazma, SE of the Evciler village (Figure 4.2).

4.5.1. Endoskarn

Endoskarn formation begins with epidotization, and is coincident with sericitization during metasomatic reactions. Endoskarn consists mainly of epidote and pyroxene. Along the contact with exoskarn, replacement of granodiorite by massive epidote and minor garnet-pyroxene endoskarns over widths of centimeters to 0.5 m may result in complete destruction of the original igneous texture. This zone

consists of fine- to medium-grained epidote accompanied by interstitial quartz (Figure 4.3a & b). Endoskarn located at Evciler also contains garnet and pyroxene accompanying the above mineral association. Further within the granite, endoskarns occur only as disseminated epidote skarns, and are enriched in garnet towards the marble. The garnet-rich skarn predominantly comprises exoskarn. However, garnet was locally developed by the dissolution and replacement of primary igneous minerals, particularly feldspar, in the granodiorite (Figure 4.3c & d). Most garnets in the granodiorite are isotropic, whereas some garnets display anisotrophy as well as sector and oscillatory zoning (Figure 4.3e & f).

4.5.2. Exoskarn

The alteration of the host rock (marble and gneiss) at the Evciler district is marked by the formation of coarsely crystalline skarn lenses due to the introduction of Si-, Al-, Fe-, and Mg-rich fluids in the host rock. At the contact between Evciler granitoid and Kazdağ Massif, the earliest changes observed in the protolith involve recrystallization to fine-grained, dark grey-green hornfels containing an assemblage of clinopyroxene-feldspar-quartz. Metasomatism of carbonate litology in Evciler produced grossular-andradite/pyroxene exoskarn. The dominant minerals of the exoskarn are pyroxene and garnet as prograde assemblages, and epidote, tremolite/actinolite, chlorite and/or calcite and quartz as retrograde mineral assemblages.

In the Evciler skarn, the exoskarn shows slight zoning to pyroxene-epidote assemblages, with plagioclase, scapolite and sphene, close to the contact with the marble front (distal skarn) and as garnet-pyroxene with chlorite, epidote, close to the endoskarn zone (proximal skarn). The width of individual zones ranges from centimeters scale to 2-3 m (even locally 15-25 m). Epidote, tremolite/actinolite, chlorite and/or quartz and calcite typically represent the retrograde assemblages formed by the alteration of pyroxene and garnet at the advanced stages of skarn formation.

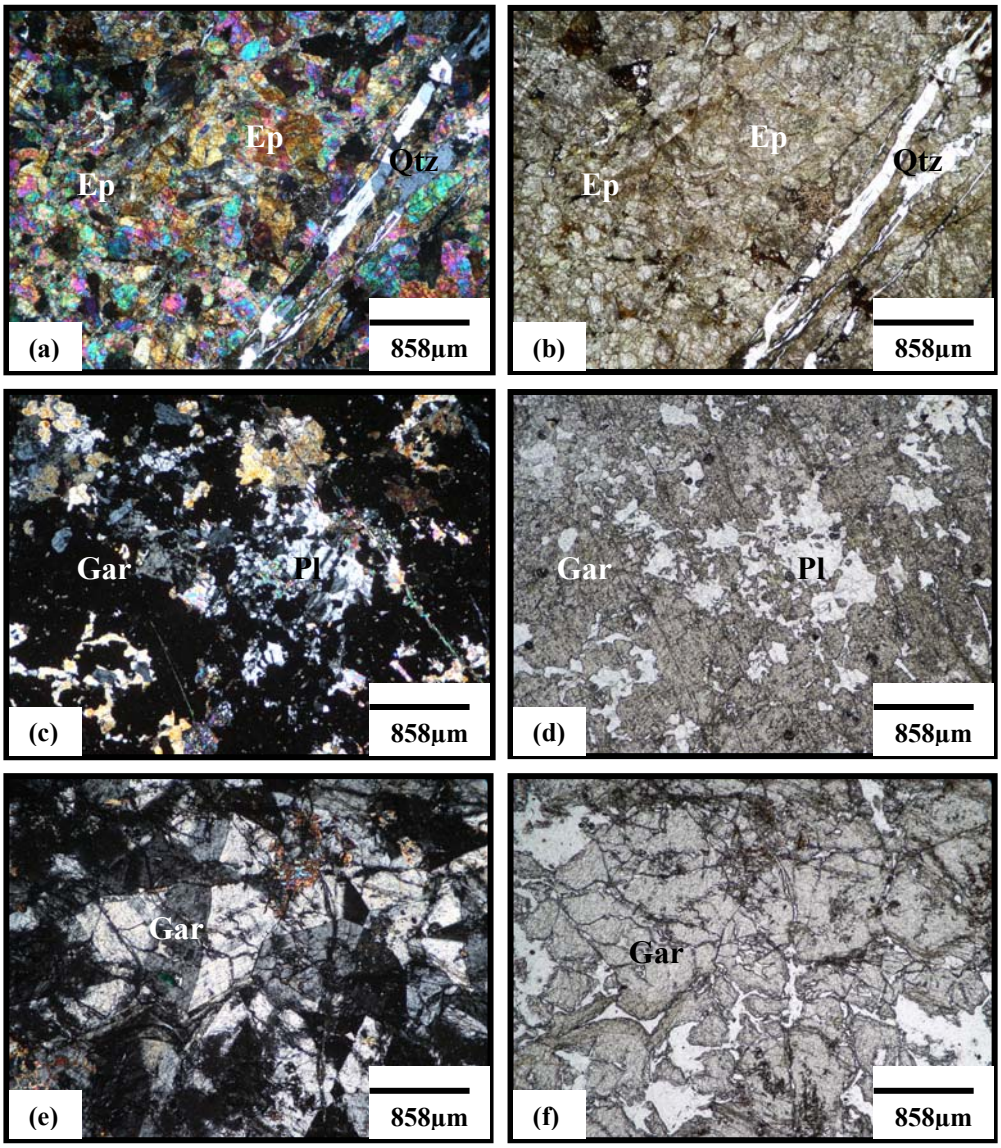

Figure 4.3. Typical endoskarn textures in the Evciler district; (a, b) massive epidote with interstitial quartz, (CPL & PPL); (c, d) replacement of primary igneous minerals (plagioclase) by garnet (CPL & PPL); (e, f) garnet showing oscillatory and sector zoning within the granodiorite (CPL & PPL). Ep= Epidote, Qtz= Quartz, Gar= Garnet, Pl= Plagioclase, Px= Pyroxene.

The prograde skarn mineral assemblage comprises garnet, clinopyroxene and scapolite (Figure 4.4a & b). Garnet and pyroxene are intimately intergrown, suggesting synchronous growth of these minerals. The garnet consists of anisotropic and isotropic zoned andradite to grossular ($Ad_{70\text{-}50}Gr_{30\text{-}50}$). Two types of garnets are observed in exoskarns, smaller and isotropic garnets and largely anisotropic garnets (with oscillatory-zoning) (Figure 4.4c & d). Their compositions are close to those of

garnets from Au-Cu and Fe-Cu skarns (Einaudi *et al.* 1981; Meinert, 1992). Pyroxenes are generally anhedral to subhedral, and hedenbergitic to diopsidic in composition ($Hd_{50-75}Di_{50-25}$) and are close to those of pyroxenes from Au-Cu and Fe-Cu skarns (Einaudi *et al.* 1981; Meinert, 1992). These were converted into tremolite/actinolite during the retrograde stages. Calcic-scapolite (meionite) is commonly formed during prograde alteration. Its presence in the Evciler exoskarn indicates a low-temperature scapolite variety or a former skarn assemblage. As the Ca-scapolite grains are intergrown with clinopyroxene and garnets, the latter hypothesis is favored (Figure 4.4c & d).

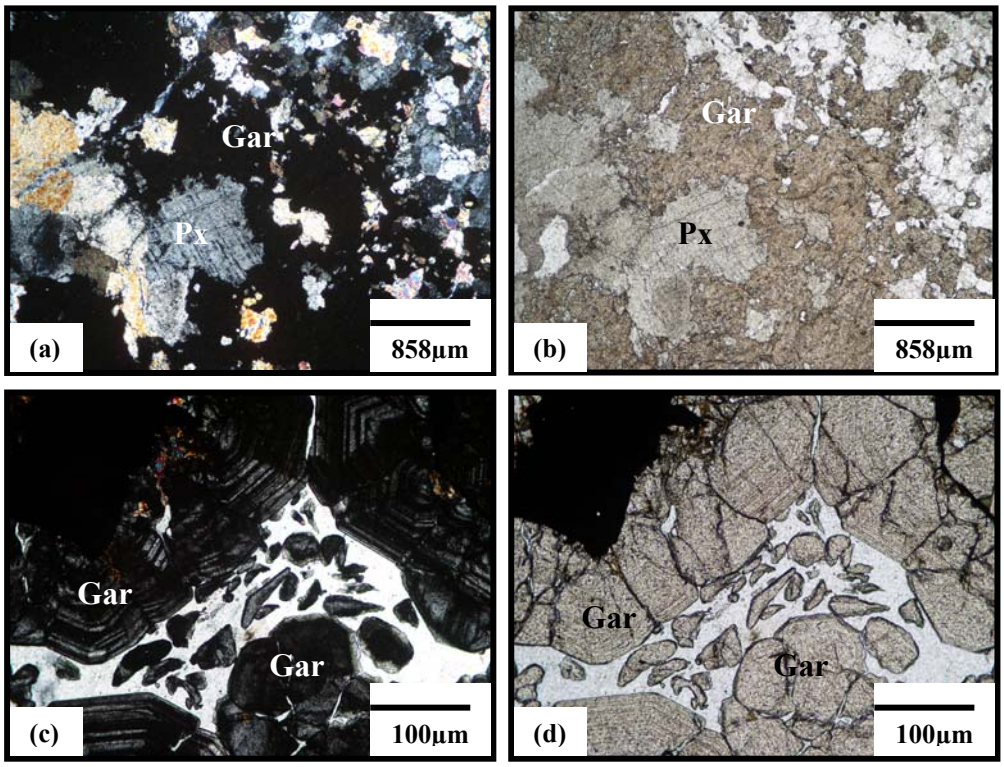

Figure 4.4. Typical exoskarn textures in the Evciler district; (a, b) the prograde skarn mineral assemblage comprising garnet, clinopyroxene and scapolite (CPL & PPL) ; (c, d) the garnet exoskarn consisting of anisotropic and isotropic zoned andradite to grossular (CPL & PPL).

The main pyrrhotite-rich mineralization is observed within the exoskarn and is related to the retrograde alteration of prograde calc-silicate assemblages to chlorite and/or calcite. Magnetite-pyrrhotite-chalcopyrite assemblage is common and magnetite is replaced by both pyrrhotite and chalcopyrite (Figure 4.5a & b).

Pyrrhotite occur as the main sulfide phase that was replaced by chalcopyrite (Figure 4.5c & d). The sulfide mineralization typically developed within the pyroxene exoskarns and occurs intermittently along ca. 600 m of the contact between gneiss and marble belong to the Sutuven formation (Kazdağ Massif).

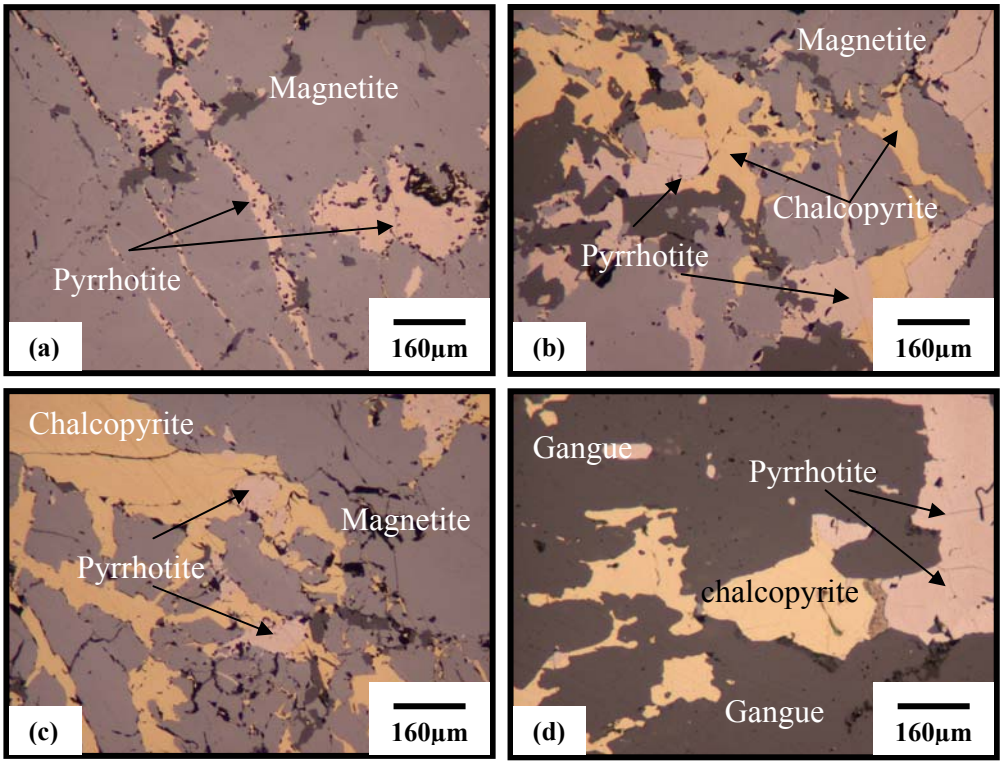

Figure 4.5. Polished sections showing (a-d) magnetite - pyrrhotite - chalcopyrite assemblage. Magnetite is replaced by both pyrrhotite and chalcopyrite.

4.6. Preparation and Analysis

Pure samples of skarn minerals were prepared using standard magnetic and heavy liquid techniques (Zussman, 1977). Some silicate samples were treated in acetic acid to remove any carbonate contamination. Finally, pure samples for isotopic analysis were seperated by handpicking.

Stable isotope analyses were performed at the University of Tübingen in the geochemical laboratory, using standard extraction and mass spectrometric techniques. Analytical results are reported in the normal δ notation, relative to

standard mean ocean water for oxygen (V-SMOW, Craig, 1961a; Baertschi, 1976) and hydrogen (Craig, 1961a).

The oxygen isotope composition (^{18}O, ^{16}O) of the samples were measured using a method similar to that described by Sharp (1990) and Rumble and Hoering (1994). Between 0.5 to 2 mg of sample was loaded onto a small Pt-sample holder and pumped out to a vacuum of about 10^{-6} mbar. After preflourination of the sample chamber overnight, the samples were heated with a CO_2-laser in 50 mbars of pure F_2. Excess F_2 is seperated from the O_2 produced by conversion to Cl_2 using KCl held at 150^{o}C. The extracted O_2 is collected on a molecular sieve (13X) and subsequently expanded and analyzed using a Finnigan MAT 252 isotope ratio mass spectrometer. Replicate oxygen isotope analyses of the standards used (NBS-28 quartz (n= 31) and UWG-2 garnet (n= 6); Valley et al., 1995) had an average accuracy of ±0.1 for $\delta^{18}O$. The precision of $\delta^{18}O$ values was better than 0.2‰ compared to accepted $\delta^{18}O$ values for NBS-28 of 9.64‰ and UWG-2 of 5.8‰.

The hydrogen isotope composition (D/H) of the hydrous samples were measured using the closed tube technique described by Vennemann and O'Neil (1993). This closed tube technique involves quantitative reduction of the H_2O in hydrous minerals by Zn reagent where sample and Zn are inserted into quartz tubes and, after evacuation, are heated to 1200^{o}C in a resistance furnace (Vennemann & O'Neil, 1993).

Minerals are heated in the quartz tube to extract water. The water and any H_2 gas produced are then passed over hot CuO to oxidize the H_2 and all hydrogen is frozen into a tube containing zinc. Zinc and water are reacted for 10 minutes at 500 ^{o}C to quantitavely convert all water to H_2 gas for mass spectrometric analysis.

4.7. Isotopic Studies

4.7.1. Evciler granitoid

Because of its proximity to the skarn mineralization and its possible role in genesis of the ore-forming fluids, we analyzed samples of seperated minerals from the Evciler granitoid collected close to the pyrrhotite-bearing mineralization. Oxygen isotope analyses of the granite reported here (Table 4.1) were performed on mineral seperates (quartz, feldspar and amphibole) in preference to whole-rock powders because oxygen isotope ratios of the whole-rock are vulnerable to effects of post-crystallization, sub-solidus alteration.

Table 4.1. $\delta^{18}O$ values and locations of samples from Evciler granitoid.

Sample no.	$\delta^{18}O$ (‰)				$\delta^{18}O_{magma}$ (‰)
	Quartz	Feldspar	Amphibole	Whole rock	
195	10.2				
193	10.4				
112/2	10.4	7.0	6.6	7.2	8.0
191	8.9			8.1	
79	10.9	13.4		8.3	
192/2	1.3			6.1	
109	7.2			6.0	
58	10.2	8.9		8.7	
76/1	7.2			5.7	
42/2	10.2	2.2	5.9	2.5	7.2
148/2	9.0		5.2	6.5	6.5
184	3.7		-0.6		7.2
140/S_5	4.5			7.1	
222/1	8.5		5.2	4.8	6.6

In all cases, whole rock data show a greater variation in O-isotope composition than quartz. The whole rock $\delta^{18}O$ values of the Evciler granitoid decrease toward the intrusive contact, which happens to be the region closest to the pyrrhotite-bearing mineralization at the Evciler district (Figure 4.6). The whole-rock $\delta^{18}O$ values of samples, collected only a few meters from the skarn mineralization are 2.5, 5.7 and

6.0 ‰, lower than the normal range for fresh granites (Taylor, 1968), and suggest that granite at this locality has been altered.

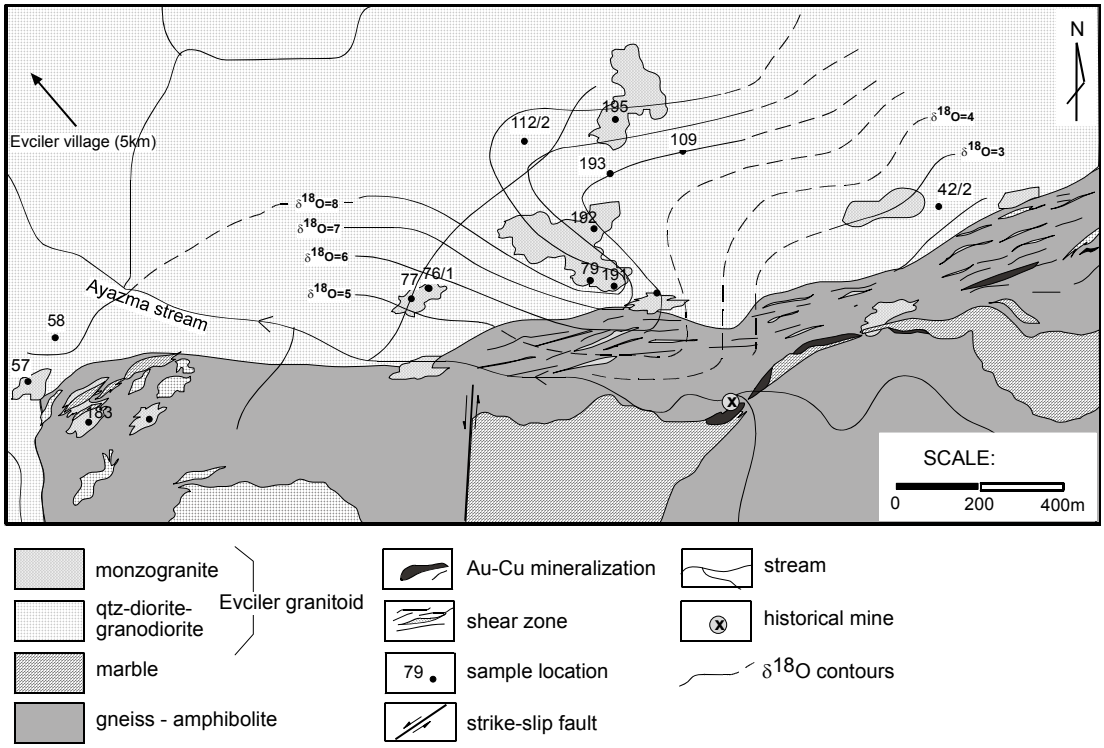

Figure 4.6. Geological map showing $\delta^{18}O$ values of the Evciler qtz diorite-granodiorite (after Yücel-Öztürk et al., 2005).

Note that the range of $\delta^{18}O$ values for quartz from the granite samples collected furthest from the skarn mineralization is restricted, ranging from +7.2 to +10.9 ‰, which may be close to the primary unaltered value for this intrusive rock. This range is normal for I-type granitic rocks (e.g., Taylor & Sheppard 1986; +8 ‰ - +10 ‰).

4.7.1.1. Mineral-Mineral Fractionation

Under equilibrium conditions, the O-isotope fractionation between quartz and constituent minerals (e.g., $\Delta_{qtz\text{-}feld}$) should fall in the range of 0.5-2.0 ‰ at magmatic temperatures (Chiba *et al.* 1989). For the granitoid at the Evciler district, the only readily applicable fractionation for equilibrium conditions was quartz-feldspar. Quartz-feldspar, the fractionation most often chosen for felsic igneous rocks is

applicable at Evciler. The average $\Delta_{qtz\text{-}feld.}$ observed in the Evciler granitoid ranges from -2.5 to 8.0 ‰, indicating that the O-isotopes did not reach equilibrium in these samples. Therefore, the present isotopic characteristics demonstrate that the Evciler granitoid has experienced post emplacement open-system hydrothermal alteration. Meteoric water was the most probable fluid involved in the water-rock interactions for the granitic intrusion.

Oxygen isotope results for quartz-feldspar pairs from Evciler are plotted in Figure 4.7. In this type of diagram minerals from unaltered pluton of all ages typically have quartz-feldspar fractionations of 0.5 to 2.0 per mil (Pollard et al., 1991). Granites which have exchanged with meteoric waters usually have larger fractionations due to lowering of $\delta^{18}O_{feldspar}$ during subsolidus reactions with meteoric hydrothermal fluids (Taylor, 1979). In Figure 4.7, following Gregory and Criss (1986) and Gregory et al. (1989), two diagonal lines denote the probable equilibrium isotopic fractionation between quartz and feldspar at magmatic temperatures. Data points of Evciler similar to those of the Lamashan and Xinhuatun pluton (NE China) (F. Wu et al., 2003) fall below or above the equilibrium range. This isotopic disequilibrium is mainly due to the fact that feldspar exchanges oxygen isotopes with the fluid more rapidly than quartz during water-rock interaction (F. Wu et al., 2003).

Oxygen isotope fractionation between quartz and biotite in sample 288/1 yields a temperature of 510, using the equation of Zheng (1993) for $\alpha_{quartz\text{-}biotite}$ (T). This temperature suggests reequilibration below the solidus temperature. We can calculate the oxygen isotope composition of the fluid in equilibrium with these minerals and obtain $\delta^{18}O_{water}$ = 7.3 per mil.

4.7.1.2. Estimation of the $\delta^{18}O$ value of the original magmas (δ_{magma})

In this section, the $\delta^{18}O$ value for the original magma (δ_{magma}) has been estimated from the $\delta^{18}O$ values of quartz. In theory, the $\delta^{18}O$ value of the fresh rock (and hence δ_{magma}) can be calculated from the mineral $\delta^{18}O$ values and modal proportions, provided that oxygen isotope data are available for all of the constituent minerals

(Harris *et al.* 1997). The $\delta^{18}O$ values calculated for the granite magmas from quartz $\delta^{18}O$ values at the Evciler granitoid range from 6.0 to 8.0 ‰.

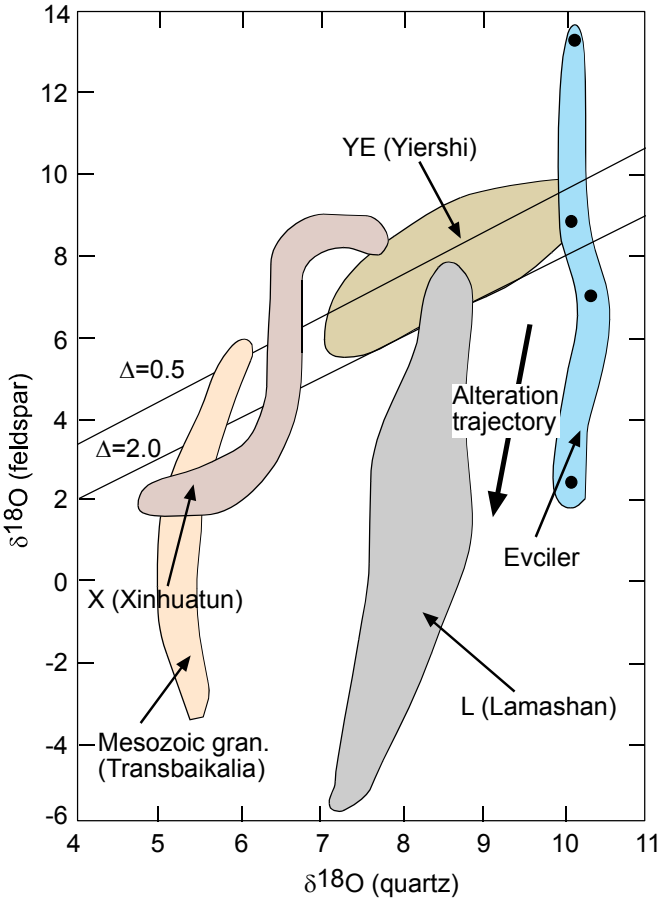

Figure 4.7. Feldspar $\delta^{18}O$ vs. quartz $\delta^{18}O$ diagram. Two lines with constant $\Delta_{qtz\text{-}feld}$ values represent possible isotopic fractionations between quartz and feldspar at magmatic temperatures. The data for the rocks from Transbaikalia and Yiershi, Xinhuatun, Lamashan are from Wichkam et al. (1996) and F. Wu et al. (2003) respectively.

In slowly cooled coarse-grained rocks (e.g., the Cape granites, Harris *et al.* 1997), the difference between the $\delta^{18}O$ value of quartz and δ_{magma} is not only dependent on $\Delta_{qtz\text{-}melt}$, but is also dependent on grain-size, the rate of cooling, and the temperature of closure of the mineral to oxygen diffusion (e.g., Giletti, 1986; Jenkin *et al.* 1991). Larger grain size generally results from slower cooling, which in turn means that oxygen diffusion and re-equilibrium continues for a greater period of time.

The difference between the $\delta^{18}O$ value of quartz and the other constituent minerals in a slowly cooled rock will be larger than for a more rapidly cooled rock. To correct for these 'closure' effects $\Delta_{quartz\text{-}magma}$ was assumed to be +1‰ in the quartz porphyries (e.g., Taylor & Sheppard 1986) and +2 ‰ in the remaining granites which relatively coarse-grained (see Giletti 1986). Calculated $\Delta_{quartz\text{-}magma}$ for the Evciler granitoid range from +1.8 to +3.0 ‰.

4.7.2. Isotopic studies of the skarn silicates

4.7.2.1. Oxygen Isotope Geothermometry

Oxygen isotope geothermometry was conducted using quartz-garnet, quartz-pyroxene pairs from stage I skarn, and quartz-epidote, quartz amphibole pairs from stage II skarn. The geothermometric equations of Matthews *et al.* (1983), Matthews (1994), and Zheng (1993) are shown in Table 4.2.

Table 4.2. Oxygen isotope geothermometric equations

Mineral pair (a-b)	Equation coefficients[1]	T range (°C)	Reference
Quartz-biotite	A=0.64, B= 3.99, C=–1.67	0-1200	Zheng, Y.F. (1993)
Quartz-garnet	A=3.03, B= 0.00, C=0.00	400-800	Matthews, A. (1994)
Quartz-pyroxene	A=2.08, B= 0.00, C=0.00	400-800	Matthews, A. et al.,(1983)
Quartz-epidote	A=1.50, B= 0.00, C=0.00	0-1200	Matthews, A. (1994)
Quartz-amphibole	A=4.18, B= 0.00, C=-1.67	520-680	Zheng, Y.F. et al. (1994)

[1]from $\Delta_{a-b} = 1000 \ln \alpha = A\left(10^6 T^{-2}\right) + B\left(10^3 T\right) + C$

Table 4.3 gives 41 isotopic analyses of garnets, pyroxene, epidote, amphibole, and quartz from massive ore-bearing skarn and pluton at Evciler. The data summarizes the results of oxygen isotope compositions of samples in ore-generating granite and skarn from Ayazma (Evciler) location. The $\delta^{18}O$ values of quartz associated with skarn minerals in contact between gneiss and granite and in ore body are –0.6 ‰ and 3.5 – 10.9 ‰ respectively. There is a well defined trend of decreasing $\delta^{18}O_{quartz}$ values towards the sulfide mineralization at the district (Figure

4.8). The range of $\delta^{18}O$ values for garnets is restricted, ranging from +4.6 to +8.2‰. The pyroxene $\delta^{18}O$ values range from +6.2 to +9.3‰. Amphibole and epidote $\delta^{18}O$ values range from +6.3 to +8.2‰ (in one sample –0.6‰) and from –3.3 to +6.8‰, respectively. These data permit limits to be placed on the degree and temperature of equilibrium as well as on the source of skarn-forming fluids.

Table 4.3. Stable Isotope Analyses - Silicates

Sample no.	Min.	$\delta^{18}O_{min}$ (‰)	δD_{min} (‰)	T (°C) Calc.	T_{est} (°C)	$\delta^{18}O_{fluid}$[1] (‰)	$\delta^{18}O_{fluid}$[2] (‰)	δD_{fluid}[2] (‰)
		measured				Calc.		
Granite								
42/2	Amph	5.9	-97.2	Qtz-Amph 554			8.1	-70.2
112/2	Amph	6.6			750			
222/1	Amph	5.2			750			
148/2	Amph	5.2			750			
288/1	Bio	4.8		Qtz-Bio 510		7.3		
112/2	Feld	7.0						
79	Feld	13.4						
58	Feld	8.9						
42/2	Feld	2.2						
42/2	Qtz	10.2			750		8.9	
58	Qtz	10.2			750		8.9	
112/2	Qtz	10.4			750		9.1	
222/1	Qtz	8.5			750		7.2	
148/2	Qtz	9.0			750		7.7	
288/1	Qtz	9.3			750		8.0	
Stage 1								
79	Qtz	10.9						
96/2	Qtz	9.7						
140/S_{3A}	Qtz	13.2						
191	Qtz	8.9						
193	Qtz	10.4						
195	Qtz	10.2						
71	Px	8.1			750		10.2	
79	Px	7.9		Qtz-Cpx 560	750	9.9	10.0	
80/2	Px	7.8			750		9.9	
109	Px	8.4			750		10.5	
140/S_{3A}	Px	8.0		Qtz-Cpx 455	750	9.8	10.1	
140/S_5	Px	8.4			750		10.5	
140/S_{11}	Px	9.3			750		11.4	
144	Px	6.2			750		8.3	
191	Px	8.0			750		10.1	
191	Px	7.8			750		9.9	

Table 4.3 *(Cont.)*

Sample no.	Min.	$\delta^{18}O_{min}$ (‰)	δD_{min} (‰)	T (°C) Calc.	T_{est} (°C)	$\delta^{18}O_{fluid}$[1] (‰)	$\delta^{18}O_{fluid}$[2] (‰)	δD_{fluid}[2] (‰)
		measured				Calc.		
193	Px	8.0		Qtz-Cpx 655	750	10.0	10.1	
195	Px	8.4		Qtz-Cpx 820	750	10.4	10.5	
76/1	Gros	7.7			750		10.5	
79	Gros	7.9		Qtz-Gros 740	750	10.4	10.7	
96/2	Gar	6.3		Qtz-Gar 700	750	8.9	9.1	
96/2	Gar	4.6		Qtz-Gar 495	750	6.3	7.4	
191	Gros	6.9		Qtz-Gros 957	750	9.8	9.7	
192/2	Gros	5.3			750		8.1	
193	Gros	8.2		Qtz-Gros 884	750	10.9	11.0	
Stage II								
80/2	Qtz	2.1						
144	Qtz	-0.6						
155	Qtz	3.5						
184	Qtz	3.7						
80/2	Amph	7.9	-99.1		550		9.8	-77.4
96/2	Amph	6.3			550		8.2	
109	Amph	7.0			550		8.9	
184	Amph[3]	-0.6	-85.7	Qtz-Amph 465	550	1.0	1.3	-64.0
191	Amph	7.9	-91.0		550		9.8	-69.3
192	Amph	8.2			550		10.1	
57/4	Epid	-3.3	-53.6		450		-2.5	-17.7
76/1	Epid	0.7	-58.9		450		1.4	-23.0
109	Epid	6.8	-61.4		450		7.5	-25.5
155	Epid	-1.3	-66.8	Qtz-Epid 285	450	-2.6	-0.5	-30.9
184	Epid	-2.1		Qtz-Epid 237	450	-4.6	-1.3	
193	Epid	7.9			450		8.6	
195	Epid	5.1	-65.0		450		5.8	-29.1

Oxygen isotope analyses of silicate minerals were performed at the University of Tubingen. Calculated fluid compositions for garnet, pyroxene, amphibole and epidote are based on fractionation factors of Zheng (1993).

Abbreviations: Amph=Amphibole, Gros=Grossular, Gar=Garnet, Px=Pyroxene, Epid=Epidote, T_{est}=Estimated temperature of mineral formation

[1] Calculated at T °C, calculated from quartz-mineral pairs

[2] Calculated at T_{est} °C

[3] Sample showed textural and/or isotopic evidence of retrograde alteration during subsequent skarn stage

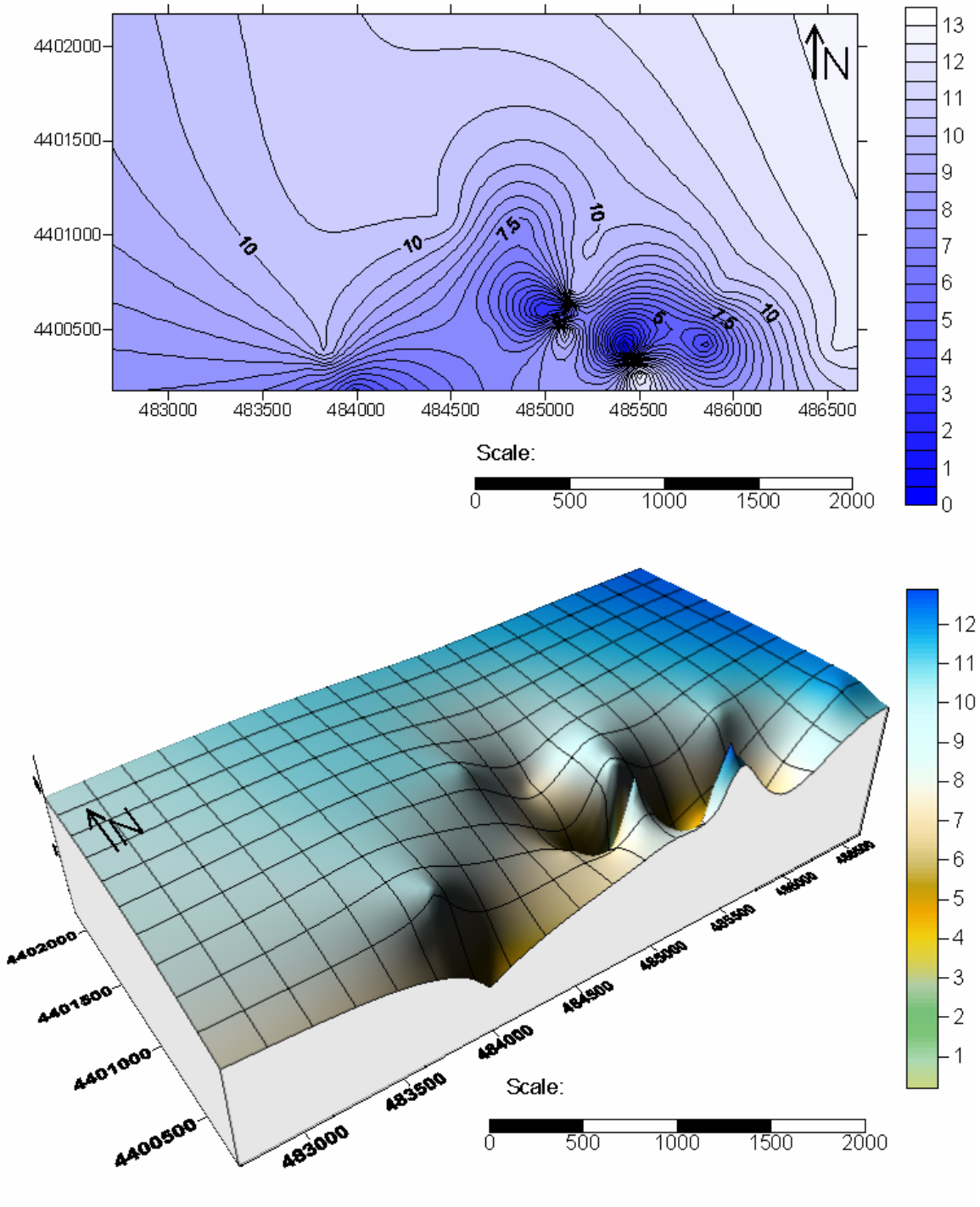

Figure 4.8 (a) Contour and (b) surface map of the $\delta^{18}O_{quartz}$ from the Evciler skarn district.

4.7.2.2. Stage I

In order to estimate oxygen isotopic compositions of ore-forming fluids, twelve clinopyroxene samples were provided from the Evciler skarn district. Clinopyroxene is a main constituent of skarns in most deposits, and is noticed as a reliable recorder of the oxygen isotopic compositions of fluids prevailed (Brown et al., 1985). In the study area, pyroxene and quartz samples have ranges of $\delta^{18}O$ values of 6.2 to 9.3 and 8.9 to 13.2 permil, respectively (Table 4.3, Figure 4.9). Using experimental data of Matthews (1994) and Zheng (1993) for $\delta^{18}O$ fractionation for quartz-mineral, oxygen isotope temperatures were calculated from the measured quartz-pyroxene fractionations. In four out of six quartz-pyroxene pairs, calculated temperatures are in the range 455^{o}C to 820^{o}C. For this temperature range, calculated $\delta^{18}O$ values of H_2O in equilibrium with pyroxene and quartz are in the range from 9.8 to 10.4 permil. These values agree fairly well with values of fluid in equilibrium with the Evciler granitoid. The oxygen isotope data are consistent with a predominantly magmatic source of the early skarn-forming fluids. Six samples of the skarn body in the district have negative quartz-pyroxene fractionations. These samples contain significant amounts of cavity infill and retrograde alteration quartz (e.g. -0.6 to 4.5‰) in addition to primary quartz. The disequilibrium quartz-pyroxene fractionations observed in the Evciler skarn reflect retrograde alteration by hydrothermal fluid-rock interaction at lower temperatures. This stage involves interaction with meteoric hydrothermal fluids at relatively low temperatures.

However, twelve pyroxene samples from stage I skarn rocks yield calculated $\delta^{18}O$ values for the coexisting fluid (8.3 to 11.4 ‰; Table 4.3) which are similar to those of magmatic water at Evciler granitoid. These are the values at an estimated temperature of 750ºC, near the probable maximum for contact metamorphism. A lower temperature of formation would yield even higher $\delta^{18}O$ values for the stage I fluid.

Figure 4.10 shows that pyroxene-garnet fractionations vary from 4.0 to 10.5 permil, this range is greater than possible if both are to be in equilibrium with a

common fluid (Brown *et al.*, 1985). The number locating each anlaysis on the ^{18}O axis gives the sample number. Tie lines join analyses from the same sample. The analyses in Figure 4.10 are grouped together as skarn with no consideration of mineralogy or position in space between the marble and the gneiss close to the intrusion contact.

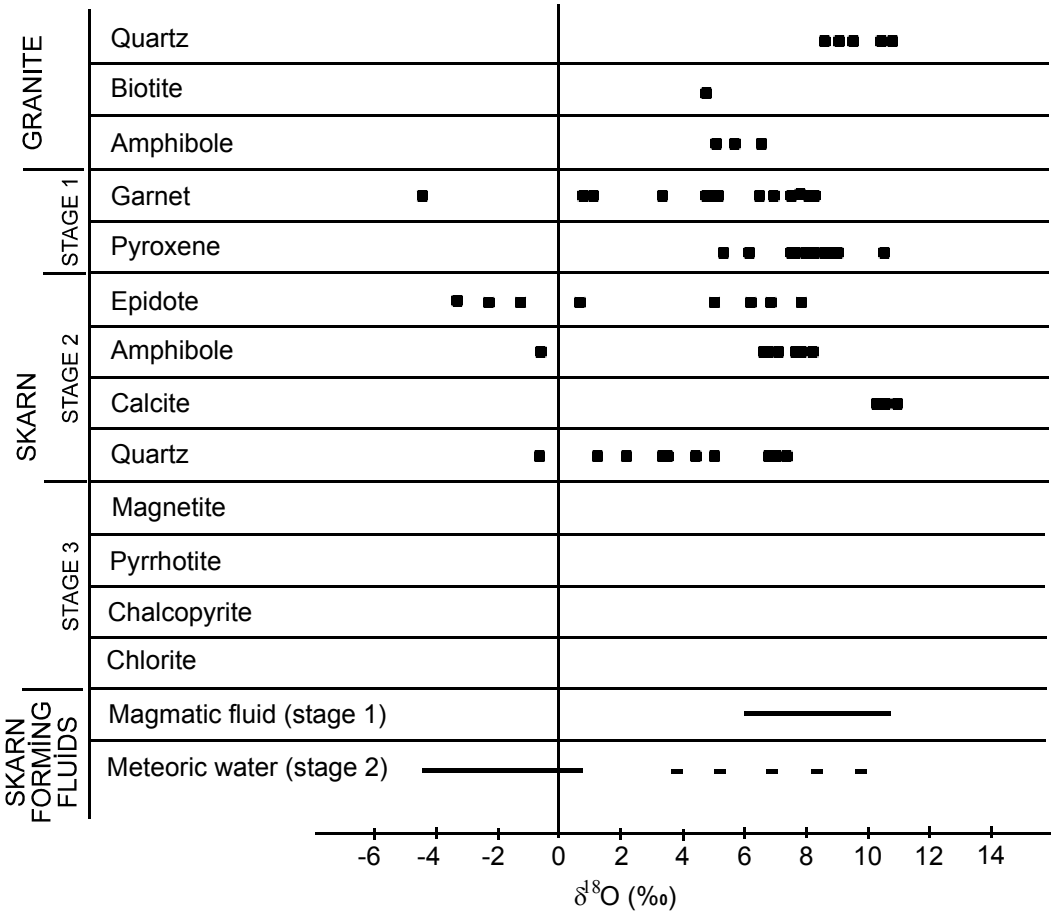

Figure 4.9. Distribution of paragenesis and $\delta^{18}O$ values for minerals from Evciler skarn.

Garnet samples display a wide range of $\delta^{18}O$ values (4.6 to 8.2‰) (Table 4.3, Figure 4.9). The positive garnet values are similar to those reported from other skarn deposits (Brown *et al.*, 1985; Taylor & O'Neil, 1977). Fluids in equilibrium with this garnet, at an estimated maximum temperature of 750 ^{o}C for stage I, have $\delta^{18}O$ values of 7.4 to 11.0 permil, in the middle of the range for magmatic water associated with the Evciler granitoid.

However, using experimental data of Matthews (1994) and Zheng (1993) for $\delta^{18}O$ fractionation for quartz-mineral, oxygen isotope temperatures were calculated from the measured quartz-garnet fractionations. In five quartz-garnet pairs, calculated temperatures are in the range 495°C to 957°C. For this temperature range, calculated $\delta^{18}O$ values of H_2O in equilibrium with garnet and quartz are in the range from 6.3 to 10.9 permil. These values agree fairly well with values of fluid in equilibrium with the Evciler granitoid. The oxygen isotope data are consistent with a predominantly magmatic source of the early skarn-forming fluids.

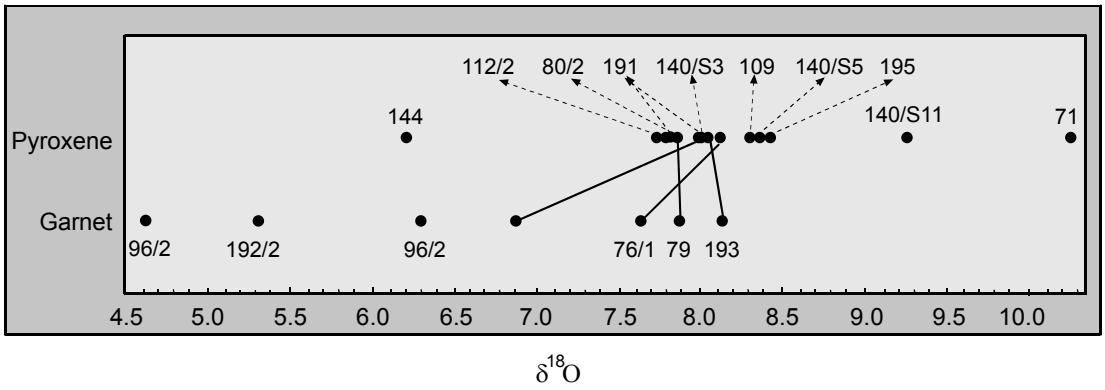

Figure 4.10. Garnet and pyroxene data plotted against oxygen isotope values. The numbers within the figure indicate the sample numbers. The lateral position is determined by the measured isotopic ratio. There is no significance to vertical position. Tie lines join garnets and pyroxenes that occur in the same sample.

Some minerals are depleted in 18-O compared to the same minerals in normal igneous rocks or skarns associated with magmatic intrusions, clearly indicating a meteoric water influence during growth of these minerals (Vazquez et al., 1998) (Figure 4.9). Low $\delta^{18}O$ values of these minerals (-4.5 to +5.5‰) prove water of metasomatic fluids to have mainly supplied from heavy oxygen depleted source.

4.7.2.3. Stage II

In addition, there is patchy development of retrograde assemblages such as epidote-calcite-quartz after garnet, and actinolite after pyroxene. This stage

subsequent to the main-stage growth of the garnet+pyroxene may have reset some or all of the isotope ratios of the earlier minerals (Brown *et al.*, 1985).

Epidote and amphibole have ranges of $\delta^{18}O$ values of -3.3 to 5.1 permil, except two samples (6.8 and 7.9 permil) and -0.6 to 8.2 permil, respectively (Table 4.3, Figure 4.9). Using experimental data of Matthews (1994) and Zheng (1993) for $\delta^{18}O$ fractionation for quartz-mineral, oxygen isotope temperatures were calculated from the measured quartz-epidote and quartz-amphibole fractionations.

Six amphibole samples from stage II skarn rocks yield calculated $\delta^{18}O$ values for the coexisting fluid (8.2 to 10.1 permil; Table 4.3), except one sample (1.3 permil), which are similar to those of magmatic water mixing with meteoric water. These are the values at an estimated temperature of 550ºC. However, in only one quartz-amphibole pair, calculated temperature is 465^{o}C. For this temperature, calculated $\delta^{18}O$ value of H_2O in equilibrium with amphibole 1.0 permil. These value agrees fairly well with values of fluid mixing with meteoric water.

Epidote was the predominant rock-forming mineral at stage II. For quartz-epidote pairs, calculated temperatures are in the range 237^{o}C to 285^{o}C. For this temperature range, calculated $\delta^{18}O$ values of H_2O in equilibrium with epidote are in the range of -2.6 to 4.6 permil. These values agree fairly well with values of fluid mixing with meteoric water. The oxygen isotope data are consistent with a predominantly magmatic and meteoric source of the later skarn-forming fluids. However, seven epidote samples from stage II skarn rocks yield calculated $\delta^{18}O$ values for the coexisting fluid (-2.5 to 5.8 permil; Table 4.3), except two samples (7.5 and 8.6 permil), which are similar to those of meteoric water. These are the values at an estimated temperature of 450ºC.

The range of stage II fluid compositions partially overlaps that of primary magmatic water at Evciler but trends toward lower $\delta^{18}O$ values, suggesting the involvement of both magmatic and low $\delta^{18}O$ meteoric water in the fluid system at this stage.

Preliminary data for D/H ratios in the hydrous phases amplify the information on fluid sources derived from the carbon and oxygen isotope data. The δD value of primary igneous amphibole at Evciler is -97.2 permil, whereas skarn amphibole record values from -85.7 permil through -91.0 to -99.1 permil. The amphibole sample from Evciler record a range of δD fluid composition, ranging from -64.0 to -77.4 permil (Figure 4.11). This fluid is isotopically lighter than that extracted from garnet-clinopyroxene skarn, suggesting even greater meteoric water, influx during later stages of skarn evolution.

However, as shown in Table 4.3, the massive epidotes as a retrograde alteration mineral from Evciler have δD values of -66.8 to -53.6 permil. It is not clear to what extent the early magmatic fluids were mixed with highly depleted meteoric waters. The epidote samples from Evciler record a range of δD fluid composition, from -17.7 to -30.9 permil. Calculated $\delta^{18}O$ and δD fluid compositions from Evciler skarn epidote (Table 4.3) trend toward meteoric water line (Figure 4.11).

This observation suggest that the formation of retrograde alteration minerals in general, and amphibole-epidote in particular, cannot only result from evolution of a single magmatic hydrothermal system, since there is an evidence in the Evciler skarn system for mixing with a significant component of meteoric water.

Certainly the δD values are all compatible with either a magmatic or a meteoric origin the overlap between these fluids in this region is too large and one cannot distinguish on the basis of D/H ratios alone. The combination of oxygen (and temperature-equilibrated fluids) as well as hydrogen is required to make this distinction between magmatic and/or mixed magmatic-meteoric and/or meteoric fluids.

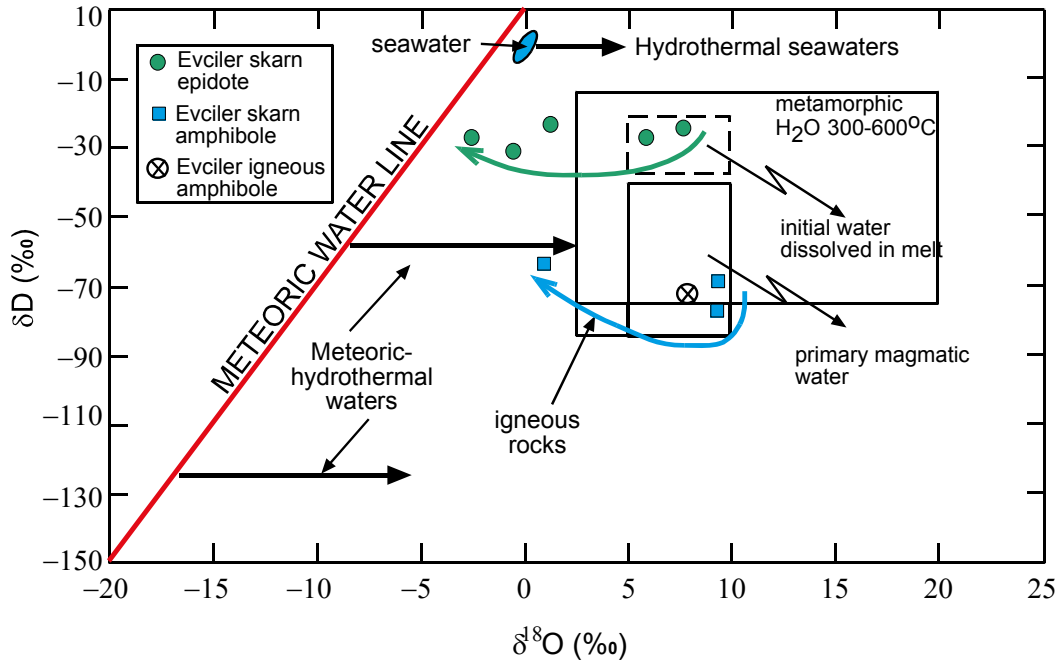

Figure 4.11. Calculated $\delta^{18}O$ versus δD compositions of fluids in equilibrium with epidote and amphibole (Table 4.3) from the Evciler skarn deposit.

4.8. Discussion and Conclusion

4.8.1. Granite

For some granites, little or no interaction with external fluids seems to have taken place (e.g., the Berridale batholith in eastern Australia, O'Neil & Chappell 1977; Manaslu granite, Himalaya, France-Lanord *et al.* 1988) and the whole-rock oxygen isotope ratios probably reflect quite closely the original magma values. Other granites have been subjected to extensive exchange with external fluids which has changed the original magmatic $\delta^{18}O$ values. Some Hercynian granites of the Pyrenees (Wickham & Taylor 1987), the Idaho batholith and many other Tertiary batholiths of the western USA (Criss *et al.* 1991) and some Caledonian granites of Britain (Harmon 1984) can be classified in this category.

Whole rock samples from Evciler granitoid, collected only a few meters from the skarn mineralization have $\delta^{18}O$ between 4.8 and 6.0 ‰, with the most altered samples having lowest $\delta^{18}O$ value like other world skarn granitoids (e.g., Edough granitoid, Annaba, Northeast Algeria; Laouar *et al.* 2002). In order to create granites with low $\delta^{18}O$ values observed in the Evciler samples, it is necessary to call upon hydrothermal alteration. Compared to normal granites, meteoric waters have relatively low $\delta^{18}O$ values (Figure 4.12). Given fluid-rock exchange between a granite and meteoric waters with distinctly lower 18-O and D contents, such exchange will lead to lowering of the $\delta^{18}O$ values (and δD values but depending on the actual values) of the granites. Thus, the Evciler granitoid $\delta^{18}O$ values would decrease to lower values during hydrothermal alteration and skarn formation at the district.

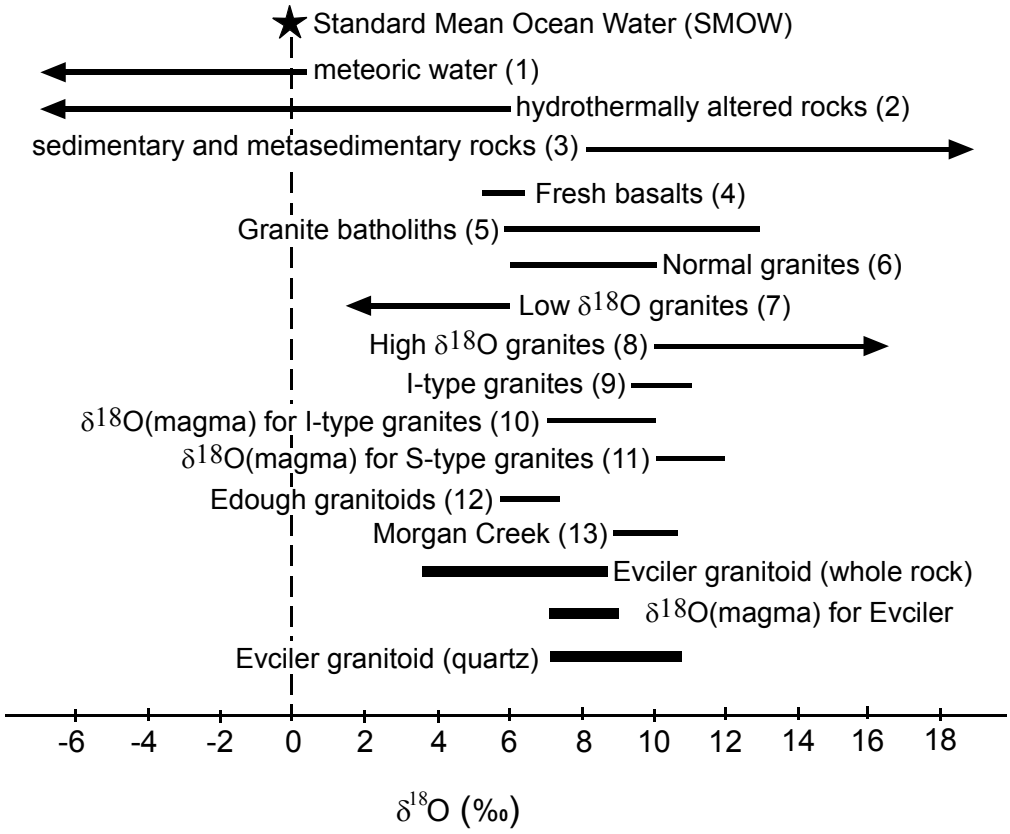

Figure 4.12. Oxygen isotopic composition of the Evciler granitoid compared to those of typical terrestrial materials and other world skarn granitoids. (1) Craig (1961); (2) Ohmoto (1986); (3), (4) and (5) Taylor & Sheppard (1986); (6), (7) and (8) Taylor (1978); (9), (10) and (11) Harris *et al.* (1997); (12) Laouar *et al.* (2002); and (13) Brown *et al.* (1985).

4.8.2. Origin of hydrothermal fluid

The oxygen, hydrogen and whole-rock isotope analyses contribute to a general picture of the geologic history of the Evciler skarn mineralization as follows: the Evciler pyrrhotite skarn mineralization was precipitated in a faulted zone between Evciler granitoid and Kazdağ metamorphic rocks at the south of the pluton. The paragenetic studies at Evciler show that skarn evolution occurred three stages. Stage I mineral assemblage is dominated by clinopyroxene and garnet. This stage is considered to represent prograde anhydrous skarn development, whereas stage II, which is dominated by hydrous minerals (amphibole, epidote) and stage III, which comprises pyrrhotite, pyrite, chalcopyrite, chlorite and/or quartz are considered to represent retrograde hydrous skarn development.

The isotopic compositions of the hydrothermal fluid, from which skarn was precipitated, can be calculated if (1) a fractionation factor at a given temperature, (2) isotopic compositions of skarn silicates and (3) equilibrium temperature of skarn silicates from the fluid are known. Consequently, with all the information given, $\delta^{18}O$ values were calculated for the stable isotope compositions of the skarn-forming fluid.

The fluid associated with prograde skarn formation at Evciler was a high temperature fluid. The calculated $\delta^{18}O$ value of the fluid in equilibrium with garnet and pyroxene from the deposit is within the range of values for magmatic fluids (Taylor & Sheppard, 1986). The fluid associated with the retrograde alteration stage is lower temperature than that of the prograde skarn fluid.

The water in the hydrothermal solution precipitating the pyrrhotite-rich ore body could have been magmatic water at first, but meteoric water played an increasing role toward the end of the depositional history. The evidence of the presence of a meteoric component in the hydrothermal solution suggests that with passage of time the hydrothermal fluid mixed to a progressively greater extent with invading meteoric water which may have encouraged cooling of the fluid; precipitation of ore may have been induced by this process.

In conclusion, the stable isotope evidence suggests some involvement of meteoric water in the genesis of the mineralization, but the high-temperature history of that water, its interaction with the granite and the temperature of ore mineralization are unclear. Further measurements of salinity and fluid inclusion chemistry and $\delta^{34}S$-values of sulfide minerals are essential to establish the complete history.

4.9. References

Baertschi, P. (1976). Absolute ^{18}O content of standard mean ocean water. *Earth & Planetary Science Letters*, *31*, 341-344.

Bowman, J. R., & Essene, E. J. (1984). Contact skarn formation at Elkhorn, Montana. I: P-T-component activity conditions of early skarn formation. *American Journal of Sciences*, *284*, 597-650.

Bowman, J. R., O'Neil, J. R., & Essene, E. J. (1985a). Contact skarn formation et Elkhorn, Montana, II: Origin and evolution of C-O-H skarn fluids. *American Journal of Sciences*, *285*, 621-660.

Bowman, J. R., Covert, J. J., Clark, A. H., & Mathieson, G. A. (1985a). The CanTung E-zone scheelite skarn orebody, tungsten, North-west Territories: oxygen, hydrogen and carbon isotope studies. *Economic Geology*, *80*, 1872-1895.

Brown, P. E., Bowman, J. R., & Kelly, W. C. (1985). Petrologic and stable isotope constraints on source and evolution of skarn-forming fluids at Pine Creek, California. *Economic Geology*, *80*, 72-95.

Chiba, H., Chacko, T., Clayton, R.N., & Goldsmith, J.R. (1989). Oxygen isotope fractionations involving diopside, forsterite, magnetite and calcite: application to geothermometry. *Geochimica Cosmochimica Acta*, *53*, 2985-2995.

Craig, H. (1961a). Standards for reporting concentrations of deuterium and oxygen 18 in natural waters. *Science*, *133*, 1833-1834.

Criss, R.E., Fleck, R.J., & Taylor, H.P. (1991). Tertiary meteoric hydrothermal systems and their relation to ore deposition, northwestern United States and southern British Columbia. *Journal of Geophysical Research*, *96*, 13335-13356.

Einaudi, M.T., Meinert, L.D., & Newberry, R.J. (1981). Skarn deposits. *Economic Geology (75th anniversary volume)* 317-391.

France-Lanord, C., Sheppard, S.M.F., & Le Fort, P. (1988). Hydrogen and oxygen isotope variations in the High Himalaya peraluminous Manaslu leucogranite: evidence for heterogeneous sedimentary source. *Geochimica Cosmochimica Acta*, *52*, 513-526.

Wu, F., Jahn, B., Wilde, S.A., Lo, C.-H., Tzen, F.Y., Lin, Q., Ge, W., & Sun, D. (2003). Highly fractionated I-type granites in NE China (II): isotopic geochemistry and implications for crustal growth in Phanerozoic. *Lithos, 67*, 191-204.

Genç, Ş., C. (1998). Evolution of the Bayramiç magmatic complex, northwestern Anatolia. *Journal of Volcanology and Geothermal Research*, *85*, 233-249.

Giggenbach, W.F. (1997). The origin and evolution of fluids in magmatic-hydrothermal systems, *in:* Barnes, H.L. (eds), *Geochemistry of hydrothermal ore deposits, 3rd edition: New York, John Wiley and Sons*, 737-796.

Giletti, B.J. (1986). Diffusion effects on oxygen isotope temperatures of slowly cooled igneous and metamorphic rocks. *Earth & Planetary Science Letters*, *77*, 218-228.

Graham, C. M., Sheppard, S. M. F., & Heaton, T. H. E. (1980). Experimental hydrogen studies-I. Systematics of hydrogen fractionation in the system epidote-H_2O, zoisite-H_2O and AlO(OH)-H_2O. *Geochimica Cosmochimica Acta*, *44*, 353-364.

Gregory, R.T., & Criss, R.E. (1986). İsotope Exchange in open and closed systems. In: Valley, J.W., Taylor, Jr., H.P., O'Neil, J.R. (eds.) Satble Isotopes in High Temperature Geological Processes. *Mineralogical Society of America, Review in Mineralogy, 16*, 91-127.

Gregory, R.T., Criss, R.E., & Taylor, H.P. (1989). Oxygen isotope exchange kinetics of mineral pairs in closed and open systems: applications to problems of hydrothermal alteration of igneous rocks and Precambrian iron formations. *Chemical Geology, 75*, 1-42.

Hall, D. L., Sterner, S. M., & Bodnar, R. J. (1988). Freezing point depression of NaCl-KCl-H_2O solutions. *Economic Geology*, *83*, 197-202.

Harmon, R.S. (1984). Stable isotope geochemistry of Caledonian granitoids from the British Isles and east Greenland. *Physics of the Earth and Planetary Interiors*, *35*, 105-120.

Harris, C., Faure, K., Diamond, R.E., & Scheepers, R. (1997). Oxygen and hydrogen isotope geochemistry of S- and I-type granitoids: the Cape granite suite, south Africa. *Chemical Geology*, *143*, 95-114.

Jenkin, G.R.T., Fallick, A.E., Farrow, C.M., & Bowes, G.M. (1991). COOL: A FORTRAN 77 computer program for modelling stable isotopes in cooling closed systems. *Computer Geosciences*, *17*, 391-412.

Layne, G. D., Longstaffe, F. J., & Spooner, E. T. C. (1991). The JC tin skarn deposit, southern Yukon territory: II. A carbon, oxygen, hydrogen and sulfur stable isotope study. *Economic Geology*, *86*, 48-65.

Laouar, R., Boyce, A.J., Ahmed-Said, Y., Ouabadi, A., Fallick, A.E., & Toubal, A. (2002). Stable isotope study of the igneous, metamorphic and mineralized rocks of the Edough complex, Annaba, Northeast Algeria. *Journal of African Earth Sciences*, *35*, 271-283.

Mathieson, G.A., & Clark, A.H. (1984). The CanTung E-zone scheelite skarn orebody, Tungsten, Northwes Territories: A revised genetic model. *Economic Geology*, *79*, 883-901.

Matthews, A., Goldsmith, J. R., & Clayton, R. N. (1983). Oxygen isotope fractionations involving pyroxenes: the calibration of mineral-pair geothermometers, *Geochimica Cosmochimica Acta*, *47*, 631-644.

Matthews, A. (1994). Oxygen isotope geothermometers for metamorphic rocks. *Journal of Metamorphic Geology*, *12*, 211-219.

Meinert, L.D. (1992). Skarns and skarn deposits: *Geoscience Canada*, *19*, 145-162.

Meinert, L.D., Hedenquist, J.W., Satoh, H., & Matsuhisa, Y. (2003). Formation of anhydrous and hydrous skarn in Cu-Au ore deposits by magmatic fluids. *Economic Geology*, *98*, 147-156.

Okay, A.I., & Satır, M. (2000). Coeval plutonism and metamorphism in a latest Oligocene metamorphic core complex in northwest Turkey. *Geological Magazine*, *137* (5), 495-516.

O'Neil, J.R. (1986). Thereotical and experimental aspects of isotopic fractionation. *In* Stable Isotopes in High Temperature Geologic Processes (Valley, J.W., Taylor, Jr, H.P. & O'Neil, J.R., eds.). *Reviews in Mineralogy*,, *16*, 1-40.

Öngen, S. (1992). Les échances métasomatiques entre granitoides et encaissant particuliers (calcaires, dolomies, ultrabasites, series manganiferes): I'example de la Turquie-NW. *Doctorat These. Université de Nancy, Faculté des Sciences de la Terre*, 554 p.

Pollard, P.J., Andrew, A.S., & Taylor, R.G. (1991). Fluid inclusion and stable isotope evidence for interaction between granites and magmatic hydrothermal fluids during formation of disseminated and pipe-style mineralization at the Zaaiplaats Tin Mine. *Economic Geology, 86,* 121-141.

Rose, A. W., Herrick, D. C., & Deines, P. (1985). An oxygen and sulfur isotope study of skarn-type magnetite deposits of the Cornwall type, southeasthern Pennsylvania. *Economic Geology*, *80*, 418-443.

Rumble, D. III., & Hoering, T. C. (1994). Analysis of oxygen and sulfur isotope ratios in oxide and sulfide minerals by spot heating with a carbon dioxide laser in a fluorine atmosphere. *Accounts of Chemical Research*, *27*, 237-241.

Sharp, Z. D. (1990). A laser-based microanalytical method for in situ determination of oxygen isotope ratios in silicates and oxides. *Geochimica Cosmochimica Acta*, *54*, 1353-1357.

Sheppard, S.M.F. (1986). Characterization and isotopic variations in natural waters. *Mineralogy*, *16*, 165-183.

Taylor, H.P. (1968). The oxygen isotope geochemistry of igneous rocks. *Contributions to Mineralogy and Petroogy*, *19*, 1-71.

Taylor, H.P. (1979). Oxygen and hydrogen isotope relationships in hydrothermal mineral deposits. In: Barnes, H.L. (eds.) *Geochemistry of Hydrothermal Ore Deposits: New York, Wiley Intersci.*, 236-277.

Taylor, B. E., & O'Neil, J. R. (1977). Stable isotope studies of metasomatic Ca-Fe-Al-Si skarns and associated metamorphic and igneous rocks, Osgood Mountains, Nevada. *Contribution to Mineralogy and Petrology*, *63*, 1-49.

Taylor, H. P., & Sheppard, S. M. F. (1986). Igneous rocks. I. Processes of isotopic fractionation and isotope systematics. In: Valley J. W., Taylor H. P., O'Neil J. R. (eds) Stable Isotopes in High temperature geological processes . *Reviews in mineralogy, Mineral Society of America, Washington, DC*, *16*, 227-272.

Taylor, H.P. (1997). Oxygen and hydrogen isotope relationships in hydrothermal mineral deposits, *in:* Barnes, H.L. (eds), *Geochemistry of hydrothermal ore deposits, 3rd edition: New York, John Wiley and Sons*, 229-302.

Valley, J. W., Kitchen, N., Kohn, M. J., Niendorf, C. R., & Spicuzza, M. J. (1995). UWG-2, a garnet standard for oxygen isotope ratios: strategies for high precision and accuracy with laser heating. *Geochimica Cosmochimica Acta*, *59*, 5223-5231.

Vazquez, R., Venneman, T.W., Kesler, S.E., & Russell, N. (1998). CArbon and oxygen isotope halos in the host limestone, El Mochito Zn, Pb (Ag) skarn massive sulfide/oxide deposit, Honduras. *Economic Geology*, *93*, 15-31.

Vennemann, T. W., & O'Neil, J. R. (1993). A simple and inexpensive method of hydrogen isotope and water analyses of minerals and rocks based on zinc reagent. *Chemical Geology (Isotope Geoscience Section)*, *103*, 227-234.

Wichkam, S.M., & Taylor, H.P. (1987). Stable isotope evidence for large-scale seawater infiltration in a regional metamorphic terrane: the Trois Seigneurs Massif, Pyrenees, France. *Contribution to Mineralogy and Petrology*, *91*, 122-137.

Wichkam, S.M., Alberts, A.D., Zanvilevich, A.N., Litvinovsky, B.A., Bindeman, I.N., & Schauble, E.A. (1996). A stable isotope study of anorogenic magmatism in East Central Asia. *Journal of Petrology, 37*, 1063-1095.

Yücel-Öztürk, Y., Helvacı, C., & Satır, M. (2005). Genetic relations between skarn mineralization and petrogenesis of the Evciler granitoid (Kazdağ, Çanakkale-Turkey) and comparison with world skarn granitoids. *Turkish Journal of Earth Sciences, 14*, 255-280.

Zheng, Y.F. (1993). Calculation of oxygen isotope fractionation in hydroxyl-bearing silicates. *Earth and Planetary Science Letter*, *120*, 247-263.

Zussman, J. (1977). *Physical methods in determinative mineralogy, 2nd ed. London, Academic Press*, 720 pp.

CHAPTER FIVE
GENERAL CONCLUSION

This study focuses on the Evciler Cu-Au skarn deposit, supplements the geological and petrographic features with the analytical data obtained by the electron microprobe and stable isotope analyses of the skarn mineral assemblage of Evciler, determine the geology and alteration-mineralization style of the Evciler district. It also draws upon the similarities of this occurrence with the other skarns of the world, some of which are well known for their ore potential.

Pyrrhotite-bearing calcic skarn mineralization occur at the contact between Evciler quartz diorite-granodiorite and marble lenses belong to the Kazdağ Massif at the south of the Evciler granitoid. Major element chemistry indicates that the Evciler granitoid has a metaluminous, mildly peraluminous and calc-alkaline character. In terms of trace-element data, the Evciler granitoid is classified as VAG (volcanic arc granites) and syn-collision granites. In the study area two different rock types are observed: the mezocratic-type Evciler is quartz diorite to granodiorite in composition, whereas the leucocratic-type Evciler is monzogranite in composition and they both show I-type characteristics.

Relative metal abundances in magmas and different types of intrusion-related deposits are a function of compositional evolution, fractionation and oxidation state. It is the core element association that most closely relates to magma composition. Cu-Au deposits are associated with oxidized, relatively unevolved to moderately evolved suites. The Evciler quartz diorite-granodiorite are characterized by relatively unevolved to moderately evolved and oxidized suite and are fairly close to Au-Cu deposits. The geochemical characteristics of the Evciler quartz diorite-granodiorite, Çavuşlu monzodiorite and Karaköy granodiorite are also similar to some of the Cu-, Fe-, Cu-Au-, and Fe-Cu skarn granitoids. However, the geochemical characteristics of the Evciler monzogranite are similar to the averages for Sn- and Mo- skarn granitoids.

The results of this study suggest that the composition and petrologic evolution of the Evciler pluton are the primary controls on skarn alteration, mineralization, and metal content (e.g. copper, gold, iron). The combination of all these parameters can be used on a district to regional scale to interpret relationships between Evciler pluton and related ore deposits. However, the Evciler pluton is analoguous with Au-Cu association of the core metal associations.

For some granite, little or no interaction with external fluids seems to have taken place and the whole-rock oxygen isotope ratios probably reflect quite closely the original magma values. Other granites have been subjected to extensive exchange with external fluids which has changed the original magmatic $\delta^{18}O$ values (e.g.; Hercynian granites of the Pyrenees, the Idaho batholith and many other Tertiary batholiths of the western USA and some Caledonian granites of Britain).

Whole rock samples from Evciler granitoid, collected only a few meters from the skarn mineralization have $\delta^{18}O$ between 4.8 and 6.0 ‰, with the most altered samples having lowest $\delta^{18}O$ value like other world skarn granitoids. In order to create granites with low $\delta^{18}O$ values observed in the Evciler samples, it is necessary to call upon hydrothermal alteration. Compared to normal granites, meteoric waters have relatively low $\delta^{18}O$ values. During water-rock interaction at the Evciler district, each isotopic value of the granitoid and meteoric water normalize the value of other as $\delta^{18}O$ is exchanged. Thus, the Evciler granitoid $\delta^{18}O$ values would decrease to lower values during hydrothermal alteration and skarnization at the district. $\delta^{18}O$ values of the original magma of the Evciler granitoid (δ_{magma}), calculated from quartz $\delta^{18}O$ values, range from 6.0 to 8.0 ‰, suggesting similar to those of slowly cooled coarse-grained I-type granites. Although, range of $\delta^{18}O$ value for quartz (7.2-10.9 ‰) of fresh granitoid samples is normal for I-type granitic rocks.

The Evciler phyrrothite-rich skarn mineralization was precipitated in a faulted zone between Evciler granitoid and Kazdağ metamorphic rocks at the south of the pluton. Both endoskarn and exoskarn occur within the study area. Endoskarn represents the skarnization of the Evciler granitoid. Exoskarn is classified as calcic

exoskarn. The paragenetic studies at Evciler show that skarn evolution occurred three stages. Stage I mineral assemblage is dominated by clinopyroxene and garnet. This stage is considered to represent prograde anhydrous skarn development, whereas stage II, which is dominated by hydrous minerals (amphibole, epidote) and stage III, which comprises pyrrhotite, pyrite, chalcopyrite, chlorite and/or quartz are considered to represent retrograde hydrous skarn development. The Evciler deposit is extremely rich-in pyrrhotite, magnetite and chalcopyrite, and appear to be oxidized, but pyrrhotite characterizes a reduced environment. The difference in oxidation levels of the skarn is revealed by varying Fe^{2+}/Fe^{3+} ratios which are generally manifested in the type of garnet and clinopyroxene formed.

During the early stage (stage I), skarn-forming fluids are largely anhydrous and derived from granite, and no convection cell to focus fluids from meteoric sources from the country rocks has formed. Major pyrrhotite-bearing mineralization occurs within the pyroxene skarn. In the late stage (stage II), magmatic fluids mix with meteoric fluids, and are formed into permeable early-formed skarns and unreplaced carbonate unit to form late-stage skarns and mineralization, which are dominantly hydrous. This late-stage is also accompanied by the formation of endoskarn due to metasomatic alteration of the igneous protolith in areas where fluids have permeated intensely.

Chemical determinations of minerals from the Evciler skarn showed that large proportions of minerals at these locations are calcium-rich (grossular-andradite, amphibole, epidote, sphene). This observation suggests high calcium activity during skarn formation, most likely emanating from the dissolution of calcic carbonate protolith (Kazdağ marble lenses). Mineral chemistry also provide information, which can be used to classify the skarn type. On the basis of garnet and pyroxene compositions, the Evciler skarn occurrences show many similarities with other calcic Fe-Cu and Au skarns. The deposits occur in carbonate host litologies of various ages that are associated with felsic intrusions of varying ages. Other important features associated with these deposits include oxidation state of the skarns, plumbing system or channel ways for fluids, metal source, and level of emplacement of the associated

intrusion. These deposits are generally characterized by early anhydrous mineral assemblages that are overprinted by later hydrous retrograde mineral assemblages.

The oxygen, hydrogen and whole-rock isotope analyses contribute to a general picture of the geologic history of the Evciler skarn mineralization. The isotopic compositions of the hydrothermal fluid, from which skarn was precipitated, can be calculated if (1) a fractionation factor at a given temperature, (2) isotopic compositions of skarn silicates and (3) equilibrium temperature of skarn silicates from the fluid are known. Consequently, with all the information given, $\delta^{18}O$ values were calculated for the stable isotope compositions of the skarn-forming fluid.

The fluid associated with prograde skarn formation at Evciler was a high temperature liquid. The calculated $\delta^{18}O$ value of the fluid in equilibrium with garnet and pyroxene from the deposit is within the range of values for magmatic fluids. The fluid associated with the retrograde alteration stage is lower temperature than that of the prograde skarn fluid.

The water in the hydrothermal solution precipitating the phyrrothite-rich ore body could have been magmatic water at first, but meteoric water played an increasing role toward the end of the depositional history. The evidence of the presence of a meteoric component in the hydrothermal solution suggests that with passage of time the hydrothermal fluid mixed to a progressively greater extent with invading meteoric water which may have encouraged cooling of the fluid; precipitation of ore may have been induced by this process.

In conclusion, the stable isotope evidence suggests some involvment of meteoric water in the genesis of the mineralization, but the high-temperature history of that water, its interaction with the granite and the temperature of ore mineralization are unclear.